Springer Theses
Recognizing Outstanding Ph.D. Research

Rong Wang

Global Emission Inventory and Atmospheric Transport of Black Carbon

Evaluation of the Associated Exposure

Springer

Springer Theses

Recognizing Outstanding Ph.D. Research

Aims and Scope

The series "Springer Theses" brings together a selection of the very best Ph.D. theses from around the world and across the physical sciences. Nominated and endorsed by two recognized specialists, each published volume has been selected for its scientific excellence and the high impact of its contents for the pertinent field of research. For greater accessibility to non-specialists, the published versions include an extended introduction, as well as a foreword by the student's supervisor explaining the special relevance of the work for the field. As a whole, the series will provide a valuable resource both for newcomers to the research fields described, and for other scientists seeking detailed background information on special questions. Finally, it provides an accredited documentation of the valuable contributions made by today's younger generation of scientists.

Theses are accepted into the series by invited nomination only and must fulfill all of the following criteria

- They must be written in good English.
- The topic should fall within the confines of Chemistry, Physics, Earth Sciences, Engineering and related interdisciplinary fields such as Materials, Nanoscience, Chemical Engineering, Complex Systems and Biophysics.
- The work reported in the thesis must represent a significant scientific advance.
- If the thesis includes previously published material, permission to reproduce this must be gained from the respective copyright holder.
- They must have been examined and passed during the 12 months prior to nomination.
- Each thesis should include a foreword by the supervisor outlining the significance of its content.
- The theses should have a clearly defined structure including an introduction accessible to scientists not expert in that particular field.

More information about this series at http://www.springer.com/series/8790

Rong Wang

Global Emission Inventory and Atmospheric Transport of Black Carbon

Evaluation of the Associated Exposure

Doctoral Thesis accepted by College
of Urban and Environmental Sciences,
Peking University, Beijing, China

Springer

Author
Dr. Rong Wang
Laboratory for Earth Surface Processes,
College of Urban and Environmental Sciences
Peking University
Beijing
China

Supervisor
Prof. Shu Tao
Laboratory for Earth Surface Processes,
College of Urban and Environmental Sciences
Peking University
Beijing
China

ISSN 2190-5053 ISSN 2190-5061 (electronic)
Springer Theses
ISBN 978-3-662-46478-6 ISBN 978-3-662-46479-3 (eBook)
DOI 10.1007/978-3-662-46479-3

Library of Congress Control Number: 2015933152

Springer Heidelberg New York Dordrecht London

Printed on acid-free paper

Springer-Verlag GmbH Berlin Heidelberg is part of Springer Science+Business Media (www.springer.com)

Parts of this thesis have been published in the following journal articles:

Wang, R., Tao, S., Shen, H.Z., Huang, Y., Chen, H., Balkanski, Y., Boucher, O., Ciais, P., Shen, G.F., Li, W., Zhang, Y.Y., Chen, Y., Lin, N., Su, S., Li, B., Liu, J.F., Li, W. Trend in Global Black Carbon Emissions from 1960 to 2007. *Environ. Sci. Technol.* 2014, 48(12), 6780–6787. (Reproduced with Permission. Copyright (2014) American Chemical Society).

Wang, R., Tao, S., Balkanski, Y., Ciais, P., Boucher, O., J.F. Liu, Piao, S.L., Shen, H., Vuolo, M., Chen, H., Chen, Y., Cozic, A., Huang, Y., Li, B.G., Li, W., Shen, G.F., Wang, B., Zhang, Y.Y. Exposure to ambient black carbon derived from a unique inventory and high resolution model. *Proc. Natl. Acad. Sci. USA.* 2014, 111(7), 2459–2463. (Reproduced with Permission).

Wang, R., Tao, S., Ciais, P., Shen, H.Z., Huang, Y., Chen, H., Shen, G.F., Wang, B., Li, W., Zhang, Y.Y., Lu, Y., Zhu, D., Chen, Y.C., Liu, X. P., Wang, W. T., Wang, X. L., Liu, W. X., Li, B. G., Piao, S. L. High resolution mapping of combustion processes and implications for CO_2 emissions. *Atmos. Chem. Phys.* 2013, 13, 5189–5203. (Reproduced with Permission).

Wang, R., Tao, S., Wang, W.T., Liu, J., Shen, H.Z., Shen, G.F., Wang, B., Liu, X., Li, W., Huang, Y., Zhang, Y.Y., Lu, Y., Chen, H., Chen, Y.C., Wang, C., Zhu, D., Wang, X., Li, B.G., Li, W., Ma, J. Black carbon emissions in China from 1949 to 2050. *Environ. Sci. & Technol.* 2012, 46, 7595–7603. (Reproduced with Permission. Copyright (2012) American Chemical Society).

Wang, R., Tao, S., Shen, H.Z., Wang, X.L., Li, B.G., Shen, G.F., Wang, B., Li, W., Liu, X., Huang, Y., Zhang, Y.Y., Lu, Y., Ouyang, H. Global emission of black carbon from motor vehicles from 1960 to 2006. *Environ. Sci. & Technol.* 2012, 46, 1278–1284. (Reproduced with Permission. Copyright (2011) American Chemical Society).

Supervisor's Foreword

Particulate matter in air affects both climate and health. Among various compositions of atmospheric particulate matter, black carbon is an important one in terms of both climate forcing and health impact. Over the past decade, many efforts have been made to improve our understanding on sources, emission, and transport of black carbon in regional and global environment. Still, large uncertainty remains in emission inventory prevent us to quantitatively model spatiotemporal distribution of black carbon satisfactorily. In his thesis study, Dr. Rong Wang has compiled a global fuel consumption data product (PKU-Fule-2007) and a global black carbon emission inventory (PKU-BC-2007), modeled transport of black carbon in global scale, and estimated inhalation exposure to ambient black carbon at population level. The major improvement in the inventory developed was spatial (0.1°) and sectorial (more than 60 sources) high resolutions, which provides necessary information for high-resolution modeling, exposure assessment, and abatement policy evaluation. To create the high-spatial resolution inventory, a subnational method was taken. It was well demonstrated that the spatial bias caused by national fuel data-based spatial disaggregation using population density as a proxy can be reduced substantially. A per-capital GDP (gross domestic product)-based regression model was also developed for predicting emission factors of black carbon from motor vehicles for given country and given year. Historical emissions at country resolution have also been compiled and compared with those reported previously. The results of the east-Asia-nested transport modeling not only showed the detailed geographical distribution and hot areas of black carbon in atmosphere, but also revealed that model resolution is critical in the modeling. It was found that coarse resolution can lead underestimation in severely contamination sites. An emission-based method was developed to downscale the model-predicted concentrations. In sum, the results and major findings of the study can help us to understand global-scale source, fate, and impacts of black carbon better.

Beijing, December 2014 Prof. Shu Tao

Abstract

Black carbon (BC), or soot, is a particulate component produced in the combustion of carbon fuels. Due to the special role of BC in climate change and air quality, this short-lived climate forcer is particularly concerned in atmospheric science. In this thesis, we revisited the emission inventory of BC by updating the emission factors of BC and improving the spatial allocation of fuel consumption. In detail, a global high-resolution emission inventory of BC was constructed for the year 2007, covering 64 fuel subtypes and 222 countries/territories. A subnational disaggregation method was developed to allocate the fuel consumption and BC emissions to grids, which reduces the disaggregation errors in the national disaggregation method. In addition, the temporal trend in BC emissions will be studied for a period from 1949 to 2050 in China and was studied from 1960 to 2007 in all countries. Uncertainties associated with estimated BC emissions were characterized following a Monte Carlo approach. As a result, global total BC emissions had increased from 5.3 Tg year^{-1} (3.4–8.5 as an interquartile range of uncertainty) in 1960 to 9.1 Tg year^{-1} (5.6–14.4) in 2007. Comparing with previous BC emission inventories, our estimations are 11–16 % higher than those reported previously, mainly due to the update of BC emission factors by recent measurements and use of fuel consumption data from local energy statistics. An underestimation in BC emissions by previous inventories was found in the north and southwest of China, the northeast of India, Central Africa, where traditional fuels were intensively burnt in residential stoves or industrial boilers with poor dust abatement facilities.

Subsequently, the new emission inventory of BC was introduced to an atmospheric general circulation model LMDz-OR-INCA zoomed to a resolution of 0.51° in latitude and 0.66° in longitude over Asia. In comparison, a reference emission inventory of BC (MACCity) and the LMDz-OR-INCA at a regular grid of 1.27° in latitude and 2.50° in longitude were also used. In comparison with other three combinations of emission inventory and model resolutions, the combination of new inventory and high-resolution model produces a field of BC which better agrees with observations. The model-data misfit was reduced from −88 to −35 % in Asia where the new emission inventory and high-resolution transport model replaced a previous inventory and coarse-resolution model. However, as illustrated in an

offline regional chemistry transport model CHIMERE, the discrepancy of model and observations can be further reduced when BC concentrations were simulated at a resolution of $0.1° \times 0.1°$. Therefore, a nonlinear downscaling method was developed to disaggregate BC concentrations to a resolution of $0.1° \times 0.1°$ globally. As a result, the model-data misfit could be further reduced to -12 % globally using the nonlinear downscaling method. In addition to the magnitude of BC concentrations, acceptable agreements between the modeled and observed seasonal trend and vertical distribution of BC were also obtained using the new emission inventory and high-resolution model.

According to simulated BC concentrations, ambient exposure and lifetime average daily intake of BC were estimated globally. The ambient exposure to BC was assessed at a resolution of 10 km based on the simulated surface BC concentrations using the new emission inventory and nonlinear downscaling method. The highest BC exposure concentration as a population-weighted average was found over the North China Plain (6.68 $\mu g\ m^{-3}$), the Sichuan Basin (5.49 $\mu g\ m^{-3}$), and the Indo-Gangetic Plain (4.31 $\mu g\ m^{-3}$). The results are sensitive to the emission inventory and model resolution. When a coarse model resolution is used, the exposure concentration of BC among population living in "hot-spots" regions could be "diluted" and the population-weighted BC exposure concentration could be underestimated significantly. The estimated global average BC exposure concentration constrained by observations is 2.14 $\mu g\ m^{-3}$, 130 % higher than that using a less-detailed emission inventory and coarse-resolution transport model. Regionally, 18 and 11 % populations in East Asia and South Asia were exposed to a high BC concentration with significant health effects reported in a Chinese city. The lifetime average daily intake of BC was estimated by country using a standard exposure model. The top 10 lifetime average daily intake countries were China (132 ng/kg/day), Bangladesh (123 ng/kg/day), Pakistan (87 ng/kg/day), India (81 ng/kg/day), Nepal (80 ng/kg/day), Vietnam (79 ng/kg/day), Bhutan (75 ng/kg/day), North Korea (70 ng/kg/day), Cambodia (66 ng/kg/day), and Nigeria (51 ng/kg/day). Although there is still no exposure standard for BC due to lack of epidemiological data, a high exposure risk of BC could be expected. At last, since the BC exposure concentration was much higher over urban areas than that over rural areas in developing countries, an accelerated urbanization would lead to a higher BC exposure in the coming decades.

Keywords Black carbon · Fuel consumption · Emission factors · Emission inventory · Uncertainty analysis · Atmospheric model · Model resolution · Exposure · Air pollution

Acknowledgments

In 2004, I have entered Peking University and began a 9-year study in this beautiful campus. Many colleagues and friends have helped me in my study. I would like to take this opportunity to express my gratitude to all of them.

First, I would like to thank Prof. Tao, who supervised me in my undergraduate and graduate study. His passion for science and intelligence in research impresses me so much and help in shaping me to a potential scientist. In the 9 years, he teaches me how to work and how to think, which will benefit me for the rest of my career. In particular, this thesis cannot be completed without his patient and expert guidance.

Second, I would like to thank three reputable scientists in France. In the fourth year of my graduate study, I got an opportunity for a visit study at Laboratoire des Sciences du Climat et de l'Environnement, France. Prof. Balkanski gave me great help in learning the atmospheric models. He showed me how to work in a rigorous manner and taught me how to cooperate with other colleagues. Also in this year, I recognized Prof. Boucher and Prof. Ciais, who are both the topping scientists in climate change. They taught me how to perform original researches. Under the help by them, I obtained a better understanding of climate change and a distinctive way to think.

Third, I would like to thank all my colleagues in the laboratory. Many professors have given me useful guidance in my study. For example, Prof. Bengang Li has taught me how to use professional software in preparing high-quality graphs and Prof. Wenxin Liu gave me lots of guidance in studying the fugacity model. Meanwhile, many friends have helped me. For example, Chang Lang, Yu Yang, and Yanxu Zhang gave me great help when I was starting my study. Huizhong Shen and Ye Huang had worked together with me in developing the emission inventory. Guofeng Shen and Bing Wang had provided important data for my research.

At last, I would like to thank H. Ouyang for format-editing and proof-reading. I also thank her for encouraging me whenever I come to problems in the study.

The research carried out in the thesis was funded by the National Natural Science Foundation of China (Grant 41390240, 41390243 and 41130754), the 111 Program (B14001), the Beijing Municipal Government (YB20101000101), and the Agence Nationale de la Recherche' (project: ANR-09-CEP-005-03/PAPRIKA). Some of the computation was performed using HPC resources from GENCI-TGCC.

Contents

Chapter 1
Introduction

1.1 Background

Emission sources, environment fate, health effects and climate impacts of black carbon (BC) are increasingly concerned by the public and policy makers. BC, or soot, as a distinct type of carbonaceous material that strongly absorbs incoming solar radiation, is emitted by incomplete combustion of carbon fuels, such as coal, petroleum, biofuels and biomass. BC is widely found in the environment, including soils, ices, sediments, and the air. It was found that BC makes up 12–31 % of the sedimentary organic materials at two deep ocean sites, which has an age of thousands of years (Masiello and Druffel 1998). During the industrial-era, the consumption of fossil fuels and biofuels have been increased rapidly, leading to a significant increase of BC emissions to the atmosphere (Novakov et al. 2003; Ito and Penner 2005; Dentener et al. 2006; Bond et al. 2007; McConnell et al. 2007; He and Zhang 2009; Hirdman et al. 2010; Skeie et al. 2011). With a lifetime spanning from 1 to 10 days (Penner et al. 1993), BC can contribute to air pollution as a component in fine particulate matter (Brimblecombe 1987). The climate impact of BC, in addition to its impact on human health, has been recognized and highlighted in recent decades (Andreae 1995; Haywood and Shine 1995; Hansen et al. 1998; Myhre et al. 1998; Penner et al. 1998; Jacobson 2001b; Hansen and Nazarenko 2004). Now, BC has been widely concerned for its dual role in air pollution and climate change (Anenberg et al. 2012; Shindell et al. 2012).

As a driving agent for global warming, BC absorbs solar light at all visible wavelengths. Up to now, BC has been recognized as a species with the strongest light absorption per unit mass in the atmosphere, although the abundance is much lower than that of carbon dioxide (CO_2), the most well-known greenhouse gas. The second assessment report of Intergovernmental Panel on Climate Change adopted a direct radiative forcing of $+0.1$ W m^{-2} for BC (Houghton 1996), based on the work by Andreae (1995), Haywood and Shine (1995), Hansen et al. (1998)

R. Wang, *Global Emission Inventory and Atmospheric Transport of Black Carbon*,
Springer Theses, DOI 10.1007/978-3-662-46479-3_1

and Haywood and Ramaswamy (1998). Subsequently, with the development of a comprehensive atmospheric transport model for aerosols, Jacobson reported a direct radiative forcing of BC as high as +0.55 W m^{-2} (Jacobson 2000, 2001a, b), by considering the internal mixing state of BC in particles. Furthermore, when the first global observational network of light absorption by aerosols was established, the estimated direct radiative forcing of BC was raised to 0.7–0.9 W m^{-2} using the observation as a constraint (Sato et al. 2003; Chung and Seinfeld 2005; Ramanathan and Carmichael 2008; Chung et al. 2012; Bond et al. 2013). In the latest assessment report of Intergovernmental Panel on Climate Change, a comprehensive estimate based on recent modelling studies of BC suggests a direct radiative forcing of +0.4 W m^{-2} (+0.05 to +0.8 as 90 % confidence interval) for BC from fossil fuels and biofuels, and +0.2 W m^{-2} (+0.03 to +0.4) for BC from biomass burning (Stocker et al. 2013).

In addition to light absorption, BC can also affect the Earth's radiative budget by interacting with the cloud and changing the snow/ice albedo. In the atmosphere, BC particles can act as an effective cloud condensation nuclei or ice nuclei. Then, it can inhibit the freezing of droplets, increase the reflectivity of clouds, and change cloud droplet number and size distributions of cloud droplet (Jacobson 2004; Lohmann and Feichter 2005; Menon and Rotstayn 2006; Levy et al. 2013). When BC is deposited over the surface of ice/snow, it decreases the reflectivity, increases the ability of ground in absorbing solar radiation, and finally leads to a positive radiative forcing in the Earth system. Moreover, due to the increase of light absorption by ground, ice or snow may melt and lead to additional climate impact due to the change of surface albedo. Due to BC deposition in snow and ice, there is a positive radiative forcing of +0.04 W m^{-2} (+0.02 to +0.09) according to the fifth assessment report of Intergovernmental Panel on Climate Change (Stocker et al. 2013). Therefore, BC is playing an important role in Earth climate system due to its direct and indirect effects.

In addition to climate change, the role of BC in air quality has also been increasingly noticed in recent studies. Fine particles, or $PM_{2.5}$ (defined as the ambient particles less than two and a half micrometers in size), can induce significant adverse impacts on human healths, which result in millions of premature deaths every year globally (Lim et al. 2013). In an authoritative assessment of the benefits of mitigation of short-lived climate species, namely BC and methane (Shindell et al. 2012), it is found that when sufficient measures are adopted to mitigate methane and BC, the global mean warming can be cut off by ~0.5 ° by 2050 while 0.7–4.7 million annual premature deaths can be avoided due to outdoor air pollution (Shindell et al. 2012). These authors performed the calculation by considering BC as a normal component of $PM_{2.5}$, and applied the exposure-response relationship based on $PM_{2.5}$ for BC (Pope III et al. 2002; Roman et al. 2008). However, the unique role of BC, distinct to other species such as sulfate and nitrate, has not been well identified. In the latest assessment report released by U.S. Environmental Protection Agency (http://www.epa.gov/research/airscience/air-blackcarbon.html), the health effects of BC have been highlighted. According to this report, it is recognized that BC exposure is associated with lots of health

effects, such as respiratory diseases (e.g. asthma), low birth weights, heart attacks and lung cancer. As a component of $PM_{2.5}$, in the report by U.S. Environmental Protection Agency, BC is recognized as a valuable indicator for a larger category of primary combustion particles, such as trace metals and hydrocarbons. Almost at the same time, the World Health Organization released a similar report to review all BC-related epidemiological studies systematically and investigated the evidences of the health effects of BC (Janssen et al. 2012). According to that report, it's concluded that short-term epidemiological studies have provided sufficient evidences to justify the association of the daily variation in BC exposure concentrations and short-term health indices, including all-cause and cardiovascular mortality and cardiopulmonary hospital admissions. Meantime, some evidences are also found from cohort studies for the association of all-cause and cardiopulmonary mortality with the long-term exposure of BC. According to the short-term health effects studies, BC is shown as a better indicator of harmful species in particles than the total mass of particulate matter. It should be noted that there is still a lack of evidences for the association of BC exposure and health effects in long-term studies. As a conclusion, BC should be regarded as a "universal carrier" of toxic substances in the particulate matter, and BC can be used as an indirect indicator for the health effects associated with PM in air quality assessments. In addition to the studies reviewed by U.S. Environmental Protection Agency and World Health Organization, there are a series of studies which have investigated the relationship between the mortality outcomes and the exposure to BC in a Chinese city (Geng et al. 2013; Wang et al. 2013; Hua et al. 2014). It is found that an interquartile range increase (2.7 $\mu g\ m^{-3}$) of the concentration of BC exposure could lead to an increase by 2.3, 3.2 and 0.6 % in the total, cardiovascular and respiratory mortality, respectively. More importantly, this relationship remains robust when the correlation is adjusted for $PM_{2.5}$. This is the first time to identify the health effects of BC in an Asian developing country, which highlights the importance of including BC as an additional indicator for air quality assessment.

However, current studies simulating the BC concentrations and light absorption due to BC in the atmosphere all found large discrepancies between model and observations, preventing a clear assessment of the role of BC in climate change and air pollution. Koch et al. (2009) performed a model-intercomparison study by using different sources of measurement to evaluate the modelling of BC in the atmosphere. As a result, the surface BC concentrations were generally underestimated by 2-fold in Asia, and overestimated by 2-fold in Europe in 17 AeroCom (Aerosol Comparisons between Observations and Models) Phase-I models (Koch et al. 2009). Meantime, the observed aerosol absorption optical depth were underestimated in all regions by AeroCom models by a factor spanning from 2 to 6 (Koch et al. 2009; Bond et al. 2013). Chung et al. (2012) performed another study to isolate the aerosol absorption optical depth induced by BC and brown carbon, resulting in an observation-constrained BC aerosol optical depth (AOD) higher than all modelling studies. Recently, in the Atmospheric Chemistry and Climate Model Intercomparison Project (ACCMIP) study as a support to the fifth assessment report of Intergovernmental Panel on Climate Change, Shindell et al. (2013)

found that current models have generally underestimated the AAOD by roughly a factor of two when compared with either the Ozone Monitoring Instrument (OMI) (Torres et al. 2007) or the Aerosol Robotic Network (AERONET) (Holben et al. 1998; Dubovik et al. 2000; Dubovik et al. 2002) observations. It was suggested that the underestimated BC surface concentrations and light absorption in models are caused by the bias in the BC emission inventories (Chung and Seinfeld 2005; Koch et al. 2009; Chung et al. 2012; Bond et al. 2013). These results suggested that BC emissions is likely underestimated, in particular for Asia, in present emission inventories. It is urgently necessary to re-visit the emission inventory of BC in order to provide a better understanding of the role of BC in both climate change and air pollution.

1.2 Main Objectives

This thesis targets at developing a global BC emission inventory, simulating the global distribution of BC in an atmospheric transport model, and assessing the population exposure to BC. The main objectives include:

(1) developing a global $0.1° \times 0.1°$ inventory of fuel consumptions as a basis for the emission inventory of BC;
(2) constructing a comprehensive database of BC emission factors using the latest measurements;
(3) developing a global $0.1° \times 0.1°$ inventory of BC with the high-resolution fuel inventory and the updated database of BC emission factors in 2007;
(4) investigating the historical trend of regional and global BC emissions;
(5) running a high-resolution atmospheric transport model with the new BC emission inventory, and evaluating the model by observed BC concentrations globally;
(6) estimating the exposure to ambient BC globally, and investigating the effects of using the new emission inventory and high-resolution transport model.

1.3 Thesis Structure

Chapter I Introduction. A brief introduction about the background, research objectives and structure of the thesis.

Chapter II Research background. In this section, previous studies on emission estimations, atmospheric modelling, climate effects and health impacts of black carbon are reviewed.

Chapter III Research method. The methodology used to develop the emission inventory of black carbon is described, including the collection of black carbon emission factors, compilation of high-resolution fuel consumption data,

technology divisions, and calculation of black carbon emissions. In addition, the atmospheric transport model used to simulate the global distribution of black carbon and the method used to calculate the exposure of black carbon are also described in this section.

Chapter IV Global high-resolution inventory of fuel consumptions. In this section, the high-resolution fuel consumption inventory based upon a sub-national disaggregation method with detailed sectors is introduced. This new data product is compared with the inventory developed based upon the nightlight data set and the inventory using the traditional national disaggregation method. The implications of this new inventory of fuel consumption at a high spatial resolution for carbon emissions are also discussed.

Chapter V Emissions of black carbon from motor vehicles. In this section, models predicting the emission factors of black carbon for different motor vehicles were developed based upon the measured data collected in this study. Based on these models, black carbon emissions from motor vehicles are predicted globally from 1960 to 2007.

Chapter VI Emissions of black carbon in China from 1949 to 2050. In this section, black carbon emissions in China from 1949 to 2007 are estimated based on the compiled black carbon emission factors and data of fuel consumption. The impact of the major technology transfers in the historical period in this country are discussed. At last, the emissions of black carbon in China are predicted to 2050 under different scenarios.

Chapter VII Global emissions of black carbon from 1960 to 2007. In this section, the historical global emissions of black carbon are estimated. Black carbon emissions are estimated at a resolution of $0.1^\circ \times 0.1^\circ$ for year 2007. The estimated black carbon emissions and the spatial patterns are compared with previous inventories, and the differences are discussed.

Chapter VIII Concentrations, exposure, and inhalation intake of black carbon. The surface concentrations of black carbon simulated by an atmospheric transport model are validated by observations worldwide. The results based on models at different resolution and using different emission inventories are compared. At last, the exposure and inhalation intake of black carbon are assessed, and the effects of using a high-resolution transport model and a new emission inventory are discussed.

Chapter IX Conclusions. In this section, we summary the main conclusions of this thesis.

References

Andreae, M. O. (1995). Climatic effects of changing atmospheric aerosol levels. *World Survey of Climatology, 16*, 347–398.

Anenberg, S. C., Schwartz, J., Vignati, E., Emberson, L., Muller, N. Z., West, J. J., et al. (2012). Global air quality and health co-benefits of mitigating near-term climate change through methane and black carbon emission controls pp. (831–839). doi: 10.1289/ehp.1104301.

Bond, T. C., Bhardwaj, E., Dong, R., Jogani, R., Jung, S., Roden, C., et al. (2007). Historical emissions of black and organic carbon aerosol from energy-related combustion. *Global Biogeochemical Cycles, 21*(2), 1850–2000. doi:10.1029/2006GB002840.

Bond, T. C., Doherty, S. J., Fahey, D., Forster, P., Berntsen, T., DeAngelo, B., et al. (2013). Bounding the role of black carbon in the climate system: A scientific assessment. *Journal of Geophysical Research: Atmospheres, 118*(11), 5380–5552.

Brimblecombe, P. (1987). *The big smoke: A history of air pollution in London since medieval times*. Methuen: Hardcover Publisher.

Chung, C. E., Ramanathan, V., & Decremer, D. (2012). Observationally constrained estimates of carbonaceous aerosol radiative forcing. *Proceedings of the National Academy of Sciences, 109*(29), 11624–11629.

Chung, S. H., & Seinfeld, J. H. (2005). Climate response of direct radiative forcing of anthropogenic black carbon. *Journal of Geophysical Research: Atmospheres (1984–2012), 110*(D11).

Dentener, F., Kinne, S., Bond, T., Boucher, O., Cofala, J., Generoso, S., et al. (2006). Emissions of primary aerosol and precursor gases in the years 2000 and 1750 prescribed data-sets for AeroCom. *Atmospheric Chemistry and Physics, 6*(12), 4321–4344.

Dubovik, O., Smirnov, A., Holben, B., King, M., Kaufman, Y., Eck, T., & Slutsker, I. (2000). Accuracy assessments of aerosol optical properties retrieved from Aerosol Robotic Network (AERONET) Sun and sky radiance measurements. *Journal of Geophysical Research: Atmospheres (1984–2012), 105*(D8), 9791–9806.

Dubovik, O., Holben, B., Eck, T. F., Smirnov, A., Kaufman, Y. J., King, M. D., et al. (2002). Variability of absorption and optical properties of key aerosol types observed in worldwide locations. *Journal of the Atmospheric Sciences, 59*(3), 590–608.

Geng, F., Hua, J., Mu, Z., Peng, L., Xu, X., Chen, R., & Kan, H. (2013). Differentiating the associations of black carbon and fine particle with daily mortality in a Chinese city. *Environmental Research, 120*, 27–32.

Hansen, J., & Nazarenko, L. (2004). Soot climate forcing via snow and ice albedos. *Proceedings of the National Academy of Sciences of the United States of America, 101*(2), 423–428.

Hansen, J. E., Sato, M., Lacis, A., Ruedy, R., Tegen, I., & Matthews, E. (1998). Climate forcings in the industrial era. *Proceedings of the National Academy of Sciences, 95*(22), 12753–12758.

Haywood, J., & Shine, K. (1995). The effect of anthropogenic sulfate and soot aerosol on the clear sky planetary radiation budget. *Geophysical Research Letters, 22*(5), 603–606.

Haywood, J., & Ramaswamy, V. (1998). Global sensitivity studies of the direct radiative forcing due to anthropogenic sulfate and black carbon aerosols. *Journal of Geophysical Research: Atmospheres (1984–2012), 103*(D6), 6043–6058.

He, Y., & Zhang, G.-L. (2009). Historical record of black carbon in urban soils and its environmental implications. *Environmental Pollution, 157*(10), 2684–2688.

Hirdman, D., Burkhart, J., Sodemann, H., Eckhardt, S., Jefferson, A., Quinn, P., et al. (2010). Long-term trends of black carbon and sulphate aerosol in the Arctic: Changes in atmospheric transport and source region emissions. *Atmospheric Chemistry and Physics, 10*(19), 9351–9368.

Holben, B., Eck, T., Slutsker, I., Tanre, D., Buis, J., Setzer, A., et al. (1998). AERONET—a federated instrument network and data archive for aerosol characterization. *Remote Sensing of Environment, 66*(1), 1–16.

Houghton, J. T. (1996). *Climate change 1995: The science of climate change: Contribution of working group I to the second assessment report of the Intergovernmental Panel on Climate Change* (Vol. 2). Cambridge: Cambridge University Press.

Hua, J., Yin, Y., Peng, L., Du, L., Geng, F., & Zhu, L. (2014). Acute effects of black carbon and PM _{2.5} on children asthma admissions: A time-series study in a Chinese city. *Science of the Total Environment, 481*, 433–438.

Ito, A., & Penner, J. E. (2005). Historical emissions of carbonaceous aerosols from biomass and fossil fuel burning for the period. *Global Biogeochemical Cycles, 19*(2), 1870–2000.

Jacobson, M. Z. (2000). A physically-based treatment of elemental carbon optics: Implications for global direct forcing of aerosols. *Geophysical Research Letters, 27*(2), 217–220.

Jacobson, M. Z. (2001a). Global direct radiative forcing due to multicomponent anthropogenic and natural aerosols. *Journal of Geophysical Research: Atmospheres (1984–2012), 106*(D2), 1551–1568.

Jacobson, M. Z. (2001b). Strong radiative heating due to the mixing state of black carbon in atmospheric aerosols. *Nature, 409*(6821), 695–697.

Jacobson, M. Z. (2004). Climate response of fossil fuel and biofuel soot, accounting for soot's feedback to snow and sea ice albedo and emissivity. *Journal of Geophysical Research: Atmospheres (1984–2012), 109*(D21).

Janssen, N. A. H., et al. (2012). Health effects of black carbon. In R. Bohr (Ed.) *World Health Organization Regional office for Europe: Warlich Druck Rhein Ahr GmbH*.

Koch, D., Schulz, M., Kinne, S., McNaughton, C., Spackman, J., Balkanski, Y., et al. (2009). Evaluation of black carbon estimations in global aerosol models. *Atmospheric Chemistry and Physics, 9*(22), 9001–9026.

Levy, H., Horowitz, L. W., Schwarzkopf, M. D., Ming, Y., Golaz, J. C., Naik, V., & Ramaswamy, V. (2013). The roles of aerosol direct and indirect effects in past and future climate change. *Journal of Geophysical Research: Atmospheres, 118*(10), 4521–4532.

Lim, S. S., Vos, T., Flaxman, A. D., Danaei, G., Shibuya, K., Adair-Rohani, H., et al. (2013). A comparative risk assessment of burden of disease and injury attributable to 67 risk factors and risk factor clusters in 21 regions, 1990–2010: A systematic analysis for the Global burden of disease study 2010. *The Lancet, 380*(9859), 2224–2260.

Lohmann, U., & Feichter, J. (2005). Global indirect aerosol effects: A review. *Atmospheric Chemistry and Physics, 5*(3), 715–737.

Masiello, C., & Druffel, E. (1998). Black carbon in deep-sea sediments. *Science, 280*(5371), 1911–1913.

McConnell, J. R., Edwards, R., Kok, G. L., Flanner, M. G., Zender, C. S., Saltzman, E. S., et al. (2007). 20th-century industrial black carbon emissions altered arctic climate forcing. *Science, 317*(5843), 1381–1384.

Menon, S., & Rotstayn, L. (2006). The radiative influence of aerosol effects on liquid-phase cumulus and stratiform clouds based on sensitivity studies with two climate models. *Climate Dynamics, 27*(4), 345–356.

Myhre, G., Stordal, F., Restad, K., & Isaksen, I. S. (1998). Estimation of the direct radiative forcing due to sulfate and soot aerosols. *Tellus B, 50*(5), 463–477.

Novakov, T., Ramanathan, V., Hansen, J., Kirchstetter, T., Sato, M., Sinton, J., & Sathaye, J. (2003). Large historical changes of fossil-fuel black carbon aerosols. *Geophysical Research Letters, 30*(6).

Penner, J., Eddleman, H., & Novakov, T. (1993). Towards the development of a global inventory for black carbon emissions. *Atmospheric Environment. Part A. General Topics, 27*(8), 1277–1295.

Penner, J., Chuang, C., & Grant, K. (1998). Climate forcing by carbonaceous and sulfate aerosols. *Climate Dynamics, 14*(12), 839–851.

Pope III, C. A, I. I. I., Burnett, R. T., Thun, M. J., Calle, E. E., Krewski, D., Ito, K., & Thurston, G. D. (2002). Lung cancer, cardiopulmonary mortality, and long-term exposure to fine particulate air pollution. *JAMA, 287*(9), 1132–1141.

Ramanathan, V., & Carmichael, G. (2008). Global and regional climate changes due to black carbon. *Nature Geoscience, 1*(4), 221–227.

Roman, H. A., Walker, K. D., Walsh, T. L., Conner, L., Richmond, H. M., Hubbell, B. J., & Kinney, P. L. (2008). Expert judgment assessment of the mortality impact of changes in ambient fine particulate matter in the US. *Environmental Science and Technology, 42*(7), 2268–2274.

Sato, M., Hansen, J., Koch, D., Lacis, A., Ruedy, R., Dubovik, O., et al. (2003). Global atmospheric black carbon inferred from AERONET. *Proceedings of the National Academy of Sciences, 100*(11), 6319–6324.

Shindell, D., Kuylenstierna, J. C., Vignati, E., van Dingenen, R., Amann, M., Klimont, Z., et al. (2012). Simultaneously mitigating near-term climate change and improving human health and food security. *Science, 335*(6065), 183–189.

Shindell, D. T., Lamarque, J.-F., Schulz, M., Flanner, M., Jiao, C., Chin, M., et al. (2013). Radiative forcing in the ACCMIP historical and future climate simulations. *Atmospheric Chemistry and Physics, 13*(6), 2939–2974.

Skeie, R., Berntsen, T., Myhre, G., Pedersen, C. A., Ström, J., Gerland, S., & Ogren, J. (2011). Black carbon in the atmosphere and snow, from pre-industrial times until present. *Atmospheric Chemistry and Physics, 11*(14), 6809–6836.

Stocker, T. F., Qin, D., Plattner, G.-K., Tignor, M., Allen, S. K., Boschung, J., et al. (2013). Climate Change 2013. The Physical Science Basis. Working Group I Contribution to the Fifth Assessment Report of the Intergovernmental Panel on Climate Change-Abstract for decision-makers : Groupe d'experts intergouvernemental sur l'evolution du climat/ Intergovernmental Panel on Climate Change-IPCC, C/O World Meteorological Organization, 7bis Avenue de la Paix, CP 2300 CH-1211 Geneva 2 (Switzerland).

Torres, O., Tanskanen, A., Veihelmann, B., Ahn, C., Braak, R., Bhartia, P. K., et al. (2007). Aerosols and surface UV products from Ozone Monitoring Instrument observations: An overview. *Journal of Geophysical Research: Atmospheres (1984–2012), 112*(D24).

Wang, X., Chen, R., Meng, X., Geng, F., Wang, C., & Kan, H. (2013). Associations between fine particle, coarse particle, black carbon and hospital visits in a Chinese city. *Science of the Total Environment, 458*, 1–6.

Chapter 2
Research Background

2.1 Sources of Black Carbon in the Atmosphere

The sources of black carbon (BC) in the atmosphere include wildfires, volcanoes eruption, energy-related combustion of fossil fuels and biofuels and some industrial activities (Penner et al. 1993; Streets et al. 2001; Bond et al. 2004). For the present-day, over two thirds of BC emissions are coming from anthropogenic sources due to a rapid increase of fossil fuel and biofuel consumptions by industry and by domestic activities (Bond et al. 2004). In addition, some natural processes also produce BC to the atmosphere, in particular from forest fires and savanna fires (Andreae and Merlet 2001). Based on past emission inventories of BC (Turco et al. 1983; Penner et al. 1993; Cooke and Wilson 1996; Liousse et al. 1996; Andreae and Merlet 2001; Novakov et al. 2003; Bond et al. 2004, 2007; Ito and Penner 2005; Dentener et al. 2006; Junker and Liousse 2008; Zhang et al. 2009; Lamarque et al. 2010; Granier et al. 2011; Lu et al. 2011; Diehl et al. 2012), the major emission sources of BC in the atmosphere include: (1) combustion of carbon-based fuels, including coal, oil, natural gas, crop residues and fuel wood by power plants, industrial sector, transportation and residential sector; (2) coke production, including the refining processes, the gas heating and the leakage processes; (3) brick production, including the material conveying processes, the product drying and fuel firing processes; (4) waste incineration, including combustion of municipal and industrial waste; (5) outdoor biomass burning, including the natural fires (forests fires, grassland fires, woodland fires and peat fires) and human-induced fires (deforestation and open burning of agricultural waste in the field). Previous studies show that domestic heating, residential cooking, on-road diesel vehicles, coke and brick production, and wildfires are the most important emission sources of BC in the atmosphere.

R. Wang, *Global Emission Inventory and Atmospheric Transport of Black Carbon*,
Springer Theses, DOI 10.1007/978-3-662-46479-3_2

2.2 Climate Effects of Black Carbon

BC can strongly absorb incoming solar light in both visible and near-infrared spectra, and its absorption per mass is tens of times of that for carbon dioxide, the well-known greenhouse gas. In addition to BC, there are some other light-absorbing species in aerosols, such as dust and non-soot organic carbon (e.g. brown carbon), but the absorption ability by any of them is much weaker in comparison to BC. The mass absorption cross section is an efficient index to evaluate the light absorbing ability of aerosols. For freshly generated BC, the mass absorption cross section is 7.5 ± 1.2 m^2 g^{-1} at 550 nm (Bond et al. 2013), and the mass absorption cross section will be enhance significantly when the emitted BC is mixed with other scattering matter (e.g. sulfate or nitrate). In comparison, the mass absorption cross section is less than 1 m^2 g^{-1} at 550 nm for non-soot organic carbon, and about 0.01 m^2 g^{-1} at 550 nm for dust (Clarke et al. 2004). As a result, due to its strong ability in absorbing light, BC is the most concerned particulate species heating the atmosphere in the Earth climate system (Stocker et al. 2013).

The impact of aerosols on the radiation budget of the Earth system has been studied for half a century. McCormick and Ludwig (1967) pointed out, for the first time, that atmospheric aerosols could cool the earth by increasing the planetary albedo. Charlson and Pilat (1969) then argued that the effect of aerosols on the radiation depends on both the size distribution of the particles and the scattering and absorption cross sections. The light-scattering components may lead to a cooling effect while the light-absorbing components may lead to a warming effect. Haywood and Shine (1995) derived the first estimate of the radiative forcing of BC at top-of-atmosphere ($+0.04$ to $+0.18$ W m^{-2}), by applying a constant specific extinction coefficient of 6.4 m^2 g^{-1} at 700 nm for BC. This estimate was subsequently adopted in the Second Assessment Report of Intergovernmental Panel on Climate Change (Houghton 1996). However, a complete estimation of the radiative forcing of BC calls for a quantitative understanding of the mixing state of BC in aerosols, because the optical properties of BC are very different when it exists distinctly from other aerosol species or becomes well mixed with them. Haywood and Shine highlight the important of considering the degree of external and internal mixing state of BC to obtain a definite description of the optical properties of BC (Haywood and Shine 1995). Haywood et al. (1997) then investigated the radiative effects of BC under different relative humidities, chemical compositions of particles, and internal and external mixing states of BC and sulfate. As a result, a larger direct radiative forcing of BC was derived, ranging from $+0.20$ to $+0.36$ W m^{-2}, which corresponds to an external and internal mixture, respectively. Almost at the same time, Myhre et al. derived an estimate of $+0.16$ W m^{-2} for BC in an external mixture, and $+0.42$ W m^{-2} in an internal mixture with a three-dimensional chemistry-transport-model and a multistream radiative transfer code (Myhre et al. 1998). Penner et al. (1998) gave a comparable estimate of $+0.20$ W m^{-2} for fossil fuel BC alone, and of $+0.16$ W m^{-2} for the fossil fuel BC and OC together in a general circulation model coupled with a chemistry

model. Jacobson (2001) simulated the evolution of the chemical composition of aerosols explicitly and estimated a positive radiative forcing of BC as high as +0.55 W m^{-2}, listing BC as the second most important component of global warming after carbon dioxide. Recently, to understand the differences in describing the chemical and physical states of aerosols in different models, a model intercomparison study was initialized under the framework of AeroCom (Aerosol Comparisons between Observations and Models) (http://nansen.ipsl.jussieu.fr/AEROCOM/). According to the AeroCom Phase-I study, a model-averaged estimate of radiative forcing of BC was +0.34 W m^{-2} for BC from fossil fuels, biofuels and biomass burning (Schulz et al. 2006), which was adopted in the coming Fourth Assessment Report of Intergovernmental Panel on Climate Change (Solomon et al. 2007). According to the AeroCom Phase-II study, the RF of BC was revised downward to +0.18 W m^{-2} for BC from fossil fuels and biofuels, and +0.00 W m^{-2} for OC and BC from biomass burning (Myhre et al. 2013), but with large uncertainties due to large discrepancies between model and observations.

In addition to the bottom-up estimates, there are also many studies using the top-down approach to estimate the radiative forcing of BC using observed light absorption by aerosols. The Aerosol Robotic Network (AERONET) provided a global network of automatic sun and sky scanning radiometers for aerosol at over 500 sites worldwide (Holben et al. 1998; Dubovik et al. 2000, 2002). Sato et al. (2003) derived the first top-down estimate of BC RF at about ~1 W m^{-2}, regardless of whether it is internally or externally mixed, based on the aerosol absorption optical depths observed by AERONET. In that study, Sato et al. compared the aerosol absorption simulated by two atmospheric transport models developed in (Koch 2001; Chin et al. 2002), yielding a scale factor that was used to optimize the BC climatologies to achieve the best agreement with AERONET observations. Chung et al. (2005) further improved the top-down estimate by integrating satellite and ground-based observations with the models of aerosol chemistry, transport, and radiative transfer. The global aerosol optical depths observed by satellite are optimized by data from ground-based network AERONET, and then used together to reconcile the BC climatologies generated by an global chemical-transport model. As a result, it yielded an annual mean radiative forcing of BC of +0.9 W m^{-2} at the top of atmosphere, which was adopted in a review study (Ramanathan and Carmichael 2008). Further, Bond et al. (2013) used the aerosol absorption optical depths retrieved from the AERONET network to constrain the absorption optical depths due to BC and thus the radiative forcing simulated by 8 AeroCom Phase-I models. As a result, Bond et al. estimated the observation-constrained radiative forcing of BC to be +0.71 W m^{-2}, with a very wide uncertainty from +0.08 to +1.29 W m^{-2} due to large discrepancies between model and observations (Bond et al. 2013). Finally, the latest Fifth Assessment Report of Intergovernmental Panel on Climate Change adopted a central radiative forcing of BC from the bottom-up and top-down approaches, resulting a radiative forcing of +0.4 W m^{-2}, with an 90 % uncertainty range from +0.05 to +0.8 W m^{-2}, for BC from fossil fuels and biofuels (Stocker et al. 2013). The sources of errors in the estimations, including the emissions, the transport errors, and the optical properties of BC, should be better understood to reduce the uncertainty.

In addition to the direct radiative effect due to light absorption, BC can also interact with clouds by altering the thermal structure of clouds, changing the number concentrations and size distributions of liquid cloud droplets, changing the lifetime of clouds, and changing the number of ice particles in clouds. Clouds cover roughly two thirds of the area of earth, and play an important role in the radiation budget of the atmosphere. By enhancing the planetary albedo, the global mean radiative effect of cloud at the top of atmosphere is $+29.5$ W m^{-2} in the longwave and -46.6 W m^{-2} in the shortwave, with a net radiative effect of -17.1 W m^{-2} (Loeb et al. 2009). As a result, there is an additional radiative effect of BC when it is interacting with clouds in the atmosphere. According to a recent study, the central estimate of the BC semi-direct effect is -0.1 W m^{-2} as an industrial-era radiative forcing, with a wide uncertainty from -0.44 to $+0.1$ W m^{-2} as the 90 % uncertainty range (Bond et al. 2013). In particular, the indirect radiative forcing of BC was estimated to be -0.1 W m^{-2} by changing the number concentrations of liquid cloud droplets, $+0.2$ W m^{-2} by changing the thermal structure of clouds, $+0.2$ W m^{-2} by acting as an ice nuclei and increasing the ice fall-out (Bond et al. 2013). It should be noted these estimates all involve high uncertainties, due to a large variability in both the simulations of aerosols and clouds (Bond et al. 2013; Carslaw et al. 2013), which needs more studies in the future. At last, BC deposited over the surface of ice and snow changes the surface albedo and decreases the reflection of light (Wiscombe and Warren 1980; Podgorny and Grenfell 1996). According to the estimations by Hansen and Nazarenko (2004) and Jacobson (2004), this effect is responsible for a indirect radiative forcing of $+0.10 \pm 0.10$ W m^{-2}, and adopted as $+0.04$ ($+0.02$ to $+0.09$) W m^{-2} in the lastest Fifth Assessment Report of Intergovernmental Panel on Climate Change (Stocker et al. 2013).

In summary, BC can impact on the Earth climate system by absorbing solar light in the atmosphere, interacting with clouds, and changing the surface albedo after deposition over the surface of snow or ice. According to a systematic assessment, the total radiative forcing of BC is $+1.1$ W m^{-2} (Bond et al. 2013), which is 59 % of that from carbon dioxide (Stocker et al. 2013). However, this estimate is associated with a wide uncertainty range (90 % confidence interval from $+0.17$ to $+2.1$ W m^{-2}). Parameters in the estimations are very uncertain, such as the emission inventory, the transport model, the optical properties of BC, and the radiative transfer scheme used in the model, which have not been well understood yet (Stier et al. 2013). Improving the emission inventory of BC and reducing the discrepancies between model and observations are the major targets in this thesis.

2.3 Health Effects of Black Carbon

The health effects of BC have not been studied as much as its climate impact (Anenberg et al. 2011), because it is very hard to separate the individual health effects induced by BC from other components in air particles (Wilkinson et al. 2009; Janssen et al. 2011, 2012). As already recognized, BC can cause adverse

effects on human health as an important component of fine particles, which can be inhaled into human bodies (Saikawa et al. 2009; Anenberg et al. 2011, 2012; Shindell et al. 2012). The adverse effects of fine particles on human health have been well documented. It's evidenced that long-term or short-term exposure to fine particles can lead to a significant increase of the cardiovascular and respiratory diseases and the premature mortality (Dockery et al. 1993; Laden et al. 2000; Katsouyanni et al. 2001; Pope III et al. 2002; Roemer and van Wijnen 2002; Englert 2004; Morgenstern et al. 2007; Ostro et al. 2007; Sarnat et al. 2008). The super-fine particles like $PM_{2.5}$ (particles less than 2.5 μm in diameter) and $PM_{1.0}$ (particles less than 10.0 μm in diameter) are found to be more associated with the human health that total particulate matter (Dockery et al. 1993; Delfino et al. 1997, 2005; Goss et al. 2004; Kim et al. 2004; Dominici et al. 2006; Lipfert et al. 2006; Chimonas and Gessner 2007; Miller et al. 2007; Woodruff et al. 2008; Krewski et al. 2009; Pope III et al. 2009). However, the individual health effects of BC are yet not well understood. It is still not clear if the toxicity of various PM components is different and if the individual effects for each species can be differentiated, which needs more studies by epidemiologists and toxicologists.

As BC is rarely measured in field sampling studies, some studies try to link the measured concentration of black smoke with the health outcomes, since BC and black smoke are strongly correlated (Janssen et al. 2011). Hoek et al. (2002) have collected data on daily mortality and air pollutants measured from 1986 to 1994 in Netherlands, including black smoke. They found that sulphate, nitrate and black smoke are more associated with total mortality than for PM_{10}. Similarly, Filleul et al. (2006) have investigated the health effects of air pollutants (sulphur dioxide, total suspended particles, black smoke, nitrogen dioxide, and nitric oxide) on chronic respiratory diseases in the Pollution Atmosphe´rique et Affections Respiratoires Chroniques/Air pollution and chronic respiratory diseases survey within 24 districts of seven towns for a period of 1975–1976 in France. They found, after adjusting for age, sex, body mass index, educational level, smoking habits, and occupational exposure, the total suspended particles, black smoke, nitrogen dioxide, and nitric oxide are all significantly associated with non-accidental mortality. The relative risk associated with an increase of black-smoke concentration by 10 $\mu g\ m^{-3}$ is 1.14 (1.03–1.25 as 95 % confidence intervals).

Smith et al. (2010) have reviewed the health effects of three short-lived greenhouse pollutants (BC, ozone and sulphate) via a meta-analyses of existing time-series studies and an analysis of a cohort of 352,000 people in 66 U.S.A. cities during a 18-year follow-up study. As a result, they found the toxicology of BC and sulphate existing in pure form cannot be identified statistically while their health effects are associated with other aerosol species. It is concluded that the health effects of BC and sulphate should be interpreted as representing mixtures rather than independent forms. In addition, the U.S.A. cohort study shows a stronger effect for elemental carbon (very close to BC) on the mortality than fine particles. However, the results are not robust when also including other air pollutants in the model. As a result, it's yet very hard to assess the differential effects of different aerosol components on mortality and identify the individual health effect of BC from the long-term cohort study.

Extremely high concentrations of BC are always found in the Asian developing countries, in particular for China and India (Anenberg et al. 2011). However, there are few studies that examine the health effects of BC in these developing regions. Lin et al. (2011) have examined the association between the acute respiratory inflammation in school children and the concentrations of BC and $PM_{2.5}$ in ambient air before and during the 2008 Beijing Olympic Games. In that study, the relative importance of BC and $PM_{2.5}$ was assessed by a two-pollutant model. As a result, the exhaled nitric oxide, as an acute respiratory inflammation biomarker, has increased by 16.6 % (95 % confidence interval, 14.1–19.2 %) and 18.7 (15.0–22.5 %) per interquartile range increase of the concentration of BC (4.0 $\mu g\ m^{-3}$) and $PM_{2.5}$ (149 $\mu g\ m^{-3}$). Moreover, the health effect of BC is robust in the two-pollutant model, while the relationship between $PM_{2.5}$ and exhaled nitric oxide would decrease when the model was adjusted for BC. Geng et al. (2013) have investigated the association between the total and cause-specific mortality and the exposure concentrations of BC and $PM_{2.5}$ in Shanghai, China. It's found that an interquartile range increase in the concentration of BC (2.7 $\mu g\ m^{-3}$) corresponds to a 2.3 % (95 % confidence interval, 0.6–4.1 %), 3.2 % (0.6–5.7 %), and 0.6 % (−4.5 to 5.7 %) increase in total, cardiovascular and respiratory mortality, respectively. When adjusted for $PM_{2.5}$, the effect of BC on mortality is robust. In comparison, the effect of $PM_{2.5}$ on mortality decreased and became insignificant when the model was adjusted for BC, indicating that BC is a better air quality indicator for the health risks of particulate pollution than $PM_{2.5}$.

It should be noted that epidemiological evidences alone cannot substantiate the toxicity of BC without toxicological studies, even though the exposure of BC is strongly associated with the adverse effects on human health. Frampton et al. (2006) have investigated the vascular effect of elemental carbon ultrafine particles (diameter < 100 nm) on healthy and asthmatic subjects. It's found that the inhalation of elemental carbon ultrafine particles can cause phenotypic alterations in blood leukocytes at a low concentration of 10 $\mu g\ m^{-3}$ or 2×10^6 particles cm^{-3}. Routledge et al. (2006) examined the effects of controlled concentrations of carbon particles on the inflammatory and autonomic responses of healthy humans and patients with coronary artery disease. Among the healthy volunteers, a short-term exposure to pure carbon particles does not lead to adverse effects on heart rate variability or cause a systematic inflammatory response (Routledge et al. 2006). Sawant et al. (2008) used an idling medium-duty diesel truck to produce diesel exhaust, rich in elemental carbon (close to BC), for controlled human exposure experiments. As a result, there is no significant change in the conventional lung function tests among eleven volunteer subjects after a exposure to diesel exhaust for 2 h (Sawant et al. 2008). Similarly, Biswas et al. (2009) have investigated the oxidative potential of diesel exhausts from motor vehicles and found that there is no measurable changes in oxidative activity due to the exposure. It showed that the oxidative potential is associated with organic carbon, in particular for the water soluble organic carbon, more than any other species in particles (Biswas et al. 2009). Barath et al. (2010) reported that diesel exhaust with a higher soot content may cause an additional effect on vascular smooth muscle. However, Barath et al. also

implies that the effect might be attributed to the organic compounds absorbed on soot, rather than on soot itself (Barath et al. 2010). Mills et al. (2011) compared the in vivo effects of inhalation of dilute diesel exhaust, pure carbon nanoparticulate, filtered diesel exhaust, and filtered clean air. Increased systolic blood pressure and attenuated vasodilatation to bradykinin, acetylcholine, and sodium nitroprusside were noticed for inhalation of diesel exhaust, but not for inhalation of pure carbon nanoparticulate. Therefore, it's suggested that adverse vascular effects of diesel exhaust inhalation is attributable to the soluble and insoluble components on the surface of soot (Mills et al. 2011).

As a conclusion, epidemiological studies show a certain relationship between BC exposure and adverse health effects, while there are insufficient evidences for the toxicity of BC. Some studies indicated that BC is an important carrier of toxic compounds, including volatile carbon matters (e.g. polycyclic aromatic hydrocarbons), heavy metals and water-soluble organics. So far, there is no evidence that the health effects of BC can be identified from other components in air particles. Nevertheless, it's well convinced that BC is a valuable indicator for ambient particulate pollution, especially for developing countries. Estimation of the exposure of BC is important to evaluate the adverse effects on human health caused by ambient particles, and mitigation of BC can effectively reduce the health risks due to air particulate pollution by reducing the co-emissions of many toxic components in particles.

2.4 Emission Inventories of Black Carbon

BC has been recognized as an aerosol component that strongly absorbs solar light (Rosen et al. 1978). Since the 1980s, there are lots of studies estimating the emissions of atmospheric BC, at either regional scale (Streets et al. 2001; Reddy and Venkataraman 2002a, b; Streets et al. 2003; Kupiainen and Klimont 2004; Cao et al. 2006; Ohara et al. 2007; Klimont et al. 2009; Zhang et al. 2009; Lu et al. 2011; Qin and Xie 2012; Kurokawa et al. 2013) or global scale (Turco et al. 1983; Penner et al. 1993; Cooke and Wilson 1996; Liousse et al. 1996; Penner et al. 1998; Novakov et al. 2003; Bond et al. 2004; Ito and Penner 2005; Dentener et al. 2006; Cofala et al. 2007; Junker and Liousse 2008; Lamarque et al. 2010; Granier et al. 2011; Diehl et al. 2012; Bond et al. 2013). These emission inventories provide the input for atmospheric transport models that estimate the contribution of BC to global warming. Over the past decades, continuous efforts have been made to develop the emission inventories of BC by measuring more emission factors for BC and developing new methods to estimate emissions. In the inventories developed via bottom-up approaches, the emission of BC is calculated based on the fuel consumed by a specific emission source and the associated emission factor, which is defined as the mass of BC emitted per fuel consumed or product produced. In need of a large number of data in different sectors, the emission inventories of BC are associated with large uncertainties due to limitation of data, including the fuel consumptions, technology divisions and BC emission factors.

Turco et al. (1983), for the first time, estimated the global BC emissions (2.2–22 Tg/year) from fossil fuels, wood fuels and biomass burning. Penner et al. (1993) adopted two distinct methods to construct the global emissions inventories of BC using the concentration ratios of BC and sulfur dioxide measured at global stations and the published inventories of sulfur, or using BC emissions factors and fuel consumptions. Penner et al. found that the difference between the two estimates is less than a factor of two (Penner et al. 1993). Cooke and Wilson (1996) constructed a global BC inventory from fossil fuel combustion and biomass burning, and the modelled BC concentrations based on the constructed emission inventory compared within a factor of two against the observed concentrations over continental regions. Cooke et al. (1999) have further improved the BC emission inventory from fossil fuels by discriminating the emission factors among different types of countries and combustion processes, generating an emission inventory at a resolution of $1° \times 1°$. Meantime, Streets et al. focused on BC emissions in Asia, by paying particular attention to BC emission factors for China (Streets et al. 2001, 2003). Streets et al. also revealed that the uncertainty of the estimated BC emission is approximately a factor of eight, mainly due to the variability of BC emission factors. Bond et al. (2004) developed the first global BC inventory by taking into detailed consideration of the variation of BC emission factors by fuel type, combustion process, and control technology. This method has been widely used in the following bottom-up emission inventories (Dentener et al. 2006; Bond et al. 2007; Zhang et al. 2009; Lamarque et al. 2010; Granier et al. 2011; Lu et al. 2011).

Novakov et al. (2003) made the first attempt to estimate BC emission back to the 19th century. According to that study, the global fossil-fuel BC emissions increased rapidly in the latter half of 1800s, leveled off in the first half of the 1900s, and got re-accelerated again in the latter half of the 1900s. This study indicates that it is necessary to take the historical trend of BC into consideration when analyzing the temporal evolution of climate. Subsequently, Ito and Penner (2005) have estimated BC emissions from biomass burning and fossil fuels for a period from 1870 to 2000 by inversing the open vegetation inventories from observations, implying the importance of realistically representing emissions of aerosols from biomass burning in climate simulations. By extending the technology-based method developed in (Bond et al. 2004), Bond et al. (2007) constructed the historic BC emissions from all energy-related sources for a period from 1850 to 2000. The methodology used by Bond et al. (2007) had been adopted to generate a historical gridded BC inventory (Lamarque et al. 2010; Granier et al. 2011; Diehl et al. 2012), which was used as inputs driving the climate simulations used in the Climate Model Intercomparison Program #5 (CMIP5) in support of the fifth Assessment Report of Intergovernmental Panel on Climate Change (Stocker et al. 2013).

The estimated BC emissions vary greatly due to large variability of input parameters. Table 2.1 compares the BC emissions estimated by different inventories. It shows that the variation of global and regional BC emissions is large among different inventories. The estimated global BC emission ranges from 4500 to 12,600 Gg/year. For China, which contributes approximately 25 % to the global total BC emission, there is a range of 1000–1700 Gg/year for the estimated

Table 2.1 Comparison of BC emission estimations by different inventories

Emission inventories	Scale	Year	Emissions (Gg/year)
Penner et al. (1993)	Global	1980	12,600
Cooke et al. (1999), Liousse et al. (1996)	Global	1984	6100
Ito and Penner (2005)	Global	2000	4800
Junker and Liousse (2008)	Global	1997	4800
SPEW (Bond et al. 2007)	Global	2000	4530
GAINS (Cofala et al. 2007)	Global	2000	4700
Streets et al. (2003)	China	2000	1000
Cao et al. (2006)	China	2000	1500
Zhang et al. (2009)	China	2006	1800
Klimont et al. (2009)	China	2000	1200
Lu et al. (2011)	China	2000	1200
GAINS (Cofala et al. 2007)	China	2000	1100
SPEW (Bond et al. 2007)	China	2000	1200
Reddy and Venkataraman (2002a, b)	India	1997	400
Ohara et al. (2007)	India	2000	800
Streets et al. (2003)	India	2000	600
Klimont et al. (2009)	India	2000	750
Lu et al. (2011)	India	2000	680
GAINS (Cofala et al. 2007)	India	2000	580
SPEW (Bond et al. 2007)	India	2000	500
Reff et al. (2009)	U.S.A.	2000	440
SPEW (Bond et al. 2007)	U.S.A.	2000	350
GAINS (Cofala et al. 2007)	U.S.A.	2000	260

BC emission. In addition to the change of fuel consumption for different years, the difference is mainly attributable to variability of BC emission factors, methods used to consider the technology divisions, and sources of data used for fuel consumptions. It should be noted that the emissions listed in Table 2.1 are corresponding to the central estimates by different inventories, and the uncertainty within each inventory should be large (Streets et al. 2001; Bond et al. 2004; Zhang et al. 2007a, 2009; Lu et al. 2011). Reviewing the input data used by different inventories, analyzing the difference in methodologies, and understanding the uncertainties of technologies are essential to improve the reliability of the emission inventory and reduce the uncertainties in BC emissions.

There are several factors contributing to uncertainties in the emission inventories of BC. Variation in the BC emission factors, which often ranges up to several orders of magnitude, has been regarded as the major contributor to uncertainties in the emission inventory. BC emission factors, defined as the amount of BC emitted per fuel consumed or product produced, are derived by *in-lab* or in situ measurements. BC emission factors are highly dependent on the condition of combustion, the methods of sampling and the method of sample analysis. For instance,

the BC emission factors for industrial coal boilers can be influenced by many factors, including the boiler type, the boiler age, the coal property and the operation condition (Ge et al. 2001; Bond et al. 2004; Kupiainen and Klimont 2004). As a result, due to the variation of the technologies and emission standards, BC emission factors for industrial coal boilers differ by country and year (Bond et al. 2007; Junker and Liousse 2008). Unfortunately, the BC emission factors of industrial boilers burning coal are mainly measured in several developed countries and thus applying these measurements for developing countries may lead to underestimation of the BC emission factors for the industrial boilers equipped with poor emission abatement facilities (Penner et al. 1993; Cooke and Wilson 1996). Similarly, the BC emission factors for motor vehicles reported in the literature varied over 4 orders of magnitude (Wang et al. 2012) due to many factors including vehicle type, fuel composition, vehicle model year, marketing country, operation mode, ambient temperature, analytical method. Adoption of any single statistics of these values for global emission estimation should lead to large uncertainties (Bond et al. 2004; Kupiainen and Klimont 2004). In addition, since the majority of BC emission factors were measured in developed countries, it is very likely that the application of these measurements to other countries can cause prediction bias. Development and application of a quantitative emission model for characterizing major factors affecting the BC emission factors for specific emission activities is the effective way to downscale these uncertainties.

In addition, the *in-lab* or in situ measurements of the BC emission factors are also influenced greatly by the analyzing methods. There are three methods widely used to analyze the mass of BC in samples. The first one is the optical method, which is based on the light absorption of BC. However, this method can be largely biased when the variability of the mixing state of aerosol samples is uncertain (Reid et al. 1998). The second one is the thermal method, which is based on the different volatility of element carbon and organic carbon. In this method, the sample is heated to volatilize organic carbon and then heated again with sufficient oxygen to volatilize element carbon, which is regarded to be equivalent to BC (Bond et al. 1999; Chow et al. 2001). The last method is using laser-induced incandescence, namely the refractory BC. In this method, refractory BC is heated to the vaporization temperature and then detected using an infrared intra-cavity laser (Schwarz et al. 2006). However, most of the BC emission factors are measured using the thermal method in terms of early studies, which are applied in most emission inventories. It should be noted that the difference of BC emission factors measured by different methods is very large. For example, in the diesel exhaust, the measured BC emission factors using the thermal and optical methods differ significantly that BC emission factors measured using the thermal method is only 60 % of that using the optical method (Kim Oanh et al. 2010). More studies comparing the BC emission factors by different methods can reduce this uncertainty.

Due to the large variation of BC emission factors under different technologies, it's necessary to identify the fraction of fuel under each combustion technology in the development of emission inventories (Bond et al. 2004). However, information on technology divisions are always very limited, particularly for certain

sectors in developing countries in lack of systematic records. For example, large differences of BC emission factors are observed in coal combustion in residential stoves, depending on the coal species and the technology of combustion (Chen et al. 2005, 2006; Zhang et al. 2008; Zhi et al. 2008; Chen et al. 2009). Zhi et al. (2008) reported that the emission factors of BC measured for raw coal chunk burned in high-efficiency chunk stoves could be 46 times of that for honeycomb coal briquette burned in high-efficiency briquette stoves. As an important emission source of BC, however, the ratio of raw coal chunk burned in high-efficiency chunk stoves and honeycomb coal briquette burned in high-efficiency briquette stoves is very uncertain in China. The International Energy Agency statistics and the China Energy Statistical Yearbook both reported very small portion of coal used as briquette (less than 10 %) (National Bureau of Statistics and National Energy Administration 2009; International Energy Agency 2010a, b), but coal briquettes are widely used in the residential sector in China. As a result, it leads to a high uncertainty when applying a uniform BC emission factor for all residential coal over all regions in China (Zhang et al. 2009). Moreover, for some industrial processes, like the production of coke and brick, limited data are available for the distribution of different technologies, such as beehive and battery coke ovens. Reducing this uncertainty needs more data to be released.

At last, the fuel consumption data used to estimate emissions are also associated with a high uncertainty. Akimoto et al. (2006) compared the coal consumption data in China during 1996–2003 among three different official energy statistics: the province-by-province statistic from the China Energy Statistics Yearbook (National Bureau of Statistics and National Energy Administration 2009), the country-total statistic from the China Energy Statistics Yearbook (National Bureau of Statistics and National Energy Administration 2009), and the energy balance tables by International Energy Agency statistics (International Energy Agency 2010b). As a result, there are significant differences in the data between province-by-province statistic from the China Energy Statistics Yearbook and the International Energy Agency statistics since 1997, and the discrepancy is larger than 10 % after 1999 (Akimoto et al. 2006). Meanwhile, the amount of coal consumption given by country-total statistic from the China Energy Statistics Yearbook doesn't agree with either of the another two statistics, and the number in country-total statistic from the China Energy Statistics Yearbook is lower. The disagreement of data between the country-total and province-by-province statistic in the China Energy Statistics Yearbook is even larger than 30 % during 1999–2001, and larger than 20 % in 2003. Thus, a simple application of the Chinese fuel consumption data from the country-total statistic from the China Energy Statistics Yearbook or the International Energy Agency statistics could lead to a significant underestimation of BC emissions when developing the inventory (Ohara et al. 2007). Guan et al. (2012) have further studied these discrepancies between the two sets of fuel consumption data in China compiled in the China Energy Statistics Yearbook by the agency of the National Bureau of Statistics. They found that the discrepancy of calculated CO_2 emissions using the two official energy data sets can reach 10 % in 2003 and 18 % in 2010. More than 70 % of the discrepancy

is originated from the statistics for coal consumption, while that for petroleum, natural gas, and other fuels contribute 12, 2, and 14 %, respectively. In fact, the energy statistics in the consumption of biofuels like wood and crop residue fuels are also particularly uncertain (Bond et al. 2004), and there is a lack of a quantitative assessment of these uncertainties.

In addition to the facts above, there are other factors contributing to the uncertainty in the bottom-up emission inventory, such as the spatial allocation of emissions to grids. Gridded BC emissions are needed by the atmospheric model to simulate the climate and health effects of BC, and spatial allocation of BC emissions can influence the spatial pattern of BC concentrations. Emission inventories in administrative units (countries, provinces) are always geo-referenced into gridded maps using the spatial distribution of population as a proxy (Andres et al. 1996; Bond et al. 2004; Lamarque et al. 2010). This method, however, can create a large spatial bias if the per capita emission is not uniform in space (Zhang et al. 2007b; Gurney et al. 2009). According to these studies (Zhang et al. 2007b; Gurney et al. 2009), using sub-national fuel data to estimate the fuel consumptions and emissions at a fine spatial resolution can reduce this uncertainty.

2.5 Health Assessments of Black Carbon

It has been recognized that emissions of the short-lived greenhouse pollutants should be mitigated in addition to regulating the carbon dioxide emissions, since the short-lived greenhouse pollutants are making a substantial contribution to global warming while causing significant damages to human health (Smith et al. 2010). Among all short-lived greenhouse pollutants, BC and ozone are most concerned, and BC draws more focus due to the its great climate effect with a high radiative forcing, which is recently reported to be second to carbon dioxide (Ramanathan and Carmichael 2008; Bond et al. 2013). The measures targeted at mitigating BC emissions can produce a significant "win-win" benefit for both near-term climate change and regional air pollution (Shindell et al. 2012).

Saikawa et al. (2009) have made a first attempt to estimate the contribution of aerosols emitted from China to global annual premature mortality and radiative forcing in 2000 and 2030 using a global chemical transport model. They found that mitigation of anthropogenic BC, organic carbon, and sulfur dioxide in China can avoid a premature death of 480 and 30 thousands in and outside of China, respectively, in 2030. Based on a global chemical transport model (MOZART-4), Anenberg et al. (2011) have investigated the effects on the surface concentrations of $PM_{2.5}$ and the premature mortality by halving anthropogenic BC emissions globally and regionally. As a result, when global anthropogenic BC emissions are halved, the global outdoor population-weighted average concentration of $PM_{2.5}$ can be reduced by 542 ng m^{-3}. Due to a lower exposure concentration of $PM_{2.5}$, an annual total premature death of 157,000 (95 % confidence interval, 120,000–194,000) can be avoided. It should be noted that these results are very sensitive to the choice

of the concentration-response factor and the health effect thresholds, which are associated with high uncertainties.

In a recent study, Shindell et al. (2012) have conducted a comprehensive study of the climate and health benefits by measures reducing the emissions of methane and BC. As a result, the health benefits from BC measures are much larger than those from the CH_4 measures, and it is due to the fact that the health effect is more sensitive to the exposure to $PM_{2.5}$ than to surface ozone. It's estimated that a total of 0.7–4.7 million premature deaths can be avoided in 2030 by all climate mitigation measures, which is comparable to other causes of premature death, such as tuberculosis, traffic accidents, or tobacco use. In addition, it is predicted that these measures can avoid another 373,000 premature deaths by improving the indoor air quality. As a conclusion, the BC measures are likely to produce substantial climate benefits and result in a large regional human health benefit, making these measures distinct from and complementary to the expensive measures targeted at controlling carbon dioxide emissions.

However, the three global assessments of the health impact of BC (Saikawa et al. 2009; Anenberg et al. 2011; Shindell et al. 2012) are all obtained by assuming that BC can be regarded as a species in aerosols that has the same health effect as other components. Up to now, there are no studies which assessed the individual health effects of BC by discriminating the effects of BC from other aerosol components. An assessment of the exposure of BC alone is urgently important once the concentration-response relationship become available for BC (Janssen et al. 2011).

References

Akimoto, H., Ohara, T., Kurokawa, J.-I., & Horii, N. (2006). Verification of energy consumption in China during 1996–2003 by using satellite observational data. *Atmospheric Environment, 40*(40), 7663–7667.

Andreae, M. O., & Merlet, P. (2001). Emission of trace gases and aerosols from biomass burning. *Global Biogeochemical Cycles, 15*(4), 955–966.

Andres, R. J., Marland, G., Fung, I., & Matthews, E. (1996). A 1 × 1 distribution of carbon dioxide emissions from fossil fuel consumption and cement manufacture, 1950–1990. *Global Biogeochemical Cycles, 10*(3), 419–429.

Anenberg, S., Talgo, K., Arunachalam, S., Dolwick, P., Jang, C., & West, J. (2011). Impacts of global, regional, and sectoral black carbon emission reductions on surface air quality and human mortality. *Atmospheric Chemistry and Physics, 11*(14), 7253–7267.

Anenberg, S. C., Schwartz, J., Vignati, E., Emberson, L., Muller, N. Z., West, J. J., et al. (2012). Global air quality and health co-benefits of mitigating near-term climate change through methane and black carbon emission controls. *Environmental Health Perspectives*, 831–839. doi:10.1289/ehp.1104301.

Barath, S., Mills, N. L., Lundbäck, M., Törnqvist, H., Lucking, A. J., Langrish, J. P., et al. (2010). Impaired vascular function after exposure to diesel exhaust generated at urban transient running conditions. *Particle and Fibre Toxicology, 7*, 19.

Biswas, S., Verma, V., Schauer, J. J., Cassee, F. R., Cho, A. K., & Sioutas, C. (2009). Oxidative potential of semi-volatile and non volatile particulate matter (PM) from heavy-duty vehicles retrofitted with emission control technologies. *Environmental Science and Technology, 43*(10), 3905–3912.

Bond, T. C., Anderson, T. L., & Campbell, D. (1999). Calibration and intercomparison of filter-based measurements of visible light absorption by aerosols. *Aerosol Science and Technology, 30*(6), 582–600.

Bond, T. C., Streets, D. G., Yarber, K. F., Nelson, S. M., Woo, J. H., & Klimont, Z. (2004). A technology-based global inventory of black and organic carbon emissions from combustion. *Journal of Geophysical Research: Atmospheres (1984–2012), 109*(D14), 1–43.

Bond, T. C., Bhardwaj, E., Dong, R., Jogani, R., Jung, S., Roden, C., et al. (2007). Historical emissions of black and organic carbon aerosol from energy-related combustion, 1850–2000. *Global Biogeochemical Cycles, 21*(2). doi:10.1029/2006GB002840.

Bond, T. C., Doherty, S. J., Fahey, D., Forster, P., Berntsen, T., DeAngelo, B., et al. (2013). Bounding the role of black carbon in the climate system: A scientific assessment. *Journal of Geophysical Research: Atmospheres, 118*(11), 5380–5552.

Cao, G., Zhang, X., & Zheng, F. (2006). Inventory of black carbon and organic carbon emissions from China. *Atmospheric Environment, 40*(34), 6516–6527.

Carslaw, K., Lee, L., Reddington, C., Pringle, K., Rap, A., Forster, P., et al. (2013). Large contribution of natural aerosols to uncertainty in indirect forcing. *Nature, 503*(7474), 67–71.

Charlson, R., & Pilat, M. (1969). Climate: The influence of aerosols. *Journal of Applied Meteorology, 8*(6), 1001–1002.

Chen, Y., Sheng, G., Bi, X., Feng, Y., Mai, B., & Fu, J. (2005). Emission factors for carbonaceous particles and polycyclic aromatic hydrocarbons from residential coal combustion in China. *Environmental Science and Technology, 39*(6), 1861–1867.

Chen, Y., Zhi, G., Feng, Y., Fu, J., Feng, J., Sheng, G., et al. (2006). Measurements of emission factors for primary carbonaceous particles from residential raw-coal combustion in China. *Geophysical Research Letters, 33*(20).

Chen, Y., Zhi, G., Feng, Y., Liu, D., Zhang, G., Li, J., et al. (2009). Measurements of black and organic carbon emission factors for household coal combustion in China: Implication for emission reduction. *Environmental Science and Technology, 43*(24), 9495–9500.

Chimonas, M.-A. R., & Gessner, D. B. (2007). Airborne particulate matter from primarily geologic, non-industrial sources at levels below National Ambient Air Quality Standards is associated with outpatient visits for asthma and quick-relief medication prescriptions among children less than 20 years old enrolled in Medicaid in Anchorage, Alaska. *Environmental Research, 103*(3), 397–404.

Chin, M., Ginoux, P., Kinne, S., Torres, O., Holben, B. N., Duncan, B. N., et al. (2002). Tropospheric aerosol optical thickness from the GOCART model and comparisons with satellite and Sun photometer measurements. *Journal of the Atmospheric Sciences, 59*(3), 461–483.

Chow, J. C., Watson, J. G., Crow, D., Lowenthal, D. H., & Merrifield, T. (2001). Comparison of IMPROVE and NIOSH carbon measurements. *Aerosol Science and Technology, 34*(1), 23–34.

Chung, C. E., Ramanathan, V., Kim, D., & Podgorny, I. (2005). Global anthropogenic aerosol direct forcing derived from satellite and ground-based observations. *Journal of Geophysical Research: Atmospheres (1984–2012), 110*(D24).

Clarke, A., Shinozuka, Y., Kapustin, V., Howell, S., Huebert, B., Doherty, S., et al. (2004). Size distributions and mixtures of dust and black carbon aerosol in Asian outflow: Physiochemistry and optical properties. *Journal of Geophysical Research: Atmospheres (1984–2012), 109*(D15).

Cofala, J., Amann, M., Klimont, Z., Kupiainen, K., & Höglund-Isaksson, L. (2007). Scenarios of global anthropogenic emissions of air pollutants and methane until 2030. *Atmospheric Environment, 41*(38), 8486–8499.

Cooke, W., Liousse, C., Cachier, H., & Feichter, J. (1999). Construction of a 1 × 1 fossil fuel emission data set for carbonaceous aerosol and implementation and radiative impact in the ECHAM4 model. *Journal of Geophysical Research: Atmospheres (1984–2012), 104*(D18), 22137–22162.

Cooke, W. F., & Wilson, J. J. (1996). A global black carbon aerosol model. *Journal of Geophysical Research: Atmospheres (1984–2012), 101*(D14), 19395–19409.

Delfino, R. J., Sioutas, C., & Malik, S. (2005). Potential role of ultrafine particles in associations between airborne particle mass and cardiovascular health. *Environmental Health Perspectives*, 113, 934–946.

Delfino, R. J., Murphy-Moulton, A. M., Burnett, R. T., Brook, J. R., & Becklake, M. R. (1997). Effects of air pollution on emergency room visits for respiratory illnesses in Montreal, Quebec. *American Journal of Respiratory and Critical Care Medicine, 155*(2), 568–576.

Dentener, F., Kinne, S., Bond, T., Boucher, O., Cofala, J., Generoso, S., et al. (2006). Emissions of primary aerosol and precursor gases in the years 2000 and 1750 prescribed data-sets for AeroCom. *Atmospheric Chemistry and Physics, 6*(12), 4321–4344.

Diehl, T., Heil, A., Chin, M., Pan, X., Streets, D., Schultz, M., et al. (2012). Anthropogenic, biomass burning, and volcanic emissions of black carbon, organic carbon, and SO2 from 1980 to 2010 for hindcast model experiments. *Atmospheric Chemistry and Physics Discussions, 12*(9), 24895–24954.

Dockery, D. W., Pope, C. A., Xu, X., Spengler, J. D., Ware, J. H., Fay, M. E., et al. (1993). An association between air pollution and mortality in six US cities. *New England Journal of Medicine, 329*(24), 1753–1759.

Dominici, F., Peng, R. D., Bell, M. L., Pham, L., McDermott, A., Zeger, S. L., et al. (2006). Fine particulate air pollution and hospital admission for cardiovascular and respiratory diseases. *JAMA, 295*(10), 1127–1134.

Dubovik, O., Smirnov, A., Holben, B., King, M., Kaufman, Y., Eck, T., et al. (2000). Accuracy assessments of aerosol optical properties retrieved from Aerosol Robotic Network (AERONET) Sun and sky radiance measurements. *Journal of Geophysical Research: Atmospheres (1984–2012), 105*(D8), 9791–9806.

Dubovik, O., Holben, B., Eck, T. F., Smirnov, A., Kaufman, Y. J., King, M. D., et al. (2002). Variability of absorption and optical properties of key aerosol types observed in worldwide locations. *Journal of the Atmospheric Sciences, 59*(3), 590–608.

Englert, N. (2004). Fine particles and human health—A review of epidemiological studies. *Toxicology Letters, 149*(1), 235–242.

Filleul, L., Cassadou, S., Médina, S., Fabres, P., Lefranc, A., Eilstein, D., et al. (2006). The relation between temperature, ozone, and mortality in nine French cities during the heat wave of 2003. *Environmental Health Perspectives*, *114*, 1344–1347.

Frampton, M. W., Stewart, J. C., Oberdörster, G., Morrow, P. E., Chalupa, D., Pietropaoli, A. P., et al. (2006). Inhalation of ultrafine particles alters blood leukocyte expression of adhesion molecules in humans. *Environmental Health Perspectives*, *114*, 51–58.

Ge, S., Bai, Z., Liu, W., Zhu, T., Wang, T., Qing, S., et al. (2001). Boiler briquette coal versus raw coal: Part I—Stack gas emissions. *Journal of the Air and Waste Management Association, 51*(4), 524–533.

Geng, F., Hua, J., Mu, Z., Peng, L., Xu, X., Chen, R., et al. (2013). Differentiating the associations of black carbon and fine particle with daily mortality in a Chinese city. *Environmental Research, 120*, 27-32.

Goss, C. H., Newsom, S. A., Schildcrout, J. S., Sheppard, L., & Kaufman, J. D. (2004). Effect of ambient air pollution on pulmonary exacerbations and lung function in cystic fibrosis. *American Journal of Respiratory and Critical Care Medicine, 169*(7), 816–821.

Granier, C., Bessagnet, B., Bond, T., D'Angiola, A., Van Der Gon, H. D., Frost, G. J., et al. (2011). Evolution of anthropogenic and biomass burning emissions of air pollutants at global and regional scales during the 1980–2010 period. *Climatic Change, 109*(1–2), 163–190.

Guan, D., Liu, Z., Geng, Y., Lindner, S., & Hubacek, K. (2012). The gigatonne gap in China's carbon dioxide inventories. *Nature Climate Change, 2*(9), 672–675.

Gurney, K. R., Mendoza, D. L., Zhou, Y., Fischer, M. L., Miller, C. C., Geethakumar, S., et al. (2009). High resolution fossil fuel combustion CO2 emission fluxes for the United States. *Environmental Science and Technology, 43*(14), 5535–5541.

Hansen, J., & Nazarenko, L. (2004). Soot climate forcing via snow and ice albedos. *Proceedings of the National Academy of Sciences of the United States of America, 101*(2), 423–428.

Haywood, J., & Shine, K. (1995). The effect of anthropogenic sulfate and soot aerosol on the clear sky planetary radiation budget. *Geophysical Research Letters, 22*(5), 603–606.

Haywood, J., Roberts, D., Slingo, A., Edwards, J., & Shine, K. (1997). General circulation model calculations of the direct radiative forcing by anthropogenic sulfate and fossil-fuel soot aerosol. *Journal of Climate, 10*(7), 1562–1577.

Hoek, G., Brunekreef, B., Goldbohm, S., Fischer, P., & van den Brandt, P. A. (2002). Association between mortality and indicators of traffic-related air pollution in the Netherlands: A cohort study. *The Lancet, 360*(9341), 1203–1209.

Holben, B., Eck, T., Slutsker, I., Tanre, D., Buis, J., Setzer, A., et al. (1998). AERONET—A federated instrument network and data archive for aerosol characterization. *Remote Sensing of Environment, 66*(1), 1–16.

Houghton, J. T. (1996). *Climate change 1995: The science of climate change: Contribution of working group I to the second assessment report of the intergovernmental panel on climate change* (Vol. 2). Cambridge: Cambridge University Press.

International Energy Agency. (2010a). Energy Statistics and Balances of OECD Countries 1960–2006 (Press release).

International Energy Agency. (2010b). Energy Statistics and Balances of Non-OECD Countries 1970–2006 (Press release).

Ito, A., & Penner, J. E. (2005). Historical emissions of carbonaceous aerosols from biomass and fossil fuel burning for the period 1870–2000. *Global Biogeochemical Cycles, 19*(2).

Jacobson, M. Z. (2001). Strong radiative heating due to the mixing state of black carbon in atmospheric aerosols. *Nature, 409*(6821), 695–697.

Jacobson, M. Z. (2004). Climate response of fossil fuel and biofuel soot, accounting for soot's feedback to snow and sea ice albedo and emissivity. *Journal of Geophysical Research: Atmospheres (1984–2012), 109*(D21).

Janssen, N., Hoek, G., Simic-Lawson, M., Fischer, P., van Bree, L., ten Brink, H., et al. (2011). Black carbon as an additional indicator of the adverse health effects of airborne particles compared with PM10 and PM2.5. *Environmental Health Perspectives, 119*(12), 1691–1699.

Janssen, N. A., Gerlofs-Nijland, M. E., Lanki, T., Salonen, R. O., Cassee, F., Hoek, G., et al. (2012). *Health effects of black carbon*. Copenhagen: World Health Organization.

Junker, C., & Liousse, C. (2008). A global emission inventory of carbonaceous aerosol from historic records of fossil fuel and biofuel consumption for the period 1860–1997. *Atmospheric Chemistry and Physics, 8*(5), 1195–1207.

Katsouyanni, K., Touloumi, G., Samoli, E., Gryparis, A., Le Tertre, A., Monopolis, Y., et al. (2001). Confounding and effect modification in the short-term effects of ambient particles on total mortality: Results from 29 European cities within the APHEA2 project. *Epidemiology, 12*(5), 521–531.

Kim, J. J., Smorodinsky, S., Lipsett, M., Singer, B. C., Hodgson, A. T., & Ostro, B. (2004). Traffic-related air pollution near busy roads: The East Bay Children's Respiratory Health Study. *American Journal of Respiratory and Critical Care Medicine, 170*(5), 520–526.

Kim Oanh, N. T., Thiansathit, W., Bond, T. C., Subramanian, R., Winijkul, E., & Paw-armart, I. (2010). Compositional characterization of PM_{2.5}emitted from in-use diesel vehicles. *Atmospheric Environment, 44*(1), 15–22.

Klimont, Z., Cofala, J., Xing, J., Wei, W., Zhang, C., Wang, S., et al. (2009). Projections of SO2, NOx and carbonaceous aerosols emissions in Asia. *Tellus B, 61*(4), 602–617.

Koch, D. (2001). Transport and direct radiative forcing of carbonaceous and sulfate aerosols in the GISS GCM. *Journal of Geophysical Research: Atmospheres (1984–2012), 106*(D17), 20311–20332.

Krewski, D., Jerrett, M., Burnett, R. T., Ma, R., Hughes, E., Shi, Y., et al. (2009). *Extended follow-up and spatial analysis of the American Cancer Society study linking particulate air pollution and mortality.* Boston, MA: Health Effects Institute.

Kupiainen, K., & Klimont, Z. (2004). Primary emissions of submicron and carbonaceous particles in Europe and the potential for their control. *International Institute for Applied Systems Analysis (IASA), Interim Report IR-04-79, Schlossplatz, 1.*

Kurokawa, J., Ohara, T., Morikawa, T., Hanayama, S., Janssens-Maenhout, G., Fukui, T., et al. (2013). Emissions of air pollutants and greenhouse gases over Asian regions during 2000–2008: Regional Emission inventory in ASia (REAS) version 2. *Atmospheric Chemistry and Physics, 13*(21), 11019–11058.

Laden, F., Neas, L. M., Dockery, D. W., & Schwartz, J. (2000). Association of fine particulate matter from different sources with daily mortality in six US cities. *Environmental Health Perspectives, 108*(10), 941.

Lamarque, J.-F., Bond, T. C., Eyring, V., Granier, C., Heil, A., Klimont, Z., et al. (2010). Historical (1850–2000) gridded anthropogenic and biomass burning emissions of reactive gases and aerosols: Methodology and application. *Atmospheric Chemistry and Physics, 10*(15), 7017–7039.

Lin, W., Huang, W., Zhu, T., Hu, M., Brunekreef, B., Zhang, Y., et al. (2011). Acute respiratory inflammation in children and black carbon in ambient air before and during the 2008 Beijing Olympics. *Environmental Health Perspectives, 119*(10), 1507.

Liousse, C., Penner, J., Chuang, C., Walton, J., Eddleman, H., & Cachier, H. (1996). A global three-dimensional model study of carbonaceous aerosols. *Journal of Geophysical Research: Atmospheres (1984–2012), 101*(D14), 19411–19432.

Lipfert, F., Wyzga, R., Baty, J., & Miller, J. (2006). Traffic density as a surrogate measure of environmental exposures in studies of air pollution health effects: Long-term mortality in a cohort of US veterans. *Atmospheric Environment, 40*(1), 154–169.

Loeb, N. G., Wielicki, B. A., Doelling, D. R., Smith, G. L., Keyes, D. F., Kato, S., et al. (2009). Toward optimal closure of the Earth's top-of-atmosphere radiation budget. *Journal of Climate, 22*(3), 748–766.

Lu, Z., Zhang, Q., & Streets, D. G. (2011). Sulfur dioxide and primary carbonaceous aerosol emissions in China and India, 1996–2010. *Atmospheric Chemistry and Physics, 11*(18), 9839–9864.

McCormick, R. A., & Ludwig, J. H. (1967). Climate modification by atmospheric aerosols. *Science, 156*(3780), 1358–1359.

Miller, K. A., Siscovick, D. S., Sheppard, L., Shepherd, K., Sullivan, J. H., Anderson, G. L., et al. (2007). Long-term exposure to air pollution and incidence of cardiovascular events in women. *New England Journal of Medicine, 356*(5), 447–458.

Mills, N. L., Finlayson, A. E., Gonzalez, M. C., Törnqvist, H., Barath, S., Vink, E., et al. (2011). Diesel exhaust inhalation does not affect heart rhythm or heart rate variability. *Heart, 97*(7), 544–550.

Morgenstern, V., Zutavern, A., Cyrys, J., Brockow, I., Gehring, U., Koletzko, S., et al. (2007). Respiratory health and individual estimated exposure to traffic-related air pollutants in a cohort of young children. *Occupational and Environmental Medicine, 64*(1), 8–16.

Myhre, G., Stordal, F., Restad, K., & Isaksen, I. S. (1998). Estimation of the direct radiative forcing due to sulfate and soot aerosols. *Tellus B, 50*(5), 463–477.

Myhre, G., Samset, B., Schulz, M., Balkanski, Y., Bauer, S., Berntsen, T., et al. (2013). Radiative forcing of the direct aerosol effect from AeroCom Phase II simulations. *Atmospheric Chemistry and Physics, 13*(4), 1853–1877.

National Bureau of Statistics and National Energy Administration. (2009). China Energy Statistical Yearbook, 1986, 1989–2008 editions (Press release).

Novakov, T., Ramanathan, V., Hansen, J., Kirchstetter, T., Sato, M., Sinton, J., et al. (2003). Large historical changes of fossil-fuel black carbon aerosols. *Geophysical Research Letters, 30*(6), 57–61.

Ohara, T., Akimoto, H., Kurokawa, J.-I., Horii, N., Yamaji, K., Yan, X., et al. (2007). An Asian emission inventory of anthropogenic emission sources for the period 1980–2020. *Atmospheric Chemistry and Physics, 7*(16), 4419–4444.

Ostro, B., Feng, W.-Y., Broadwin, R., Green, S., & Lipsett, M. (2007). The effects of components of fine particulate air pollution on mortality in California: results from CALFINE. *Environmental Health Perspectives*, *115*, 13–19.

Penner, J., Eddleman, H., & Novakov, T. (1993). Towards the development of a global inventory for black carbon emissions. *Atmospheric Environment. Part A. General Topics, 27*(8), 1277–1295.

Penner, J., Chuang, C., & Grant, K. (1998). Climate forcing by carbonaceous and sulfate aerosols. *Climate Dynamics, 14*(12), 839–851.

Podgorny, I. A., & Grenfell, T. C. (1996). Partitioning of solar energy in melt ponds from measurements of pond albedo and depth. *Journal of Geophysical Research: Oceans (1978–2012), 101*(C10), 22737–22748.

Pope III, C. A., Burnett, R. T., Krewski, D., Jerrett, M., Shi, Y., Calle, E. E., et al. (2009). Cardiovascular mortality and exposure to airborne fine particulate matter and cigarette smoke shape of the exposure-response relationship. *Circulation, 120*(11), 941–948.

Pope III, C. A., Burnett, R. T., Thun, M. J., Calle, E. E., Krewski, D., Ito, K., et al. (2002). Lung cancer, cardiopulmonary mortality, and long-term exposure to fine particulate air pollution. *JAMA, 287*(9), 1132–1141.

Qin, Y., & Xie, S. (2012). Spatial and temporal variation of anthropogenic black carbon emissions in China for the period 1980–2009. *Atmospheric Chemistry and Physics, 12*(11), 4825–4841.

Ramanathan, V., & Carmichael, G. (2008). Global and regional climate changes due to black carbon. *Nature Geoscience, 1*(4), 221–227.

Reddy, M. S., & Venkataraman, C. (2002a). Inventory of aerosol and sulphur dioxide emissions from India. Part II—Biomass combustion. *Atmospheric Environment, 36*(4), 699–712.

Reddy, M. S., & Venkataraman, C. (2002b). Inventory of aerosol and sulphur dioxide emissions from India: I—Fossil fuel combustion. *Atmospheric Environment, 36*(4), 677–697.

Reff, A., Bhave, P. V., Simon, H., Pace, T. G., Pouliot, G. A., Mobley, J. D., et al. (2009). Emissions inventory of PM2. 5 trace elements across the United States. *Environmental Science and Technology, 43*(15), 5790-5796.

Reid, J. S., Hobbs, P. V., Liousse, C., Martins, J. V., Weiss, R. E., & Eck, T. F. (1998). Comparisons of techniques for measuring shortwave absorption and black carbon content of aerosols from biomass burning in Brazil. *Journal of Geophysical Research: Atmospheres (1984–2012), 103*(D24), 32031–32040.

Roemer, W. H., & van Wijnen, J. H. (2002). Pollution and daily mortality in Amsterdam. *Epidemiology, 13*(4), 491.

Rosen, H., Hansen, A., Gundel, L., & Novakov, T. (1978). Identification of the optically absorbing component in urban aerosols. *Applied Optics, 17*(24), 3859–3861.

Routledge, H. C., Manney, S., Harrison, R., Ayres, J., & Townend, J. N. (2006). Effect of inhaled sulphur dioxide and carbon particles on heart rate variability and markers of inflammation and coagulation in human subjects. *Heart, 92*(2), 220–227.

Saikawa, E., Naik, V., Horowitz, L. W., Liu, J., & Mauzerall, D. L. (2009). Present and potential future contributions of sulfate, black and organic carbon aerosols from China to global air quality, premature mortality and radiative forcing. *Atmospheric Environment, 43*(17), 2814–2822.

Sarnat, J. A., Marmur, A., Klein, M., Kim, E., Russell, A. G., Sarnat, S. E., et al. (2008). Fine particle sources and cardiorespiratory morbidity: An application of chemical mass balance and factor analytical source-apportionment methods. *Environmental Health Perspectives, 116*(4), 459.

Sato, M., Hansen, J., Koch, D., Lacis, A., Ruedy, R., Dubovik, O., et al. (2003). Global atmospheric black carbon inferred from AERONET. *Proceedings of the National Academy of Sciences, 100*(11), 6319–6324.

Sawant, A. A., Cocker, I., David, R., Miller, J. W., Taliaferro, T., Diaz-Sanchez, D., et al. (2008). Generation and characterization of diesel exhaust in a facility for controlled human exposures. *Journal of the Air and Waste Management Association, 58*(6), 829–837.

Schulz, M., Textor, C., Kinne, S., Balkanski, Y., Bauer, S., Berntsen, T., et al. (2006). Radiative forcing by aerosols as derived from the AeroCom present-day and pre-industrial simulations. *Atmospheric Chemistry and Physics, 6*(12), 5225–5246.

Schwarz, J., Gao, R., Fahey, D., Thomson, D., Watts, L., Wilson, J., et al. (2006). Single-particle measurements of midlatitude black carbon and light-scattering aerosols from the boundary layer to the lower stratosphere. *Journal of Geophysical Research: Atmospheres (1984–2012), 111*(D16).

Shindell, D., Kuylenstierna, J. C., Vignati, E., van Dingenen, R., Amann, M., Klimont, Z., et al. (2012). Simultaneously mitigating near-term climate change and improving human health and food security. *Science, 335*(6065), 183–189.

Smith, K. R., Jerrett, M., Anderson, H. R., Burnett, R. T., Stone, V., Derwent, R., et al. (2010). Public health benefits of strategies to reduce greenhouse-gas emissions: Health implications of short-lived greenhouse pollutants. *The Lancet, 374*(9707), 2091–2103.

Solomon, S., Qin, D., Manning, M., Chen, Z., Marquis, M., Averyt, K., et al. (2007). IPCC, 2007: Climate change 2007: The physical science basis. *Contribution of Working Group I to the Fourth Assessment Report of the Intergovernmental Panel on Climate Change.*

Stier, P., Schutgens, N., Bellouin, N., Bian, H., Boucher, O., Chin, M., et al. (2013). Host model uncertainties in aerosol radiative forcing estimates: Results from the AeroCom Prescribed intercomparison study. *Atmospheric Chemistry and Physics, 13*(6), 3245–3270.

Stocker, T. F., Qin, D., Plattner, G.-K., Tignor, M., Allen, S. K., Boschung, J., et al. (2013). Climate change 2013. The physical science basis. *Working Group I Contribution to the Fifth Assessment Report of the Intergovernmental Panel on Climate Change-Abstract for decision-makers: Groupe d'experts intergouvernemental sur l'evolution du climat/ Intergovernmental Panel on Climate Change-IPCC*, C/O World Meteorological Organization, 7bis Avenue de la Paix, CP 2300 CH-1211 Geneva 2 (Switzerland).

Streets, D., Bond, T., Carmichael, G., Fernandes, S., Fu, Q., He, D., et al. (2003). An inventory of gaseous and primary aerosol emissions in Asia in the year 2000. *Journal of Geophysical Research: Atmospheres (1984–2012), 108*(D21), 8809.

Streets, D. G., Gupta, S., Waldhoff, S. T., Wang, M. Q., Bond, T. C., & Yiyun, B. (2001). Black carbon emissions in China. *Atmospheric Environment, 35*(25), 4281–4296.

Turco, R., Toon, O., Whitten, R., Pollack, J., & Hamill, P. (1983). The global cycle of particulate elemental carbon: A theoretical assessment. *Precipitation Scavenging, Dry Deposition, and Resuspension*, 1337–1351.

Wang, R., Tao, S., Shen, H., Wang, X., Li, B., Shen, G., et al. (2012). Global emission of black carbon from motor vehicles from 1960 to 2006. *Environmental Science and Technology, 46*(2), 1278–1284.

Wilkinson, P., Smith, K. R., Davies, M., Adair, H., Armstrong, B. G., Barrett, M., et al. (2009). Public health benefits of strategies to reduce greenhouse-gas emissions: Household energy. *The Lancet, 374*(9705), 1917–1929.

Wiscombe, W. J., & Warren, S. G. (1980). A model for the spectral albedo of snow. I: Pure snow. *Journal of the Atmospheric Sciences, 37*(12), 2712–2733.

Woodruff, T. J., Darrow, L. A., & Parker, J. D. (2008). Air pollution and postneonatal infant mortality in the United States, 1999–2002. *Environmental Health Perspectives*, *116*, 110–115.

Zhang, Q., Streets, D. G., He, K., & Klimont, Z. (2007a). Major components of China's anthropogenic primary particulate emissions. *Environmental Research Letters, 2*(4), 045027.

Zhang, Y., Tao, S., Cao, J., & Coveney, R. M. (2007b). Emission of polycyclic aromatic hydrocarbons in China by county. *Environmental Science and Technology, 41*(3), 683–687.

Zhang, Q., Streets, D. G., Carmichael, G. R., He, K., Huo, H., Kannari, A., et al. (2009). Asian emissions in 2006 for the NASA INTEX-B mission. *Atmospheric Chemistry and Physics, 9*(14), 5131–5153.

Zhang, Y., Schauer, J. J., Zhang, Y., Zeng, L., Wei, Y., Liu, Y., et al. (2008). Characteristics of particulate carbon emissions from real-world Chinese coal combustion. *Environmental Science and Technology, 42*(14), 5068–5073.

Zhi, G., Chen, Y., Feng, Y., Xiong, S., Li, J., Zhang, G., et al. (2008). Emission characteristics of carbonaceous particles from various residential coal-stoves in China. *Environmental Science and Technology, 42*(9), 3310–3315.

Chapter 3
Research Method

3.1 Global High-Resolution Fuel Database in 2007 (PKU-FUEL-2007)

Data of fuel consumed by a specific source is an important input parameter used in developing the bottom-up emission inventory. For black carbon (BC), the basic fuel consumption data is the fuel consumed in each type of combustion process. BC is either emitted in the combustion as a byproduct of incomplete combustion of fuels, or in the non-combustion processing of fuels. Therefore, developing a high-resolution emission inventory of BC requires a reliable high-resolution inventory of fuel consumption. This section will introduce a new global high-resolution fuel consumption inventory (PKU-FUEL-2007, Peking University Fuel Inventory) which was created by a sub-national disaggregation method. In addition, a resultant global high-resolution emission inventory of CO_2, namely PKU-CO2-2007, was developed to evaluate the new inventory of fuel consumptions.

3.1.1 Combustion Sources

The PKU-FUEL-2007 inventory was constructed based on 64 combustion-related emission sources in 5 fuel categories (coal, petroleum, natural gas, solid waste and biomass) for 5 human-related sectors (energy production, industry, residential and commercial, transportation, agriculture) and 1 natural sector (wildfires). Table 3.1 lists all sources that are covered by the PKU-FUEL-2007 inventory. The definition of most sources are decided according to that in the International Energy Agency (IEA) database (International Energy Agency 2010a, b). In the sector of energy production, we included electrical plants, thermal plants, and combined heat and power (CHP) plants. Fossil fuels and biofuels used in commercial and public

R. Wang, *Global Emission Inventory and Atmospheric Transport of Black Carbon*,
Springer Theses, DOI 10.1007/978-3-662-46479-3_3

Table 3.1 Classification of the 64 fuel sub-types included in the PKU-FUEL-2007 inventory

Sector	Coal	Petroleum	Natural gas	Solid wastes	Biomass
Energy production	• Anthracite (100 %) • Bituminous coal (97.3 %) • Lignite (99.4 %) • Coking coal (100 %) • Peat (100 %)	• Gas/diesel (98.7 %) • Residue fuel oil (96.7 %) • Natural gas liquids (99.9 %)	• Dry natural gas (95.9 %) • Natural gas flaring	• Municipal waste (99.9 %) • Industrial waste (99.3 %)	• Solid biomass (85.3 %) • Biogas (100 %)
Industry	• Anthracite excluding aluminum production (98.1 %) • Bituminous coal excluding coke and brick production (98.0 %) • Lignite (99.4 %) • Coking coal (100 %) • Peat (100 %) • Bituminous coal used in coke production (99.1 %) • Bituminous coal used in brick production • Anthracite used in aluminum production	• Gas/diesel (99.4 %) • Residue fuel oil (95.7 %) • Crude oil used in petroleum refinery (96.6 %) • Natural gas liquids (98.6 %)	• Dry natural gas (88.5 %)	• Municipal waste (99.7 %) • Industrial waste (99.5 %)	• Solid biomass (99.2 %) • Biogas (100 %)

(continued)

Table 3.1 (continued)

Sector	Coal	Petroleum	Natural gas	Solid wastes	Biomass
Transportation		• Vehicles gasoline (98.0 %) • Vehicles diesel (98.1 %) • Aviation gasoline (99.6 %) • Jet kerosene (99.5 %) • Ocean tanker • Ocean container • Ocean bulk and combined carries • General cargo vessels • Non-cargo vessels • Auxiliary engines • Military vessels			• Liquid biofuels (100 %)
Residential and commercial	• Anthracite (94.4 %) • Bituminous coal (97.3 %) • Lignite (100 %) • Coking coal (100 %) • Peat (100 %)	• Kerosene (99.2 %) • Liquid petroleum gas (94.9 %) • Natural gas liquids (96.0 %)	• Dry natural gas (96.0 %)	• Non-organized waste incineration (86.2 %)	• Firewood (90.1 %) • Straw (98.8 %) • Dung cake • Biogas (100 %)
Agriculture		• Gas/diesel (99.9 %)		• Open burning of agriculture solid waste (98.5 %)	
Natural					• Forest fire • Deforestation fire • Woodland fire • Savanna fire • Peat fire

The fuels are classified into 5 fuel-categories and 6 sectors

services are included in the residential and commercial sector, which is referred to as the residential sector hereinafter. The sector of transportation includes on-road motor vehicles consuming petroleum and biodiesel, ships and aircrafts. The agricultural sector includes fuels combusted in agriculture, forestry, and fishing. It should be noted that our fuel database was constructed in order to estimate the emissions of BC, and thus non-energy use of fuels are not taken into account, because BC is mainly generated in the combustion process. Percentages of fuel consumption collected from the literature are listed in the parenthesis in Table 3.1, while consumption of remaining fuels were calculated using regression models (Wang et al. 2013).

The PKU-FUEL-2007 data set includes 223 countries/territories in 11 regions (East and South Africa, North Africa, West and Central Africa, East Asia, South and Southeast Asia, West and Central Asia, Oceania, Europe, North America, Caribbean and Central America, and South America) worldwide, which are classified into developing/developed countries based on the World Bank's criteria for 2007 (The World Bank 2010). This is shown in Table 3.2. As a country extending across the northern Asia and part of Eastern Europe, Russia was divided into two territories (European Russia and Asian Russia), since more detailed fuel consumption data were applied for European Russia (Wang et al. 2013).

3.1.2 Compilation of Fuel Consumption Data

Fuel consumption data were compiled from global, national or local energy statistics. Due to differences in data sources and data availability, we divided the 64 combustion sources in Table 3.1 into 8 groups. These groups are: (1) wildfire, (2) aviation/shipping, (3) power-stations, (4) natural gas flaring, (5) agricultural solid wastes, (6) non-organized waste incineration, (7) dung cakes, and (8) others. Generally, the amount of fuel consumed in each combustion source were compiled at global, national, or gridded level and subsequently allocated to $0.1^\circ \times 0.1^\circ$ grids using a certain proxy, except for some sources that are already produced by another data source at the resolution of $0.1^\circ \times 0.1^\circ$. The methodology and data sources used to compile fuel consumption for all these sources are summarized in Table 3.3 and described in the text below.

For wildfires (Group 1), global $0.5^\circ \times 0.5^\circ$ wildfire carbon emissions from Global Fire Emissions Database (GFED) version 3.0 (van der Werf et al. 2010) were converted to fuel consumption based on the carbon emission factors used by van der Werf et al. (2010). Then, the amount of biomass burned at the resolution of $0.5^\circ \times 0.5^\circ$ were further disaggregated to $0.1^\circ \times 0.1^\circ$ using vegetation density in the dataset constructed by Friedl et al. (2002) as a proxy. Group 2 includes aviation and shipping fuels. For aviation, fuel consumptions of aviation were collected from the International Energy Agency database (International Energy Agency 2010a, b) as a global total and then allocated to $0.1^\circ \times 0.1^\circ$ using aviation carbon monoxide emissions in the Emissions Database for Global Atmospheric Research (EDGAR) (European Commission Joint Research Centre/Netherlands

Table 3.2 List of 223 countries/territories in 11 regions

E. and S. Africa	N. Africa	W. and C. Africa	E. Asia	S. and SE. Asia	W. and C. Asia
Angola	Algeria	Benin	China	Bangladesh	Afghanistan
Botswana	Burkina Faso	Burundi	*Japan*	Bhutan	Armenia
British Indian Ocean	Chad	Cameroon	North Korea	*Brunei*	Azerbaijan
Comoros	Djibouti	Cape Verde	*South Korea*	Cambodia	*Bahrain*
Kenya	Egypt	Central African Republic	Mongolia	India	*Cyprus*
Lesotho	Eritrea	Congo	Asian Russia	Indonesia	Georgia
Madagascar	Ethiopia	Congo, Democratic Republic of the		Laos	Iran
Malawi	Libya	Cote d'Ivoire		Malaysia	Iraq
Mauritius	Mali	*Equatorial Guinea*		Maldives	*Israel*
Mayotte	Mauritania	Gabon		Myanmar	Jordan
Mozambique	Morocco	Ghana		Nepal	Kazakhstan
Namibia	Niger	Guinea		*Pakistan*	*Kuwait*
Reunion	Somalia	Guinea-Bissau		Philippines	Kyrgyzstan
Seychelles	Sudan	Liberia		*Singapore*	Lebanon
South Africa	Tunisia	Nigeria		Sri Lanka	*Oman*
Swaziland	Western Sahara	Rwanda		Thailand	*Qatar*
Tanzania		Sao Tome and Principe		Timor-Leste	*Saudi Arabia*
Uganda		Senegal		Vietnam	Syria
Zambia		Sierra Leone			Tajikistan
Zimbabwe		St. Helena			Turkey
		Togo			Turkmenistan
					United Arab Emirates
					Uzbekistan
					Yemen
Oceania	Europe	N. America	Carib. and C. America	S. America	
American Samoa	Albania	*Canada*	Anguilla	Argentina	
Australia	*Andorra*	Greenland	*Antigua and Barbuda*	Bolivia	
Cook Islands	*Austria*	Mexico	*Aruba*	Brazil	

(continued)

Table 3.2 (continued)

Oceania	Europe	N. America	Carib. and C. America	S. America
Fiji	Belarus	St. Pierre and Miquelon	*Bahamas, The*	Chile
French Polynesia	*Belgium*	*United States*	*Barbados*	Colombia
Guam	Bosnia and Herzegovina		Belize	Ecuador
Kiribati	Bulgaria		*Bermuda*	Falkland Islands (Islas Malvinas)
Marshall Islands	Croatia		*British Virgin Islands*	French Guiana
Nauru	*Czech Republic*		*Cayman Islands*	Guyana
New Caledonia	*Denmark*		Costa Rica	Paraguay
New Zealand	*Estonia*		Cuba	Peru
Niue	*Faroe Islands*		Dominica	South Georgia and the South Sandwich Is
N. Mariana Islands	*Finland*		Dominican Republic	Suriname
Palau	*France*		El Salvador	Uruguay
Papua New Guinea	*Germany*		Grenada	Venezuela
Pitcairn Islands	Gibraltar		Guadeloupe	
Samoa	*Greece*		Guatemala	
Solomon Islands	*Hungary*		Haiti	
Tokelau	*Iceland*		Honduras	
Tonga	*Ireland*		Jamaica	
Tuvalu	*Italy*		Martinique	
Vanuatu	Latvia		Montserrat	
Wallis and Futuna	*Liechtenstein*		Netherlands Antilles	
	Lithuania		Nicaragua	
	Luxembourg		Panama	
	Macedonia		*Puerto Rico*	
	Malta		St. Kitts and Nevis	
	Moldova		St. Lucia	
	Monaco		St. Vincent and the Grenadines	

(continued)

Table 3.2 (continued)

Oceania	Europe	N. America	Carib. and C. America	S. America
	Netherlands		*Trinidad* and *Tobago*	
	Norway		Turks and Caicos Islands	
	Poland			
	Portugal			
	Romania			
	European Russia			
	San Marino			
	Serbia and Montenegro			
	Slovakia			
	Slovenia			
	Spain			
	Sweden			
	Switzerland			
	Ukraine			
	United Kingdom			

Russia is divided into two territories of European Russia and Asian Russia. Developing (normal font) and developed (italic font) countries are marked

Environmental Assessment Agency 2011) as a proxy. For shipping, similarly, the global total fuel consumption was collected from the World Merchant Fleet database (Equasis 2008) and then allocated to $0.1^\circ \times 0.1^\circ$ using shipping carbon monoxide emissions in a database constructed by global shipping inventories (Eyring et al. 2005; Wang et al. 2008) as a proxy.

For power-stations (Group 3), we first compiled data of fuel consumption by 26,239 major power stations from CARMA v2.0 database (available on-line at: http://carma.org/) (Wheeler and Ummel 2008; Ummel 2012), and the fuel were allocated to the individual $0.1^\circ \times 0.1^\circ$ grid-points where power plants are reported. However, the total fuel consumption compiled by CARMA is lower than that reported in the International Energy Agency database (International Energy Agency 2010a, b), indicating that not all power plants are included in the CARMA database. It's understandable because CARMA compiles data as much as possible, and there are still many small-scale power plants that cannot be included, especially for developing countries where the information are limited (Wheeler and Ummel 2008; Ummel 2012). Therefore, we collected the total fuel consumption in the sector of energy production from the International Energy Agency database for each country (International Energy Agency 2010a, b). National fuel consumptions by power stations that are not included by CARMA were calculated by subtracting

Table 3.3 Schematic methods to construct the 0.1° × 0.1° fuel consumption database

No.	Group	Coverage	Raw data	Resolution	Conversion and prediction	0.1° × 0.1° disaggregation
1	Wildfire (5)	Globe	CO emissions	0.5° × 0.5°	Converted to 0.5° × 0.5° fuel consumptions using CO emission factors	Biomass (grass/trees) proxy
2	Aviation and shipping (9)	Globe	Fuel consumption	Global	None	CO emission proxy
3	Power stations (13)	Globe	Fuel consumptions of 26,239 major stations	Locations	None	Allocated directly to grids
		Globe	Fuel consumptions of other stations in 139 countries	National	Predicted for the other 84 small countries/territories using region-specific models	National population proxy
4	Natural gas flaring (1)	Globe	Nighttime lights for gas flaring	0.1° × 0.1°	Converted to 0.1° × 0.1° fuel consumptions based on a regression model	Allocated directly to grids
5	Agricultural solid wastes (1)	China	Crop productions	Provincial	Converted to provincial fuel consumptions based on crop-specified production-to-residue ratios and province-specific percentages of crop residues burned in the field	Sub-national population proxy
		Other countries	Crop productions of 206 countries/territories	National	Converted to national fuel consumptions based on crop-specified production-to-residue ratios and region-specific percentages of crop residues burned in the field (those for the remained 17 small countries/territories were omitted)	National population proxy
6	Non-organized waste incineration (1)	Globe	Municipal waste of 102 countries/territories	National	Converted to national fuel consumptions using 1 and 5 % incineration rates for developed and developing countries, respectively and predicted for the other 111 small countries/territories using region-specific models	National population proxy

(continued)

Table 3.3 (continued)

No.	Group	Coverage	Raw data	Resolution	Conversion and prediction	0.1° × 0.1° disaggregation
7	Dung cakes (1)	SEA13[a]	India consumption	National	Predicted for other 12 countries assuming a same per capita consumption	National population proxy
8	Other fuels (33)	EUCS-36[b]	(1) Fuel consumptions except for aluminum, coke, and brick productions. National data for 132 countries and state/provincial data for U.S.A., China and C-6 (2) Coke, aluminum, bricks productions for 132, 83, and 113 countries[e]	National	Converted to 0.5° × 0.5° fuel consumptions using CO emission proxy	Sub-national population/ road proxy[f]
		Mexico		National	Converted to county fuel consumptions using CO emission proxy	Sub-national population/ road proxy[f]
		U.S.A		State	Converted to county fuel consumptions using CO emission proxy	Sub-national population/ road proxy[f]
		China		Provincial	Predicted for 2373 counties using region-specific models	Sub-national population/ road proxy[f]
		C-6[c]		Provincial/ state	None	Sub-national population/ road proxy[f]
		C-178[d]		National	Predicted for other 84 small countries/ territories using region-specific models in Table S3 (aluminum and brick productions for 140 and 110 small countries/territories not included were omitted)	National population/road proxy[f]

For each of the eight source groups using different disaggregation approaches, the numbers of fuel sub-types are shown in the parenthesis

[a]SEA13: 13 South Asian countries including India, Bangladesh, Bhutan, Brunei, Cambodia, Laos, Maldives, Myanmar, Nepal, Pakistan, Sri Lanka, Timor-Leste, and Vietnam

[b]EUCS-36: 36 European countries including Albania, Andorra, Austria, Belarus, Belgium, Bosnia and Herzegovina, Bulgaria, Croatia, Czech Republic, Denmark, Estonia, Finland, France, Germany, Greece, Hungary, Iceland, Italy, Latvia, Lithuania, Macedonia, Moldova, Netherlands, Norway, Poland, Portugal, Romania, Russia, Serbia and Montenegro, Slovakia, Slovenia, Spain, Sweden, Switzerland, Ukraine, and United Kingdom

[c]C-6: 6 countries with state/province data collected, including India, Brazil, Canada, Australia, Turkey, and South Africa

[d]C-178: 178 countries other than EUCS-36, C-6, U.S.A., China, or Mexico

[e]Consumptions of bituminous (coke and bricks productions) and anthracite (aluminum production) were converted from the production volumes (1.25, 1.06, and 3 ton coal/ton coke, bricks, and aluminum produced, respectively)

[f]Population proxy was applied to disaggregate fuel consumptions (the 15197 SDUs for the 45 countries and remaining 178 countries) to 0.1° × 0.1° grids (ORNL 2008) except for on-road gasoline and diesel vehicles, for which 0.1° × 0.1° CO emission from road transportation in EDGARv4.2 (JRC/PBL 2011) was used as a proxy

that included in the CARMA v2.0 dataset from the national total for coal, petroleum and natural gas. At last, these fuels were disaggregated to 0.1° × 0.1° using the population distribution as a proxy (Oak Ridge National Laboratory 2008). It should be noticed that the CARMA database covers 77 % of the global total fuels and 40 % of the global total fossil fuel CO_2 emissions reported by the International Energy Agency database (International Energy Agency 2010a, b), which enhances the spatial resolution.

The accuracy of the locations of power-plants reported by CARMA was examined in our study. In brief, the locations of 350 randomly selected power-plants were checked one by one in Google imagery except for these in the U.S.A., where the geo-locations have been validated in (Wheeler and Ummel 2008; Ummel 2012). All stations recorded in CARMA v2.0 were divided into 10 categories of equal sample sizes of fuel consumptions. Using a stratified sampling method, a total of 50 stations (20 in China and 30 in other countries except the U.S.A.) were randomly selected from each category of sample size. Then, the exact locations of the power stations were derived using Google Earth by searching the names of the stations and inspecting Google Earth images of power plants (mainly through identifying the chimneys and cooling towers). Generally, 3 out of 4 stations selected can be successfully found in the Google Earth images, and 1 out of 4 stations could not be identified. At last, a total of 350 power stations with locations from Google Earth images (100 in China and 250 in other countries except the U.S.A.) were selected after searching for 476 stations. The locations recorded by CARMA and identified by Google Earth are compared, which is shown in Fig. 3.1. As a result, 45 % (China) and 89 % (countries other than China and the U.S.A.) of the stations were located in the same 0.1° × 0.1° grid-points, and the remaining 42 and 9 % of stations are located in grids adjacent to the one recorded in CARMA. It suggests that the accuracy of the CARMA v2.0 locations are satisfactory for 0.1° × 0.1° resolution mapping in countries other than China. For 87 and 95 % of power stations in China, the differences between the CARMA v2.0 reported locations and that identified by Google imagery are no more than 2 and 3 grids, respectively. Since CARMA is the best product for global power-stations that can be used when conducting this study, we relied on this database which is used in the allocation of power plants. However, the associated inaccuracy of locations of power plants in developing countries should be notified, which is ready to be updated when an improved version of CARMA or another power-plant data product is available.

For gas flaring (Group 4), the amount of fuel consumed in natural gas flaring were derived from satellite night-light data from the Defense Meteorological Satellite Program (NOAA Earth Observation Group 2011). Elvedge et al. identified a total of 2500 gas flare sites using Google Earth, and developed a regression model based on night-light and natural gas flaring (Elvidge et al. 2009), which is used estimated the 0.1° × 0.1° gridded data of natural gas flaring. In our study, the 0.1° × 0.1° night-light data is collected from the Version 4 DMSP-OLS Nighttime Lights Time Series (http://www.ngdc.noaa.gov/dmsp/downloadV4composites.html#AXP), and converted to the amount of fuel consumed using the regression models by Elvidge et al. (2009).

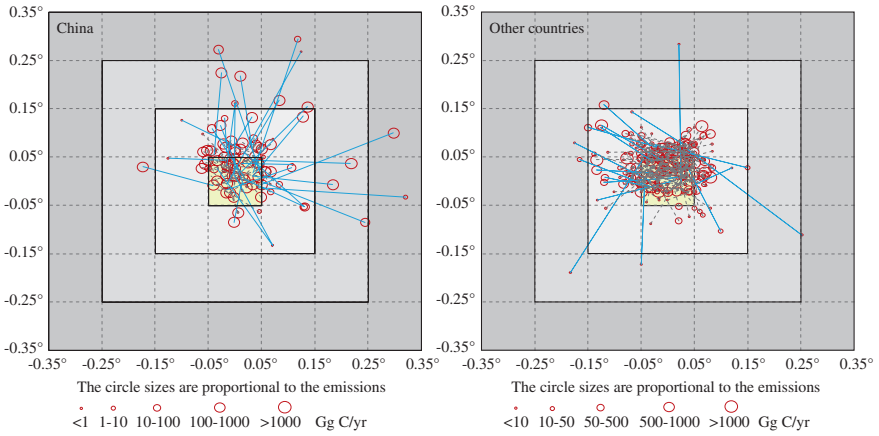

Fig. 3.1 Test of the accuracy of position of randomly selected power stations recorded in the CARMA v2.0. The geographic positions of randomly selected 350 power stations (100 stations in China and 250 stations outside of China and U.S.A.) recorded by the CARMA v2.0 database are compared with that identified by Google imagery. The *red circles* are the locations identified from Google imagery, which are linked by *blue lines* to the locations recorded in CARMA v2.0. The size of power plant is shown using circle size. Reproduced from with Permission (Wang et al. 2013); link to the original image: http://www.atmos-chem-phys.net/13/5189/2013/acp-13-5189-2013.html

Figure 3.2 shows the distribution of natural gas flaring expressed as the carbon released. It illustrates that the natural gas flaring was mainly distributed over the Northern Europe, Central Africa, North Africa and North America, and high densities were found over the Ural Mountains and Caucasian region at the border of Europe and Asia, and the Baltic Sea area in Northern Europe and Central Europe, where a large number of natural gas miners were distributed.

For agricultural solid wastes burnt in the field (Group 5), the quantities of agricultural wastes burned in each country were converted from the production of crop using the ratios of production to residue and the fraction of crop straw burned in the field. Production of five types of crop (wheat, rice, cotton, beans, maize) and a total of other agricultural species were collected from the Food and Agriculture Organization of the United Nations (FAO) database (FAOSTAT food and agriculture statistics, available at: http://faostat.fao.org/default.aspx, 2010). For China, the crop data were compiled by province from the China Agriculture Yearbook (Ministry of Agriculture of China 2008). We applied the production-to-residue ratios from Bond et al. (Streets et al. 2003; Yevich and Logan 2003; Bond et al. 2004; Cao et al. 2006; Zhang and Tao 2009) and the percentage of field burned residues (by province for China and by nation for other countries) (Bond et al. 2004; Cao et al. 2006) to estimate the quantities of agricultural wastes burnt in the field by province in China and by nation for other countries.

For non-organized waste combustion (Group 6), the total quantities of municipal waste generated in each country were collected from the United Nation statistics (United Nations Statistics Division 2010). An incineration rate of 1 and 5 %

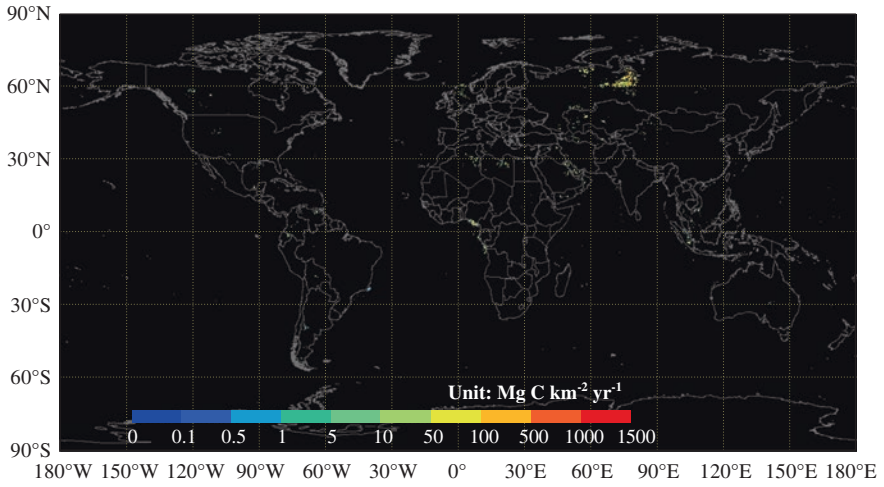

Fig. 3.2 Global distribution of natural gas flaring inferred from the version 4 DMSP-OLS nighttime lights time series data set

was adopted for the developed and developing countries, respectively (Bond et al. 2004; Zhang and Tao 2009) to calculate the quantities of municipal waste burnt. For dung cakes (Group 7), the consumption data in India was compiled from the Indian energy statistics (Tata Energy Research Institute 2008). We assumed that only 12 other South and Southeast Asian countries (Bangladesh, Bhutan, Brunei, Cambodia, Laos, Maldives, Myanmar, Nepal, Pakistan, Sri Lanka, Timor-Leste, and Vietnam) also consume dung cake, and the consumption of dung cake in India was interpolated to these countries based on national population. Then, non-organized waste combustion and consumption of dung cake were disaggregated to $0.1° \times 0.1°$ using the spatial distribution of population from a global 0.8×0.8 km^2 dataset (Oak Ridge National Laboratory 2008) as a proxy.

The remaining sources are included in Group 8, for which sub-national data were compiled and a sub-national disaggregation method was used to produce the $0.1° \times 0.1°$ fuel data. For these sources, all countries were divided into 4 groups. In the first country group, national fuel consumptions of 36 European countries including Albania, Andorra, Austria, Belarus, Belgium, Bosnia and Herzegovina, Bulgaria, Croatia, Czech Republic, Denmark, Estonia, Finland, France, Germany, Greece, Hungary, Iceland, Italy, Latvia, Lithuania, Macedonia, Moldova, Netherlands, Norway, Poland, Portugal, Romania, Russia, Serbia and Montenegro, Slovakia, Slovenia, Spain, Sweden, Switzerland, Ukraine, and United Kingdom were collected from the International Energy Agency database (International Energy Agency 2010a, b). Then, national fuel consumptions were first disaggregated to $0.5° \times 0.5°$ grids (a total of 7094 $0.5° \times 0.5°$ grids) using CO emission proxies from the European Monitoring and Evaluation Programme by sector (Centre on Emission Inventories and Projections 2011), and then disaggregated to $0.1° \times 0.1°$ grids using

on-road CO emission (European Commission Joint Research Centre/Netherlands Environmental Assessment Agency 2011) as a proxy for transportation and population as a proxy for other sources (Oak Ridge National Laboratory 2008). In the second country group, provincial fuel consumption data (a total of 161 states of provinces) were compiled for 6 countries (India, Brazil, Canada, Australia, Turkey, and South Africa) from local energy statistics (Australian Bureau of Agricultural and Resource Economics and Sciences 2008; Tata Energy Research Institute 2008; Statistics South Africa 2009; Brazil Energy Ministry 2010; Environment Canada/Natural Resource Canada 2010; Turkish Statistical Institute 2010). Then, the fuel data at province or state level were disaggregated to $0.1^\circ \times 0.1^\circ$ grids using on-road CO emissions (European Commission Joint Research Centre/Netherlands Environmental Assessment Agency 2011) as a proxy for transportation and population as a proxy for other sources (Oak Ridge National Laboratory 2008). The third country group includes China, U.S.A., and Mexico, where country (Mexico), state (U.S.A.) or province (China) -level fuel data were first collected from energy statistics (US Energy Information Administration 2008; National Bureau of Statistics and National Energy Administration 2009; International Energy Agency 2010a). Then, the national fuel consumption data in Mexico were allocated to counties (a total of 2428 counties) using CO emissions by county in 1999 as a proxy by sector (United States Environmental Protection Agency 2006), while the state fuel consumptions of U.S.A. were allocated to counties (a total of 3141 counties) using CO emissions by county in 2008 as a proxy by sector (United States Environmental Protection Agency 2011). In China, county-level fuel consumptions (a total of 2373 counties) were determined based on the provincial fuel consumption compiled above and county-level social-economic data (total and rural populations and secondary plus tertiary GDPs by county, and annual mean temperature for the capital city of each province) (National Bureau of Statistics and National Energy Administration 2009) using a set of provincial-data-based regression models developed by Zhang et al. (2007). Then, the county-level fuel consumptions in China, U.S.A., and Mexico were disaggregated to $0.1^\circ \times 0.1^\circ$ grids using on-road CO emissions (European Commission Joint Research Centre/Netherlands Environmental Assessment Agency 2011) as a proxy for transportation and population as a proxy for other sources (Oak Ridge National Laboratory 2008). In the last country group, the national fuel consumptions for countries without sub-national fuel data were taken from the International Energy Agency database (International Energy Agency 2010a, b) and then disaggregated to $0.1^\circ \times 0.1^\circ$ grids using on-road CO emissions (European Commission Joint Research Centre/Netherlands Environmental Assessment Agency 2011) as a proxy for transportation and population as a proxy for other sources (Oak Ridge National Laboratory 2008).

In processing the sub-national data for these sectors in Group 8, the sub-national fuel database covers part of the 33 fuel sub-types in Group 8. Table 3.4 lists the fuel sub-types for the sub-national data compiled in the 45 countries (China, U.S.A., Mexico, 6 countries with provincial data, and 36 European countries with gridded data). For fuel sub-types without detailed data, we assume that the shares of these sub-types in sub-national units were equal to the shares in the

Table 3.4 Sub-national fuel data available for the 45 countries (China, U.S.A., Mexico, 6 countries with provincial data, and 36 European countries (EUCS36) with gridded data)

Country	Fuel sub-types with detailed sub-national data available
EUCS36	Power coal, power oil, industry coal, industry oil, coke production[#], aluminum production[#], brick production[#], petroleum refinery[#], residential coal, residential biofuel, waste incineration[#], vehicle diesel[#], vehicle gasoline[#]
China	Power coal, industry coal, aluminum production[#], brick production[#], petroleum refinery[#], residential coal, residential straw[#], residential firewood[#], vehicle diesel[#], vehicle gasoline[#]
U.S.	Power coal, power gas, industry coal, industry oil, industry gas, coke production[#], aluminum production[#], brick production[#], petroleum refinery[#], residential coal, residential LPG[#], residential gas[#], residential biofuel, vehicle diesel[#], vehicle gasoline[#]
Mexico	Power coal, industry coal, residential oil, residential LPG[#], residential gas, residential biomass, open solid waste incineration[#], vehicle diesel[#], vehicle gasoline[#]
India	Power coal, industry coal, coke production[#], residential coal, residential biofuel, residential dung cake[#], vehicle diesel[#], vehicle gasoline[#]
South Africa	Power coal, industry coal, coke production[#], residential coal, residential biofuel, vehicle diesel[#], vehicle gasoline[#]
Brazil	Power coal, industry coal, coke production[#], residential coal, residential biofuel, vehicle diesel[#], vehicle gasoline[#]
Turkey	Power coal, industry coal, coke production[#], residential coal, residential biofuel, vehicle diesel[#], vehicle gasoline[#]
Canada	Power coal, industry coal, coke production[#], petroleum refinery[#], residential coal, residential LPG[#], residential gas, vehicle diesel[#], vehicle gasoline[#], residential biofuel
Australia	Power coal, power oil, power biofuel, industry coal, industry oil, industry gas, industry biofuel, coke production[#], residential coal, residential LPG[#], residential gas, residential biofuel, vehicle diesel[#], vehicle gasoline[#]

The fuel subtypes in Group 8 with fuel consumption data in the local database are marked with a superscript ([#])

national total, which are derived from the International Energy Agency database (International Energy Agency 2010a, b).

When compiling the national fuel data, there are some countries that are not included in the statistics. For example, the International Energy Agency database only includes a total of 138 Organization for Economic Co-operation and Development (OECD) and non-OECD countries (International Energy Agency 2010a, b). For the remaining countries without fuel data, a set of region-specific regression models were developed to predict their fuel consumptions based on data from countries in the same region (Wang et al. 2013). The region-specific regression models were developed for 11 regions defined in Table 3.2 based on data for these countries in the same regions. Total population, rural population, and/or gross domestic production were used individually or collectively as independent variables (The World Bank 2010). The overall uncertainty of the inventory would not be affected significantly since fuel consumptions in these countries/territories contributed 4.2 % to the global total.

As a summary, the fuel consumptions in China, U.S.A., Mexico, 6 countries with provincial data, and 36 European countries with gridded data were compiled at sub-national level, namely the Sub-nationally Disaggregated Units before being disaggregated to $0.1° \times 0.1°$ for 33 fuel-subtypes in Group 8. In contrast to the traditional method of disaggregating fuels from national data, the new method developed here, namely the sub-national disaggregation method, can reduce the disaggregation bias and thus reduces the uncertainty associated with the gridded fuel data in these fuel-consuming countries. Figure 3.3 summaries the method to produce the $0.1° \times 0.1°$ data set for each fuel sub-type.

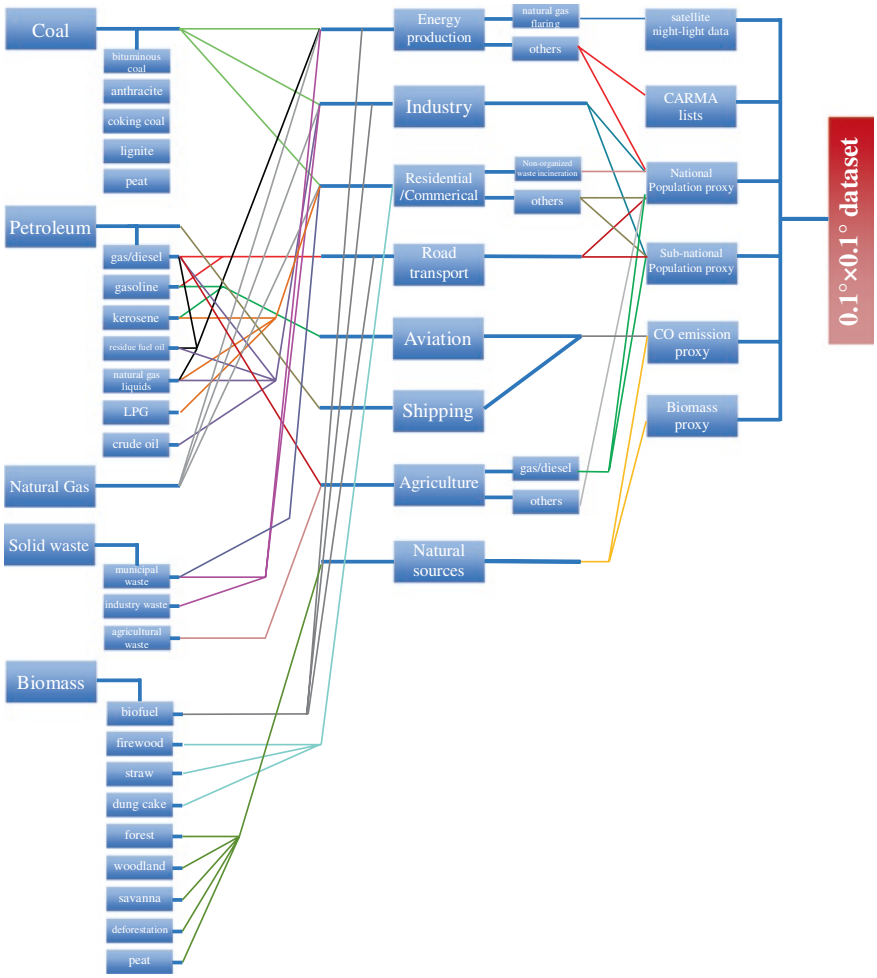

Fig. 3.3 A schematic map of compiling the fuel consumption data for 64 fuel sub-types at the resolution of $0.1° \times 0.1°$ using various proxies

Table 3.5 Mean CO_2 emission factors (EF_C) and combustion rates (R) of various fuel sub-types

Fuels	EF_c, Mg C/TJ	R, %
Anthracite used in power stations	26.07	98.0
Coking coal used in power stations	28.04	98.0
Bituminous coal used in power stations	24.30	98.0
Lignite used in power stations	25.74	98.0
Peat used in power stations	27.45	98.0
Bituminous coal consumed in coke production	24.30	98.0
Bituminous coal consumed in brick production	24.30	98.0
Anthracite consumed in aluminum production	26.07	98.0
Anthracite used in industry	26.07	98.0
Coking coal used in industry	28.04	98.0
Bituminous coal used in industry	24.30	98.0
Lignite used in industry	25.74	98.0
Peat used in industry	27.45	98.0
Anthracite used residentially/commercially	26.07	98.0
Coking coal used residentially/commercially	28.04	98.0
Bituminous coal used residentially/commercially	24.30	98.0
Lignite used residentially/commercially	25.74	98.0
Peat used residentially/commercially	27.45	98.0
Gas/Diesel used in power stations	19.19	99.0
Residue fuel oil used in power stations	20.22	99.0
Natural gas liquids used in power stations	16.34	99.0
Gas/diesel used in industry	19.19	99.0
Residue fuel oil used in industry	20.22	99.0
Crude oil consumed in petroleum refinery	13.74	99.0
Natural gas liquids used in industry	16.34	99.0
Liquid petroleum gas used residentially/commercially	16.33	99.0
Natural gas liquids used residentially/commercially	16.34	99.0
Kerosene used residentially/commercially	18.62	99.0
Gas/diesel used in agriculture	19.19	99.0
Motor vehicle gasoline	18.17	99.0
Aviation gasoline	17.92	99.0
Liquid biofuels used by vehicles	19.19	99.0
Jet kerosene	18.48	99.0
Motor vehicle gas/diesel	19.19	99.0
Oil used by ocean tanker	16.90	99.0
Oil used by ocean container ships	16.90	99.0
Oil used by ocean bulk and combined carriers	17.20	99.0
Oil used by general cargo vessels	17.20	99.0
Oil used by non-cargo vessels	17.50	99.0
Oil used by auxiliary engines	17.62	99.0
Oil used by military vessels	22.55	99.0

(continued)

Table 3.5 (continued)

Fuels	EF_c, Mg C/TJ	R, %
Dry natural gas used in power stations	13.76	99.5
Natural gas flaring	13.76	99.5
Dry natural gas used in industry	13.76	99.5
Dry natural gas used in residential/commercial	13.76	99.5
Solid biomass used in power stations	28.41	98.0
Biogas used in power stations	16.34	98.0
Solid biomass used in industry	28.41	98.0
Biogas used in industry	16.34	98.0
Biogas used residentially/commercially	16.34	98.0
Firewood used residentially/commercially	38.84	88.7/78.9
Straw used residentially/commercially	22.68	91.9
Dung cake used residentially/commercially	26.10	88.7
Biomass burned in forest fires	34.07	90.1
Biomass burned in deforestation fires	34.07	90.1
Biomass burned in peat fires	34.07	90.1
Biomass burned in woodland fires	34.07	90.1
Biomass burned in savanna fires	28.50	90.1
Municipal waste used in power stations	22.54	98.0
Industrial waste used in power stations	22.54	98.0
Municipal waste used in industry	22.54	98.0
Industrial waste used in industry	22.54	98.0
Small-scaled solid waste burning	22.54	98.0
Open burning of agriculture waste	25.14	90.1

All data are taken from (Intergovernmental Panel on Climate Change 1996; US Department of Energy 2000; American Petroleum Institute 2001; URS 2003; Nyboer et al. 2006; van der Werf et al. 2010)

3.1.3 Construction of CO_2 Emission Maps

CO_2 emission map (PKU-CO_2-2007) is one of the major by-products of PKU-FUEL-2007, and a product that was used to evaluate the generated fuel data set. Based on the PKU-FUEL-2007 inventory, CO_2 emissions were estimated from the CO_2 emission factors and the combustion rates of different fuel sub-types. CO_2 emission factors for different fuel sub-types were derived as the means of data collected from the literature, listed in Table 3.5. Combustion rate of fuel is defined as the ratio of fuel burnt in the combustion. Fixed combusted rates were applied to petroleum (0.990), coal (0.980), natural gas (0.995), solid municipal and industrial waste fuel (0.980), biomass burned in the field (0.901), firewood burned in cook stoves (0.887), firewood burned in fireplaces (0.789), crop residue burned in cook stoves (0.919), and open burning of agriculture waste (0.901), respectively, which were collected from the measurements (Lee et al. 2005; Johnson et al. 2008; Zhang et al. 2008a; Oda and Maksyutov 2011).

Our product focuses on fuel and CO_2 emissions from fuel burning. However, in order to be comparable with other inventories, CO_2 emissions from cement production were also included in PKU-CO_2-2007, based on the cement production data in 155 countries compiled from the U.S. Geological Survey database (US Geological Survey 2010) and the corresponding CO_2 emission factors from Andres et al. (1996). National CO_2 emissions from cement production were disaggregated to $0.1^\circ \times 0.1^\circ$ grids using the distribution of industrial coal consumption from PKU-FUEL-2007 as a proxy.

3.1.4 Uncertainty of the Fuel and CO_2 Inventory

To assess the uncertainty, Monte Carlo ensemble simulations of the PKU-FUEL-2007 and PKU-CO_2-2007 emission models were run 1000 times on all grids globally. We randomly varied all input data from priori uncertainty distributions with coefficients of variation (CVs). A constant CV of fuel consumptions from ships/aviation and wildfires are set to be 20 and 18 %, respectively, with normal distributions according to the literature (Endresen et al. 2007; Wang et al. 2008; van der Werf et al. 2010). For the remaining fuel sub-types, the uncertainty in fuel consumption was assumed to follow uniform distributions with coefficients of variation (30 % for non-organized waste incineration, 20 % for residential biofuel, 20 % for open biomass burning, and 10 % for other sources) (Marland et al. 2003; Bond et al. 2004; Akimoto et al. 2006; Ciais et al. 2010). The CVs of literature reported EF_C range from 3.8 to 5.1 % (Intergovernmental Panel on Climate Change 1996; US Department of Energy 2000; American Petroleum Institute 2001; URS 2003). Thus, a constant value of 5 % was adopted with a normal distribution for EF_C of all fuel sub-types. For the combustion rate, a fixed CV of 20 % was applied with a normal distribution.

To assess the uncertainty associated with the spatial disaggregation method, a normal distribution was applied in the disaggregation. For each sub-national disaggregation unit or country (where no sub-national data exists), the CV of the fraction of fuel allocated to each grid was defined according to the size, using a formula as:

$$CV = 1000\,\% \times \frac{N_i}{225829} \tag{3.1}$$

where N_i is the number of grid-points in a certain sub-national disaggregation unit or country, and 225,829 is the number of grid-points in Asian Russia. Asian Russia is the largest sub-national disaggregation unit in the disaggregation system, for which a CV of 1000 % was assigned. It assumes that uncertainty is proportional to the number of grid-points in each disaggregation unit. Finally, the results of Monte Carlo simulations are presented as R_{90} (the range between 95th and 5th percentiles) and R_{90}/M (the ratio of R_{90} and the median) for absolute and relative errors on a map, respectively.

3.2 Estimation of BC Emissions

Following the bottom-up approach (Bond et al. 2004), the emissions of BC can be estimated based on the BC emission factors (defined mass of BC emitted per mass fuel consumed or product produced) and the corresponding fuel consumption. To develop the emission inventory of BC, the measured emission factors of BC are collected from the literature as many as possible. Then, statistics methods are used to derive the BC emission factors under different technology, and the fraction of each technology is determined from statistic reports or based on some assumption. At last, the high-resolution fuel consumption data compiled in PKU-FUEL-2007 were applied to generate a global $0.1° \times 0.1°$ gridded emission inventory of BC in 2007. Meanwhile, long-term fuel data (1949–2007 in China, and 1960–2007 for all countries) are used to study the time series of BC emissions in the history.

3.2.1 Emission Factors of BC

In this study, a new data set of the emission factors of BC has been developed from a total of 706 EF_{BC} data measured in 13 countries from 1985 to 2011. The original data of BC emission factors includes those used in previous global emission inventories (Bond et al. 2004; Junker and Liousse 2008; Lamarque et al. 2010), those that are recently measured by other groups in the literature (Chen et al. 2005, 2006, 2009; Parashar et al. 2005; Cao et al. 2006, 2008; Roden et al. 2006, 2009; Li et al. 2007, 2009; Bi et al. 2008; Kleeman et al. 2008; Olivares et al. 2008; Zhang et al. 2008b; Zhi et al. 2008; Saud et al. 2012), and those measured in our group (Shen et al. 2010, 2012, 2013). Determination of the emission factors of BC for all sources is listed in Table 3.6.

Note that the collected data includes both BC (optically measured) and EC (elemental carbon, thermally measured). The ratio of EC to BC varies with the nature and aging of the deposited particles (Watson et al. 2005). According to Kim Oanh et al. (2010), the optically measured BC in diesel exhaust is higher than the thermally measured EC. However, they also noticed a good linear relationship between BC and EC ($EC = 0.6$ BC with a correlation coefficient of 0.88), and they found that the relationship between BC and EC is dependent on the thickness of filters used for particles deposit in the measurement. When the sampling filter is thick enough (>20 $\mu g\ cm^{-2}$ of filter area), only a single layer of particles can be measured by the optical method, leading to a high uncertainty in the measurement (Kim Oanh et al. 2010). Unfortunately, not all studies have measured both BC and EC, and the relationship between BC and EC is not well understood. To ensure the sample number of EF_{BC}, all emission factors measured as EC was used as equivalent to BC in this study. As a result, the uncertainty due to the difference between BC and EC is unknown at present stage.

Table 3.6 Emission factors of BC used in this study

Emission source	Technology division	Mean	SD	Sample number
Anthracite/coking coal/bituminous coal/lignite/peat used in power plants	PC/cyclone	−1.76 (0.017)	0.50	1
	PC/scrubber	−3.64 (0.00023)	0.50	1
	PC/ESP	−2.73 (0.0018)	0.55	3
	SC/cyclone	−1.81 (0.015)	0.36	4
	SC/scrubber	−2.46 (0.0035)	0.20	7
	SC/ESP	−2.43 (0.0037)	0.26	4
	No control	−1.31 (0.049)	0.23	4
Anthracite/coking coal/bituminous coal/lignite/peat used in industry	PC/cyclone	−1.76 (0.017)	0.50	1
	PC/scrubber	−3.64 (0.00023)	0.50	1
	PC/ESP	−2.73 (0.0018)	0.55	3
	SC/cyclone	−1.81 (0.015)	0.36	4
	SC/scrubber	−2.46 (0.0035)	0.20	7
	SC/ESP	−2.43 (0.0037)	0.26	4
	No control	−1.31 (0.049)	0.23	4
Brick production	Traditional	0.65 (4.5)	0.50	1
	Tunnel kilns	−0.27 (0.54)	0.50	1
Aluminum production	–	−1.82 (0.015)	0.50	1
Anthracite used in residential	–	−1.85 (0.014)	0.21	11
Coking coal used in residential	–	−0.10 (0.79)	0.41	2
Bituminous coal used in residential (chunk)	–	0.66 (4.57)	0.35	15
Bituminous coal used in residential (briquette)	–	−1.73 (0.018)	0.25	14
Lignite used in residential	–	−0.73 (0.18)	0.50	1
Peat used in residential	–	−0.74 (0.18)	0.50	1
Gas/Diesel used in power stations	–	0.38 (2.4)	0.14	2
Residue fuel oil used in power stations	–	−2.86 (0.0014)	0.31	1
Natural gas liquids used in power stations	–	−1.81 (0.015)	0.50	1
Gas/diesel used in industry	–	0.38 (2.4)	0.14	2
Residue fuel oil used in industry	–	−2.86 (0.0014)	0.31	1
Crude oil consumed in petroleum refinery	–	−3.82 (0.00015)	0.50	1
Natural gas liquids in industry	–	−1.81 (0.015)	0.50	1
LPG in residential	–	−1.27 (0.054)	0.50	1
Natural gas liquids in residential	–	−1.81 (0.015)	0.50	1

(continued)

Table 3.6 (continued)

Emission source	Technology division	Mean	SD	Sample number
Kerosene used in residential	–	−0.82 (0.15)	0.11	1
Gas/diesel used in agriculture	–	0.38 (2.4)	0.14	2
Aviation gasoline	–	−0.70 (0.20)	0.50	1
Biodiesel used by vehicles	–	−0.45 (0.35)	0.25	1
Jet kerosene	–	−0.70 (0.20)	0.50	1
Oil used by ocean tanker	–	−0.42 (0.38)	0.23	3
Oil used by ocean container ships	–	−0.10 (0.79)	0.11	2
Oil by bulk and combined carriers	–	−0.42 (0.38)	0.15	5
Oil used by general cargo vessels	–	−0.40 (0.40)	0.20	5
Oil used by non-cargo vessels	–	−0.44 (0.36)	0.22	3
Oil used by auxiliary engines	–	−0.01 (0.98)	0.23	5
Oil used by military vessels	–	−0.42 (0.38)	0.22	5
Dry natural gas in power stations	–	−3.60 (0.00025)	0.50	1
Natural gas flaring	–	−0.08 (0.83)	0.50	1
Dry natural gas used in industry	–	−3.60 (0.00025)	0.50	1
Dry natural gas used in residential	–	−3.60 (0.00025)	0.50	1
Solid biomass in power stations	–	−2.71 (0.00195)	0.50	1
Biogas used in power stations	–	$-5.49\ (3.2 \times 10^{-6})$	0.50	1
Solid biomass used in industry	–	−2.71 (0.00195)	0.26	1
Biogas used in industry	–	$-5.49\ (3.2 \times 10^{-6})$	0.50	1
Biogas used in residential	–	$-5.49\ (3.2 \times 10^{-6})$	0.50	1
Firewood used in residential	Fireplace	−0.52 (0.30)	0.23	14
	Cook stoves	0.0 (1.0)	0.38	21
Straw used in residential	–	−0.14 (0.72)	0.18	23
Dung cake used in residential	–	−0.43 (0.37)	0.30	7
Biomass burned in forest fires	–	−0.34 (0.46)	0.31	34
Biomass burned in deforestation	–	−0.24 (0.58)	0.50	1
Biomass burned in peat fires	–	−0.24 (0.58)	0.50	4
Biomass burned in woodland fires	–	−0.28 (0.52)	0.50	9
Biomass burned in savanna fires	–	−0.23 (0.58)	0.14	14

(continued)

Table 3.6 (continued)

Emission source	Technology division	Mean	SD	Sample number
Open burning of agriculture	Wheat	−0.51 (0.31)	0.26	7
	Rice	−0.62 (0.24)	0.27	6
	Cotton	−0.20 (0.63)	0.16	8
	Beans	−0.02 (0.95)	0.20	6
	Maize	−0.02 (0.95)	0.18	6
	Other	−0.30 (0.50)	0.11	5
Municipal waste in power stations	–	−1.91 (0.012)	0.50	1
Industrial waste in power stations	–	−1.91 (0.012)	0.50	1
Municipal waste in industry	–	−1.91 (0.012)	0.50	1
Industrial waste in industry	–	−1.91 (0.012)	0.50	1
Small-scaled solid waste burning	–	0.74 (5.5)	0.50	1
on-road gasoline vehicles	Four-stroke	Emission factors of BC were collected from the literature, as listed in Wang et al. (2012a), which were used to develop a regression model predicting emission factors of BC for gasoline vehicles		
	Two-stroke	5 times of that for four-stroke gasoline vehicles		
	Superemitters	−0.54 (0.29)	0.50	1
On-road diesel vehicles	Normal	Emission factors of BC were collected from the literature, as listed in Wang et al. (2012a), which were used to develop a regression model predicting emission factors of BC for diesel vehicles		
	Superemitters	0.71 (5.1)	0.50	1
Coke production	Beehive	0.79 (6.2)	0.50	1
	Battery coking	The emission factors of fine particles are collected from the literature, which is used to develop a regression model (Wang et al. 2012b)		

Means and standard deviations (*SD*) were calculated for $\log_{10}$-transformed BC emission factors, because BC emission factors collected in the literature are log-normally distributed. Arithmetic average BC emission factors are given in brackets. The unit is g/kg, except for gas fuels (g/m^3) and coke/aluminum production (g/kg product). Data sources are listed in published papers (Wang et al. 2012a, b, 2014a, b)

The frequency distributions of collected BC emission factors for different emission sources were analyzed using standard statistical methods. First, a few outliers were detected using Grubb's test after log-transformation ($P = 0.05$) and removed from the database. These data include the BC emission factors measured for residential chunk coal of 28.5 g/kg by Zhi et al. (2008) and 0.2 g/kg by Chen et al. (2006); residential briquette of 0.675 g/kg by Chen et al. (2005), on-road motor vehicles of 0.0059 g/kg by Williams et al. (1989). Then, the normal or log-normal distribution of are tested for BC emission factors of the sources with enough measured data.

For motor vehicles, to analyze the factors governing the distribution of BC emission factors, information relevant to BC emissions measurements were collected. These relevant factors included the vehicle type, vehicle in-use country, model year, measured year, method for the measurement, run cycle, vehicle odometer, and ambient air temperature. For the BC emission factors measured for diesel or gasoline vehicle fleets on roads, they are not corresponding to a single model year. Thus, the vehicle model year was calculated by subtracting the year when the measurement was conducted by the average on-road vehicle ages of 4 (Lin et al. 2009; Westerdahl et al. 2009) and 6 (Fraser et al. 1999; Sjödin and Andréasson 2000) for developing and developed countries, respectively. The factors of the vehicle in-use country, model year, measured year, method for the measurement, run cycle, vehicle odometer, and ambient air temperature were tested individually for their influences on BC emission factors using an analysis of variance. As a result, among all factors, in-use country, model year, and T were tested to be significant. By recognizing that per capital gross domestic product (purchasing power parity) (GDP_c) is an ideal indicator representing differences both among countries and over years, regression models were developed using GDP_c to predict BC emission factors of gasoline and diesel vehicles in different countries and for different years. Later, it was found that the transfer of technical from developed to developing countries contributes to reduce the emission factors in developing countries. As a result, another parameter, Y_{3000} defined as the year when a country's GDP_c reaching 3000 USD, was introduced into the models of BC emission factors.

For other sources, the frequency distributions of the BC emission factors are shown in Fig. 3.4. BC emission factors for residential firewood, residential crop residues, residential chunk coal, agriculture waste burning, forest fire and savanna fire follow log-normal distributions. Therefore, the means and standard deviations (SD) were calculated for $\log_{10}$-transformed BC emission factors, as listed in Table 3.6. For sources with only single reported BC emission factors, the value was used as the mean and the SD of $\log_{10}$-transformed BC emission factors was assigned as 0.50. The means and SD were used to estimate the emissions and the uncertainties, respectively. Although we collect as many BC emission factors as possible from various countries including developed, developing, and in-transition economies, the data availability is still a major limit of this study. For example, in our data set of BC emission factors for motor vehicles, approximately 70 % of them were from the United States. Hopefully, more measurements in a wider range of countries will help validate our data and reduce the uncertainty.

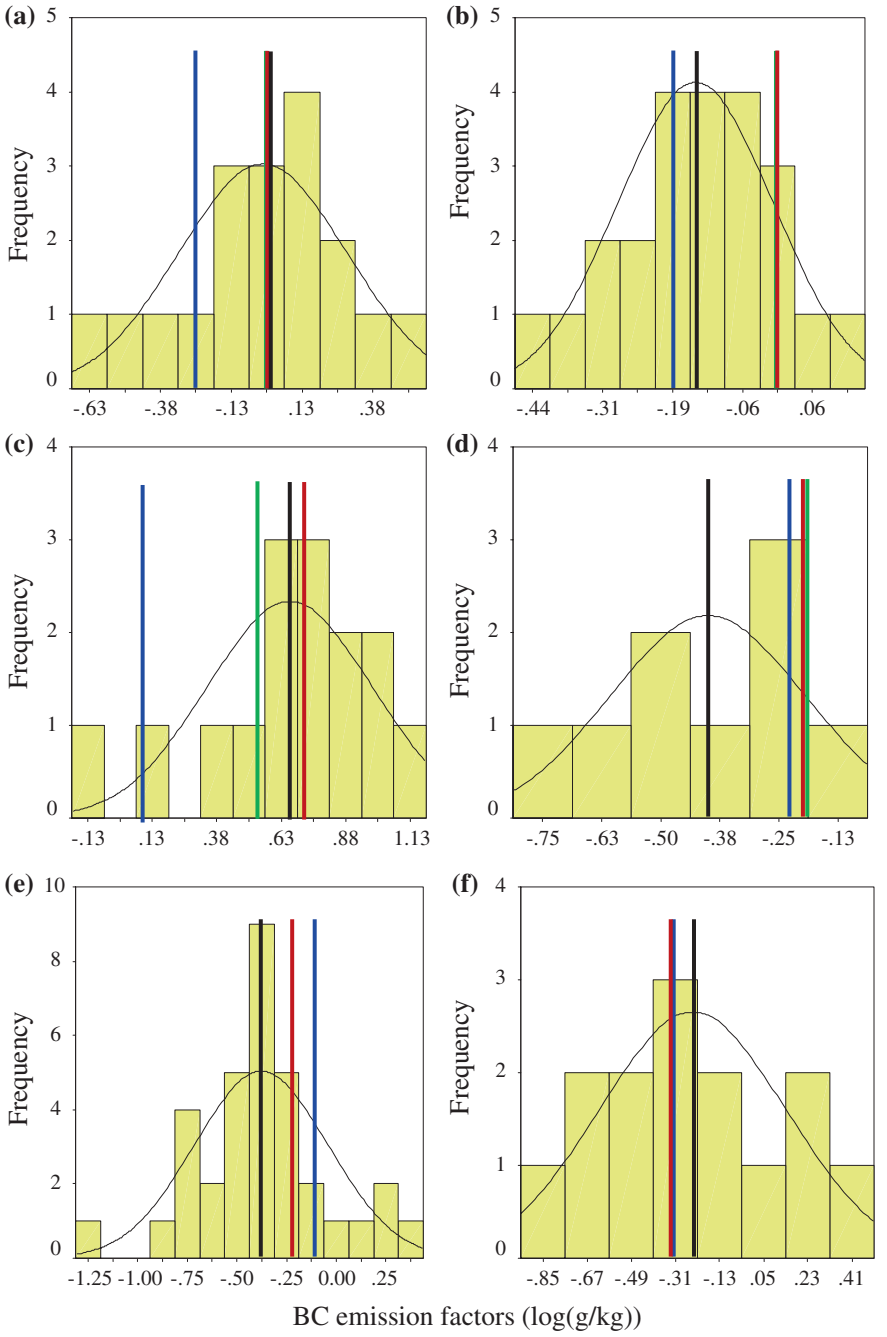
(a)
Frequency
-.63 -.38 -.13 .13 .38
(b)
Frequency
-.44 -.31 -.19 -.06 .06
(c)
Frequency
-.13 .13 .38 .63 .88 1.13
(d)
Frequency
-.75 -.63 -.50 -.38 -.25 -.13
(e)
Frequency
-1.25 -1.00 -.75 -.50 -.25 0.00 .25
(f)
Frequency
-.85 -.67 -.49 -.31 -.13 .05 .23 .41
BC emission factors (log(g/kg))

Fig. 3.4 Frequency distribution of the BC emission factors measured for residential firewood (**a**), residential crop residues (**b**), residential chunk coal (**c**), agriculture waste burning (**d**), forest fire (**e**) and savanna fire (**f**). The BC emission factors used by Streets et al. (2001, 2003), Cao et al. (2006), and Zhang et al. (2009) were marked as *green*, *blue* and *red lines*, respectively, in each graph for a comparison to BC emission factors used in our study (*black line*). (Reproduced with Permission)

3.2.2 Technology Splits

BC emission factors from coal combustion in power plants and industrial boilers, brick kilns, coke production, on-road motor vehicles (diesel and gasoline), residential firewood, residential coal, and agriculture residue burned in the field was strongly affected by the process type or abatement technology (Table 3.6). These fuel sub-types should be divided into more detailed technology in order to reduce the uncertainty of the emission inventory. Accordingly, a total of 17 of the 64 sub-types in PKU-FUEL-2007, which are associated with a wide spread of BC emission factors, were further divided into sub-categories. For each sub-category, the adequate BC emission factors could be applied. For example, coal consumptions in power plants and industrial boilers were divided into 2 types of combustion boilers (pulverized-coal or stoker/cyclone boilers) and 3 types of control facilities (cyclone, scrubber, electrostatic precipitators); coke production was divided into two sub-categories as beehive and recovery battery ovens; motor vehicles using either diesel or gasoline were classified into two sub-categories: normal and *super-emitters* (vehicles with high emission factors due to poor maintenance) (Bond et al. 2004); normal gasoline vehicles were further allocated to two-stroke and four-stroke vehicle sub-categories; agriculture residues were classified into 6 species as crop straws of wheat, rice, cotton, beans, maize, and others. As a result, the 17 emission sources were further divided into 39 sub-type sources and individual BC emission factors were applied for each. Table 3.7 lists the emission sources with technology splits and the methodology to calculate the fraction of each sub-category.

Coal used in power plants and industrial boilers were divided into 7 technologies of 2 types of combustion boilers: pulverized-coal (PC) or stoker/cyclone boilers (SC); and 3 types of control facilities: cyclone, scrubber, electrostatic precipitators (ESP); and those without any control facilities. The share of each technology was calculated using the S-shaped curves used by Bond et al. (2004):

$$F(t) = (F_0 - F_\mathrm{f})\exp\left[-(t - t_0)2/2s^2\right] + F_\mathrm{f} \tag{3.2}$$

where F_0 and F_f are the initial and final fractions of the technology division, t_0 is transition beginning time, and s is transition rate. Input parameters were applied to developing or developed countries, respectively, referring to those used by Bond et al. (2004) and Streets et al. (2005). All input parameters are listed in Table 3.8. The coal consumptions under the 6 technologies were calculated by Eq. 3.2, and

Table 3.7 Technology splits of the emission sources with different BC emission factors

Sector	Fuel/activity	Sub-sources	Descriptions
Energy	Anthracite	a. PC/cyclone b. PC/scrubber c. PC/ESP d. SC/cyclone e. SC/scrubber f. SC/ESP g. SC/no control	Combustions of coal in power plants and industry were divided into 7 types according to the combusting boilers (pulverized-coal firing boilers (PC) and stokers/cyclone (SC)) and exhaust treatment facility (cyclone, scrubber, electrostatic precipitators (ESP), and no control). Fractions of different technologies were calculated using the S-shaped models as follows: $F(t) = (F_0 - F_f)$ exp $[-(t - t_0)2/2\ s^2] + F_f$, where F_0 and F_f are the initial and final fractions of the technology division, t_0 is transition beginning time, and s is transition rate. Parameters were determined for developing or developed countries, respectively (Wang et al. 2014b)
	Bituminous coal		
	Lignite		
	Coking coal		
	Peat		
Industry	Anthracite		
	Bituminous coal		
	Lignite		
	Coking coal		
	Peat		
Industry	Coke production	a. Beehive b. Battery coking	Fractions of beehive coking ovens were assumed to be 0 in developed countries and 20 % for developing countries except China, for which country the data was compiled by Wang et al. (2012b)
Industry	Brick production	a. Traditional b. Tunnel kilns	Fractions of tunnel kilns are assumed to be 100 % for developed countries and 10 % for developing countries
Residential	Bituminous coal	a. Chunk b. Briquette	The consumption data of briquette in residential sector were compiled for China from local statistics (by province for the period 1980–2007, and by nation from 1960 to 1979) (Wang et al. 2012b). The briquette used in countries other than China was neglected

(continued)

Table 3.7 (continued)

Sector	Fuel/activity	Sub-sources	Descriptions
Residential	Firewood	a. Fireplace b. Stoves	We assumed that 75 % of firewood was burned in fireplaces in Europe and North America, and the other 25 % was burned in stoves. In other countries, it was assumed that all the firewood was burned in stoves
Transportation	Diesel vehicles (on road)	a. Normal b. Superemitters	Fractions of superemitters were assumed to be 5 % for developed countries and 10 % for developing countries
Transportation	Gasoline vehicles (on road)	a. Normal (2-stroke) b. Normal (4-stroke) c. Superemitters	Fractions of four-stroke vehicle are derived from the International Road Federation. Fractions of superemitters was assumed to be 5 % for developed countries and 10 % for developing countries
Agriculture	Agriculture residue burned in the field	a. Wheat b. Rice c. Cotton d. Beans e. Maize f. Others	Mass of residue of individual crops burned in the field were calculated from the crop production by species (wheat, rice, cotton, beans, maize, and others)

the remaining coal was burnt without any control facilities. However, in China, many control devices might not be operating at all times (Sun 2006; Xu 2010). According to Xu (2010), 20 % of scrubbers in power plants were not in operation. According to the report by the National Development and Reform Commission, this non-compliance ratio can reach 60 % in China (Sun 2006). Based on these estimates, a median value of 20 % non-compliance was adopted for the operation of control devices in power plants and industry in China.

For residential coal, the consumption of briquette were collected for China by province for the period from 1980 to 2007 and by nation from 1960 to 1979 according to the national energy yearbook (National Bureau of Statistics and National Energy Administration 2009). Since there are limited data for countries except for China and the fraction of briquette in residential coal is less than 3 % for 3 countries with records (United Nations Statistics Division 1995), the residential briquette used in countries other than China was not considered. For brick kilns, 10 and 100 % tunnel kilns were applied to the developing and developed countries, respectively. For coke ovens, the ratios of beehive to recovery battery coking were derived for

Table 3.8 Parameters of the S-shaped curves of coal consumption in power plants and industry

Power stations	Developed countries				Developing countries			
	F_0 (%)	F_f (%)	s	t_0	F_0 (%)	F_f (%)	s	t_0
PC/cyclone	0	2–5	20	1955	0	3–5	20	1955
PC/scrubber	0	2–5	20	1955	0	3–5	20	1955
PC/ESP	60	80–96	25	1980	0	84–90	25	1960
SC/cyclone	5	2–3	30	1955	20	1–5	30	1960
SC/scrubber	5	2–8	30	1955	20	1–5	30	1960
SC/ESP	0	2–10	36	1955	0	8–13	36	1960
Industry								
PC/cyclone	0	4–6	20	1955	0	2–4.5	20	1955
PC/scrubber	0	4–6	20	1955	0	2–4.5	20	1955
PC/ESP	0	15–25	25	1960	0	10–16	25	1980
SC/cyclone	30	10–15	30	1960	5	43–58	30	1960
SC/scrubber	30	10–15	30	1960	5	22–29	30	1960
SC/ESP	0	40–50	36	1955	0	4–11	36	1960

each year from the national energy yearbook (National Bureau of Statistics and National Energy Administration 2009) for China. For other countries, constant ratios were applied to the developing countries (20 %) and developed countries (0), respectively. For on-road emissions of diesel and gasoline motor vehicles, a fraction of 10 and 5 % of super-emitters were adopted for developing and developed countries, respectively (Bond et al. 2004; Subramanian et al. 2009). For normal gasoline motor vehicles, the fractions of four-stroke vehicles were derived by region from the International Road Federation (International Road Federation 2009). For firewood, we assumed that 75 % of this fuel was burnt in fireplaces in Europe and North America, and the remaining was burned in cooking stoves. In other countries, it was assumed that all firewood was burnt in cooking stoves. All agriculture residues were classified into 6 different species, and the ratios were assumed to be equal to the ratios based on the crop productions, which were collected for China (National Development and Reform Commission and Development Research Center of the State Council 2009) and other countries (Statistics at FAO, available at http://faostat.fao.org/site/291/default.aspx).

3.2.3 Fuel Consumption Data

The global high-resolution (0.1° × 0.1°) fuel consumption data in 2007 (PKU-FUEL-2007) was used to develop the 0.1° × 0.1° inventory of BC in 2007 (PKU-BC-2007). In addition to PKU-BC-2007, national fuel consumption data from 1960 to 2007 were compiled, which were used to estimate the time trend of BC emissions. Annual fuel consumptions from 1960 to 2007 for 222 countries/territories

(Russia as one country here) were taken from the International Energy Agency database (International Energy Agency 2010a, b) for fuels included in the database, and other statistics for fuels not included in the International Energy Agency database. For China, the national fuel consumptions were collected for the period 1949–1970 from the United Nations Statistics Division (United Nations Statistics Division 1995); national fuel data were collected for the period 1971–1979 from the International Energy Agency database (International Energy Agency 2010a, b); and provincial fuel data were collected for the period 1980–2007 from the China Energy Statistics Yearbook (National Bureau of Statistics and National Energy Administration 2009). Note that the national consumptions of coal, oil, natural gas, and biofuels in China taken from the provincial data from the China Energy Statistics Yearbook differ from the data taken from International Energy Agency database for the period from 1980 to 2007 (Fig. 3.5). In addition, the coal consumptions in the residential and industrial sectors from 1988–2007, petroleum consumptions from 2003–2007, and coke productions from 1980–1996 were underestimated in the International Energy Agency database. Similar conclusions were found in the literature (Akimoto et al. 2006; Guan et al. 2012). The difference can be explained by the diverse methods used by different statistics (Akimoto et al. 2006; Guan et al. 2012), and the observation data show that the provincial data are more realistic (Akimoto et al. 2006).

In addition, national data of natural gas flaring were collected from the Global Gas Flaring Database (available at: http://www.ngdc.noaa.gov/dmsp/interest/gas_flares.html); national brick production were collected from the International Yearbook of Industrial Statistics (United Nations Industrial Development Organization 2008); national aluminum production were collected from the U.S. Geological Survey database (US Geological Survey 2010); national non-organized waste incinerated were derived from the production of municipal waste by country from the United Nation statistics (United Nations Statistics Division 2010) and constant rates of incineration (1 and 5 % for developed and developing countries, respectively) (Bond et al. 2004; Zhang and Tao 2009); national consumptions of residential firewood were collected from the Food and Agriculture Organization statistics (available at: http://faostat.fao.org/site/291/default.aspx); national consumptions of residential straw were derived by subtracting the national firewood consumptions from the total solid biofuel consumption from the International Energy Agency database (International Energy Agency 2010a, b); the quantities of crop residues burned in the field were converted from the crop production by species (wheat, rice, cotton, beans, maize, and others) (from the National Bureau of Statistics Rural Social Economic Survey for China, and from Food and Agriculture Organization statistics for other countries) using region-specified production-to-residue ratios (Streets et al. 2003; Yevich and Logan 2003; Bond et al. 2004; Cao et al. 2006; Zhang and Tao 2009) and the percentage of field burned residues (Bond et al. 2004; Cao et al. 2006).

For biomass burning, we combined the data from two databases. For the period from 1997 to 2007, the $0.5° \times 0.5°$ gridded data of biomass burning from the Global Fire Emissions Database version 3 (GFED3) database (van der Werf et al. 2010)

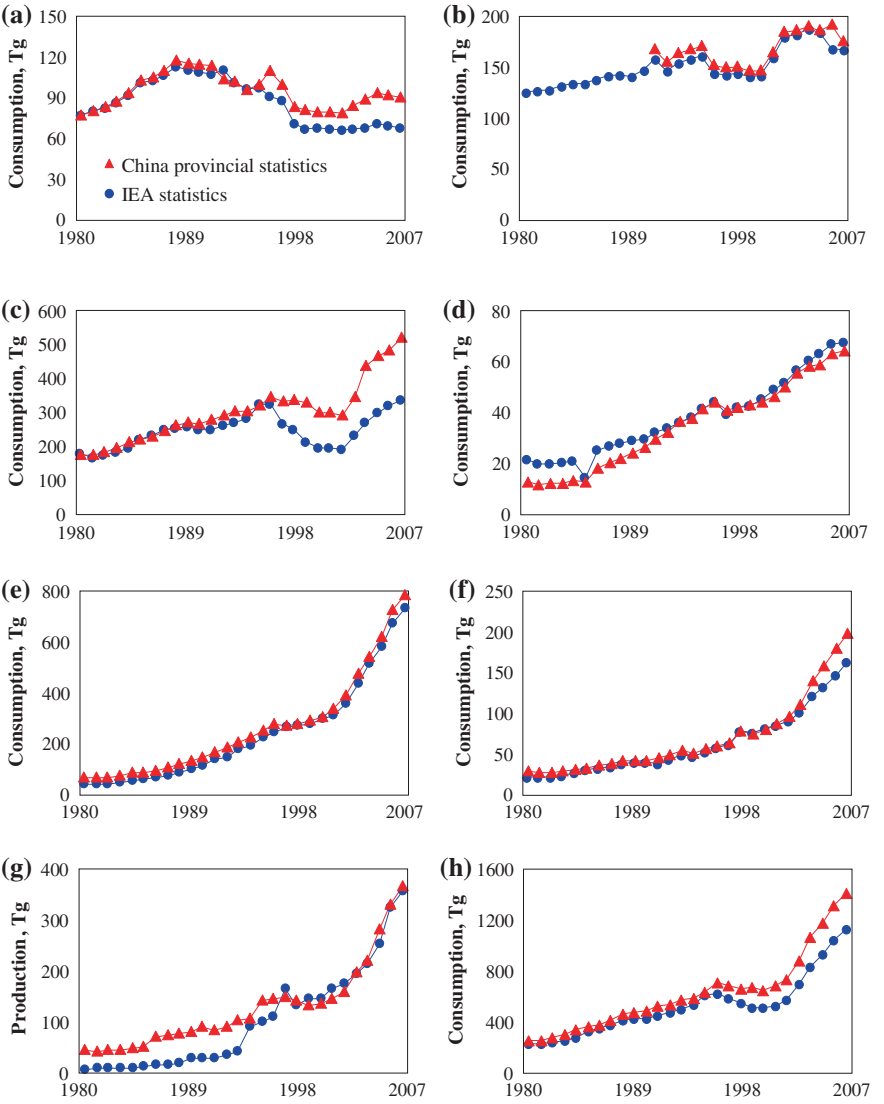

Fig. 3.5 Comparison of fuel consumptions in China between two different statistics during 1980–2007 for residential coal (**a**), residential solid biomass (**b**), coal consumed in industry (**c**), petroleum consumed in industry (**d**), coal consumed in power stations (**e**), petroleum consumed in transportation (**f**), coke production (**g**) and total coal consumption (**h**). Red lines show data from the China Energy Statistics Yearbook, while blue lines show data from the IEA database. (Reproduced with Permission)

were used. For the period from 1960 to 1996, the 0.5° × 0.5° gridded biomass burning data were derived from the RETRO (RE analysis of the TRO pospheric chemical composition over the past 40 years) database (Schultz et al. 2008).

3.3 Atmospheric Transport Models of BC

A general circulation model LMDz (Laboratoire de Météorologie Dynamique, "z" stands for zoom) coupled with an aerosol module (Interactions between Aerosols and Chemistry) and a terrestrial vegetation model ORCHIDEE (Organizing Carbon and Hydrology in Dynamic Ecosystems) was used to simulation the global atmospheric transport and distribution of BC. This model (shorted as LMDZ-OR-INCA hereinafter) is one of the 23 models used in the global multi-model exercise (CMIP5) (Szopa et al. 2013).

A latest version of the LMDZ-OR-INCA model was used in our thesis. A detailed description of the model is available in the literature (Boucher and Pham 2002; Reddy and Boucher 2004; Reddy et al. 2005; Quaas et al. 2006). In brief, the atmospheric transport of all tracers is computed following a finite volume scheme for large-scale advection (Van Leer 1977; Hourdin and Armengaud 1999), a standard scheme for turbulent mixing in the boundary layer (Reddy and Boucher 2004), and a scheme based on mass for convection (Tiedtke 1989). In the model, there are 19 vertical layers from the surface to 3.88 hPa, with 6 layers below 600 hPa and 9 layers above 250 hPa. A time step of 3 min is adopted for resolving the dynamical part of the model, and all mass fluxes are cumulated over five time steps. In addition, the physical and chemical parameterizations are updated at an interval of 30 min. All physical processes in the model are handled through operator splitting. In addition, the precipitation is discriminated as stratiform and convective precipitations. In our study, the model was driven by the meteorological wind data constrained by the reanalysis data produced by the European Centre for Medium-Range Weather Forecasts (ECMWF) (available at: http://www.ecmwf.int/products/). Simulations were run for the year 2007 after 3 months of spin-up.

The INCA module treats both gases (Hourdin et al. 2006) and particles (sulfate, black carbon, primary organic matter, dust and seasalt) (Balkanski et al. 2010). For aerosols, the INCA module adopts a computationally efficient spectral scheme to treat the size distribution of aerosols (Schulz et al. 1998). The model considers 3 independent lognormal distributions of particles with constant standard deviations, allowing the model to compute aerosol numbers and mass concentrations at the same time in the transport (Schulz et al. 1998). As an advantage, it enables the model to be computed efficiently with two tracers per mode: one representing for the mass distribution and the other for the number distribution. However, the width of the distribution is set at the beginning in the transport without accounting for the influence of atmospheric processing on size distributions (Balkanski et al. 2007, 2010). In another word, there is an implicit assumption that the hygroscopic growth, dry and wet deposition and chemical transformation do not affect the

width of the size distribution but only the mass median diameter. The modelled distributions and concentrations of carbonaceous aerosols (Reddy et al. 2005) and dust (Schulz et al. 1998; Guelle et al. 2000; Balkanski et al. 2007) can match the observation.

For all tracers, the turbulent dry deposition is computed based to the aerosol concentrations in the lowest model layer using a prescribed dry deposition velocity (0.2 cm s^{-1} for aerosol species in coarse and fine modes over land, and 0.05 cm s^{-1} over oceans). Sedimentation of lognormally distributed aerosol modes is computed following Slinn and Slinn (1980), which has been parameterized by Schulz et al. (1998). For wet deposition, different schemes are used to calculate the wet scavenging by stratiform and convective precipitations. The wet deposition is calculated following a first-order function, expressed as:

$$dC_g/dt = -\beta C_g \tag{3.3}$$

where C_g is the tracer concentrations and β is the scavenging coefficient in unit of s^{-1}. The precipitation is calculated as a function of the rain liquid water content calculated by the transport model, and the wet scavenging by snow is treated as same as that for liquid water. For convective precipitation, a scheme used by Balkanski et al. (1993) is followed with the scavenging coefficient calculated as:

$$\beta^{cv} = -f \cdot F_u \cdot g/p \tag{3.4}$$

where F_u is the upward convective mass flux in unit of kg m^{-2} s^{-1} (calculated by the transport model), g is the gravity constant, p is the air pressure, and f is the fraction of aerosol that can be taken up by the rain droplet. According to Liu et al. (2001), the fraction f can be derived as:

$$f = 1 - e^{-\alpha \Delta z} \tag{3.5}$$

where Δz is the updraft height of the convective cloud, and α is the ratio of the conversion rate of cloud water to precipitation and the velocity of air mass updraft in unit of m^{-1}. The processes above are considered for all tracers in the model. For carbonaceous aerosols, they are divided into soluble mode and insoluble mode. It is assumed that 20 % of the freshly emitted BC is soluble and the remaining is insoluble. Then, in the transport, insoluble BC is converted to soluble BC with time under an aging scheme. The half life of BC aging is set as 1.1 days, adopted from Cooke and Wilson (1996). For primary organic carbon, a similar aging process is considered, which differs from BC in that 50 % primary organic carbon is set to be soluble at the emission time. During the atmospheric transport, only soluble BC is subject to wet scavenging, and thus the aging rate influences the lifetime of BC in the model (Balkanski et al. 2010).

To study the effect of model resolution, two versions of the LMDz-OR-INCA were used in this thesis study. The first one is an Asia-zoomed version (shorted as "M_{INz}" hereafter, where "M" indicates model). In this version, the resolution was refined to 0.51° in latitude and 0.66° in longitude for an Asian region of 50–130°E, 0–55°N centered over China and India. For the region elsewhere, the resolution was reduced to 4.62° × 4.64° to ensure that the total number of model grids is

constant. The second one is a regular version (shorted as "M_{IN}" hereafter). In this version, the resolution was fixed at 1.27° in latitude and 2.50° in longitude globally. Therefore, we can run the two versions of model with different resolutions over Asia, as the most polluted region for BC, and investigate the effect of model resolution. Figure 3.6 shows the mesh systems adopted in the two versions of model.

As described above, two versions of LMDz-OR-INCA model were used to simulate the global transport and distribution of BC in 2007. In addition to LMDz-OR-INCA, a regional model, CHIMERE (Menut et al. 2000; Vautard et al. 2000; Bessagnet et al. 2004; Vautard et al. 2004, 2005, 2007), was also run to study the distribution of BC at a very high resolution of 0.1° × 0.1°. CHIMERE is a regional Eulerian off-line chemistry-transport model, and the latest version CHIMERE 2013 (Menut et al. 2014) was used in our study. The

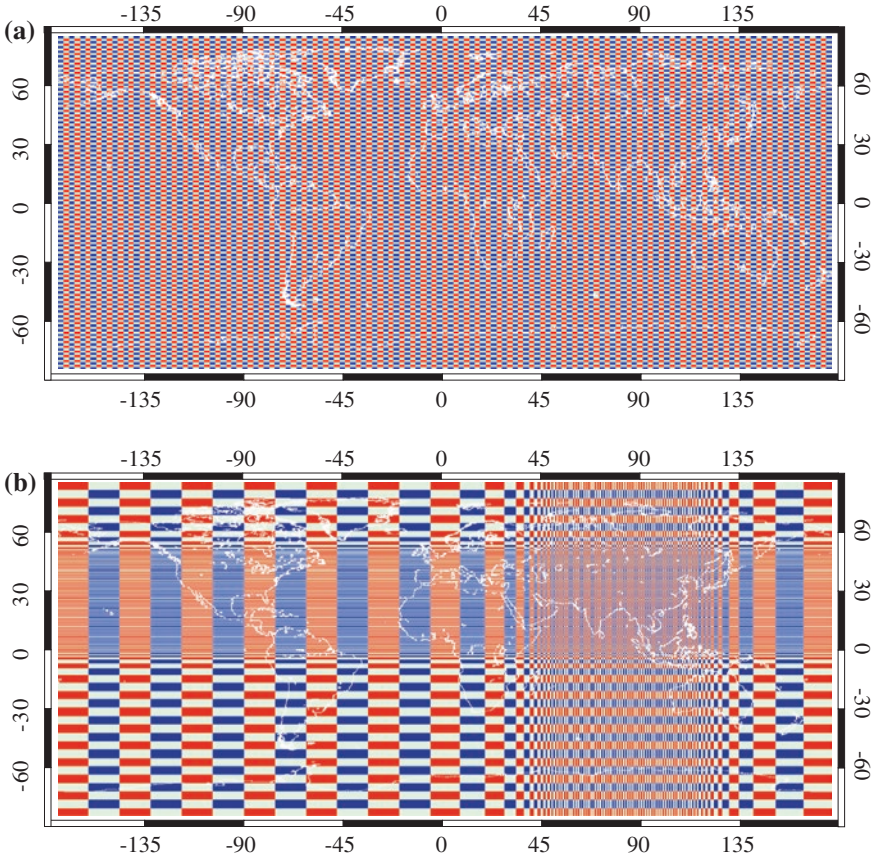

Fig. 3.6 Mesh systems used in the regular-grid (**a**) and Asia-zoomed (**b**) versions of the same atmospheric transport model

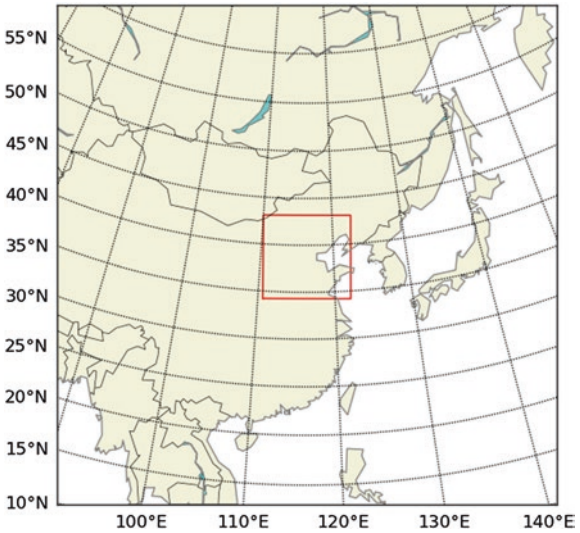

Fig. 3.7 Spatial domain covered by the CHIMERE model. The whole domain is used to run the initial and boundary conditions for the CHIMERE model, and the small domain limited by the red square represents the region where the CHIMERE model is run

model contains an aerosol module for nitrate, sulphate, ammonium, sea salt, dust, primary particulate matter (BC or primary organic carbon), and secondary organic aerosol. In the simulation, BC was divided into nine size bins. The dry deposition process is characterized by a resistance analogy. The dry deposition velocity can be expressed as:

$$v_d = v_s + \frac{1}{r_a + r_b + r_a \cdot r_b \cdot v_s} \tag{3.6}$$

where v_s is the sedimentation velocity in unit of m s^{-1}, r_a is the aerodynamical resistance in unit of s m^{-1}, and r_b is the surface resistance in unit of s m^{-1}.

The wet deposition is calculated for in-cloud rainout and below-cloud scavenging, respectively. The removing rate of in-cloud rainout is characterized as a function of the liquid water content and an empirical uptake coefficient depending on particle compositions following Tsyro (2002) and Guelle et al. (1998). The below-cloud scavenging is characterized as a function of the collision efficiency between particles and rain droplets (Seinfeld and Pandis 1998; Jung et al. 2003). More information of the model is available in the literature (Menut et al. 2014).

In our study, the CHIMERE model was run over the North China Plain region (113°E–120°E, 36°N–42°N) at the original resolution of the emission inventory of PKU-BC-2007 (0.1° × 0.1°), driven by meteorological fields produced by the Weather Research and Forecasting model. The spatial domain of the model is shown in Fig. 3.7. The initial and boundary conditions for the CHIMERE model were derived from global simulation results from LMDZ-OR-INCA.

References

Akimoto, H., Ohara, T., Kurokawa, J. -I., & Horii, N. (2006). Verification of energy consumption in China during 1996–2003 by using satellite observational data. *Atmospheric Environment, 40*(40), 7663–7667.

American Petroleum Institute. (2001). *Compendium of greenhouse gas emissions estimation methodologies for the oil and gas industry, pilot test version*. Retrieved from http://www.api.org/environment-health-and-safety/climate-change/whats-new/compendium-ghg-methodologies-oil-and-gas-industry.

Andres, R. J., Marland, G., Fung, I., & Matthews, E. (1996). A 1 × 1 distribution of carbon dioxide emissions from fossil fuel consumption and cement manufacture, 1950–1990. *Global Biogeochemical Cycles, 10*(3), 419–429.

Australian Bureau of Agricultural and Resource Economics and Sciences. (2008). *Energy in Australia 2008*. Retrieved from http://www.abares.gov.au/publications.

Balkanski, Y., Schulz, M., Claquin, T., & Guibert, S. (2007). Reevaluation of Mineral aerosol radiative forcings suggests a better agreement with satellite and AERONET data. *Atmospheric Chemistry and Physics, 7*(1), 81–95.

Balkanski, Y., Myhre, G., Gauss, M., Rädel, G., Highwood, E., & Shine, K. (2010). Direct radiative effect of aerosols emitted by transport: From road, shipping and aviation. *Atmospheric Chemistry and Physics, 10*(10), 4477–4489.

Balkanski, Y. J., Jacob, D. J., Gardner, G. M., Graustein, W. C., & Turekian, K. K. (1993). Transport and residence times of tropospheric aerosols inferred from a global three-dimensional simulation of 210Pb. *Journal of Geophysical Research: Atmospheres (1984–2012)*, *98*(D11), 20573–20586.

Bessagnet, B., Hodzic, A., Vautard, R., Beekmann, M., Cheinet, S., Honoré, C., et al. (2004). Aerosol modeling with CHIMERE—preliminary evaluation at the continental scale. *Atmospheric Environment, 38*(18), 2803–2817.

Bi, X., Simoneit, B. R., Sheng, G., & Fu, J. (2008). Characterization of molecular markers in smoke from residential coal combustion in China. *Fuel, 87*(1), 112–119.

Bond, T. C., Streets, D. G., Yarber, K. F., Nelson, S. M., Woo, J. H., & Klimont, Z. (2004). A technology-based global inventory of black and organic carbon emissions from combustion. *Journal of Geophysical Research: Atmospheres (1984–2012)*, *109*(D14).

Boucher, O., & Pham, M. (2002). History of sulfate aerosol radiative forcings. *Geophysical Research Letters, 29*(9), 22-21-22-24.

Brazil Energy Ministry. (2010). *Brazil energy statistics*. Retrieved from http://www.mme.gov.br/mme.

Cao, G., Zhang, X., & Zheng, F. (2006). Inventory of black carbon and organic carbon emissions from China. *Atmospheric Environment, 40*(34), 6516–6527.

Cao, G., Zhang, X., Gong, S., & Zheng, F. (2008). Investigation on emission factors of particulate matter and gaseous pollutants from crop residue burning. *Journal of Environmental Sciences, 20*(1), 50–55.

Centre on Emission Inventories and Projections. (2011). *Emissions as used in EMEP models*. Retrieved from http://www.ceip.

Chen, Y., Sheng, G., Bi, X., Feng, Y., Mai, B., & Fu, J. (2005). Emission factors for carbonaceous particles and polycyclic aromatic hydrocarbons from residential coal combustion in China. *Environmental Science and Technology, 39*(6), 1861–1867.

Chen, Y., Zhi, G., Feng, Y., Fu, J., Feng, J., Sheng, G., & Simoneit, B. R. (2006). Measurements of emission factors for primary carbonaceous particles from residential raw-coal combustion in China. *Geophysical Research Letters, 33*(20), L20815.

Chen, Y., Zhi, G., Feng, Y., Liu, D., Zhang, G., Li, J., et al. (2009). Measurements of black and organic carbon emission factors for household coal combustion in China: Implication for emission reduction. *Environmental Science and Technology, 43*(24), 9495–9500.

Ciais, P., Paris, J., Marland, G., Peylin, P., Piao, S., Levin, I., et al. (2010). The European carbon balance. Part 1: Fossil fuel emissions. *Global Change Biology, 16*(5), 1395–1408.

Cooke, W. F., & Wilson, J. J. (1996). A global black carbon aerosol model. *Journal of Geophysical Research: Atmospheres (1984–2012), 101*(D14), 19395–19409.

Elvidge, C. D., Ziskin, D., Baugh, K. E., Tuttle, B. T., Ghosh, T., Pack, D. W., et al. (2009). A fifteen year record of global natural gas flaring derived from satellite data. *Energies, 2*(3), 595–622.

Endresen, Ø., Sørgård, E., Behrens, H. L., Brett, P. O., & Isaksen, I. S. (2007). A historical reconstruction of ships' fuel consumption and emissions. *Journal of Geophysical Research: Atmospheres (1984–2012), 112*(D12).

Environment Canada/Natural Resource Canada. (2010). *State Energy Statistics 2007*. Retrieved from www.nrcan.gc.ca.

Equasis. (2008). *The world merchant fleet in 2007 (Lisbon)*. Retrieved from http://www.equasis.org/EquasisWeb/public/HomePage.

European Commission Joint Research Centre/Netherlands Environmental Assessment Agency. (2011). *Emission database for global atmospheric research (EDGAR), release version 4.2*. Retrieved from http://edgar.jrc.ec.europa.eu.

Eyring, V., Köhler, H., Van Aardenne, J., & Lauer, A. (2005). Emissions from international shipping: 1. The last 50 years. *Journal of Geophysical Research: Atmospheres (1984–2012), 110*(D17).

Fraser, M. P., Cass, G. R., & Simoneit, B. R. (1999). Particulate organic compounds emitted from motor vehicle exhaust and in the urban atmosphere. *Atmospheric Environment, 33*(17), 2715–2724.

Friedl, M. A., McIver, D. K., Hodges, J. C., Zhang, X., Muchoney, D., Strahler, A. H., et al. (2002). Global land cover mapping from MODIS: Algorithms and early results. *Remote Sensing of Environment, 83*(1), 287–302.

Guan, D., Liu, Z., Geng, Y., Lindner, S., & Hubacek, K. (2012). The gigatonne gap in China's carbon dioxide inventories. *Nature Climate Change, 2*(9), 672–675.

Guelle, W., Balkanski, Y., Dibb, J., Schulz, M., & Dulac, F. (1998). Wet deposition in a global size-dependent aerosol transport model: 2. Influence of the scavenging scheme on 210Pb vertical profiles, surface concentrations, and deposition. *Journal of Geophysical Research: Atmospheres (1984–2012), 103*(D22), 28875–28891.

Guelle, W., Balkanski, Y., Schulz, M., Marticorena, B., Bergametti, G., Moulin, C., Arimoto, R., & Perry, K. (2000). Modeling the atmospheric distribution of mineral aerosol: Comparison with ground measurements and satellite observations for yearly and synoptic timescales over the North Atlantic. *Journal of Geophysical Research: Atmospheres (1984–2012), 105*(D2), 1997–2012.

Hourdin, F., & Armengaud, A. (1999). The use of finite-volume methods for atmospheric advection of trace species. Part I: Test of various formulations in a general circulation model. *Monthly Weather Review, 127*(5), 822–837.

Hourdin, F., Musat, I., Bony, S., Braconnot, P., Codron, F., Dufresne, J.-L., et al. (2006). The LMDZ4 general circulation model: Climate performance and sensitivity to parametrized physics with emphasis on tropical convection. *Climate Dynamics, 27*(7–8), 787–813.

Intergovernmental Panel on Climate Change. (1996). *Revised 1996 IPCC guidelines for national greenhouse gas inventories*, Reference Manual (Vol. 3). Retrieved from http://www.ipcc-nggip.iges.or.jp/public/gl/invs1.htm.

International Energy Agency. (2010a). *Energy statistics and balances of Non-OECD countries 1970–2006* [Press release].

International Energy Agency. (2010b). *Energy statistics and balances of OECD countries 1960–2006* [Press release].

International Road Federation. (2009). *World road statistics 2009*. Geneva.

Johnson, M., Edwards, R., Alatorre Frenk, C., & Masera, O. (2008). In-field greenhouse gas emissions from cookstoves in rural Mexican households. *Atmospheric Environment, 42*(6), 1206–1222.

Jung, C. H., Kim, Y. P., & Lee, K. (2003). A moment model for simulating raindrop scavenging of aerosols. *Journal of Aerosol Science, 34*(9), 1217–1233.

Junker, C., & Liousse, C. (2008). A global emission inventory of carbonaceous aerosol from historic records of fossil fuel and biofuel consumption for the period 1860–1997. *Atmospheric Chemistry and Physics, 8*(5), 1195–1207.

Kim Oanh, N. T., Thiansathit, W., Bond, T. C., Subramanian, R., Winijkul, E., & Paw-armart, I. (2010). Compositional characterization of PM _{2.5} emitted from in-use diesel vehicles. *Atmospheric Environment, 44*(1), 15–22.

Kleeman, M. J., Robert, M. A., Riddle, S. G., Fine, P. M., Hays, M. D., Schauer, J. J., & Hannigan, M. P. (2008). Size distribution of trace organic species emitted from biomass combustion and meat charbroiling. *Atmospheric Environment, 42*(13), 3059–3075.

Lamarque, J.-F., Bond, T. C., Eyring, V., Granier, C., Heil, A., Klimont, Z., et al. (2010). Historical (1850–2000) gridded anthropogenic and biomass burning emissions of reactive gases and aerosols: Methodology and application. *Atmospheric Chemistry and Physics, 10*(15), 7017–7039.

Lee, S., Baumann, K., Schauer, J. J., Sheesley, R. J., Naeher, L. P., Meinardi, S., et al. (2005). Gaseous and particulate emissions from prescribed burning in Georgia. *Environmental Science and Technology, 39*(23), 9049–9056.

Li, X., Wang, S., Duan, L., Hao, J., & Nie, Y. (2009). Carbonaceous aerosol emissions from household biofuel combustion in China. *Environmental Science and Technology, 43*(15), 6076–6081.

Li, X., Wang, S., Duan, L., Hao, J., Li, C., Chen, Y., & Yang, L. (2007). Particulate and trace gas emissions from open burning of wheat straw and corn stover in China. *Environmental Science and Technology, 41*(17), 6052–6058.

Lin, X., Tang, D., Ding, Y., Yin, H., & Ji, Z. (2009). Study on the distribution of vehicle mileage traveled in China. *Research of Environmental Sciences, 22*(3), 377–380.

Liu, H., Jacob, D. J., Bey, I., & Yantosca, R. M. (2001). Constraints from 210Pb and 7Be on wet deposition and transport in a global three-dimensional chemical tracer model driven by assimilated meteorological fields. *Journal of Geophysical Research: Atmospheres (1984–2012), 106*(D11), 12109–12128.

Marland, G., Boden, T. A., Andres, R. J., Brenkert, A., & Johnston, C. (2003). *Global, regional, and national fossil fuel CO2 emissions* (pp. 34–43). Trends: A compendium of data on global change.

Menut, L., Vautard, R., Beekmann, M., & Honoré, C. (2000). Sensitivity of photochemical pollution using the adjoint of a simplified chemistry-transport model. *Journal of Geophysical Research: Atmospheres (1984–2012), 105*(D12), 15379–15402.

Menut, L., Bessagnet, B., Khvorostyanov, D., Beekmann, M., Blond, N., Colette, A., et al. (2014). CHIMERE 2013: A model for regional atmospheric composition modelling. Geoscientific Model Development, 6(4), 981–1028.

Ministry of Agriculture of China. (2008). *China agriculture yearbook 2008*. Beijing.

National Bureau of Statistics and National Energy Administration. (2009). *China energy statistical yearbook, 1986, 1989–2008* (editions) [Press release].

National Development and Reform Commission and Development Research Center of the State Council. (2009). *2050 China energy and CO2 emissions report*. Beijing.

NOAA Earth Observation Group. (2011). *Global gas flaring estimates*. Retrieved from http://www.ngdc.noaa.gov/dmsp/interest/gasflares.html.

Nyboer, J., Strickland, C., & Tu, J. J. (2006). *Improved CO2, CH4 and N2O emission factors for producer-consumed fuels in oil refinerie*. Canadian Industrial End-use Energy Data and Analysis Centre.

Oak Ridge National Laboratory. (2008). *LandScan global population 2007 database*. Retrieved from http://www.ornl.gov/sci/landscan/.

Oda, T., & Maksyutov, S. (2011). A very high-resolution (1 km × 1 km) global fossil fuel CO2 emission inventory derived using a point source database and satellite observations of nighttime lights. *Atmospheric Chemistry and Physics, 11*(2), 543–556.

Olivares, G., Ström, J., Johansson, C., & Gidhagen, L. (2008). Estimates of black carbon and size-resolved particle number emission factors from residential wood burning based on ambient monitoring and model simulations. *Journal of the Air and Waste Management Association, 58*(6), 838–848.

Parashar, D., Gadi, R., Mandal, T., & Mitra, A. (2005). Carbonaceous aerosol emissions from India. *Atmospheric Environment, 39*(40), 7861–7871.

Quaas, J., Boucher, O., & Lohmann, U. (2006). Constraining the total aerosol indirect effect in the LMDZ and ECHAM4 GCMs using MODIS satellite data. *Atmospheric Chemistry and Physics, 6*(4), 947–955.

Reddy, M. S., & Boucher, O. (2004). A study of the global cycle of carbonaceous aerosols in the LMDZT general circulation model. *Journal of Geophysical Research: Atmospheres (1984–2012)*, *109*(D14).

Reddy, M. S., Boucher, O., Balkanski, Y., & Schulz, M. (2005). Aerosol optical depths and direct radiative perturbations by species and source type. *Geophysical Research Letters, 32*(12).

Roden, C. A., Bond, T. C., Conway, S., & Pinel, A. B. O. (2006). Emission factors and real-time optical properties of particles emitted from traditional wood burning cookstoves. *Environmental Science and Technology, 40*(21), 6750–6757.

Roden, C. A., Bond, T. C., Conway, S., Osorto Pinel, A. B., MacCarty, N., & Still, D. (2009). Laboratory and field investigations of particulate and carbon monoxide emissions from traditional and improved cookstoves. *Atmospheric Environment*, *43*(6), 1170–1181.

Saud, T., Gautam, R., Mandal, T., Gadi, R., Singh, D., Sharma, S., et al. (2012). Emission estimates of organic and elemental carbon from household biomass fuel used over the Indo-Gangetic Plain (IGP), India. *Atmospheric Environment, 61*, 212–220.

Schultz, M. G., Heil, A., Hoelzemann, J. J., Spessa, A., Thonicke, K., Goldammer, J. G., et al. (2008). Global wildland fire emissions from 1960 to 2000. *Global Biogeochemical Cycles, 22*(2).

Schulz, M., Balkanski, Y. J., Guelle, W., & Dulac, F. (1998). Role of aerosol size distribution and source location in a three-dimensional simulation of a Saharan dust episode tested against satellite-derived optical thickness. *Journal of Geophysical Research: Atmospheres (1984–2012), 103*(D9), 10579–10592.

Seinfeld, J., & Pandis, S. (1998). *Atmospheric chemistry and physics* (pp. 1326). Hoboken, NJ: Wiley.

Shen, G., Yang, Y., Wang, W., Tao, S., Zhu, C., Min, Y., et al. (2010). Emission factors of particulate matter and elemental carbon for crop residues and coals burned in typical household stoves in China. *Environmental Science and Technology, 44*(18), 7157–7162.

Shen, G., Siye, W., Wen, W., Yanyan, Z., Yujia, M., Bin, W., et al. (2012). Emission factors, size distributions, and emission inventories of carbonaceous particulate matter from residential wood combustion in rural China. *Environmental Science and Technology, 46*(7), 4207–4214.

Shen, G., Tao, S., Wei, S., Chen, Y., Zhang, Y., Shen, H., et al. (2013). Field measurement of emission factors of PM, EC, OC, Parent, Nitro-, and Oxy-Polycyclic Aromatic Hydrocarbons for Residential Briquette, Coal Cake, and Wood in Rural Shanxi, China. *Environmental science & Technology, 47*(6), 2998–3005.

Sjödin, Å., & Andréasson, K. (2000). Multi-year remote-sensing measurements of gasoline light-duty vehicle emissions on a freeway ramp. *Atmospheric Environment, 34*(27), 4657–4665.

Slinn, S., & Slinn, W. (1980). Predictions for particle deposition on natural waters. *Atmospheric Environment (1967), 14*(9), 1013–1016.

Statistics South Africa. (2009). *Energy accounts for South Africa: 2002–2006*. Pretoria.

Streets, D., Bond, T., Carmichael, G., Fernandes, S., Fu, Q., He, D., et al. (2003). An inventory of gaseous and primary aerosol emissions in Asia in the year 2000. *Journal of Geophysical Research: Atmospheres (1984–2012), 108*(D21).

Streets, D. G., Gupta, S., Waldhoff, S. T., Wang, M. Q., Bond, T. C., & Yiyun, B. (2001). Black carbon emissions in China. *Atmospheric Environment, 35*(25), 4281–4296.

Streets, D. G., Hao, J., Wu, Y., Jiang, J., Chan, M., Tian, H., & Feng, X. (2005). Anthropogenic mercury emissions in China. *Atmospheric Environment, 39*(40), 7789–7806.

Subramanian, R., Winijkul, E., Bond, T. C., Thiansathit, W., Oanh, N. T. K., Paw-Armart, I., & Duleep, K. (2009). Climate-relevant properties of diesel particulate emissions: Results from a piggyback study in Bangkok. *Thailand. Environmental Science & Technology, 43*(11), 4213–4218.

Sun, X. (2006). *Authorities work on SO2 trade system*.

Szopa, S., Balkanski, Y., Schulz, M., Bekki, S., Cugnet, D., Fortems-Cheiney, A., et al. (2013). Aerosol and ozone changes as forcing for climate evolution between 1850 and 2100. *Climate Dynamics, 40*(9–10), 2223–2250.

Tata Energy Research Institute. (2008). *Tata energy directory and data yearbook 2007*. New Delhi, India.

The World Bank. (2010). *World development indicators.* Retrieved from http://databank.worldbank.org/ddp/home.do.

Tiedtke, M. (1989). A comprehensive mass flux scheme for cumulus parameterization in large-scale models. *Monthly Weather Review, 117*(8), 1779–1800.

Tsyro, S. (2002). First estimates of the effect of aerosol dynamics in the calculation of PM10 and PM2. 5. *EMEP Report, 4*(02).

Turkish Statistical Institute. (2010). *Turkish statistical institute regional statistics 2007*. Retrieved from http://tuikapp.tuik.gov.tr/Bolgesel/sorguSayfa.do?target=tablo.

Ummel, K. (2012). *CARMA revisited: An updated database of carbon dioxide emissions from power plants worldwide*. Center for Global Development, Working Paper 304.

United Nations Industrial Development Organization. (2008). *International yearbook of industrial statistics 2008*. Cheltenham, UK.

United Nations Statistics Division. (1995). *United Nations energy statistics, 1950–1995*. New York: United Nations Statistics Division.

United Nations Statistics Division. (2010). *Environmental indicators: Waste*. Retrieved from http://unstats.un.org/unsd/environment/qindicators.htm.

United States Environmental Protection Agency. (2006). *Mexico national emissions inventory*. Retrieved from http://www.epa.gov/ttn/chief/net/mexico.html.

United States Environmental Protection Agency. (2011). *National emissions inventory data & documentation* (NC: USEPA, Research Triangle Park). Retrieved from http://www.epa.gov/ttn/chief/net/2008inventory.html.

URS. (2003). *Corporation EME greenhouse gas emission factor review—final technical memorandum.* Austin, Texas.

US Department of Energy. (2000). *Instructions for form EIA 1605 voluntary reporting of greenhouse gases, Appendix B—Fuel and energy source codes and emission coefficients*. Retrieved from http://www.eia.gov/oiaf/1605/reportingformprelaunch.html.

US Energy Information Administration. (2008). *State energy data*. from http://www.eia.gov/state/.

US Geological Survey. (2010). *Cement statistics and information 2007*. Retrieved from http://minerals.usgs.gov/minerals/pubs/commodity/cement/.

van der Werf, G. R., Randerson, J. T., Giglio, L., Collatz, G., Mu, M., Kasibhatla, P. S., et al. (2010). Global fire emissions and the contribution of deforestation, savanna, forest, agricultural, and peat fires (1997–2009). *Atmospheric Chemistry and Physics*, *10*(23), 11707–11735.

Van Leer, B. (1977). Towards the ultimate conservative difference scheme. IV. A new approach to numerical convection. *Journal of Computational Physics, 23*(3), 276–299.

Vautard, R., Beekmann, M., Honoré, C., & Martel, F. (2000). Prévisibilité et prévision des pics de pollution en région parisienne.

Vautard, R., Honore, C., Beekmann, M., & Rouil, L. (2005). Simulation of ozone during the August 2003 heat wave and emission control scenarios. *Atmospheric Environment, 39*(16), 2957–2967.

Vautard, R., Beekmann, M., Bessagnet, B., Blond, N., Hodzic, A., Honoré, C., et al. (2004). *The use of MM5 for operational ozone/NOx/aerosols prediction in Europe: Strengths and weaknesses of MM5.* Paper presented at the Workshop Papers from the 5th WRF & 14th MM5 Users' Workshop.

Vautard, R., Builtjes, P., Thunis, P., Cuvelier, C., Bedogni, M., Bessagnet, B., et al. (2007). Evaluation and intercomparison of Ozone and PM10 simulations by several chemistry transport models over four European cities within the City Delta project. *Atmospheric Environment, 41*(1), 173–188.

Wang, C., Corbett, J. J., & Firestone, J. (2008). Improving spatial representation of global ship emissions inventories. *Environmental Science and Technology, 42*(1), 193–199.

Wang, R., Tao, S., Shen, H., Wang, X., Li, B., Shen, G., et al. (2012a). Global emission of black carbon from motor vehicles from 1960 to 2006. *Environmental Science and Technology, 46*(2), 1278–1284.

Wang, R., Tao, S., Wang, W., Liu, J., Shen, H., Shen, G., et al. (2012b). Black carbon emissions in China from 1949 to 2050. *Environmental Science and Technology, 46*(14), 7595–7603.

Wang, R., Tao, S., Ciais, P., Shen, H., Huang, Y., Chen, H., et al. (2013). High-resolution mapping of combustion processes and implications for CO2 emissions. *Atmospheric Chemistry and Physics, 13*(10), 5189–5203.

Wang, R., Tao, S., Balkanski, Y., Ciais, P., Boucher, O., Liu, J., et al. (2014a). Exposure to ambient black carbon derived from a unique inventory and high-resolution model. *Proceedings of the National Academy of Sciences, 111*(7), 2459–2463.

Wang, R., Tao, S., Shen, H., Huang, Y., Chen, H., Balkanski, Y., et al. (2014b). Trend in global black carbon emissions from 1960 to 2007. *Environmental science & technology.*

Watson, J. C., Chow, J., & Chen, L. (2005). Summary of organic and elemental carbon/black carbon analysis methods and intercompari- sons. *Aerosol Air Quality Research, 5*(1), 65–102.

Westerdahl, D., Wang, X., Pan, X., & Zhang, K. M. (2009). Characterization of on-road vehicle emission factors and microenvironmental air quality in Beijing, China. *Atmospheric Environment, 43*(3), 697–705.

Wheeler, D., & Ummel, K. (2008). *Calculating CARMA: Global estimation of CO2 emissions from the power sector*. Center for Global Development, Working Paper 145.

Williams, D. J., Milne, J. W., Quigley, S. M., Roberts, D. B., & Kimberlee, M. C. (1989). Particulate emissions from 'in-use' motor vehicles—II. Diesel vehicles. *Atmospheric Environment, 23*, 2647–2661.

Xu, Y. (2010). Improvements in the operation of SO2 scrubbers in China's coal power plants. *Environmental Science and Technology, 45*(2), 380–385.

Yevich, R., & Logan, J. A. (2003). An assessment of biofuel use and burning of agricultural waste in the developing world. *Global Biogeochemical Cycles, 17*(4).

Zhang, H., Ye, X., Cheng, T., Chen, J., Yang, X., Wang, L., & Zhang, R. (2008a). A laboratory study of agricultural crop residue combustion in China: Emission factors and emission inventory. *Atmospheric Environment, 42*(36), 8432–8441.

Zhang, Y., Schauer, J. J., Zhang, Y., Zeng, L., Wei, Y., Liu, Y., & Shao, M. (2008b). Characteristics of particulate carbon emissions from real-world Chinese coal combustion. *Environmental Science and Technology, 42*(14), 5068–5073.

Zhang, Q., Streets, D. G., Carmichael, G. R., He, K., Huo, H., Kannari, A., et al. (2009). Asian emissions in 2006 for the NASA INTEX-B mission. *Atmospheric Chemistry and Physics, 9*(14), 5131–5153.

Zhang, Y., & Tao, S. (2009). Global atmospheric emission inventory of polycyclic aromatic hydrocarbons (PAHs) for 2004. *Atmospheric Environment, 43*(4), 812–819.

Zhang, Y., Tao, S., Cao, J., & Coveney, R. M. (2007). Emission of polycyclic aromatic hydrocarbons in China by county. *Environmental Science and Technology, 41*(3), 683–687.

Zhi, G., Chen, Y., Feng, Y., Xiong, S., Li, J., Zhang, G., et al. (2008). Emission characteristics of carbonaceous particles from various residential coal-stoves in China. *Environmental Science and Technology, 42*(9), 3310–3315.

Chapter 4
Development of a High-Resolution Fuel Consumptions Database

4.1 Global Fuel Consumption by Sector in 2007

According to PKU-FUEL-2007, global total fuel consumption by 64 sub-types of combustion source in 2007 was 534 EJ/year. The total fuel consumption was mainly contributed by petroleum (154 EJ/year), coal (133 EJ/year) and natural gas (124 EJ/year), followed by biomass (11.4 EJ/year) and solid waste fuels (3.59 EJ/year). By sector, a total fuel consumption of 185, 114, 72, 93, 11, and 59 EJ/year was consumed by energy production, industry, residential/commercial sectors, transportation, agriculture, and wildfires, respectively. According to PKU-CO2-2007, a total CO_2 of 11.2 Pg C/year was emitted by all 64 fuel sub-types in 2007. The largest contribution was from energy production (3.8 Pg C/year), followed by industry (2.1 Pg C/year), wildfires (1.8 Pg C/year), transportation (1.7 Pg C/year), residential/commercial (1.7 Pg C/year), and agriculture (0.23 Pg C/year). Table 4.1 lists the fuel consumption and CO_2 emission from each fuel sub-type.

Globally, fossil fuels, biomass, and solid waste fuels emitted 7.8, 3.2, and 0.22 Pg C/year, respectively. Note that a large fraction of CO_2 emission from biomass burning can be turned back to the biosphere in the following growth of biomass after they are burnt. The CO_2 emissions from fossil fuels are comparable to the 7.87 Pg C/year reported by the International Energy Agency (International Energy Agency 2010a), because the fuel data used in PKU-FUEL-2007 are taken from the International Energy Agency (International Energy Agency 2010b, c) except for the U.S.A. and China, and the estimation methods are similar using the sector-based emission factors for each fuel sub-type (International Energy Agency 2010a). However, our estimated fossil fuel emissions of CO_2 is lower than the 9.06 Pg C/year from the U.S. Energy Information Administration (2010). It's likely due to the fact that U.S. Energy Information Administration included the fuels that are not used for purpose other for combustion (i.e. lubricant).

R. Wang, *Global Emission Inventory and Atmospheric Transport of Black Carbon*,
Springer Theses, DOI 10.1007/978-3-662-46479-3_4

Table 4.1 Energy and CO_2 emissions from 64 fuel sub-types and cement production in 2007

Sector	Fuel	Sub-type	Energy (EJ/year)	CO_2 (Tg C/year)	P (%)
Energy production	Coal	Anthracite	0.875	22.37	0.19
		Coke	0.765	21.00	0.18
		Bituminous coal	90.142	2147.28	18.47
		Lignite	20.313	512.43	4.41
		Peat	0.342	9.21	0.08
	Petroleum	Gas/diesel	2.806	49.75	0.43
		Residue fuel oil	7.696	136.78	1.18
		Natural gas liquids	0.001	0.01	0.00
	Gas	Dry natural gas	48.821	662.63	5.70
		Natural gas flaring	5.348	73.56	0.63
	Biomass	Solid biomass	6.487	150.98	1.30
		Biogas	0.099	5.57	0.05
	Waste	Municipal waste	0.951	21.02	0.18
		Industrial waste	0.222	4.76	0.04
	Sub-total		184.704	3800.02	32.68
Industry	Coal	Coke production	2.345	84.82	0.73
		Brick production	8.895	216.89	1.87
		Aluminum production	0.547	18.49	0.16
		Anthracite	1.098	28.42	0.24
		Coke	0.668	18.57	0.16
		Bituminous coal	15.581	374.74	3.22
		Lignite	0.659	16.73	0.14
		Peat	0.031	0.82	0.01
	Petroleum	Gas/diesel	5.847	111.45	0.96
		Residue fuel oil	5.108	102.65	0.88
		Petroleum refinery	15.683	216.33	1.86
		Natural gas liquids	0.059	0.97	0.01
	Gas	Dry natural gas	46.100	639.56	5.50
	Biomass	Solid biomass	6.487	180.80	1.55
		Biogas	0.099	1.61	0.01
	Waste	Municipal waste	0.015	0.33	0.00
		Industrial waste	0.226	5.09	0.04
	Sub-total		114.379	2018.27	17.36
Residential and commercial	Coal	Anthracite	0.074	2.56	0.02
		Coke	0.005	0.12	0.00
		Bituminous coal	2.620	80.37	0.69
		Lignite	0.274	10.07	0.09
		Peat	0.018	0.52	0.00
	Petroleum	Liquid petroleum gas	4.858	88.98	0.77
		Natural gas liquids	0.003	0.05	0.00
		Kerosene used	2.496	55.92	0.48

(continued)

Table 4.1 (continued)

Sector	Fuel	Sub-type	Energy (EJ/year)	CO_2 (Tg C/year)	*P* (%)
	Gas	Dry natural gas	20.048	393.32	3.38
	Biomass	Biogas	0.234	3.56	0.03
		Firewood	16.255	553.45	4.76
		Straw	17.879	375.88	3.23
		Dung cake	2.326	54.68	0.47
	Waste	Small-scaled solid waste burning	2.178	48.27	0.42
	Sub-total		72.346	1667.74	14.34
Transportation	Petroleum	Motor vehicle gasoline	41.862	755.29	6.50
		Aviation gasoline	0.057	1.02	0.01
		Jet kerosene	4.877	89.56	0.77
		Motor vehicle gas/diesel	33.334	634.98	5.46
		Ocean tanker	2.144	35.94	0.31
		Ocean container ships	1.608	26.96	0.23
		Bulk and combined carriers	1.488	25.39	0.22
		General cargo vessels	2.600	44.36	0.38
		Non-cargo vessels	1.744	30.27	0.26
		Auxiliary engines	0.616	10.76	0.09
		Military vessels	0.355	7.93	0.07
	Biomass	Liquid biofuels used by vehicles	2.231	42.44	0.36
	Sub-total		92.916	1704.91	14.66
Agriculture	Petroleum	Gas/diesel used in agriculture	6.264	85.27	0.73
	Waste	Open burning of agriculture waste	4.464	145.03	1.25
	Sub-total		10.728	230.30	1.98
Wildfires	Biomass	Forest fires	5.811	193.90	1.67
		Deforestation fires	14.570	489.52	4.21
		Peat fires	1.372	46.07	0.40
		Woodland fires	8.527	286.34	2.46
		Savanna fires	28.620	801.64	6.89
	Sub-total		58.900	1817.48	15.63
Total			533.972	11238.72	96.65

Contribution (*P*) of CO_2 emission from each fuel sub-type is shown in the last column

Figure 4.1 compares the CO_2 emissions from the U.S.A. and China between the PKU-CO2-2007 inventory and other inventories (British Petroleum 2008; Guo et al. 2010; Li et al. 2010; U.S. Energy Information Administration 2010; Wang et al. 2010; Oda and Maksyutov 2011). Our estimates are lower than that by

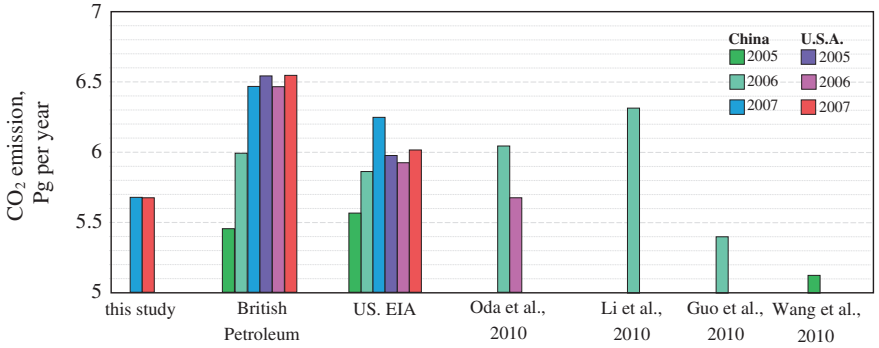

Fig. 4.1 Comparison of the national CO_2 emissions in China and U.S.A. between this study and previous inventories (British Petroleum 2008; Guo et al. 2010; Li et al. 2010; U.S. Energy Information Administration 2010; Wang et al. 2010; Oda and Maksyutov 2011)

British Petroleum (2008), U.S. Energy Information Administration (2010), the ODIAC inventory (Oda and Maksyutov 2011). The difference can be attributed to different data used for the fuel consumptions, as well as different CO_2 emission factors applied.

Figure 4.2 shows the relative contributions of different sectors to the total fuel consumption and CO_2 emissions in PKU-FUEL-2007 and PKU-CO2-2007. For both energy consumption and CO_2 emissions, the energy production is the largest contributor (34 %), followed by the industry (21 % in total fuel consumption and 18 % in total CO_2 emissions) and transportation. A lower contribution to CO_2 emissions by industry and transportation than that by energy production is due to a greater contribution of petroleum and gas used in the industry and transportation. It should be noted that our estimations are based on the fuel consumed by each sector. In fact, there is an exchange of energy produced by different sectors. For example, the fuels consumed in power plants can be used in other sectors like industry, agriculture, and residential and commercial sectors. Therefore, our profile based on the fuel consumption could be different from the profile based on terminal use of energy (Davis et al. 2010).

Figure 4.3 shows the contributions of each region to the global total fuel consumption in 2007. The largest contributor is East Asia (21 %) due to a fast rise of energy demand in developing countries (e.g. China) and several developed countries (e.g. Japan and South Korea), followed by Europe (18 %) and North America (17 %). The regional contributions should be considered when making mitigation policies in each region.

Based on the national fuel consumption, CO_2 emissions and populations (Oak Ridge National Laboratory 2008) in 2007, the global average per capital fuel consumption and CO_2 emission was 0.0733 TJ/(cap year) and 1.51 Mg C/(cap year),

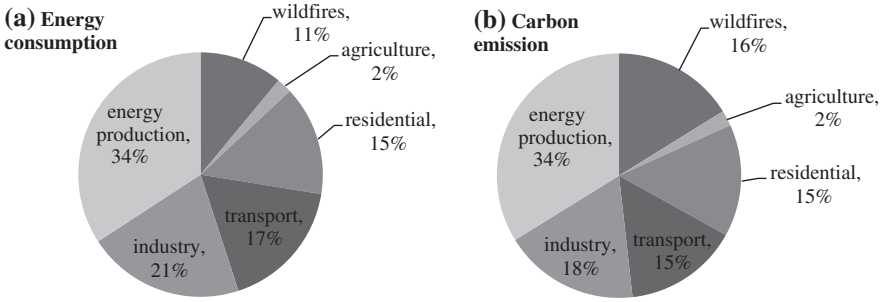

Fig. 4.2 Relative contributions of different sectors to the global total fuel consumptions (**a**) and CO_2 emissions (**b**) in 2007

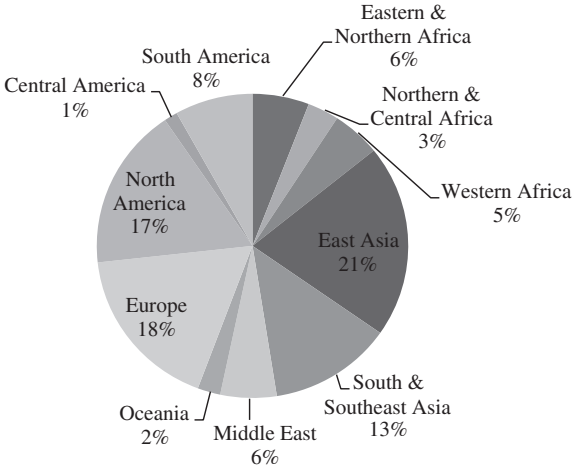

Fig. 4.3 Contributions by different regions to the global total energy consumption in 2007

respectively. For fossil fuels, the per capital fuel consumption and CO_2 emission was 0.0650 TJ/(cap year) and 1.22 Mg C/(cap year), respectively. There is a large variation of per capital fuel consumption and CO_2 emission among different countries. The per capital consumption of fossil fuels as an average of all developed countries was 0.172 TJ/(cap year)), which is approximately four times of that as an average of all developing countries (0.0414 TJ/(cap year)). Figure 4.4 shows the per capital CO_2 emission in representative developing and developed countries in 2007. The per capital CO_2 emission in developed countries was an order of 2–10 factors of that in developing countries. For example, the per capital CO_2 emission was 1.54 and 0.64 Mg C/(cap year) for China and India, compared to 5.62 and 3.62 Mg C/(cap year) in U.S.A and Germany, respectively.

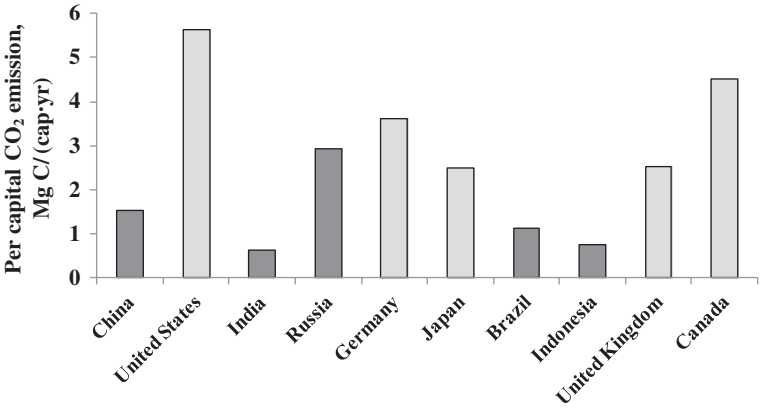

Fig. 4.4 Per capital CO_2 emission in representative developing and developed countries in 2007

4.2 High-Resolution Maps of Fuel Consumptions

According to the constructed PKU-FUEL-2007 inventory, the spatial distribution of total fuel consumptions in 2007 is mapped at a high resolution of $0.1° \times 0.1°$ (Fig. 4.5). High fuel consumption densities were mainly found over East-southeast Asia, Western Europe, the central and east-south coastal plains of the U.S.A., the Indian subcontinent, the Amazon prairie and Brazil plateau, Congo basin and surrounding highlands in central and southern Africa. The fuel consumption over ocean were contributed by shipping and aviation, which were largely distributed over Atlantic and Pacific in North Hemisphere expanding from the tropical oceans to the Arctic in latitude. The fuel consumption can be identified as the human-induced and natural sectors. The human-induced combustion occurs mainly in populated regions, and natural fires were generally distributed in the region with sufficient amounts of dry biomass. The spatial patterns of human-induced and natural activities decide the spatial pattern of total fuel consumptions, and influence the distributions of emissions of CO_2 and other air pollutants.

The relatively contributions by sector (excluding aviation and shipping, which are mainly distributed over oceans) to the total fuel consumption in 9 major regions are shown as pie charts in Fig. 4.6. Energy production was the most important single contributing sector in North America (38 %), Europe (48 %) and East Asia (49 %), while wildfires were the dominating source in South America (51 %), Africa (63 %) and Oceania (40 %). Fuels used in residential sector contributed 30, 25, 20 and 20 % to total fuel consumptions in South and Southeast Asia, Western and Central Africa, East Asia, Middle East, respectively and less than 10 % in other regions. Petroleum consumption by mobile sources was the second largest sources in North America (32 %) and Europe (20 %).

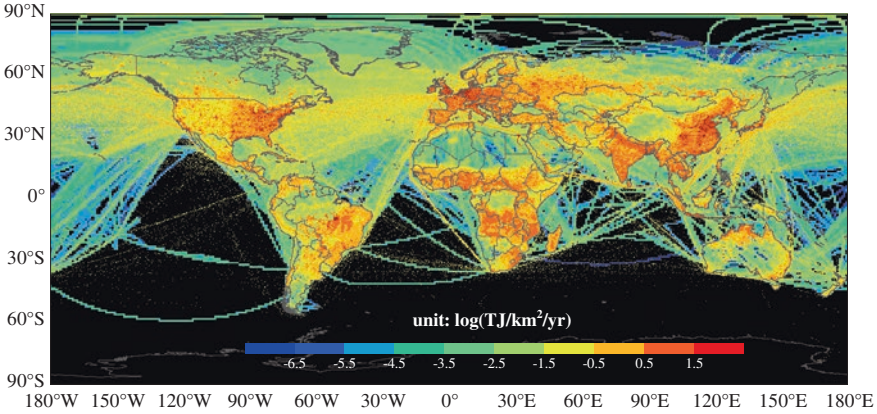

Fig. 4.5 Geographic distribution of total fuel consumptions from 64 types of fuel sub-type at a resolution of 0.1° × 0.1° in 2007. The *color* legend is in log scale

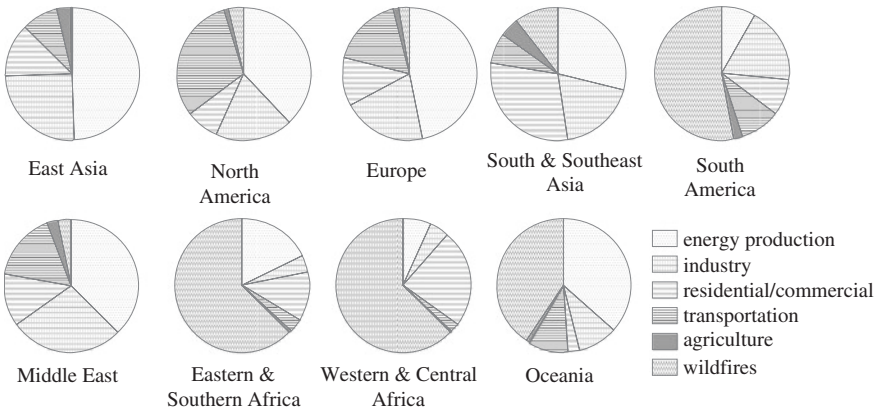

Fig. 4.6 Relative contributions by sector to the total fuel consumption in each region in 2007. Aviation and shipping, mainly distributed over oceans, are excluded

The relatively contributions by type of fuel to the total fuel consumption in the 9 major regions are also shown as pie charts in Fig. 4.7. The figure illustrates different fuel profiles in different regions. For example, coal and biomass (mainly as solid biofuel) was the dominating fuel in Africa, East Asia and South and Southeast Asia, associated with higher emission factors for pollutants, such as BC, organic matters, and mercury. In contrast, petroleum and gas fuels contribute more than half in the developed countries over North America and Europe. It is expected that the fuel profile in the developing countries will change with a larger contribution by petroleum and gas in the future (Streets et al. 2004).

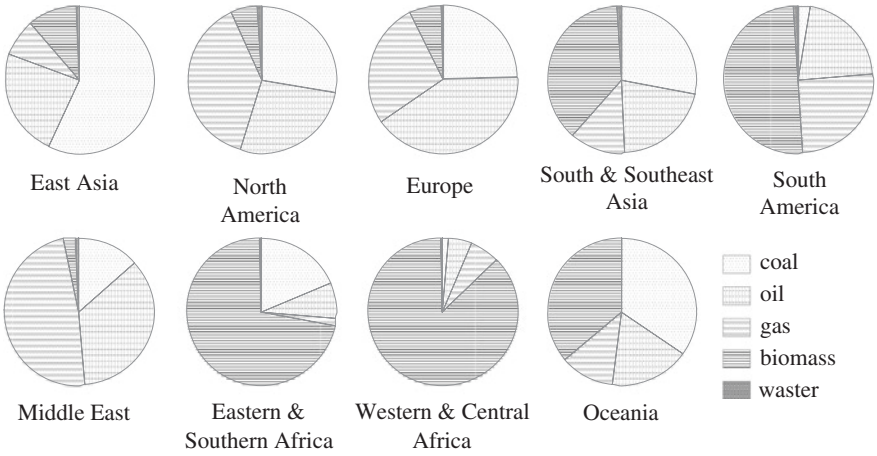

Fig. 4.7 Relative contributions by type of fuel to the total fuel consumption in each region in 2007

4.3 High-Resolution Maps of CO_2 Emissions

Based on the PKU-FUEL-2007 inventory, a global high-resolution map of CO_2 emission from combustion of 64 types of fuel (PKU-CO2-2007) was produced at a resolution of 0.1° × 0.1° (Fig. 4.8). The spatial pattern of CO_2 emissions is close to that of the fuel consumption, since the variation of CO_2 emission factors among different fuel types is less than the spatial variation of fuel consumptions. Nevertheless, the CO_2 emission densities in the east, southeast and southwest of China were higher than the west and north of China due to higher carbon contents in coal, while the CO_2 emission densities in Africa and South America are lower than Western Europe and Asia due to low contents of carbon in biomass. Globally, the Western Europe is the second most important CO_2 emission region after East Asia, due to high fuel consumptions by power plants and motor vehicles. There was a cluster of high CO_2 emissions over the Indo-Gangetic Plain in South Asia, where population density is high, leading to high fuel consumption by domestic sources. In North America, the emissions were sparsely distributed over the eastern and western of the U.S.A, in agreement with the distribution of population (Oak Ridge National Laboratory 2008).

The relatively contributions by sector (excluding aviation and shipping, mainly distributed over oceans) to total CO_2 emissions in the 9 major regions are shown as pie charts in Fig. 4.9. Regionally, energy production was the major contributor in North America (39 %), Western Europe (47 %), and East Asia (50 %), while wildfires were dominating in Africa (62 %), South America (60 %), and Oceania (41 %).

Based on the gridded CO_2 emissions (0.1° × 0.1°) and population distribution (8 × 8 km, downscaled to 0.1° × 0.1°) (Oak Ridge National Laboratory 2008), the per capital CO_2 emission from combustion excluding wildfires was mapped

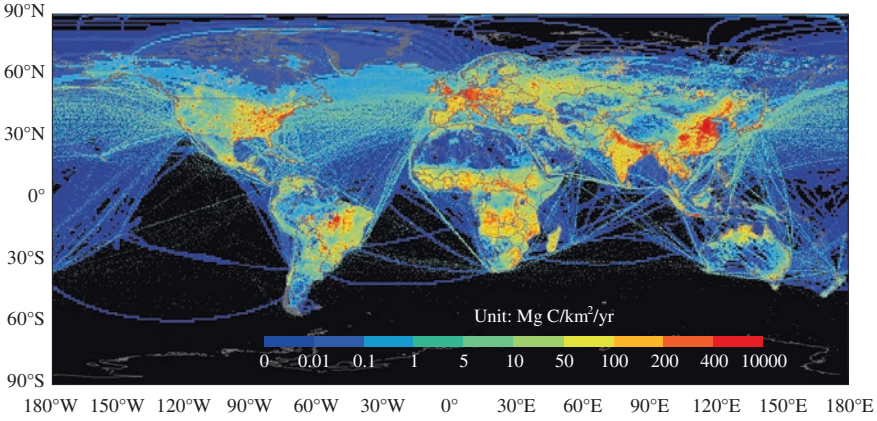

Fig. 4.8 Geographic distribution of CO_2 emissions from combustion of 64 fuel sub-types at a resolution of 0.1° × 0.1° in 2007. Reproduced from with permission (Wang et al. 2013); link to the original image: http://www.atmos-chem-phys.net/13/5189/2013/acp-13-5189-2013.html

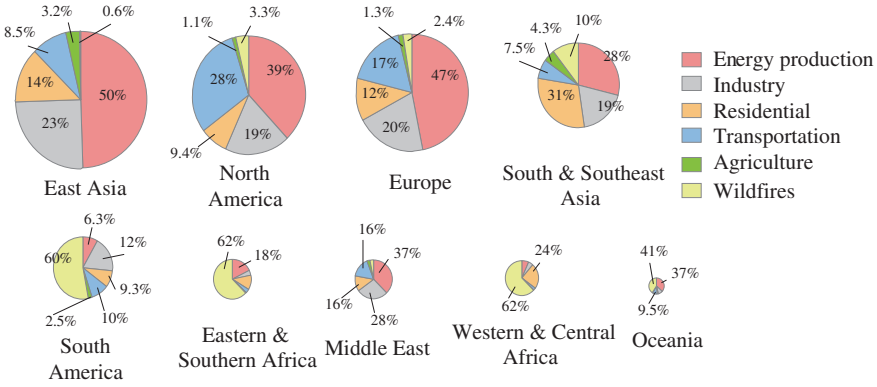

Fig. 4.9 Relative contributions by sector to total CO_2 emissions in 9 regions in 2007. Aviation and shipping, mainly distributed over oceans, are excluded. The area of each pie is proportional to total CO_2 emissions in the region

at a resolution of 0.1° × 0.1° (Fig. 4.10). Traditionally, the fuel consumptions and related emissions are compiled at provincial or national level before being disaggregated to grids using population as a proxy (Marland et al. 1985; Penner et al. 1993; Andres et al. 1996; Streets et al. 2001; Bond et al. 2004; Pacyna et al. 2006; Lamarque et al. 2010), by assuming that the per capital fuel consumption and related emissions are uniform within a province or country. However, this assumption is far from true, as illustrated by the per capital CO_2 emission produced in our work. For example, the per capital CO_2 emission in Shanxi province, Guizhou province, and the southeast coastal regions was 2–5 factors higher than that in the

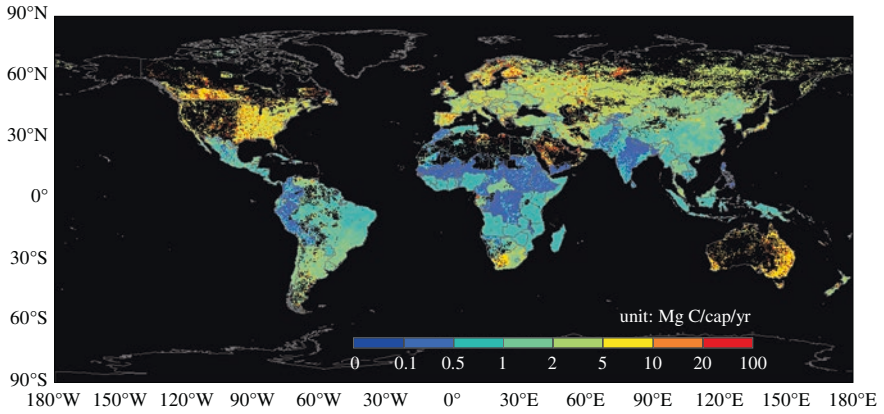

Fig. 4.10 Geographic distribution of per capital CO_2 emission from combustion excluding wildfires at a resolution of 0.1° × 0.1° in 2007. Aviation and shipping, mainly distributed over oceans, are excluded. Reproduced from with permission (Wang et al. 2013); link to the original image: http://www.atmos-chem-phys.net/13/5189/2013/acp-13-5189-2013.html

western and northern of China. In North America, higher per capital CO_2 emission was observed in the central of the U.S.A., where industry was concentrated and the population was sparsely distribution. The inhomogeneous distribution of per capital CO_2 emission in space indicates a large bias when allocating the fuel consumption to grids using population as a simple proxy.

Based on the map of per capital CO_2 emission, per capital CO_2 emission over urban and rural areas were estimated and compared to each other. To do this, in each country, a population density threshold was used to define urban and rural areas, using the urbanization rate record from the World Bank (The World Bank 2010) and the global distribution of population density in 2007 (Oak Ridge National Laboratory 2008). In brief, the population density threshold for urban region was varied from 0 to 10,000 person per km^2 at an step of 1 person per km^2, and then the fraction of urban population calculated using this threshold was calculated and compared with the recorded fraction of urban population (The World Bank 2010). The population density threshold producing an urban population closest to the recorded fraction was decided for each country, with which the global mask of urban areas was derived. Using this urban mask, per capital CO_2 emission over urban and rural areas was mapped respectively (Fig. 4.11). The per capital CO_2 emissions over urban and rural areas are dependent on the gridded CO_2 emissions. As a result, high per capital CO_2 emissions over urban areas were found in many developing countries, and per capital CO_2 emissions over rural areas were significantly lower than that in developed countries. This is understandable for the fact that industry and transportation are concentrated in cities of developing countries. Note that more and more people are moving from rural to urban areas in developing countries, namely “fast urbanization”, it will unavoidable result in more CO_2 emissions due to higher per capital CO_2 emissions over urban areas, which should be considered by policy makers.

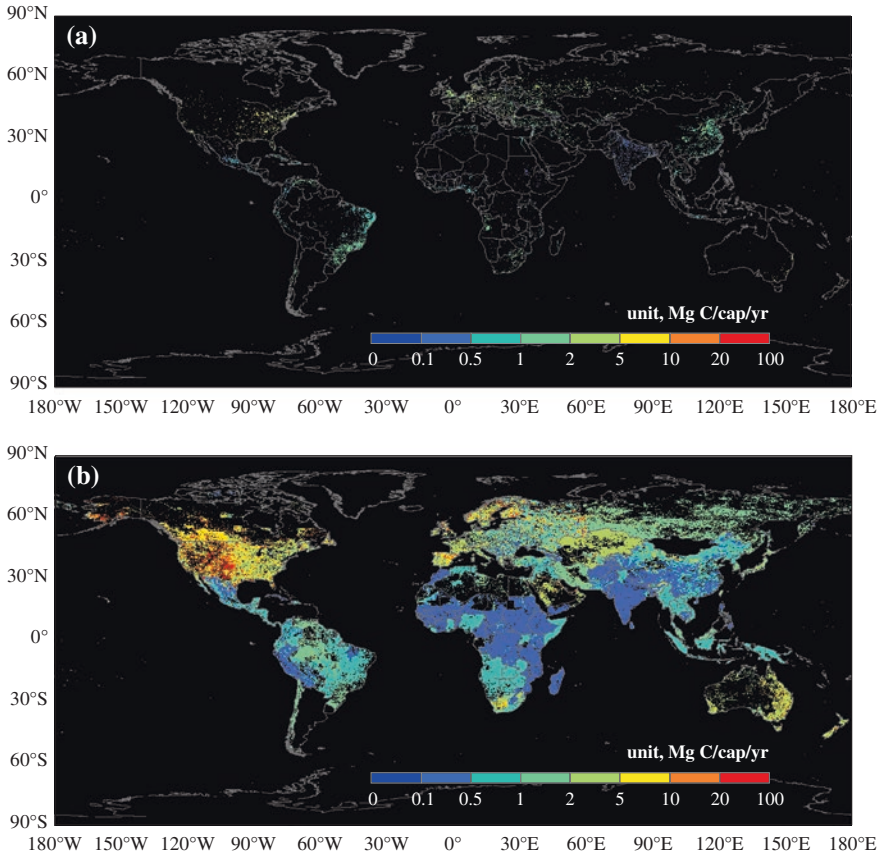

Fig. 4.11 Geographic distributions of per capital CO_2 emission from combustion excluding wildfires at a resolution of 0.1° × 0.1° over urban (**a**) and rural (**b**) areas in 2007. Aviation and shipping, mainly distributed over oceans, are excluded. Reproduced from with permission (Wang et al. 2013); link to the original image: http://www.atmos-chem-phys.net/13/5189/2013/acp-13-5189-2013.html

4.4 Comparison with a Traditionally Disaggregated Map

Different from the traditional disaggregation method, PKU-FUEL-2007 and PKU-CO2-2007 were computed from sub-national fuel consumption data in 15,197 sub-national disaggregation units, rather than disaggregated from national fuel consumptions using population as a proxy (Marland et al. 1985; Penner et al. 1993; Andres et al. 1996). The fuel consumptions by county or province or state or grid were used in 45 countries, which represent 45, 61, and 69 % of the global total area, population, and fuel consumption, respectively. To evaluate the effect of using the sub-national disaggregation method, a mock-up CO_2 emission map for sources excluding the point sources, wildfires, aviation and shipping was created

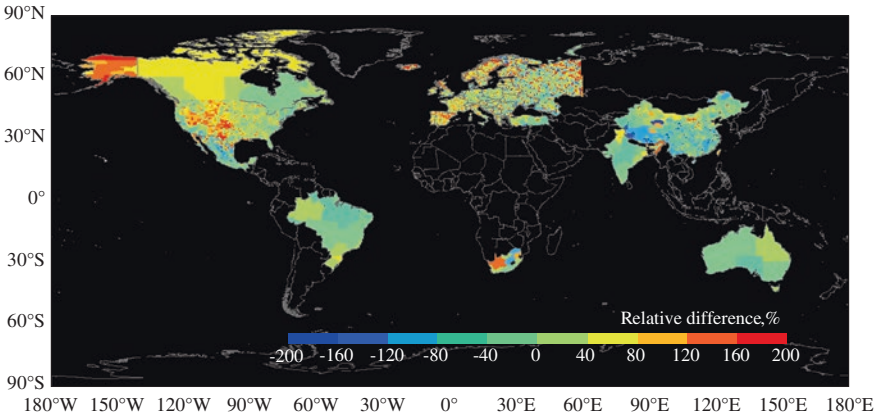

Fig. 4.12 Comparison of CO_2 emissions from combustion excluding wildfires, aviation and shipping by using our sub-national and traditional national disaggregation method. The relative differences are calculated between CO_2 emissions for each sub-national disaggregation unit. Reproduced from with permission (Wang et al. 2013); link to the original image: http://www.atmos-chem-phys.net/13/5189/2013/acp-13-5189-2013.html

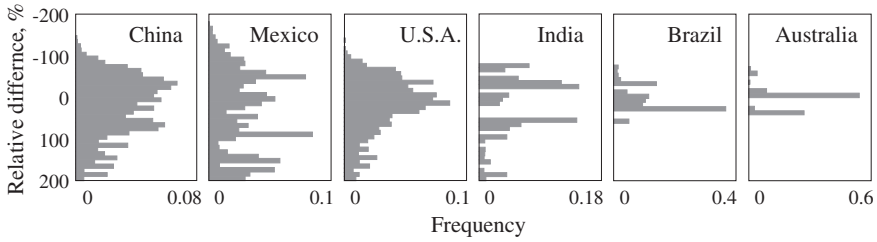

Fig. 4.13 Frequency distributions of the relative differences of CO_2 emission derived from our sub-national and traditional national disaggregation methods

using the same method as our product except that nationally aggregated fuel data and population-based proxies were applied in the 45 countries where sub-national data were used in our study. The relative differences were computed for CO_2 emission in each sub-national disaggregation unit between PKU-CO2-2007 and the mock-up CO_2 emission inventory. The fuel data in PKU-CO2-2007 were derived from the record rather than from disaggregation and thus the bias was avoided, which can be quantified by the relative differences between the two products. The relative differences of CO_2 emissions between the two products are shown in Fig. 4.12. In the 9 countries with county or state or provincial data used in our product, the relative difference as an average of sub-national disaggregation units ranges from 17.5 % (Australia) to 79.8 % (Mexico). It indicates that the bias in the disaggregated data is reduced by the same fraction.

The frequency distributions of the relative differences of CO_2 emissions for all sub-national disaggregation units between the two products were calculated

for 6 countries (Fig. 4.13). It shows that there is a large difference between the two products, indicating a systematical bias subject to traditional disaggregation method. In addition, it is found that the degree of difference between two methods (or two products) is larger in countries with higher heterogeneity of development (e.g. large developing countries) or with smaller sub-national disaggregation units used in PKU-FUEL-2007 (e.g. countries with county fuel data). In summary, it's clear that use of the fuel data at finer spatial units can help overcome the disaggregation bias in countries with higher heterogeneity of development in space.

4.5 Uncertainty of the Data

The estimated CO_2 emissions as well as the map are both associated with uncertainties. First, the fuel consumption data from the statistic varies among different energy statistics, while the input parameters used to calculate the emissions (e.g. emission factors of carbon and the prescribed combustion rates). These factors contribute to uncertainties in the estimated total CO_2 emissions. Figure 4.14 shows the frequency distribution of the estimated global CO_2 emissions in 2007 from Monte Carlo simulations. Regardless of various distributions assigned to all parameters, the estimated total CO_2 emissions follow a normal distribution. Table 4.2 lists the 90 % uncertainty ranges for each of 64 fuel sub-types. The 90 % uncertainty range varies from 18 to 20 %, depending on the input parameters for each fuel sub-type.

Table 4.2 The 90 % uncertainty ranges of the estimated CO_2 emissions for 64 fuel sub-types

Sector	Fuel	Fuel sub-type	90 % uncertainty range (Tg C/year)
Energy production	Coal	Anthracite	18.87–25.86
		Coke	17.72–24.29
		Bituminous coal	1811.35–2482.87
		Lignite	432.28–592.53
		Peat	7.77–10.65
	Petroleum	Gas/diesel	41.98–57.50
		Residue fuel oil	115.40–158.08
		Natural gas liquids	0.01–0.02
	Gas	Dry natural gas	559.04–765.87
		Natural gas flaring	62.05–85.02
	Biomass	Solid biomass	127.37–174.58
		Biogas	4.70–6.44
	Waste	Municipal waste	17.73–24.30
		Industrial waste	4.02–5.51
	Sub-total		3205.69–4393.50

(continued)

Table 4.2 (continued)

Sector	Fuel	Fuel sub-type	90 % uncertainty range (Tg C/year)
Industry	Coal	Coke production	71.59–98.05
		Brick production	182.96–250.79
		Aluminum production	15.60–21.37
		Anthracite	23.97–32.86
		Coke	15.67–21.47
		Bituminous coal	316.11–433.30
		Lignite	14.11–19.35
		Peat	0.70–0.95
	Petroleum	Gas/diesel	94.03–128.80
		Residue fuel oil	86.61–118.63
		Petroleum refinery	182.52–249.99
		Natural gas liquids	0.82–1.12
	Gas	Dry natural gas	539.58–739.27
	Biomass	Solid biomass	152.53–209.07
		Biogas	1.36–1.86
	Waste	Municipal waste	0.28–0.38
		Industrial waste	4.29–5.89
	Sub-total		1702.72–2333.17
Residential and commercial	Coal	Anthracite	2.15–2.98
		Coke	0.10–0.14
		Bituminous coal	67.50–93.32
		Lignite	8.45–11.69
		Peat	0.44–0.60
	Petroleum	Liquid petroleum gas	75.07–102.84
		Natural gas liquids	0.04–0.06
		Kerosene used	47.18–64.62
	Gas	Dry natural gas	331.83–454.64
	Biomass	Biogas	3.00–4.12
		Firewood	463.80–645.48
		Straw	316.15–435.55
		Dung cake	45.93–63.49
	Waste	Small-scaled solid waste burning	40.71–55.81
	Sub-total		1402.36–1935.34

(continued)

Table 4.2 (continued)

Sector	Fuel	Fuel sub-type	90 % uncertainty range (Tg C/year)
Transportation	Petroleum	Motor vehicle gasoline	637.21–872.88
		Aviation gasoline	0.86–1.18
		Jet kerosene	75.56–103.51
		Motor vehicle gas/diesel	535.73–733.87
		Ocean tanker	23.76–47.86
		Ocean container ships	17.82–35.90
		Bulk and combined carriers	16.78–33.80
		General cargo vessels	29.33–59.07
		Non-cargo vessels	20.01–40.31
		Auxiliary engines	7.12–14.33
		Military vessels	5.25–10.56
	Biomass	Liquid biofuels used by vehicles	35.81–49.05
	Sub-total		1405.24–2002.31
Agriculture	Petroleum	Gas/diesel used in agriculture	71.94–98.55
	Waste	Open burning of agriculture waste	121.98–168.04
	Sub-total		193.92–266.59
Wildfires	Biomass	Forest fires	128.28–258.04
		Deforestation fires	323.86–651.43
		Peat fires	30.48–61.31
		Woodland fires	189.44–381.05
		Savanna fires	530.29–1066.92
	Sub-total		1202.36–2418.75
Total			9112.29–13349.65

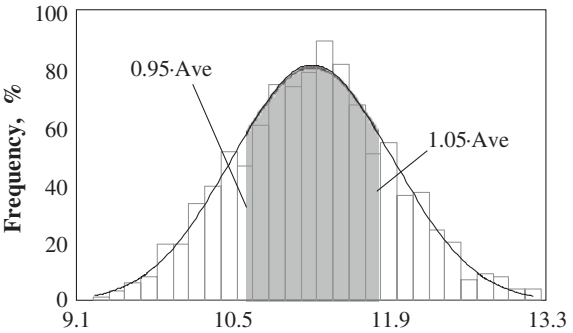

Fig. 4.14 Frequency distribution of the global total CO_2 emissions (Pg C/year) in 2007 derived from our Monte Carlo simulations

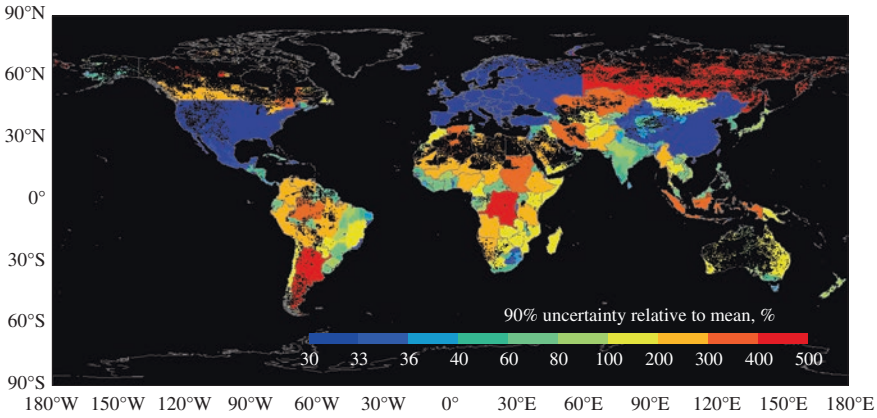

Fig. 4.15 Relative uncertainty associated with the gridded CO_2 emissions in PKU-CO2-2007. The relative uncertainty is derived as the 90 % uncertainty relative to the mean from Monte Carlo simulations for each 0.1° × 0.1° grid. Reproduced from with permission (Wang et al. 2013); link to the original image: http://www.atmos-chem-phys.net/13/5189/2013/acp-13-5189-2013.html

Second, when the fuel consumption or CO_2 emission at a spatial unit (e.g. county, province, state, or country) was disaggregated to each grid using population as a proxy, there is also a disaggregation error, since the fuel consumption or CO_2 emission is not necessarily proportional to population, just as shown in our product. An empirical equation was used by assuming that the disaggregation uncertainty is proportional to the area of sub-national disaggregation unit (see **Methods**), The uncertainty of CO_2 emission at a spatial unit and the disaggregation uncertainty were combined using a Monte Carlo simulation (see **Methods**). The 90 % uncertainty range of gridded CO_2 emission is derived and shown in Fig. 4.15. As a result, the uncertainty associated with the gridded CO_2 emission in China, U.S.A., Europe and Mexico was lower than that in other regions without using sub-national fuel data. Extremely high uncertainties were found in countries with large area and absence of local fuel data. It indicates application of sub-national fuel data at a fine resolution in these countries will further reduce uncertainty in the CO_2 emission map.

References

Andres, R. J., Marland, G., Fung, I., & Matthews, E. (1996). A 1 × 1 distribution of carbon dioxide emissions from fossil fuel consumption and cement manufacture, 1950–1990. *Global Biogeochemical Cycles, 10*(3), 419–429.

Bond, T. C., Streets, D. G., Yarber, K. F., Nelson, S. M., Woo, J. H., & Klimont, Z. (2004). A technology-based global inventory of black and organic carbon emissions from combustion. *Journal of Geophysical Research: Atmospheres (1984–2012), 109*(D14). doi:10.1029/2003JD003697.

British Petroleum. (2008). *Statistical review of world energy-2007*. Retrieved from http://www.bp.com.

Davis, S. J., Caldeira, K., & Matthews, H. D. (2010). Future CO2 emissions and climate change from existing energy infrastructure. *Science, 329*(5997), 1330–1333.

Guo, Y. Q., Zhen, J. Y., & Ge, Q. S. (2010). Study on the primary energy-related carbon dioxide emissions in China. *Geographic Research, 29*, 1027–1036.

International Energy Agency. (2010a). *CO2 emission from fuel combustion-2011 highlights*. Paris: International Energy Agency.

International Energy Agency. (2010b). *Energy statistics and balances of OECD countries 1960–2006*. Paris: International Energy Agency.

International Energy Agency. (2010c). *Energy statistics and balances of non-OECD countries 1970–2006*. Paris: International Energy Agency.

Lamarque, J.-F., Bond, T. C., Eyring, V., Granier, C., Heil, A., Klimont, Z., et al. (2010). Historical (1850–2000) gridded anthropogenic and biomass burning emissions of reactive gases and aerosols: Methodology and application. *Atmospheric Chemistry and Physics, 10*(15), 7017–7039.

Li, Y. M., Zhang, L., & Chen, X. L. (2010). A decomposition model and reduction approaches for carbon dioxide emissions in China. *Resource Science, 32*, 218–222.

Marland, G., Rotty, R., & Treat, N. (1985). CO2 from fossil fuel burning: Global distribution of emissions. *Tellus B, 37*(4–5), 243–258.

Oak Ridge National Laboratory. (2008). *LandScan global population 2007 database*. Retrieved from http://www.ornl.gov/sci/landscan/.

Oda, T., & Maksyutov, S. (2011). A very high-resolution (1 km × 1 km) global fossil fuel CO2 emission inventory derived using a point source database and satellite observations of nighttime lights. *Atmospheric Chemistry and Physics, 11*(2), 543–556.

Pacyna, E. G., Pacyna, J. M., Steenhuisen, F., & Wilson, S. (2006). Global anthropogenic mercury emission inventory for 2000. *Atmospheric Environment, 40*(22), 4048–4063.

Penner, J., Eddleman, H., & Novakov, T. (1993). Towards the development of a global inventory for black carbon emissions. *Atmospheric Environment. Part A. General Topics, 27*(8), 1277–1295.

Streets, D., Bond, T., Lee, T., & Jang, C. (2004). On the future of carbonaceous aerosol emissions. *Journal of Geophysical Research: Atmospheres (1984–2012), 109*(D24), 113.

Streets, D. G., Gupta, S., Waldhoff, S. T., Wang, M. Q., Bond, T. C., & Yiyun, B. (2001). Black carbon emissions in China. *Atmospheric Environment, 35*(25), 4281–4296.

The World Bank. (2010). *World development indicators*. Retrieved from http://databank.worldbank.org/ddp/home.do.

U.S. Energy Information Administration. (2010). *World carbon dioxide emissions from the use of fossil fuels.* Retrieved from http://www.eia.gov/cfapps/ipdbproject/IEDIndex3.cfm?tid=90&pid=44&aid=8.

Wang, J. N., Cai, B. F., Yan, G., Cao, D., & Zhou, Y. (2010). Study on carbon dioxide total emission control in the context of emission intensity commitment. *China Environmental Science, 30*, 1568–1572.

Wang, R., Tao, S., Ciais, P., Shen, H., Huang, Y., Chen, H., Shen, G., Wang, B., Li, W., & Zhang, Y. (2013). High-resolution mapping of combustion processes and implications for CO2 emissions. *Atmospheric Chemistry and Physics*, 13(10), 5189–5203.

Chapter 5
Global Black Carbon Emissions from Motor Vehicles

5.1 Regression Models of BC Emission Factors for Motor Vehicles

BC emission factors (EF_{BC}) for motor vehicles are expected to be highly variable, depending on the technology of combustion engines and dust abatement devices employed on the vehicle. Novakov et al. (2003) assumed a linear decreasing trend of diesel EF_{BC} for developed countries over time from 1965 to 1985. Bond et al. (2007) considered the decrease of EF_{BC} for gasoline and diesel vehicles based on the measured emission factors of particulate matters measured for heavy-duty vehicles in the U.S.A., and estimated the trend in BC emissions from motor vehicles. Similarly, Junker and Liousse (2008) referred to the same measurement (Yanowitz et al. 2000), and then applied a 6.8 fold decrease of EF_{BC} for gasoline and diesel vehicles between the years 1974 and 1997. In general, EF_{BC} for motor vehicles measured by various laboratories vary in orders of magnitude due to many factors including vehicle type, fuel composition, vehicle model year, marketing country, operation mode, ambient temperature, analytical method, and so on. Thus, identification of the key factors governing EF_{BC} for motor vehicles and development of a quantitative relationship between EF_{BC} and these factors is important to predict EF_{BC} for motor vehicles in countries where or years when the EF_{BC} are not measured.

A total of 385 reported EF_{BC} measured in 14 countries during the period from 1985 to 2008 were collected from 66 published papers or reports, listed in Wang et al. (2012). The data cover nine developed countries and five developing countries. Table 5.1 shows the distribution of the collected EF_{BC} by country and vehicle type. However, limitation in data availability is still a major caveat of the present work and more EF_{BC} measured over a wider range of countries will reduce the uncertainty and improve the study performed here.

R. Wang, *Global Emission Inventory and Atmospheric Transport of Black Carbon*,
Springer Theses, DOI 10.1007/978-3-662-46479-3_5

Table 5.1 Vehicle fleet compositions of collected EF_{BC} for various countries

Country	Heavy duty diesel	Light duty diesel	Light duty gasoline	Total
Australia	7	18	21	46
Austria	1	1	1	3
Canada	1	0	0	1
Finland	0	3	0	3
Germany	1	0	0	1
Greece	0	1	1	2
Switzerland	1	1	2	4
US	106	49	146	301
Brazil	1	0	1	2
China	2	0	4	6
India	2	1	1	4
Mexico	1	0	0	1
Thailand	11	0	0	11
Total	134	74	177	385

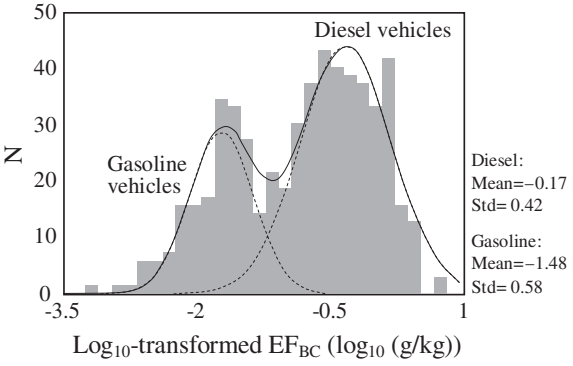

Fig. 5.1 Frequency distributions of $\log_{10}$-transformed EF_{BC} for gasoline and diesel vehicles. Log-normal distributions were fitted for diesel and gasoline vehicles. Reproduced with permission (Wang et al. 2012). Copyright (2011) American Chemical Society

First, the distributions of these EF_{BC} were tested. Among all data, after excluding the data for motorcycles and super emitters, the reported EF_{BC} varied from 0.000681 to 7.20 g/kg with a median value of 0.234 g/kg. As shown in Fig. 5.1, the frequency distribution of all EF_{BC} for motor vehicles follows a typical bimodal histogram after a log transformation ($p > 0.05$, $r^2 = 0.872$). In fact, the two populations were corresponding to gasoline and diesel vehicles, respectively. The means and standard deviations of $\log_{10}$-transformed EF_{BC} ($\log_{10}$ (g/kg)) for diesel and gasoline motor vehicles were -0.17 ± 0.42 and -1.48 ± 0.58, respectively. Therefore, the two populations were analyzed separately to evaluate other factors hereafter.

In addition, the difference of EF_{BC} for light- and heavy-duty diesel vehicles was reported in some literature (Kim Oanh et al. 2010). However, according to the data collected in our study, the difference between these two groups was not found statistically ($p = 0.946$) (see the distributions in Fig. 5.2).

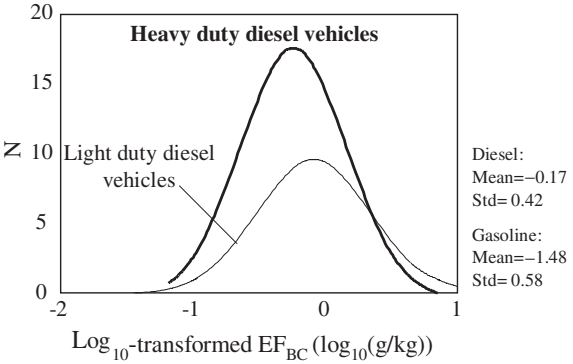

Fig. 5.2 Frequency distributions of $\log_{10}$-transformed EF_{BC} for light- and heavy-duty diesel vehicles. Reproduced with permission (Wang et al. 2012). Copyright (2011) American Chemical Society

Note that the emission factors of particulate matters for motor vehicles decreased over time due to advances in control technology and tightening of emission regulations (Yanowitz et al. 2000; Lloyd and Cackette 2001; Bond et al. 2007; Junker and Liousse 2008). For example, after the exhaust catalytic converter was introduced in mainstream gasoline vehicles in developed countries in the late 1970s, the emission factor of fine particles for motor vehicles has reduced appreciably (Hildemann et al. 1991). Since the enforcement of EURO-I and EURO-II regulations in Thailand, the emission factor of black carbon for diesel vehicles has decreased considerably (Subramanian et al. 2009). In addition, a significant difference in EF_{BC} for developed and developing countries was well anticipated (Junker and Liousse 2008). Thus, when collecting the EF_{BC} for motor vehicles, several parameters relevant to the corresponding vehicles were also recorded, including the vehicle type, vehicle in-use country, model year, measured year, method used for the analysis of BC, the run cycle of test, vehicle odometer, and ambient air temperature. These factors were tested one-by-one for their significances on the variation of EF_{BC} (after a $\log_{10}$-transformation) using analysis of variance (ANOVA) by SPSS. As a result, two factors, including the vehicle model year and the country of vehicle use (divided into three categories as the U.S.A., other developed countries, and all developing countries) were found to be significant ($p < 0.05$) for the variation of EF_{BC} (after a $\log_{10}$-transformation) for both gasoline and diesel vehicles, and ambient temperature of measurement (T) was found to be significant ($p < 0.05$) only for gasoline vehicles.

Vehicle in-use country is a category variable rather than a quantitative one, which cannot be quantified using regression models. As a common practice, separate models have been developed to predict the EF_{BC} for motor vehicles in countries in different groups (Novakov et al. 2003). This approach, however, cannot predict the differences in EF_{BC} among countries at different developing levels in a country group. To quantify the difference in EF_{BC} among different countries, a number of parameters associated with socio-technical development, including per capita gross domestic product (purchasing power parity) (GDP_c), per capita gross national income, percentage of urban population, gross domestic product per unit of energy consumption, and fuel pump prices were examined one by one. As a result, GDP_c turns out to be an ideal indicator which combines

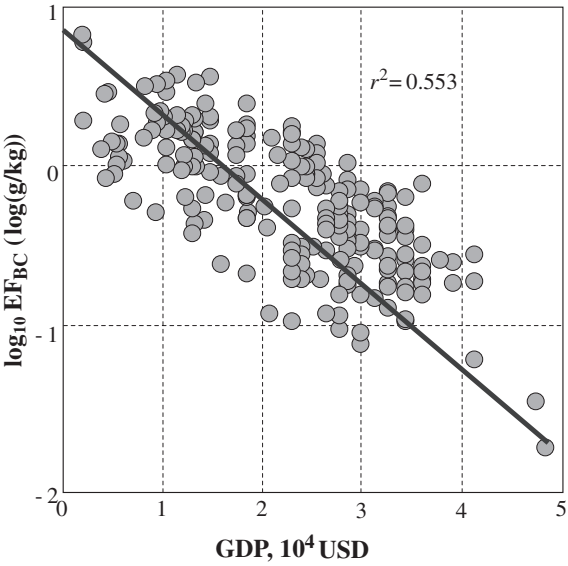

Fig. 5.3 Plots of the $\log_{10}$-transformed EF_{BC} against the independent variable GDP_c as fitting curve for diesel vehicles. Reproduced with permission (Wang et al. 2012). Copyright (2011) American Chemical Society

the impact of vehicle country and model year. The measured $\log_{10}$-transformed EF_{BC} for diesel motor vehicles is very well correlated with GDP_c (Fig. 5.3). Using GDP_c as a independent variable, the measured $\log_{10}$-transformed EF_{BC} for diesel motor vehicles can be well predicted. Note that not only the variance of EF_{BC} among countries but also the variance over time for a given country can be reflected by GDP_c.

In fact, the relationship between economic growth and technology evolution has been well evidenced. For example, in the U.S.A., a series of abatement technologies were introduced during the period from 1960 to 2007 when GDP_c has increased from 2881 to 46,723 $/cap. Since 1960s, motor vehicles engines have been enhanced by reshaping the combustion chambers, relocating the injection swirl, and modifying crevice volume and compression ratio (Yanowitz et al. 1999; Lloyd and Cackette 2001). In the late 1970s, the exhaust catalytic converter was introduced in gasoline vehicles (Hildemann et al. 1991). Since the 1980s, the transmission configuration of motor vehicle engines burning diesel fuels were improved from 3- and 4-speed to 5-speed while leaded petroleum was gradually phased out (Prucz et al. 2001). Since 1993, sulfur content in diesel was regulated to less than 50 ppm and further restricted to less than 15 ppm in 2006 (Lloyd and Cackette 2001; Ban-Weiss et al. 2008). Replacement of two-stroke by four-stroke diesel engines for and use of oxidation catalysts in transit buses occurred in 1990s (Yanowitz et al. 1999; Prucz et al. 2001). Recently, diesel particle filters have been equipped for more and more diesel engines to control the emissions of fine particles (Ban-Weiss et al. 2008; Heeb et al. 2012). Therefore, these changes were partly reflected by the increase of the GDP_c, implying a motivation of technology derived by the development of economy.

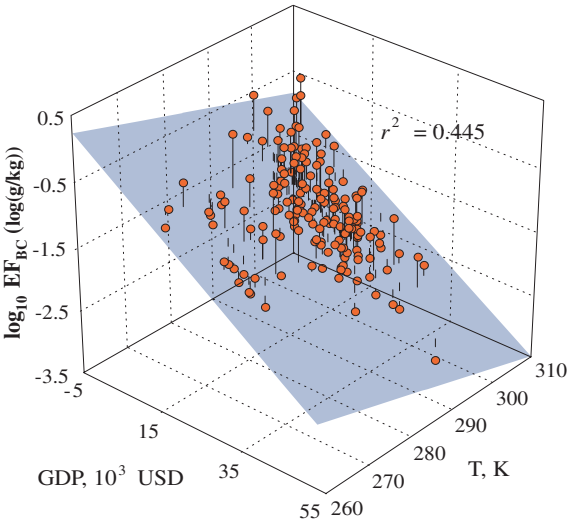

Fig. 5.4 Plots of the $\log_{10}$-transformed EF_{BC} against two independent variables (GDP_c and the ambient temperature T) as fitting plane for gasoline vehicles. Reproduced with permission (Wang et al. 2012). Copyright (2011) American Chemical Society

Similar to diesel vehicles, the $\log_{10}$-transformed EF_{BC} for gasoline vehicles were also related to GDP_c, but also ambient temperature of measurements (T), and a two-variable regression can be developed, as shown in Fig. 5.4.

Therefore, two regression models for predicting EF_{BC} for motor vehicles using GDP_c (10,000 USD/cap) and T (K, gasoline vehicle only) as independent variables were developed for diesel and gasoline vehicles respectively, expressed as:

$$\log_{10}\mathrm{EF_{BC}}(\text{diesel}) = -0.4302\,GDP_c + 0.7566, \tag{5.1}$$

$$\log_{10}\mathrm{EF_{BC}}(\text{gasoline}) = -0.7055\,GDP_c - 0.02080\,T + 5.898, \tag{5.2}$$

It should be noted that a reduced major axis method was used for regression analysis, because the dependent and independent variables were both associated with random error. As a result, loss function, defined as the quadratic sum of difference between the predicted and measured data, was used to evaluate the fitting to the models, rather than correlation coefficients.

5.2 Effect of Technology Transfer from Developed to Developing Countries

The EF_{BC} predicted by Eqs. 5.1 and 5.2 are compared with the measured ones (Fig. 5.5). This figure illustrates that a large variation in EF_{BC} can be captured using GDP_c as an independent variable. In spite of this, EF_{BC} for motor vehicles in developing countries appeared to be over adjusted by GDP_c, leading to a systematic overestimation of EF_{BC} for developing countries (solid triangles

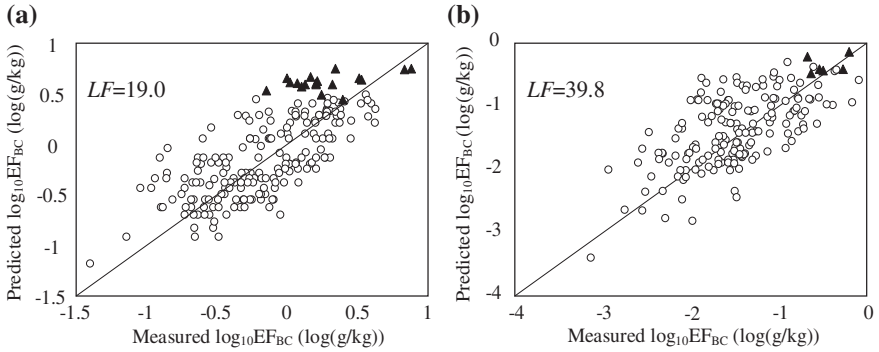

Fig. 5.5 Plot of the predicted and measured $\log_{10}$-transformed EF_{BC} for diesel (**a**) and gasoline (**b**) vehicles. Developed (*open circles*) and developing (*solid triangles*) countries are marked differently. Loss function (*LF*), defined as the quadratic sum of difference between the predicted and measured data, is used to evaluate the fitting to the model. Reproduced with permission (Wang et al. 2012). Copyright (2011) American Chemical Society

in Fig. 5.5). It implies that there is a missed factor that causes the EF_{BC} in a developing country to be lower than that in a developed country at the same GDP_c. This can be explained by the fact that developing countries are learning lessons in technology from developed countries. Consequently, the developing countries act faster in emission controls at a similar development status than the developed countries. For example, Euro III emission standards were introduced in European countries in year 2000 when GDP_c of these countries was around 20,000 USD. Equivalent standards were adopted in the U.S.A. When the GDP_c reached around 40,000 USD in 2004 (Timilsina and Dulal 2009). However, in China, a similar standard (China III) was not in force until 2007 when the GDP_c was only around 3500 USD (Timilsina and Dulal 2009).

Thus, efforts were made to account for the technology transfer from developing to developed countries when predicting the EF_{BC}. It was assumed that the later a country reached a certain level of GDP_c, the larger a possibility for the technology transfer into this country. Accordingly, a new variable Y_{3000} was introduced to quantify the effect of technology transfer, defined as the year a country's GDP_c reached 3000 USD. Note that 3035 USD is used by the World Bank to distinguish lower-middle-income and upper-middle-income economies. Consequently, new regression models can be derived using the reduced major axis method, expressed as:

$$\log_{10}\mathrm{EF_{BC}}(\text{diesel}) = -0.4302\,GDP_c - 0.01105\,Y_{3000} + 22.52, \tag{5.3}$$

$$\log_{10}\mathrm{EF_{BC}}(\text{gasoline}) = -0.7062\,GDP_c - 0.004530\,Y_{3000} - 0.02180\,T + 15.09, \tag{5.4}$$

The significantly negative slopes of Y_{3000} ($p = 0.001$ and 0.048 for diesel and gasoline vehicles, respectively) in Eqs. 5.3 and 5.4 confirms our assumption that the country that develops later (a larger Y_{3000}) is benefitting from learning lessons

from the country that develops earlier (a smaller Y_{3000}), reflected as a lower EF_{BC} at the same GDP_c. Loss function decreased from 19.0 to 16.8 for diesel vehicles and from 19.8 to 39.6 for gasoline vehicles, respectively. The mean residuals (differences between the measured and predicted $\log_{10}$-transformed EF_{BC}) for diesel vehicles was reduced from −0.02928 to 0.0003841 and from 0.3105 to −0.004177 for developed and developing countries, respectively. It confirms that inclusion of Y_{3000} in Eqs. 5.3 and 5.4 can efficiently reduce the systematic overestimation of EF_{BC} for developing countries.

5.3 Global BC Emissions from Motor Vehicles

Based on the predicted EF_{BC} and compiled fuel consumptions (United Nations Statistics Division 1995; International Energy Agency 2010a, b), annual BC emissions from motor vehicles were estimated for 222 countries/territories over a historical period from 1960 to 2006. Note that the regression models developed in this work are based on the recorded EF_{BC}. Technical advances are sometimes not in steady step and new emerging technologies may lead to fast decreases in EFs over short time. Thus, we do not apply the regression models to predict the EF_{BC} in the future. As shown in Fig. 5.6, global BC emission from motor vehicles has increased from 474 Gg in 1960 to 1294 Gg in 1978, decreased to 918 Gg in 1994, and increased again afterwards. This trend with more than one peak is a superimposition of the time trends for different countries. Compared with the study by Bond et al. (2007), our estimates are higher in the early years and lower in later years, mainly due to higher EF_{BC} predicted in early years under low GDP_c.

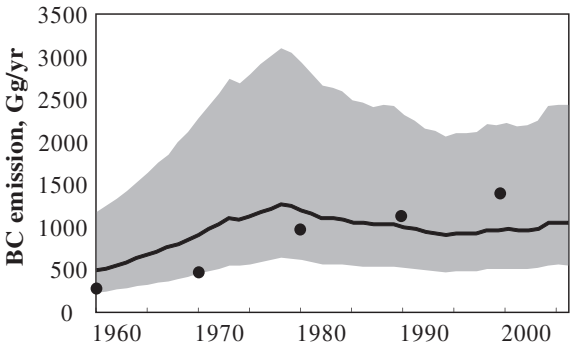

Fig. 5.6 Global historical BC emissions from motor vehicles from 1960 to 2006. The results are presented as medians (*curves*) and inter-quartile ranges (*shaded areas*) according to a Monte Carlo simulation. BC emissions from motor vehicles predicted by Bond et al. (2007) are shown as *dots* for a comparison. Reproduced with permission (Wang et al. 2012). Copyright (2011) American Chemical Society

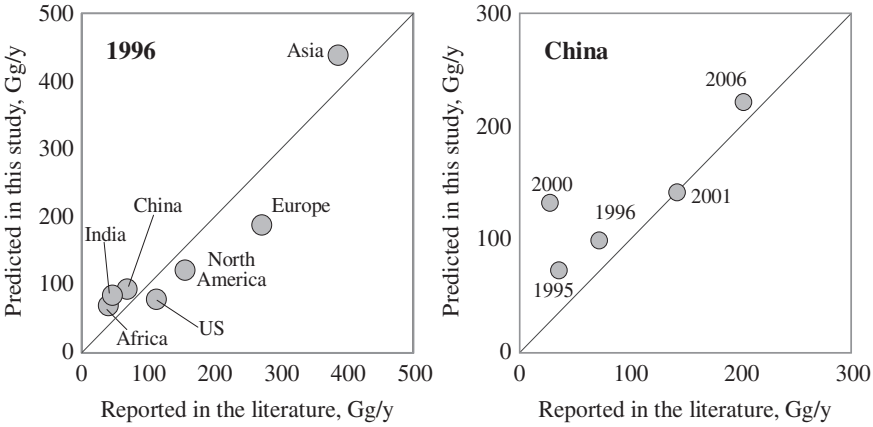

Fig. 5.7 Comparison of BC emissions estimated in this study and those reported in the literature. BC emissions in each region in 1996 are compared on the left panel (Bond et al. 2004). BC emissions in China for several years are compared on the right panel (1995: by Streets et al. (2001); 1996: by Bond et al. (2004); 2000: by Cao et al. (2006); 2001 and 2006: by Zhang et al. (2009)). Reproduced with permission (Wang et al. 2012). Copyright (2011) American Chemical Society

Our predicted emissions are also compared with those estimated in the global inventory by Bond et al. (2004), and those in China in regional inventories (Streets et al. 2001; Bond et al. 2004; Cao et al. 2006; Zhang et al. 2009) (Fig. 5.7). In comparison with the global inventory by Bond et al. (2004), our estimation is relatively higher for developing regions and lower for developed regions, although the global total emissions were close to each other. This can be explained by the dependence of EF_{BC} on the country developing level, as reflected in the Eqs. 5.3 and 5.4. For example, it is predicted that the vehicle emissions from India and the U.S.A. were 92 and 85 Gg in 1996, while 66 and 102 Gg were reported for the same year by Bond et al. (2004). Similarly, our estimated BC emissions from motor vehicles in China were generally higher than that in other inventories (Streets et al. 2001; Bond et al. 2004; Cao et al. 2006), except for the INTEX-B inventory (Zhang et al. 2009). This is expectable because the EF_{BC} measured locally were adopted in the INTEX-B inventory (Zhang et al. 2009), which account for high EF_{BC} measured in developing regions than that in developed regions.

In previous studies, inverted U-shaped environmental Kuznets curves have been noticed for many environmental indicators (Panayotou 1993; Selden and Song 1994; 1995; Barbier 1997; Hilton and Levinson 1998; Bruvoll and Medin 2003; Galeotti et al. 2006). According to the Kuznets theory, economic growth causes an initial deterioration in many environmental indicators, followed with a subsequent improvement when the economy has reached a certain criteria. According to Grossman and Krueger (1994), the turning point of this curve varies for different environmental indicators, but occurs when a country reaches a per capital income of $8000. Here, it is found that the EF_{BC} for motor vehicles decreases as the national GDP_c increase temporally, while the fuel consumed by motor vehicles

is increasing. As a combined effect, the emissions of BC from motor vehicles, as an environmental indicator, increase at the beginning due to an increase in fuel consumption, followed by a decline as a result of the reduction in emission factors. Figure 5.8 shows the national emissions of BC from motor vehicles in U.S.A. and China during 1960–2006, confirming the inverted U-shaped EKCs that the BC emission in the U.S.A. reached a peak in 1970 while the emission in China has been increasing from 1960 to 2006, with a peak to be reached in the near future.

Figure 5.9 shows the emissions of BC from motor vehicles in four country categories during 1960–2006. The emissions of BC from the OECD90 countries (states that were members of the Organisation for Economic Co-operation and

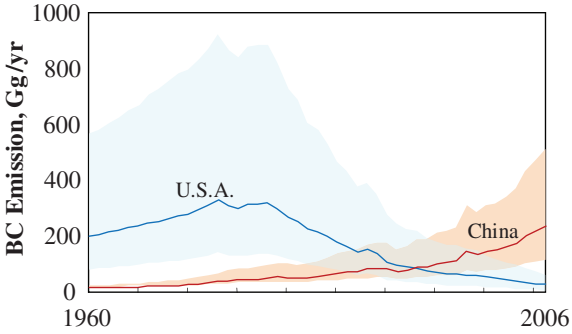

Fig. 5.8 National emissions of BC from motor vehicles in the U.S.A. and China during 1960–2006. The results are presented as medians (*curves*) and inter-quartile ranges (*shaded areas*) according to a Monte Carlo simulation. Reproduced with permission (Wang et al. 2012). Copyright (2011) American Chemical Society

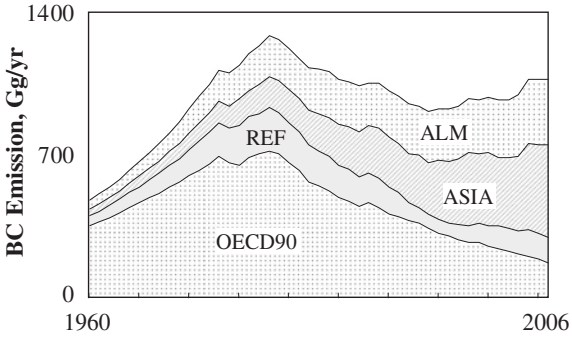

Fig. 5.9 Emissions of BC from motor vehicles in four country categories during 1960–2006. The four country categories include OECD90 (states that were members of the organisation for economic co-operation and development as of 1990), ASIA (developing countries in Asia), REF (countries undergoing economic reform), and ALM (Africa, Latin America, and the Middle East countries). Reproduced with permission (Wang et al. 2012). Copyright (2011) American Chemical Society

Development as of 1990), mostly those as developed countries, reached peak values around 1980. In contrast, BC emissions in the ASIA (developing countries in Asia) and ALM (Africa, Latin America, and the Middle East countries) countries, mainly those as developing countries, have been increasing. Notably, the increasing trends in the ASIA and ALM countries are very likely to continue in the next decade due to the fast increase of motor vehicles. As a result, the contribution of the OECD90 countries to global total BC emission from motor vehicles has decreased from 73 % in 1960 to 15 % in 2006. Meantime, the contribution of the ASIA countries has increased from 7 to 43 % over the period during 1960–2006.

Corresponding to the variation of BC emissions, the spatial pattern of BC emissions from motor vehicles has changed temporally. Figure 5.10 compares the geographic distributions of BC emissions from motor vehicles in 1976 (by country) and 2006 (at 1° × 1° resolution). In 1976, the high emissions were mainly found over Western Europe and North America. The top three emission countries were the U.S.A. (330 Gg/year), Japan (54.6 Gg/year) and Canada (47.2 Gg/year). The spatial pattern has shifted over the 30 years. As a result, in 2006, ASIA and ALM became the major source regions. In comparison, BC emissions from motor vehicles has increased 6.8 times from 1976 to 2006 in China (219 Gg/year) as the largest emission country in 2006, followed by India (85.3 Gg/year), and Brazil (63.1 Gg/year). Meanwhile, BC emissions from motor vehicles in the U.S.A., Japan, and Canada had decreased by 9177 and 90 %, respectively over the same period. In general, the emission center has shifted from Europe and North America to Asia and Africa. The different trends over these regions are important to predict the future BC emissions from motor vehicles and estimate the impact on climate, human health and agriculture (Shindell et al. 2011).

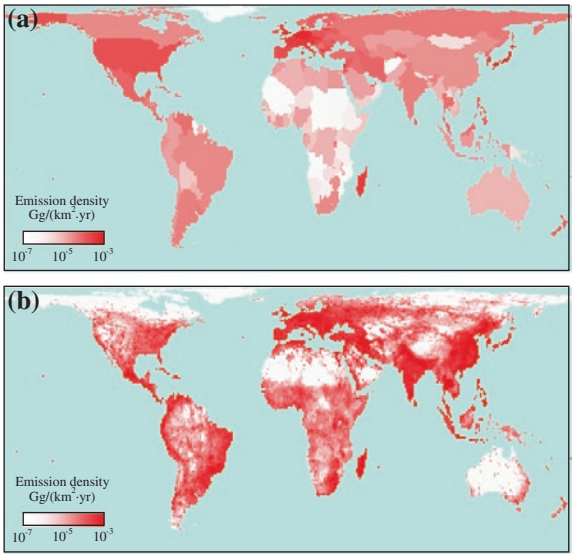

Fig. 5.10 Geographical distributions of BC emissions from motor vehicles in 1976 (**a**) and 2006 (**b**). Country-based mean values are shown for 1976 and 1° × 1° resolution is used for 2006. Reproduced with permission (Wang et al. 2012). Copyright (2011) American Chemical Society

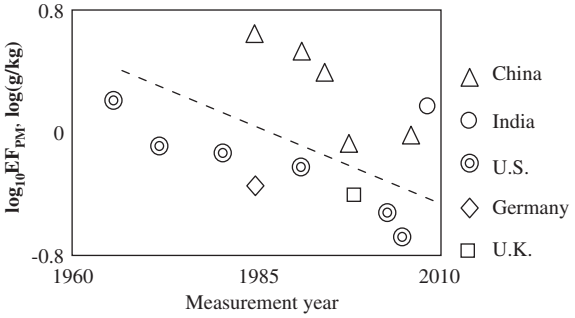

Fig. 5.11 Relationship between the emission factors of fine particles (EF_{PM}) and the year of measurement for different countries. Reproduced with permission (Wang et al. 2012). Copyright (2012) American Chemical Society

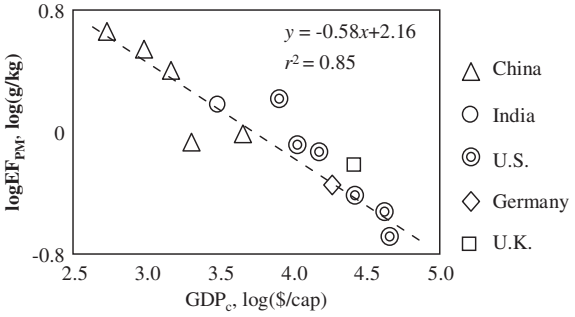

Fig. 5.12 Regression model of EF_{PM} using GDP_c as an independent variable. The data points are shown as different symbols for different countries. Reproduced with permission (Wang et al. 2012). Copyright (2012) American Chemical Society

5.4 Emission Factors for Battery Coking

As shown above, the EF_{BC} for motor vehicles can be predicted by regression models based upon the independent variables of GDP_c and Y_{3000}, which characterize the spatial and temporal variations of the measured EF_{BC}. Similar efforts were made to study the factors governing the EF_{BC} for other sources. However, there is a lack of EF_{BC} measured or relevant information, preventing us to apply a similar method to other emission sources, except for battery coking. A total of 14 emission factors of fine particles (EF_{PM}) were collected for battery coking. A relationship between $\log_{10}$-transformed EF_{PM} and the measurement year and country was also found (Fig. 5.11). It is clear that the EF_{PM} are higher in later years than those in earlier years, while the values are lower in developed countries (U.S., Germany and UK) than the values in developed countries (India and China). It reflects the dependence of EF_{PM} for battery coking on the technology, just as motor vehicles.

Following the same procedures applied for on-road motor vehicles, a good relationship was found between $\log_{10}$-transformed EF_{PM} and GDP_c corresponding to the country in the year of measurement, as shown in Fig. 5.12. Thus, a regression model was developed to predict the EF_{PM}, which was converted to EF_{BC} using a constant fraction (0.9) of BC in fine particles emitted by recovery coking (Kupiainen and Klimont 2004).

References

Ban-Weiss, G. A., McLaughlin, J. P., Harley, R. A., Lunden, M. M., Kirchstetter, T. W., Kean, A. J., et al. (2008). Long-term changes in emissions of nitrogen oxides and particulate matter from on-road gasoline and diesel vehicles. *Atmospheric Environment, 42*(2), 220–232.

Barbier, E. B. (1997), Introduction to the environmental Kuznets curve special issue. *Environment and Development Economics, 2*(04), 369–381.

Bond, T. C., Streets, D. G., Yarber, K. F., Nelson, S. M., Woo, J. H., & Klimont, Z. (2004). A technology-based global inventory of black and organic carbon emissions from combustion. *Journal of Geophysical Research: Atmospheres (1984–2012), 109*(D14).

Bond, T. C., Bhardwaj, E., Dong, R., Jogani, R., Jung, S., Roden, C., et al. (2007). Historical emissions of black and organic carbon aerosol from energy-related combustion, 1850–2000. *Global Biogeochemical Cycles, 21*(2). doi:10.1029/2006GB002840.

Bruvoll, A., & Medin, H. (2003). Factors behind the environmental Kuznets curve. A decomposition of the changes in air pollution. *Environmental and Resource Economics, 24*(1), 27–48.

Cao, G., Zhang, X., & Zheng, F. (2006). Inventory of black carbon and organic carbon emissions from China. *Atmospheric Environment, 40*(34), 6516–6527.

Galeotti, M., et al. (2006). Reassessing the environmental Kuznets curve for CO_2 emissions: a robustness exercise. *Ecological Economics, 57*(1), 152–163.

Grossman, G.M., & Krueger, A.B. (1994). *Economic Growth and the Environment*. Working Paper, National Bureau of Economic Research.

Heeb, N. V., Haag, R., Seiler, C., Schmid, P., Zennegg, M., Wichser, A., et al. (2012). Effects of a combined diesel particle filter-DeNox system (DPN) on reactive nitrogen compounds emissions: a parameter study. *Environmental Science and Technology, 46*(24), 13317–13325.

Hildemann, L. M., Markowski, G. R., & Cass, G. R. (1991). Chemical composition of emissions from urban sources of fine organic aerosol. *Environmental Science and Technology, 25*(4), 744–759.

Hilton, F. G. H., & Levinson, A. (1998). Factoring the environmental Kuznets curve: evidence from automotive lead emissions. *Journal of Environmental Economics and Management, 35*(2), 126–141.

International Energy Agency. (2010a). *Energy statistics and balances of OECD countries 1960–2006* [Press release].

International Energy Agency. (2010b). *Energy statistics and balances of Non-OECD countries 1970–2006* [Press release].

Junker, C., & Liousse, C. (2008). A global emission inventory of carbonaceous aerosol from historic records of fossil fuel and biofuel consumption for the period 1860–1997. *Atmospheric Chemistry and Physics, 8*(5), 1195–1207.

Kim Oanh, N. T., Thiansathit, W., Bond, T. C., Subramanian, R., Winijkul, E., & Paw-armart, I. (2010). Compositional characterization of PM 2.5 emitted from in-use diesel vehicles. *Atmospheric Environment, 44*(1), 15–22.

Kupiainen, K., & Klimont, Z. (2004). Primary emissions of submicron and carbonaceous particles in Europe and the potential for their control. *International Institute for Applied Systems Analysis (IASA), Interim report IR-04-79, Schlossplatz, 1.*

Lloyd, A. C., & Cackette, T. A. (2001). Diesel engines: environmental impact and control. *Journal of the Air and Waste Management Association, 51*(6), 809–847.

Novakov, T., Ramanathan, V., Hansen, J., Kirchstetter, T., Sato, M., Sinton, J., et al. (2003). Large historical changes of fossil-fuel black carbon aerosols. *Geophysical Research Letters, 30*(6).

Panayotou, T. (1993) *Empirical tests and policy analysis of environmental degradation at different stages of economic development*. ILO, Technology and Employment Programme.

Prucz, J. C., Clark, N. N., Gautam, M., & Lyons, D. W. (2001). Exhaust emissions from engines of the Detroit Diesel Corporation in transit buses: A decade of trends. *Environmental Science and Technology, 35*(9), 1755–1764.

Selden, T. M., & Song, D. (1994). Environmental quality and development: Is there a Kuznets curve for air pollution emissions? *Journal of Environmental Economics and management, 27*(2), 147–162.

Selden, T. M., & Song, D. (1995). Neoclassical growth, the J curve for abatement, and the inverted U curve for pollution. *Journal of Environmental Economics and management, 29*, 162–168.

Shindell, D., Faluvegi, G., Walsh, M., Anenberg, S. C., Van Dingenen, R., Muller, N. Z., et al. (2011). Climate, health, agricultural and economic impacts of tighter vehicle-emission standards. *Nature Climate Change, 1*(1), 59–66.

Streets, D. G., Gupta, S., Waldhoff, S. T., Wang, M. Q., Bond, T. C., & Yiyun, B. (2001). Black carbon emissions in China. *Atmospheric Environment, 35*(25), 4281–4296.

Subramanian, R., Winijkul, E., Bond, T. C., Thiansathit, W., Oanh, N. T. K., Paw-Armart, I., et al. (2009). Climate-relevant properties of diesel particulate emissions: results from a piggyback study in Bangkok, Thailand. *Environmental Science and Technology, 43*(11), 4213–4218.

Timilsina, G. R., & Dulal, H. B. (2009). *A review of regulatory instruments to control environmental externalities from the transport sector*. Washington: The World Bank.

United Nations Statistics Division. (1995). *United Nations energy statistics, 1950–1995*. New York: United Nations Statistics Division.

Wang, R., Tao, S., Shen, H., Wang, X., Li, B., Shen, G., et al. (2012). Global emission of black carbon from motor vehicles from 1960 to 2006. *Environmental Science and Technology, 46*(2), 1278–1284.

Yanowitz, J., McCormick, R. L., & Graboski, M. S. (2000). In-use emissions from heavy-duty diesel vehicles. *Environmental Science and Technology, 34*(5), 729–740.

Yanowitz, J., Graboski, M. S., Ryan, L. B., Alleman, T. L., & McCormick, R. L. (1999). Chassis dynamometer study of emissions from 21 in-use heavy-duty diesel vehicles. *Environmental Science and Technology, 33*(2), 209–216.

Zhang, Q., Streets, D. G., Carmichael, G. R., He, K., Huo, H., Kannari, A., et al. (2009). Asian emissions in 2006 for the NASA INTEX-B mission. *Atmospheric Chemistry and Physics, 9*(14), 5131–5153.

Chapter 6
Emissions of Black Carbon in China from 1949 to 2050

6.1 BC Emissions from China in 2007

Based on the updated EF_{BC} data set and a re-compiled fuel consumption data set based on local energy statistics, the total BC emission from China in 2007 was estimated to be 1957 Gg/year, in which 988, 646, 50.7, 188, and 77.7 Gg/year were emitted from the residential/commercial sectors, industry, the sector of energy production, transportation, and outdoor biomass burning, respectively. According to the Monte Carlo simulation, due to the uncertainties in EF_{BC} and fuel consumptions, the estimated BC emission was associated with a relative uncertainty from −37 to +57 % as an inter-quartile range relative to the median. Our estimate is higher than those reported in previous studies (Streets et al. 2003; Cao et al. 2006; Cofala et al. 2007; Ohara et al. 2007; Klimont et al. 2009; Zhang et al. 2009; Lu et al. 2011; Bond et al. 2013), which are listed in Table 6.1. Our estimate is the closest to the inventory INTEX-B constructed by Zhang et al. (2009), who used the EF_{BC} measured in China and fuel data from the Chinese Energy Yearbook (National Bureau of Statistics and National Energy Administration 2009).

Relative contributions by different sources to the total BC emissions in China are charted in Fig. 6.1. The residential/commercial sectors are the largest contributor, followed by industry and transportation, and the sector of energy production. Different from global BC inventories (Bond et al. 2004; Lamarque et al. 2010), wildfires were relatively negligible in Chinese BC emissions. The top five contributing emission sources were in the order of residential coal (28.0 %), residential solid biofuels (22.7 %), coke production (17.6 %), diesel vehicles (8.2 %), and brick kilns (7.4 %). Residential use of solid fuels, including coal, firewood and crop residues, contributed to more than half of the total BC emissions in China, 83 % of which were distributed over the rural areas. Among all industrial activities, coke production ranked the highest individual sector with a total BC emission of 341 Gg/year, in which 233 Gg was contributed by beehive coke ovens.

R. Wang, *Global Emission Inventory and Atmospheric Transport of Black Carbon*,
Springer Theses, DOI 10.1007/978-3-662-46479-3_6

Table 6.1 Comparison of the estimated emissions of BC in China in our work and previous studies

Emission inventory	Year	Emission of BC (Gg/year)
This work	2007	1992
Inventory A by Bond et al. (2013)	2000	1200
Inventory B by Lu et al. (2011)	2010	1700
Inventory C by Zhang et al. (2009)	2006	1800
Inventory D by Klimont et al. (2009)	2000	1200
Inventory E by Ohara et al. (2007)	2000	1093
Inventory F by Cofala et al. (2007)	2000	1100
Inventory G by Cao et al. (2006)	2000	1500
Inventory H by Streets et al. (2003)	2000	1000
Mean (± SD) of inventory A–H	–	1324 ± 302

The mean and standard deviation (SD) of the estimates in the literature are also listed

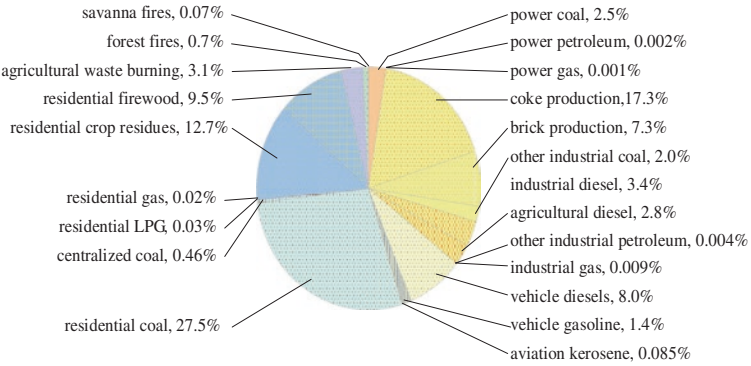

Fig. 6.1 Relative contributions by different sources to BC emissions from China in 2007. The same sector types are displayed using the same color in the chart. Reproduced with permission (Wang et al. 2012). Copyright (2012) American Chemical Society

Similar to other inventories (Streets et al. 2001; Cao et al. 2006; Zhang et al. 2009; Lu et al. 2011), BC emissions from motor vehicles were primarily from diesel engines (85 %), of which the BC emission factors are almost one magnitude higher than that for gasoline ones.

6.2 County-Level BC Emissions in China

BC emissions were estimated for all 2373 counties in 2007 based on the county-level fuel consumption compiled in PKU-FUEL-2007 and the new BC emission factors data set compiled in Sect. 6.5. In particular, the BC emission factors were derived by county using the county-level per capital GDP in 2007. The county-level BC emissions are mapped in Fig. 6.2.

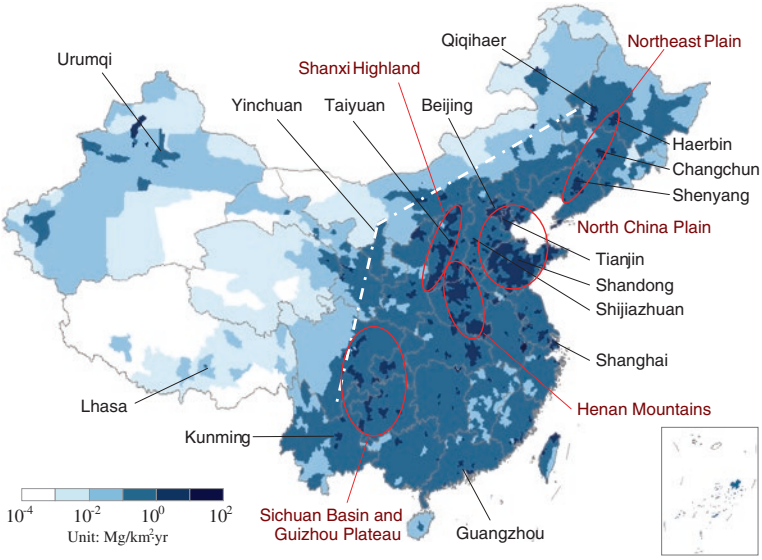

Fig. 6.2 Map of BC emissions in China by county for year 2007. East and West China are divided by a *dashed line* from Qiqihar, Yinchuan, to Kunming

In general, relatively higher BC emissions occurred in Eastern China, including most part of Northeast China, whereas relatively lower BC emissions took place in Western China, excluding east part of Inner Mongolia. These two regions can be generally separated in space by a line extending from Qiqihar to Yinchuan and Kunming. There are a cluster of cities with notably high BC emission densities, centered in and distributed around the cities of Beijing, Tianjin, Haerbin, Changchun, Shenyang, Shijiazhuang, Jinan, Zhengzhou, Taiyuan, Xi'an, Shanghai, Guangzhou, Kunming, Guiyang, and Lhasa. Over these emission centers, there are either high population densities or highly concentrated industry, or both of them. For example, Shanxi Province is the largest coal producer in China, and the BC emission densities in Taiyuan and Datong is higher than Shanghai and Guangzhou. Similarly, Henan Province is the province with the largest population in China (96 million in 2014), and most people are living in rural areas where traditional solid biofuels are widely used. It results in that the average BC emission densities by county are over 10 Mg km^{-2} year^{-1} over the most areas in this province.

Based on the county-level BC emissions, BC emissions were further allocated to $0.1^\circ \times 0.1^\circ$ grids using various proxies in space, namely the PKU-BC(China) inventory. In brief, the distribution of rural population was used as a proxy for open-burning of agricultural waste and rural residential burning of coal, firewood, and crop residues. The distribution of urban population was used as a proxy for coal consumption in urban households and centralized heating boilers, as well as aviation kerosene consumption. The distribution of CO emissions from road transportation was used as a proxy for on-road motor vehicles (European Commission

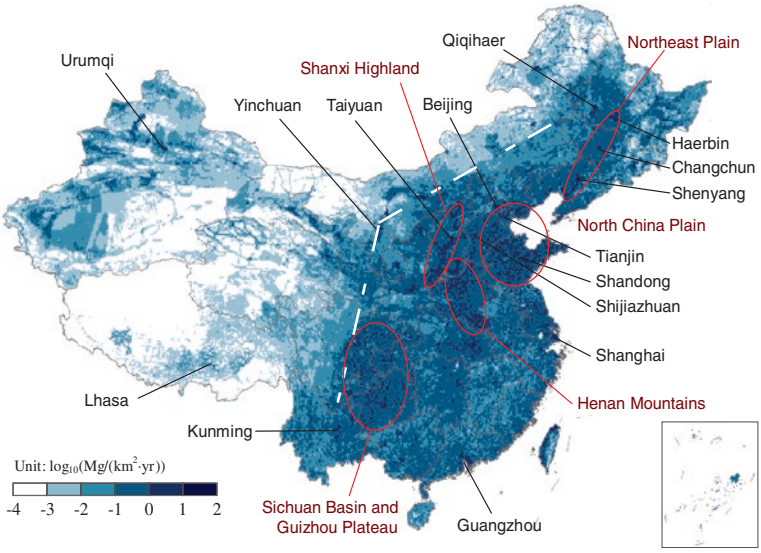

Fig. 6.3 BC emissions in China at a resolution of 0.1° × 0.1° for year 2007 by PKU-BC(China). East and West China are divided by a *dashed line* from Qiqihar, Yinchuan, to Kunming. Reproduced with permission (Wang et al. 2012). Copyright (2012) American Chemical Society

Joint Research Centre/Netherlands Environmental Assessment Agency 2011). In addition, detailed point information was collected for major power plants in China (State Power Corporation of China 2008), which covers 78 % of total coal consumption in all power stations in China. Then, BC emissions from these power plants were directly allocated to grids based on their geographic positions. The 0.5° × 0.5° GFED data for forest and grassland fires were further disaggregated to 0.1° × 0.1° (van der Werf et al. 2010), using vegetation biomass as a proxy (Friedl et al. 2002), and used a proxy for wildfires in our work. Finally, total population was used as a proxy for all other sources. In comparison to previous BC emission inventories (Streets et al. 2001, 2003; Bond et al. 2004; Lu et al. 2011), gridded BC emissions are no longer disaggregated from provincial emissions, but instead from county-level emissions, which is expected to reduce the disaggregation bias in the spatial distribution. The BC emissions according to PKU-BC(China) are mapped in Fig. 6.3.

According to PKU-BC(China), the average BC emission density over Eastern China (0.437 Mg/(km^2 year)) was much higher than that over Western China (0.033 Mg/(km^2 year)), in agreement with the spatial pattern of county-level BC emissions. High BC emission densities can be found over the North China Plain, Northeast Plain, Shanxi Highland, Henan Mountains, and Sichuan Basin-Guizhou Plateau. Extremely high BC emission densities can be found over large cities (e.g. Beijing, Shanghai, Kunming, etc.), where there are a high population density and a great number of motor vehicles and industry facilities. In addition, relatively high BC emission densities was also found over populated rural areas in the east and southwest

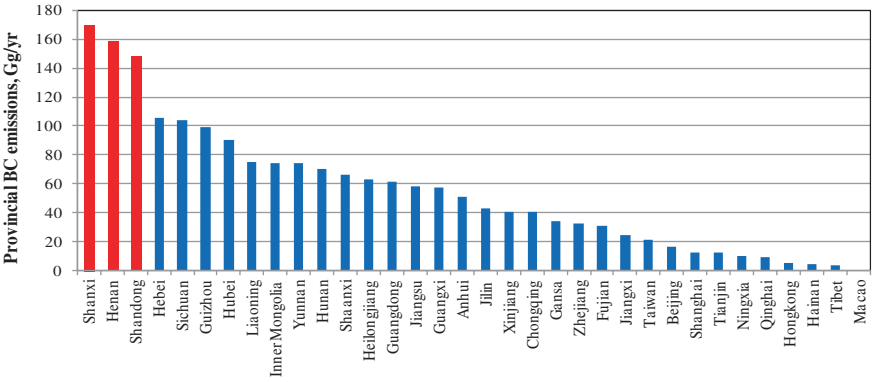

Fig. 6.4 BC emissions by province in China for the year of 2007. The top three provinces with the highest BC emissions are shown as *red bars*

of China, covering the provinces of Shandong, Henan, Shanxi, and Sichuan. The high BC emission densities over these rural areas can be attributed to the large consumption of solid biofuels and low-quality coals in the residential/commercial sectors, for which the BC emission factors are one to two magnitudes higher than that for the same fuels burnt in the industrial boilers equipped with advanced abatement facilities. In addition, the highest BC emission density was found over the Shanxi Highland, as the most polluted region in China, due to high emissions from the traditional coal-producing industry. Figure 6.4 shows the total BC emissions by province in China for year 2007. It is illustrated that the Shanxi province is the largest contributor to BC emissions in China, followed by the Henan and Shandong provinces.

6.3 Comparison with a Mock-Up Inventory

To evaluate the BC inventory constructed using the county-level emission data, a mock-up BC inventory at the same spatial resolution ($0.1° \times 0.1°$) including all anthropogenic sources was established using the same method as PKU-BC(China), but that the gridded BC emissions were disaggregated from BC emissions by province and using the provincial proxies, rather than county data, namely the PRO-BC(China) inventory. In fact, the method used in PRO-BC(China) is close to that used in previous inventories (Streets et al. 2001, 2003; Bond et al. 2004; Ohara et al. 2007; Lu et al. 2011). The produced spatial distributions in PKU-BC(China) and PRO-BC(China) are compared at a gridded level (Fig. 6.5). There are notable differences in the spatial distributions between PKU-BC(China) and PRO-BC(China). In general, the spatial distribution BC emissions are more or less smoothed in PRO-BC(China), relative to PKU-BC(China). This is understandable since the inhomogeneous distribution of BC emissions was biased to be homogeneous within each province.

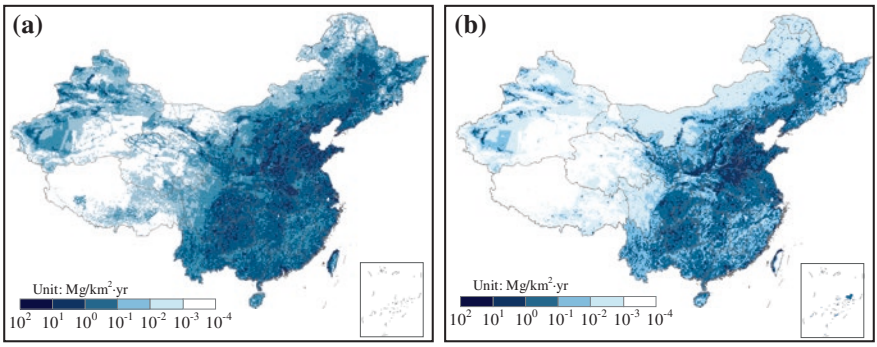

Fig. 6.5 BC emission maps at a spatial resolution of 0.1° × 0.1° in the PKU-BC(China) (**a**) and PRO-BC(China) (**b**) inventory in 2007

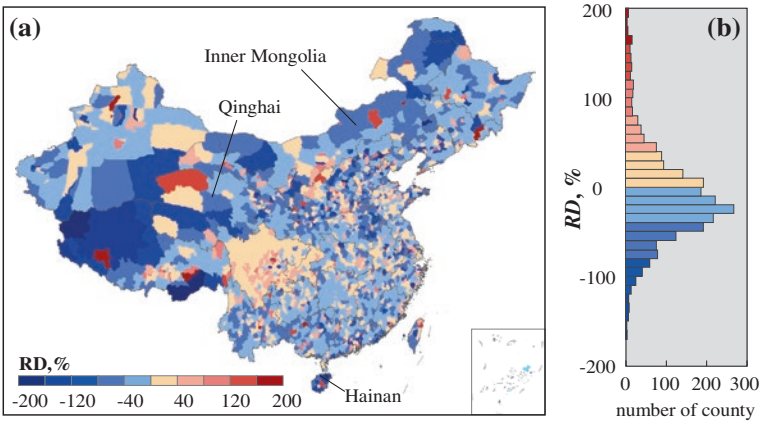

Fig. 6.6 Geographic (**a**) and frequency (**b**) distributions of the relative differences of emission between PKU-BC(China) and PRO-BC(China). A positive relative difference indicates a lower BC emissions by county in the PRO-BC(China) inventory. Reproduced with permission (Wang et al. 2012). Copyright (2012) American Chemical Society

To further illustrate the difference between PKU-BC(China) and PRO-BC(China), a relative difference was defined as $(E_1 - E_2)/((E_1 + E_2)/2)$, where E_1 and E_2 are the total BC emissions from anthropogenic sources by each county from the PKU-BC(China) and PRO-BC(China) inventory, respectively. The difference between E_1 and E_2 quantifies the bias at the county level induced by homogeneous per capital BC emissions within each province, which is identical to the improvement by using the county BC emissions. Geographic and frequency distributions of the relative difference by county are both shown in Fig. 6.6. The average absolute relative difference for all counties in China was 42.5 %. In addition, the absolute relative difference has exceeded 50 % over 30 % of counties in China, indicating a substantial

reduction in the spatial bias of BC emissions by using the county BC emissions. Large relative differences are found over the provinces where development status varied dramatically in space, such as the Inner Mongolia, Qinghai and Sichuan provinces. It indicates a more inhomogeneous distribution of emissions in these provinces.

6.4 Comparison with Previous Inventories

In addition to comparison with the mock-up PRO-BC(China) inventory, PKU-BC(China) was also compared with two previous inventories widely used in atmospheric modelling of BC, namely the REAS (anthropogenic, 0.5° × 0.5°, 2003) (Ohara et al. 2007) and INTEX-B (anthropogenic, 0.5° × 0.5°, 2006) inventory (Zhang et al. 2009), both of which were disaggregated to grids from the BC emissions from major sources by province. Similarly, the relative differences were calculated at the resolution of 0.5° × 0.5° using the same equation above. E_1 and E_2 are corresponding to the BC emissions from anthropogenic sources over each 0.5° × 0.5° grid by the PKU-BC(China) and REAS (or INTEX-B) inventory, respectively. The calculated relative differences between PKU-BC(China) and REAS or INTEX-B are mapped in Fig. 6.7. The differences in BC emissions are coming from the differences in BC emission factors and spatially disaggregated emission data. There are notable differences between PKU-BC(China) and the two previous BC inventories. High positive relative differences were found over the Tibet and Xinjiang provinces, likely due to the lack of complete fuel data for these two provinces. In addition, there were positive relative differences over northern China between PKU-BC(China) and REAS, which are attributable to the relatively higher BC emission factors applied for residential solid fuels in PKU-BC(China).

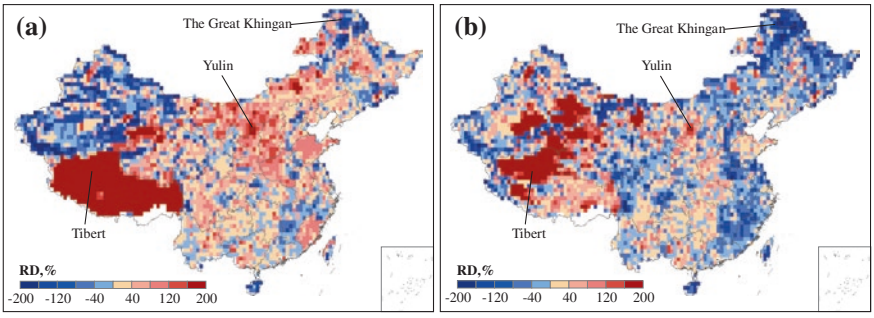

Fig. 6.7 Geographic distributions of the relative differences of anthropogenic BC emissions between PKU-BC(China) (2007) and REAS (2003) (**a**) or INTEX-B (2006) (**b**). PKU-BC(China) was downscaled to 0.5° × 0.5° for a comparison. A positive relative difference indicates a higher BC emission in the PKU-BC(China) inventory. Reproduced with permission (Wang et al. 2012). Copyright (2012) American Chemical Society

Meanwhile, there were negative relative differences over southeast China between PKU-BC(China) and INTEX-B, as a result of lower motor vehicle BC emission factors applied to counties with a high per capital GDP according to our model. In addition, high emission density abnormalities were revealed according to the county-disaggregated PKU-BC(China) model. For example, extremely high BC emission densities at Yulin, where a large volume of coal were produced and consumed, were averaged within the Shanxi province in the REAS or INTEX-B inventory, reflected as high positive relative differences.

6.5 BC Emissions in China from 1949 to 2007

Temporal trends in BC emissions from China were derived over a period from 1949 to 2007, as shown in Fig. 6.8. Over the 59 years, the Chinese total BC emissions had increased from 341 to 1957 Gg/year, equivalent to an average increasing rate of 3 % per year. The highest emission occurred in 1996 (2189 Gg/year). In comparison, our estimations are higher than those estimated for the same years in other inventories (Streets et al. 2001, 2003; Bond et al. 2004; Cao et al. 2006; Ohara et al. 2007; Zhang et al. 2009). This difference is mainly due to the update of BC emission factors, including those updated for the residential coal and biofuels, industrial activities (e.g. coke production), and motor vehicles. In addition, consideration of a non-compliance rate of dust abatements for industry also results in a higher BC emissions from industry in the PKU-BC(China) inventory. However, a lack of BC emission factors is still a major source of uncertainty in the PKU-BC(China) inventory (see the shaded area in the figure). For many important

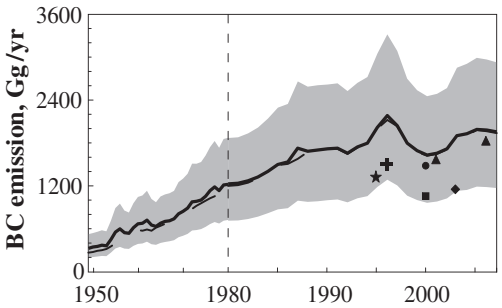

Fig. 6.8 Historical BC emissions from all sources in China from 1949 to 2007. The total emissions derived as median estimates in a Monte Carlo simulation are shown as a *black solid line*, with the inter-quartile ranges shown as *shaded areas*. The anthropogenic emissions are shown as a *dashed red line*. Our estimated annual BC emissions are compared with those reported in other inventories, which are shown as a *star* (Streets et al. 2001), a *cross* (Bond et al. 2004), a *square* (Streets et al. 2003), a *circle* (Cao et al. 2006), a *diamond* (Ohara et al. 2007) and *triangles* (Zhang et al. 2009)

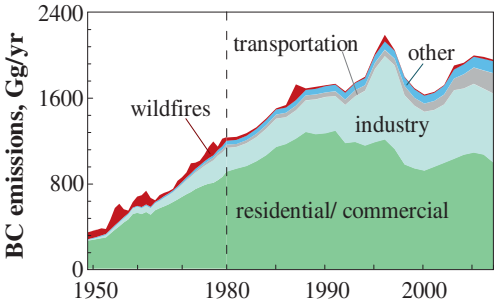

Fig. 6.9 Annual BC emissions from residential/commercial sectors, industry, transportation, wildfires, and other sectors (power generation and agricultural waste combustion in the field) in China from 1949 to 2007. Reproduced with permission (Wang et al. 2012). Copyright (2012) American Chemical Society

emission sources, including coke production, brick kilns, and small-capacity industrial boilers, more measurements on BC emission factors are essential needed to reduce the associated uncertainty in BC emissions.

The temporal trends in BC emissions from various sectors are shown in Fig. 6.9. The annual BC emissions had increased monotonically from 1949 to 1990, due to the rapid increases in population and per capital fuel consumptions, and leveled off after 1990. For example, the emissions in the residential/commercial sector declined since 1990, due to three reasons. First, rapid urbanization produced a decline in China's population in rural areas. Second, the residential coal stoves were gradually replaced with improved stoves burning liquid petroleum gas/natural gas. At last, the centralized heating systems had replaced a lot of low-efficiency traditional stoves. In addition, as an important technology change since 1996, the beehive coke ovens were gradually phased out from the Chinese coking industry, leading to a notable decline of industrial BC emissions from a peak (550 Gg) in 1996. For on-road motor vehicles, despite the fact that the BC emission factors has decreased significantly since 1990, the BC emissions were increasing steadily due to a rapid growth of the vehicle fleet in the country.

In addition, there is a significant temporal variation in the spatial pattern of BC emissions in China. The provincial BC emissions in China are compared between 1980 and 2007, as shown in Fig. 6.10. As a result, the largest increase was found in the Shanxi and Guizhou province, due to a dramatic increase in the coal-related industry, like coke production. In contrast, BC emissions had not changed too much in provinces like Sichuan and Heilongjiang, where the emissions were dominated by the residential/commercial sectors in 1980. As a result, the increase of BC emissions in industry can be partially offset by the decrease of BC emissions from the residential sectors. The different temporal trends in BC emissions in China reflect an inhomogeneous pattern of development in China.

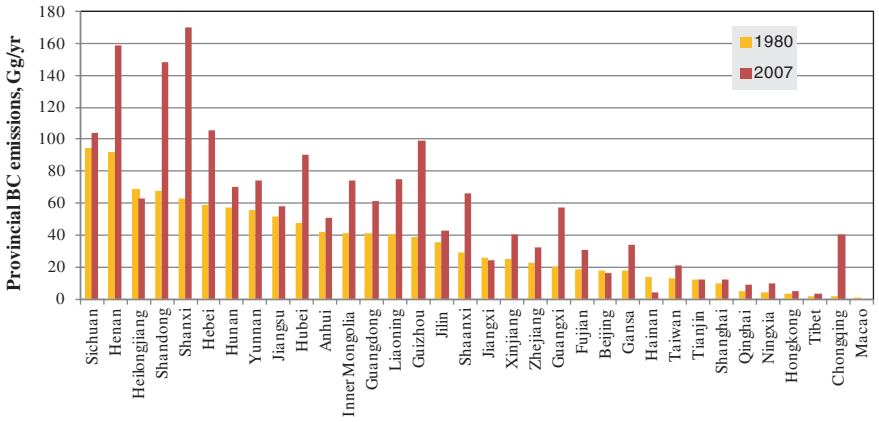

Fig. 6.10 Comparison of BC emissions by province in China between 1980 and 2007

6.6 BC Emissions in China from 2008 to 2050

Future BC emissions are concerned in future climate simulations (Shindell et al. 2012). In this study, annual BC emissions from anthropogenic sources in China were predicted for the period from 2008 to 2050 under baseline and low-carbon scenarios based on fuel consumption data predicted by National Development and Reform Commission and Development Research Center of the State Council (2009).

In addition to the predicted fuel consumption, BC emission factors for motor vehicles (diesel and gasoline) were predicted according to regression models developed in this work. The evolution of small-scaled brick kilns followed a S-shaped curve with an assumption that the phase-out of small-scaled kilns starts from 2010 with a transition time of 50 years ($t_0 = 2010$; $F_0 = 0.9$; $F_t = 0$; $s = 50$). In addition, we assumed that new regulations for off-road diesel machines start in 2020 (10 years later than the U.S.A.) ($t_0 = 2010$; $F_0 = 0$; $F_t = 1.0$; $s = 50$). Implementation of these regulations was expected to result in a reduction of BC emission factors by 80 %. Other technology changes followed the same trends as that before 2007. The scenarios with fuel consumption data under baseline and low-carbon scenarios associated with the technology change were referred to as "baseline" and "low-carbon" scenarios, respectively. In addition, to assess the impact of technology change individually, the prediction was also performed under two scenarios ("baseline-high", "low-carbon-high") using the corresponding scenarios of fuel consumption, but with BC emission factors and technologies held at the 2007 levels.

Therefore, under the four scenarios, the anthropogenic BC emissions in China were predicted from 2008 to 2050. The annual BC emissions are plotted in Fig. 6.11. It is predicted that BC emissions in China would reach 2183, 1663, 1338, and 920 Gg/year in 2050 under the baseline, low-carbon, baseline-high

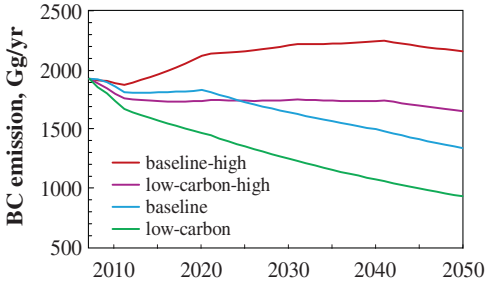

Fig. 6.11 Predicted BC emissions from anthropogenic sources in China from 2008 to 2050 under four scenarios (baseline, low-carbon, baseline-high, and low-carbon-high). Reproduced with permission (Wang et al. 2012). Copyright (2012) American Chemical Society

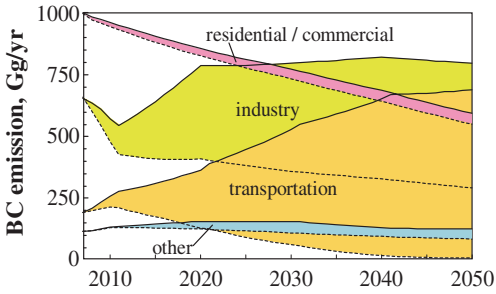

Fig. 6.12 Mitigated BC emissions by sector as a difference between the baseline-high (*solid lines*) and low-carbon (*dotted lines*) scenarios. Reproduced with permission (Wang et al. 2012). Copyright (2012) American Chemical Society

and low-carbon-high scenarios, respectively. Under the baseline-high scenario, the total BC emissions in China will reach a peak of 2273 Gg/year (1376–3719 as R50) in 2041 due to the increase of BC emissions from motor vehicles (by a factor of 3.6), off-road diesel machineries (by a factor of 3.1), coal combustions in industrial boilers and power plants (by a factor of 1.8), brick production (by a factor of 1.6), and coke production (by a factor of 2.4), due to increase in fuel consumption. If either the low-carbon strategy (low-carbon-high scenario) or technology improvement (baseline scenario) were considered, total BC emissions in China can be reduced by 92 or 29 Gg/year in 2010, 394 or 583 Gg/year in 2020, 476 or 583 Gg/year in 2030, 519 or 765 Gg/year in 2040, and 520 or 845 Gg/year in 2050, respectively. Moreover, if low-carbon strategy and technology improvement are both implemented, namely the low-carbon scenario, the reduced total BC emissions in China will be 158, 988, and 1263 Gg/year for the years of 2010, 2030, and 2050, respectively.

It is interesting to investigate the potential of BC mitigation by sector. Figure 6.12 shows BC emissions in the residential/commercial sector, industry, transportation, and other sectors (including power generation and agricultural waste burned in fields) under the worst (baseline-high) and best (low-carbon) scenarios. As illustrated by the figure, the mitigation measures would be the most

effective in the sectors of industry and transportation. In comparison to the baseline-high scenario, the annual BC emissions can be mitigated by 190 and 664 Gg in the industry and transportation sectors, respectively in 2050 if the baseline scenario can be achieved.

With a huge population, a rapid rate of industrialization and a large consumption of coal and biofuels, China is the world's largest contributor to BC emissions. Although BC emissions from China had leveled off over the last two decades, a large amount of BC emissions are still expectable in the coming decades. Traditional solid fuels including crop residues, firewood, and coal will remain the primary energy in rural areas. The number of diesel vehicles run at a less strict emission standard is still increasing rapidly. Therefore, to reduce BC emissions in these sectors, it is necessary and possible to develop and distribute simple, inexpensive, practical, and effective technologies, which make more efficient use of the fuels. For instance, biogas is used in more and more rural areas, and the so-called "improved" biomass burning stoves are welcome for its low cost. Biomass pellets and stalk gasifying furnaces are also good examples that improve the efficiency of biomass fuels use. Before the popularization and application of more expensive technologies (e.g. diesel particulate filters), these actions are expected to reduce the emissions of BC as well as other pollutants effectively in China for the near future.

References

Bond, T. C., Streets, D. G., Yarber, K. F., Nelson, S. M., Woo, J. H., & Klimont, Z. (2004). A technology-based global inventory of black and organic carbon emissions from combustion. *Journal of Geophysical Research: Atmospheres (1984–2012), 109*(D14), 203.

Bond, T. C., Doherty, S. J., Fahey, D., Forster, P., Berntsen, T., DeAngelo, B., et al. (2013). Bounding the role of black carbon in the climate system: A scientific assessment. *Journal of Geophysical Research: Atmospheres, 118*(11), 5380–5552.

Cao, G., Zhang, X., & Zheng, F. (2006). Inventory of black carbon and organic carbon emissions from China. *Atmospheric Environment, 40*(34), 6516–6527.

Cofala, J., Amann, M., Klimont, Z., Kupiainen, K., & Höglund-Isaksson, L. (2007). Scenarios of global anthropogenic emissions of air pollutants and methane until 2030. *Atmospheric Environment, 41*(38), 8486–8499.

European Commission Joint Research Centre/Netherlands Environmental Assessment Agency. (2011). *Emission database for global atmospheric research (EDGAR), release version 4.2*. Retreived from http://edgar.jrc.ec.europa.eu.

Friedl, M. A., McIver, D. K., Hodges, J. C., Zhang, X., Muchoney, D., Strahler, A. H., et al. (2002). Global land cover mapping from MODIS: Algorithms and early results. *Remote Sensing of Environment, 83*(1), 287–302.

Klimont, Z., Cofala, J., Xing, J., Wei, W., Zhang, C., Wang, S., et al. (2009). Projections of SO2, NOx and carbonaceous aerosols emissions in Asia. *Tellus B, 61*(4), 602–617.

Lamarque, J. -F., Bond, T. C., Eyring, V., Granier, C., Heil, A., Klimont, Z., et al. (2010). Historical (1850–2000) gridded anthropogenic and biomass burning emissions of reactive gases and aerosols: Methodology and application. *Atmospheric Chemistry and Physics, 10*(15), 7017–7039.

Lu, Z., Zhang, Q., & Streets, D. G. (2011). Sulfur dioxide and primary carbonaceous aerosol emissions in China and India, 1996–2010. *Atmospheric Chemistry and Physics, 11*(18), 9839–9864.

National Bureau of Statistics and National Energy Administration. (2009). *China energy statistical yearbook, 1986, 1989–2008 editions*. Cambridge: Cambridge University Press.

National Development and Reform Commission and Development Research Center of the State Council. (2009). *2050 China energy and CO2 emissions report*. Beijing.

Ohara, T., Akimoto, H., Kurokawa, J. -I., Horii, N., Yamaji, K., Yan, X., & Hayasaka, T. (2007). An Asian emission inventory of anthropogenic emission sources for the period 1980–2020. *Atmospheric Chemistry and Physics, 7*(16), 4419–4444.

Shindell, D., Kuylenstierna, J. C., Vignati, E., van Dingenen, R., Amann, M., Klimont, Z., et al. (2012). Simultaneously mitigating near-term climate change and improving human health and food security. *Science, 335*(6065), 183–189.

State Power Corporation of China. (2008). *China electricity yearbook 2007*. Beijing: China Electricity Press.

Streets, D. G., Gupta, S., Waldhoff, S. T., Wang, M. Q., Bond, T. C., & Yiyun, B. (2001). Black carbon emissions in China. *Atmospheric Environment, 35*(25), 4281–4296.

Streets, D., Bond, T., Carmichael, G., Fernandes, S., Fu, Q., He, D., et al. (2003). An inventory of gaseous and primary aerosol emissions in Asia in the year 2000. *Journal of Geophysical Research: Atmospheres (1984–2012), 108*(D21), 203.

van der Werf, G. R., Randerson, J. T., Giglio, L., Collatz, G., Mu, M., Kasibhatla, P. S., et al. (2010). Global fire emissions and the contribution of deforestation, savanna, forest, agricultural, and peat fires (1997–2009). *Atmospheric Chemistry and Physics, 10*(23), 11707–11735.

Wang, R., Tao, S., Wang, W., Liu, J., Shen, H., Shen, G., Wang, B., Liu, X., Li, W., & Huang, Y. (2012). Black carbon emissions in China from 1949 to 2050. *Environmental science & technology, 46*(14), 7595–7603.

Zhang, Q., Streets, D. G., Carmichael, G. R., He, K., Huo, H., Kannari, A., et al. (2009). Asian emissions in 2006 for the NASA INTEX-B mission. *Atmospheric Chemistry and Physics, 9*(14), 5131–5153.

Chapter 7
Global Emissions of Black Carbon from 1960 to 2007

7.1 Global BC Emissions in 2007

Global total BC emission from all sources was 8.7 Tg/year in 2007. Of the total, 2.3 Tg/year was emitted from energy-related sources. Energy production, industry, residential/commercial sectors, transportation, and agriculture contributed a total emission of 0.16, 1.6, 2.8, 1.5 and 0.47 Tg/year, respectively. Table 7.1 lists the BC emissions from 64 fuel sub-types in PKU-FUEL-2007, with the corresponding CO_2 emissions from PKU-CO_2-2007. As an indicator for energy use efficiency, the emission ratio of BC to CO_2 for each fuel sub-type is also listed in Table 7.1. The emission ratio of BC to CO_2 is the highest in residential/commercial sectors (1.69), followed by biomass burning in the field (1.29), transportation (0.90) and industry (0.70). Due to different time scales of the climate effects of BC and CO_2 (Boucher and Reddy 2008), the emission ratio of BC to CO_2 is important to evaluate the effects of climate mitigation. For example, policies regarding with the residential/commercial sectors with relatively high BC emissions are expected to slow down the global warming within short term, while policies regarding with the sector of energy production will be more important to slow down the global warming within long term.

According to the Monte Carlo simulation, the global total BC emission was ranging from 5.4 to 14.8 Tg/year, due to the variation of all parameters in the emission model. The probabilistic distributions of BC emission for global total, energy-related sources, wildfires, China total, India total, and the U.S.A. are shown in Fig. 7.1. The uncertainty in BC emissions is mainly induced by the variation of BC emission factors. For instance, if only the variation in EF_{BC} was considered, the uncertainty in global BC emission would be 5.6–14.4 Tg/year as an inter-quartile range. More measurements of EF_{BC} are needed to reduce the overall uncertainty in the inventory of BC.

R. Wang, *Global Emission Inventory and Atmospheric Transport of Black Carbon*,
Springer Theses, DOI 10.1007/978-3-662-46479-3_7

Table 7.1 Emissions of BC from 64 fuel sub-types in 2007

Sector	Type	Detailed sub-type	BC (Gg/year)	CO_2 (Tg C/year)	BC/CO_2 (×1000)
Energy production	Coal	Anthracite	0.45	22.37	0.020
		Coke	0.44	21.00	0.021
		Bituminous coal	129.75	2147.28	0.060
		Lignite	10.64	512.43	0.021
		Peat	0.11	9.21	0.012
	Petroleum	Gas/Diesel	1.08	49.75	0.022
		Residue fuel oil	2.75	136.78	0.020
		Natural gas liquids	0.00	0.01	0.000
	Gas	Dry natural gas	0.16	662.63	0.000
		Natural gas flaring	0.01	73.56	0.000
	Biomass	Solid biomass	0.83	150.98	0.005
		Biogas	0.00	5.57	0.000
	Waste	Municipal waste	11.21	21.02	0.533
		Industrial waste	2.68	4.76	0.563
	Sub-total		160.12	3800.02	0.042
Industry	Coal	Coke production	388.39	84.82	4.579
		Brick production	846.75	216.89	3.904
		Aluminum production	2.53	18.49	0.137
		Anthracite	2.34	28.42	0.082
		Coke	1.65	18.57	0.089
		Bituminous coal	34.33	374.74	0.092
		Lignite	0.51	16.73	0.030
		Peat	0.01	0.82	0.012
	Petroleum	Gas/diesel	282.00	111.45	2.530
		Residue fuel oil	1.47	102.65	0.014
		Petroleum refinery	0.52	216.33	0.002
		Natural gas liquids	0.02	0.97	0.021
	Gas	Dry natural gas	0.15	639.56	0.000
	Biomass	Solid biomass	1.00	180.80	0.006
		Biogas	0.00	1.61	0.000
	Waste	Municipal waste	0.18	0.33	0.545
		Industrial waste	2.92	5.09	0.574
	Sub-total		1564.77	2018.27	0.775
Residential and Commercial	Coal	Anthracite	0.05	2.56	0.020
		Coke	0.14	0.12	1.167
		Bituminous coal	763.64	80.37	9.502
		Lignite	3.19	10.07	0.317
		Peat	0.15	0.52	0.288

(continued)

Table 7.1 (continued)

Sector	Type	Detailed sub-type	BC (Gg/year)	CO_2 (Tg C/year)	BC/CO_2 ($\times$1000)
	Petroleum	Liquid petroleum gas	0.90	88.98	0.010
		Natural gas liquids	0.00	0.05	0.000
		Kerosene used	8.32	55.92	0.149
	Gas	Dry natural gas	0.09	393.32	0.000
	Biomass	Biogas	0.00	3.56	0.000
		Firewood	1191.72	553.45	2.153
		Straw	806.51	375.88	2.146
		Dung cake	11.22	54.68	0.205
	Waste	Small-scaled solid waste burning	36.51	48.27	0.756
	Sub-total		2822.44	1667.74	1.692
Transportation	Petroleum	Motor vehicle gasoline	209.57	755.29	0.277
		Aviation gasoline	0.23	1.02	0.225
		Jet kerosene	20.61	89.56	0.230
		Motor vehicle gas/diesel	1159.74	634.98	1.826
		Ocean tanker	20.14	35.94	0.560
		Ocean container ships	32.86	26.96	1.219
		Bulk and combined carriers	14.64	25.39	0.577
		General cargo vessels	27.51	44.36	0.620
		Non-cargo vessels	16.21	30.27	0.536
		Auxiliary engines	15.32	10.76	1.424
		Military vessels	3.45	7.93	0.435
	Biomass	Liquid biofuels used by vehicles	16.75	42.44	0.395
	Sub-total		1537.03	1704.91	0.902
Agriculture	Petroleum	Gas/diesel used in agriculture	218.85	85.27	2.567
	Waste	Open burning of agriculture waste	251.91	145.03	1.737
	Sub-total		470.76	230.30	2.044
Wildfires	Biomass	Forest fires	211.98	193.90	1.093
		Deforestation fires	662.35	489.52	1.353
		Peat fires	57.92	46.07	1.257
		Woodland fires	329.35	286.34	1.150
		Savanna fires	1078.43	801.64	1.345
	Sub-total		2340.03	1817.48	1.288
Total			8737.71	11238.72	0.777

The CO_2 emissions and the emission ratio of BC to CO_2 are listed in the table

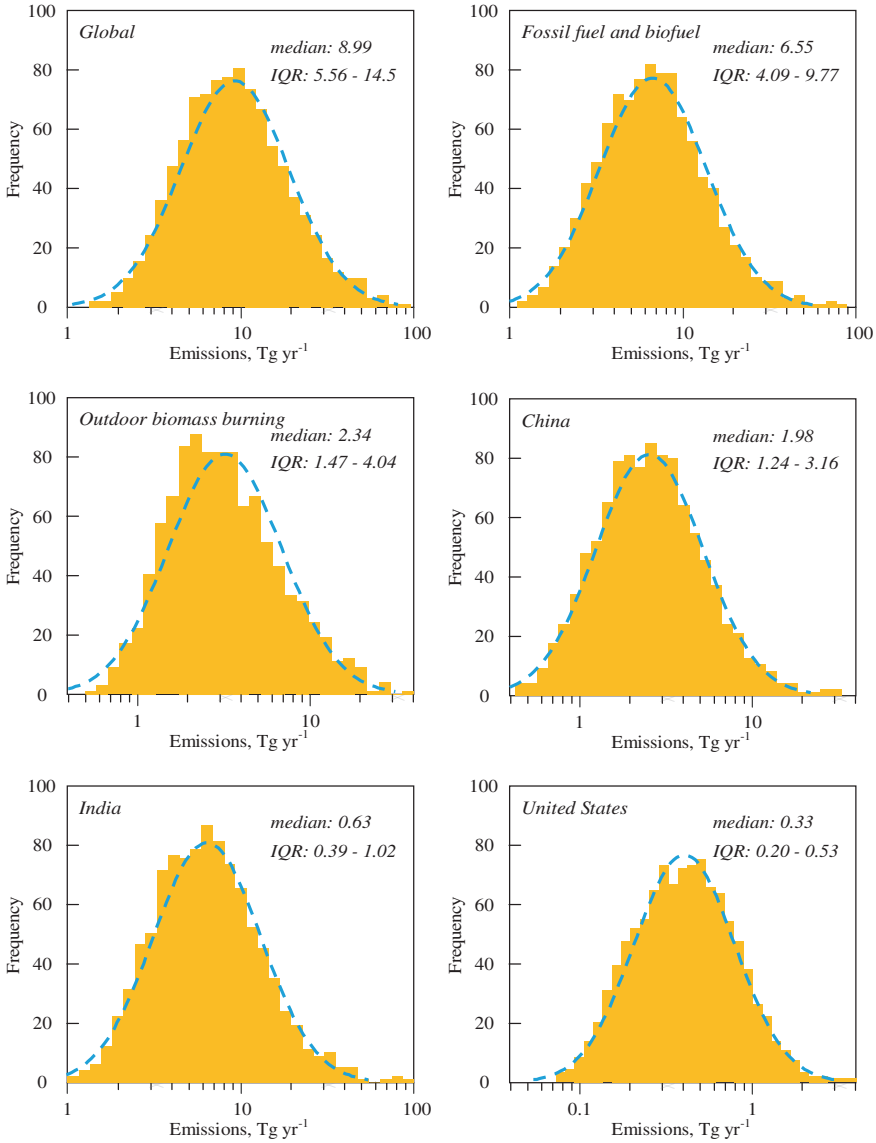

Fig. 7.1 Probabilistic distributions of BC emission for global total, energy-related sources, wildfires, China total, India total, and the U.S.A. from Monte Carlo simulations. In all of them, log-normal distributions are observed, and the median and inter-quartile ranges (IQR) are listed in each figure. Reproduced with Permission (Wang et al. 2014a)

Figure 7.2 shows the spatial distribution of BC emission at a resolution of $0.1° \times 0.1°$ according to PKU-BC-2007. High BC emission densities were mainly found over the populated regions in East Asia and South Asia, the industrialized

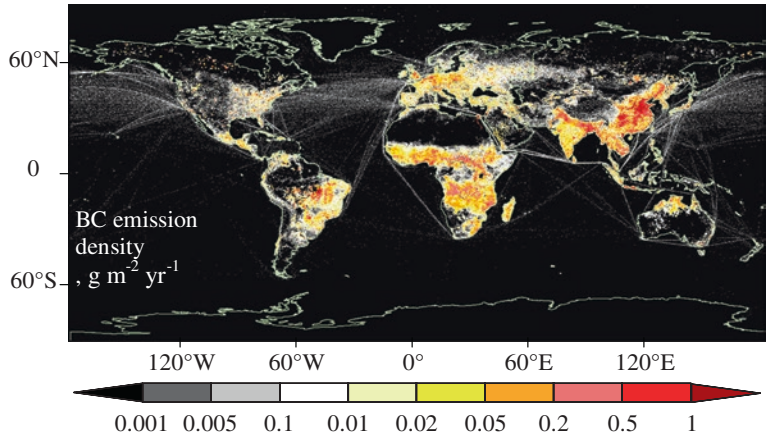

Fig. 7.2 Spatial distribution of BC emission in 2007 according to the PKU-BC-2007 inventory at a resolution of 0.1° × 0.1°. Reproduced with Permission (Wang et al. 2014a)

regions in Europe and North America, and savannas and grasslands in South America and Africa. Globally, there were three major hot-spot regions with extremely high BC emission densities (>1 g m^{-2} $year^{-1}$): the North China Plain in the north of China; the Sichuan Basin in the southwest of China; the Indo-Gangetic Plain in Indian Peninsula. In these three regions, there are either dense population distributions associated with a large consumption of domestic fuels (e.g. raw coal, straw or wood), or concentrated industry with high emission factors, such as coking or brick production.

With a total emission of 2.2 Tg/year, East Asia contributed 25 % to the global BC emissions, followed by South and Southeast Asia (18 %), South America (13 %), East and South Africa (9.3 %), West and Central Africa (9.3 %), Europe (8.5 %), North America (6.3 %), North Africa (5.6 %), Middle East (3.6 %), and Oceania (2.0 %). The relative contribution by different sectors to BC emissions in each region is charted in Fig. 7.3. Regionally, the residential/commercial sector is the most important source in East Asia and South/Southeast Asia, due to a relatively higher EF_{BC} than that in power plants and industry. In contrast, wildfire is the most important source in South America, East and South Africa, West and Central Africa, North Africa and Oceania. With less fuels consumed by the residential/commercial sector and industry, BC emission was dominated by motor vehicles in Europe and North America.

BC emissions have been concerned for the important role of BC in the Earth climate system. Bond et al. (2004) developed the first global BC emission inventory accounting for the variation of EF_{BC} among different sectors, combustion facilities, and emission control technologies. Bond et al. (2007) studied historic BC emissions from 1850 to 2000 by tracking the change of technology. Furthermore, the methodology used by (Bond et al. 2004, 2007) had been adopted to generate historical gridded BC inventories (Dentener et al. 2006; Lamarque

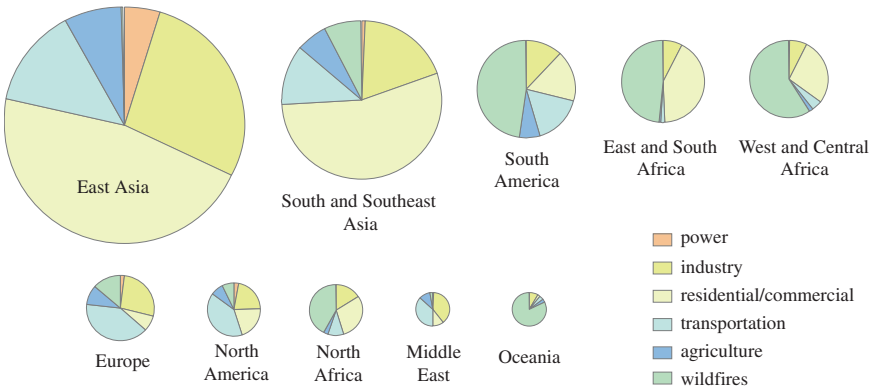

Fig. 7.3 Relative contributions by different sources in each region. The total area of the pies is proportional to the total BC emission in the region

et al. 2010; Granier et al. 2011; Diehl et al. 2012), namely the AeroCom, ACCMIP or MACCity inventory. MACCity was used to run the climate models for the Climate Model Intercomparison Program #5 in support of the IPCC Fifth Assessment report. It is important to compare our inventory with the MACCity inventory, to see the impact on modelling BC and quantifying the role of BC in the Earth climate system.

The difference in BC emissions between the PKU-BC-2007 and MACCity inventories for the same year 2007 is mapped in Fig. 7.4. The largest underestimation by MACCity is found in the north and southwest of China, as well as the northeast of India, where carbon-based fuels were intensively used in the residential sector over the rural areas. There are two major reasons to explain for the differences. First, the PKU-BC-2007 inventory update the emission factors based on some data which have not been used in the MACCity inventory (Chen et al. 2005, 2006, 2009; Cao et al. 2006, 2008; Li et al. 2007, 2009; Bi et al. 2008; Kleeman et al. 2008; Olivares et al. 2008; Zhang et al. 2008; Shen et al. 2010, 2012, 2013; Saud et al. 2012) and regression models for the emission factors of motor vehicles. The update of EF_{BC} leads to an increase of BC emissions from motor vehicles and residential sectors over the developing regions. Second, the PKU-BC-2007 inventory is highly disaggregated based on local activity data (e.g., each county in China). It induces a higher BC emission in the north and southwest of China, the northwest of India and the Ganges-Brahmaputra delta in PKU-BC-2007 than MACCity. In comparison, the MACCity inventory was developed from country-level fuel data disaggregated spatially by assuming a uniform national per capita fuel consumption for major sources (Lamarque et al. 2010; Granier et al. 2011; Diehl et al. 2012). The super-national data in PKU-FUEL-2007 shows that, for instance in China, the per capita consumption of residential coal over the North China Plain is 5.2 kg cap^{-1}, far higher than that in the southeast of China (0.90 kg cap^{-1}), whereas the MACCity inventory assumes constant per capita emissions for the

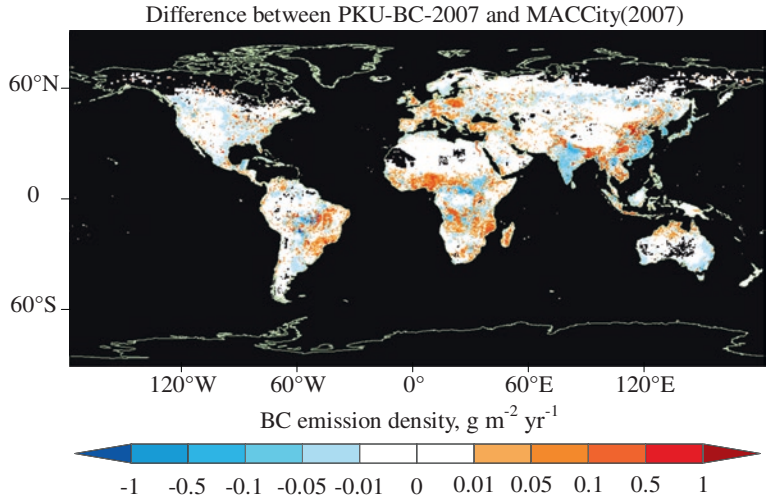

Fig. 7.4 Comparison of BC emissions between the PKU-BC-2007 and MACCity (2007) inventories. The 0.1° × 0.1° gridded BC emission in the PKU-BC-2007 inventory was downscaled to 0.5° × 0.5° to compare with that in the MACCity (2007) inventory at a resolution of 0.5° × 0.5°. Reproduced with Permission (Wang et al. 2014a)

entire country. Similarly, per capita consumption of fossil fuel is 1.1 Mg C cap^{-1} over the New Delhi region, 3.3 times larger than the Indian country mean (0.33 Mg C cap^{-1}). In addition to the contrast different in Asia, there is an increase of BC emissions over Western Africa due to a higher BC emission factors applied for the residential sector, and a decrease over Central Africa due to updating fire data from GFED2 to GFED3 (van der Werf et al. 2006, 2010).

7.2 Historical BC Emissions from 1960 to 2007

Estimation of historical BC emissions is important to understand the impact of BC on the past climate, and predict the future trend. Novakov et al. (2003) made the first attempt to track BC emissions back to the 19th century. Bond et al. (2007) studied the historic BC emissions from 1850 to 2000 by simulating the change of technology. Emissions of BC change temporally due to the change in both fuel consumption and emission factors. Based on the re-compiled national fuel consumptions and updated EF_{BC} dataset with the temporal variation quantified for certain sources, the historical trend in global BC emissions were derived for the period from 1960 to 2007. As a result, the global BC emissions from all sources were 5386 (3434–8488 as an inter-quartile range) and 9052 (5598–14,437 as an inter-quartile range) Gg $year^{-1}$ in 1960 and 2007, respectively. Of the total, anthropogenic BC emissions amounted to 3196 Gg $year^{-1}$ in 1960 and increased

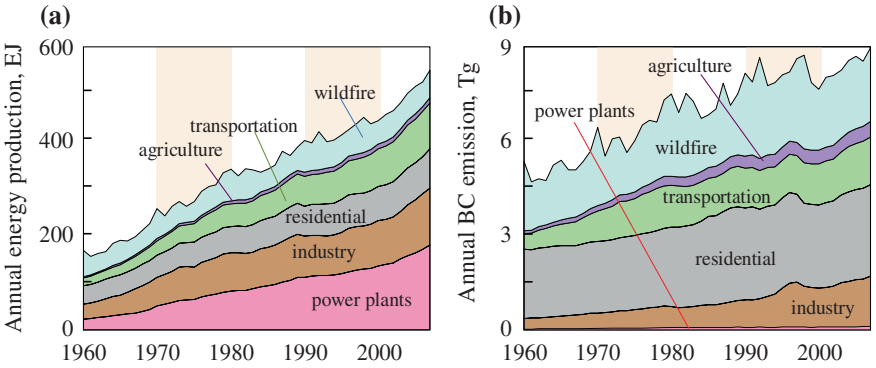

Fig. 7.5 Temporal trends of the global total energy productions (**a**) and BC emissions (**b**) from 1960 to 2007. The energy productions and BC emissions from various sectors are shown as different colors. Reproduced with Permission (Wang et al. 2014b). Copyright (2014) American Chemical Society

by 110 % to an all time high value of 6708 Gg year^{-1} in 2007, due to the increase of fuel consumption induced by population expansion and economic development.

The temporal trends of the fuel consumptions and resultant BC emissions from 1960 to 2007 from six major sectors are shown in Fig. 7.5. Different from previous studies (Bond et al. 2007; Junker and Liousse 2008), our inventory noticed series of fluctuations in total emissions after 1980, mainly due to the change of technologies in China. For example, the transfer of hard coal to oil/gas fuels in the residential and commercial sectors in Chinese cities in the late 1980s led to a peak of BC emissions in China reached in the year of 1987 (7835 Gg year^{-1}). Meantime, the increase of coking plants in early 1990s followed by a phase-out of beehive coking ovens since 1996 resulted in a peak of global BC emissions in 1997.

The global total BC emissions, together with BC emissions in China, developing countries other than China, and all developed countries from the residential sector, industry and motor vehicles are shown in Fig. 7.6.

As shown in Fig. 7.5, the residential sector is the most important energy-related source of BC emissions. From 1960 to 1988, the global BC emission from the residential sector had increased by 37 % from 2226 to 3021 Gg year^{-1}, and leveled off thereafter. The global trend in BC emissions from the residential sector before 1988 was controlled by the trend in BC emissions from the developing countries, which was increasing as a result of the rising population. After 1988, although the total population of developing countries continued to increase, there is a shift of fuels from hard coal to gas/oil fuels over the urban areas. Figure 7.7 illustrates the evolution of global fuel compositions from 1960 to 2007. In China, for instance, the domestic coal in cities had been gradually replaced by cleaner fuels (e.g. liquid petroleum gas) in the late 1980s, which decelerate the increase of BC emissions.

In the industrial sector, the total BC emissions had been increasing continuously, mainly due to the expansion of high-emission industries (e.g. coke and

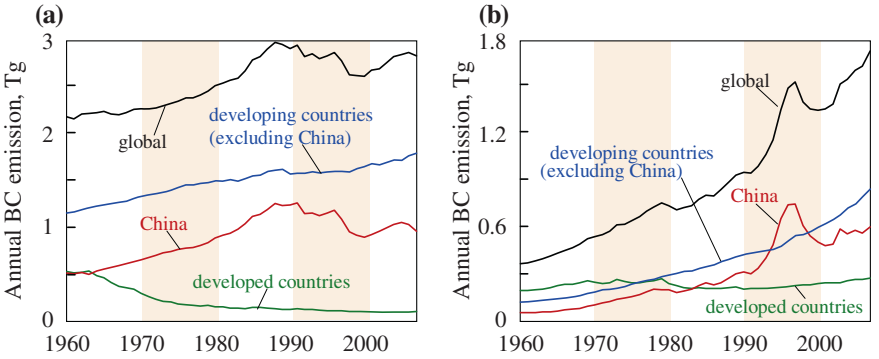

Fig. 7.6 Historical BC emissions in the residential (**a**) and industrial sector (**b**) from 1960 to 2007. The emissions are shown for China (*red*), other developing countries (*blue*), developed countries (*green*), and global total (*black*). Reproduced with Permission (Wang et al. 2014b). Copyright (2014) American Chemical Society

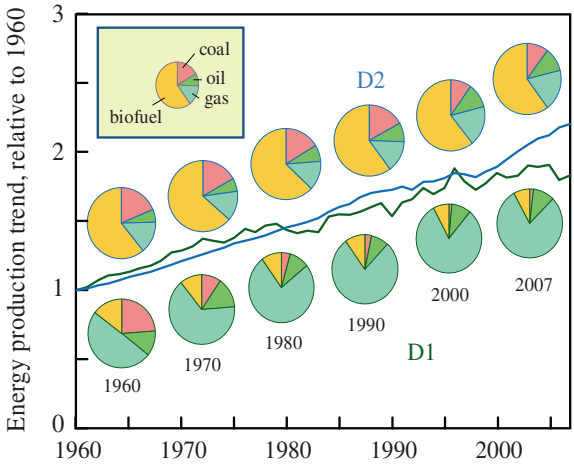

Fig. 7.7 Temporal variation of the fuel composition in the residential sector in developed (D1) and developing countries (D2). Reproduced with Permission (Wang et al. 2014b). Copyright (2014) American Chemical Society

brick production) in developing countries in the period. For example, a fast rise of beehive coke ovens in China in the middle of 1990s led to a notable increase of BC emission in the region (Fig. 7.8). It is normally well known that this source is associated with very high BC emission factors (Bond et al. 2004).

The amounts of BC emissions and the temporal trend derived from the our inventory are compared with that reported in previous work (Bond et al. 2007; Cofala et al. 2007; Junker and Liousse 2008; Lamarque et al. 2010; Granier et al. 2011; Diehl et al. 2012). The historical BC emissions from energy-related sources based on our inventory (PKU-BC) and other estimates are all shown in Fig. 7.9. The overall trend in BC emissions according to PKU-BC is similar to

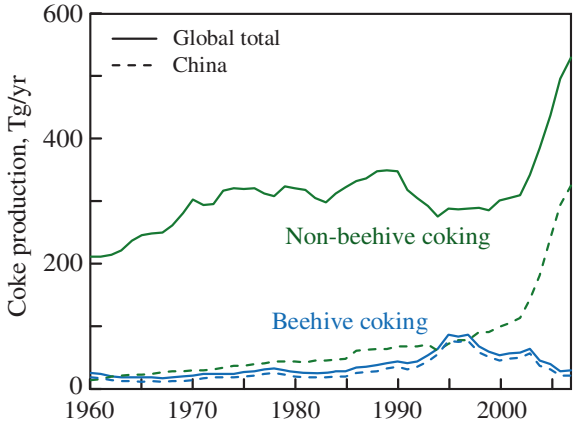

Fig. 7.8 Temporal variation of coke production from beehive coking plants and non-beehive coking plants for the global total and the total in China. Reproduced with Permission (Wang et al. 2014b). Copyright (2014) American Chemical Society

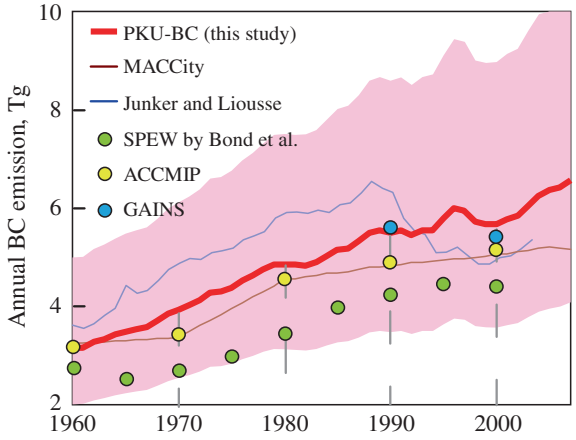

Fig. 7.9 Comparison of the energy-related BC emissions from 1960 to 2007 among different inventories. The annual BC emission and associated uncertainties according to our inventory are shown as median values (*red line*) and the inter-quartile ranges (*shaded area*) from a Monte Carlo simulation. The inventories compared with PKU-BC include ACCMIP (Lamarque et al. 2010), MACCity (Granier et al. 2011; Diehl et al. 2012), SPEW (Bond et al. 2007, 2013), GAINS (Cofala et al. 2007), and the inventory developed by Junker and Liousse (2008). Reproduced with Permission (Wang et al. 2014b). Copyright (2014) American Chemical Society

that according to ACCMIP (Lamarque et al. 2010), MACCity (Granier et al. 2011; Diehl et al. 2012), and SPEW (Bond et al. 2007, 2013). They generally show an increase in BC emissions over the period from 1960 to 2007, with an exception according to the inventory developed by Junker and Liousse (2008). According

to Junker and Liousse (2008), the global BC emissions had been increasing from 1960 to 1988, followed by a significant decrease from 1989 to 1999 (Junker and Liousse 2008). In comparison, the annual energy-related BC emissions estimated by Junker and Liousse are 10–24 % higher than our estimations over the period from 1960 to 1988, but 11–16 % lower over the period from 1995 to 2003. Lamarque et al. (2010) had compared different inventories, and noticed that the BC emission factors adopted for the coal consumed by power plants and industry by Junker and Liousse are higher than other inventories, which are likely overestimated.

In addition, the annual BC emissions from energy-related sources according to PKU-BC are close to the estimations by GAINS (Cofala et al. 2007), but higher than those according to the ACCMIP inventory (Lamarque et al. 2010), the MACCity inventory (Granier et al. 2011; Diehl et al. 2012), and the SPEW inventory (Bond et al. 2007, 2013). The annual BC emissions from energy-related sources according to PKU-BC derived as median estimates are on average 11 and 16 % higher than that according to the MACCity and SPEW inventories, respectively. This is mainly due to higher BC emission factors adopted for the residential sector and diesel vehicles in developing countries by our inventory according to new measurements. For instance, a constant fraction (20 %) of BC in fine particles was assumed to convert the emission factor of particulate matter to the emission

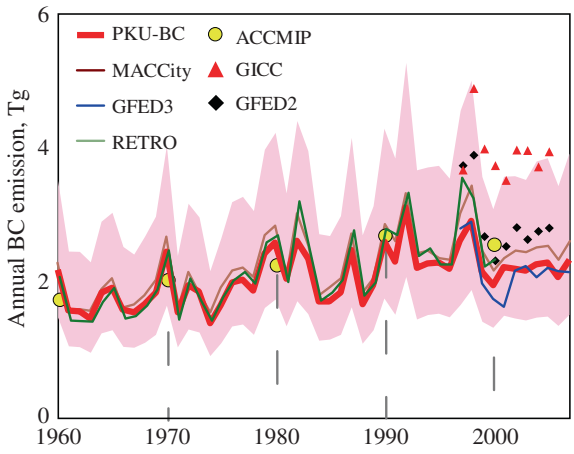

Fig. 7.10 Comparison of BC emissions from wildfires among different inventories. The annual BC emission and associated uncertainties according to our inventory are shown as median values (*red line*) and the inter-quartile ranges (*shaded area*) from a Monte Carlo simulation. The inventories compared with PKU-BC include ACCMIP (Lamarque et al. 2010), MACCity (Granier et al. 2011; Diehl et al. 2012); GFED2 (Global Fire Emissions Database version 2) (van der Werf et al. 2006); GFED3 (Global Fire Emissions Database version 3) (van der Werf et al. 2010); GICC (Le programme Gestion et Impacts du Changement climatique) (Mieville et al. 2010); and RETRO (REanalysis of the TROpospheric chemical composition over the past 40 years) (Schultz et al. 2008). Reproduced with Permission (Wang et al. 2014b). Copyright (2014) American Chemical Society

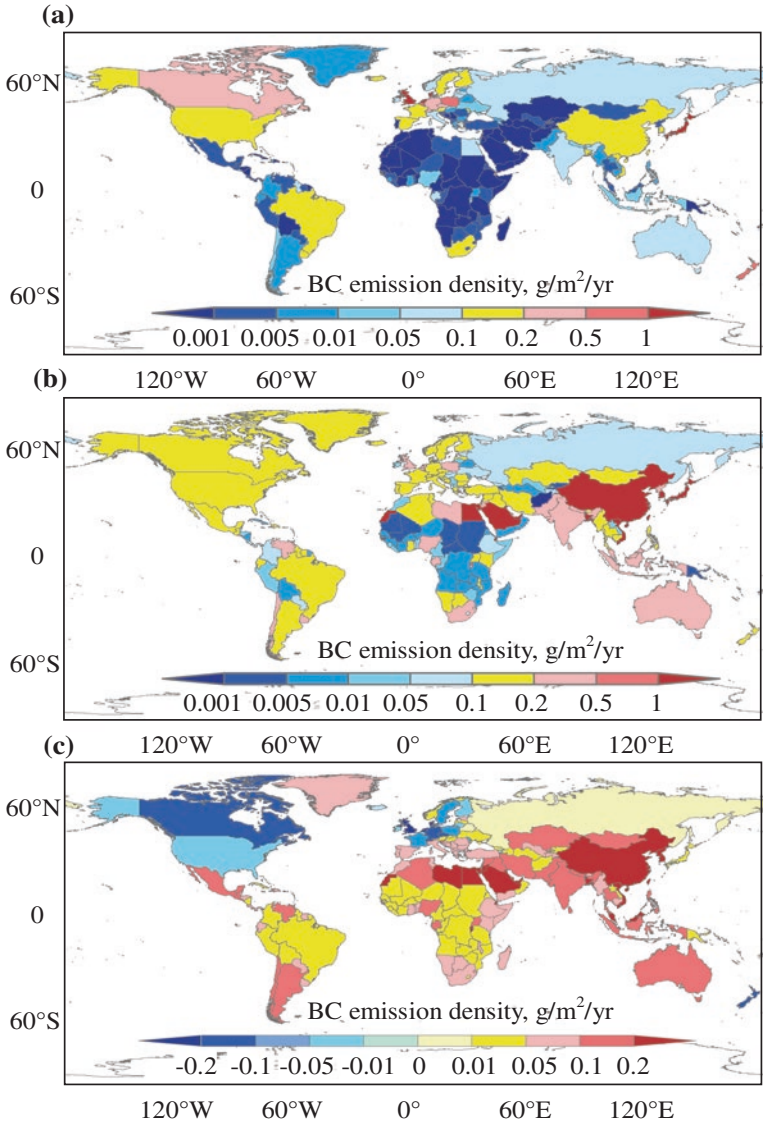

Fig. 7.11 Geographical distributions of energy-related BC emission densities in the years of 1960 (**a**) and 2007 (**b**) and the difference between the 2 years (**c**). The BC emission densities were all derived as BC emission per unit of area over grids with population density >1 cap km^{-2} based on the gridded population dataset in 2007. Reproduced with Permission (Wang et al. 2014b). Copyright (2014) American Chemical Society

factors of BC for wood burnt in stoves due to lack of measurements when developing the earlier inventories (Bond et al. 2004), but a higher value for this parameter (40–70 %) was reported in a recent measurement (Li et al. 2009). In addition,

the different data used for the fuel consumptions is also a reason for the different emissions in different emission inventories. For instance, the fuel consumption in China was taken from the national statistics in the International Energy Agency statistics or the United Nations energy database in previous inventories (Bond et al. 2007; Junker and Liousse 2008; Lamarque et al. 2010), but a more detailed provincial data from the Chinese Energy Yearbook were used in our inventory. As noticed in recent work and confirmed in our work, the Chinese fuel consumptions were underestimated by the International Energy Agency statistics or the United Nations energy database.

For wildfires, the estimations of BC emissions according to PKU-BC were also compared with other inventories (van der Werf et al. 2006, 2010; Schultz et al. 2008; Lamarque et al. 2010; Mieville et al. 2010; Granier et al. 2011; Diehl et al. 2012). The BC emissions from wildfires according to different inventories are shown in Fig. 7.10. The emissions are close to each other among different inventories, except for the GICC (Le programme Gestion et Impacts du Changement climatique) inventory (Mieville et al. 2010). This is because of that the PKU-BC inventory relies on the fuel consumption by wildfires in these inventories (Schultz et al. 2008; van der Werf et al. 2010), and the adopted BC emission factors were close to those used in previous inventories.

The geographical distributions of energy-related BC emissions over populated regions (see the definition in the figure caption) in the years of 1960 and 2007 and the difference between the 2 years are shown in Fig. 7.11. In 1960, high BC emission densities were mainly distributed over the European countries, North America, and Japan due to a large consumption of coal, and over some Asian countries like China and Vietnam due to a large consumption of biofuels. Since the energy-related BC emission densities was averaged over populated regions, high values are also found over the countries in Middle East in 2007 with population highly concentrated in cities, such as Egypt and Libya. From 1960 to 2007, there is a significant shift of BC emission centers geographically. The BC emission densities increased dramatically in the semi-developed countries, such as China and India, and the BC emission densities decreased over North America and Europe. The largest increase of BC emission densities was found in Cambodia (+0.37 g/m^2/year), China (+0.30 g/m^2/year), and India (+0.13 g/m^2/year). Meanwhile, a significant decline was found in some developed countries like UK (−1.1 g/m^2/year), Denmark (−0.27 g/m^2/year), and Netherlands (−0.21 g/m^2/year), large due to the improvement of combustion technologies.

References

Bi, X., Simoneit, B. R., Sheng, G., & Fu, J. (2008). Characterization of molecular markers in smoke from residential coal combustion in China. *Fuel, 87*(1), 112–119.

Bond, T. C., Streets, D. G., Yarber, K. F., Nelson, S. M., Woo, J. H., & Klimont, Z. (2004). A technology-based global inventory of black and organic carbon emissions from combustion. *Journal of Geophysical Research: Atmospheres (1984–2012), 109*(D14).

Bond, T. C., Bhardwaj, E., Dong, R., Jogani, R., Jung, S., Roden, C., et al. (2007). Historical emissions of black and organic carbon aerosol from energy-related combustion, 1850–2000. *Global Biogeochemical Cycles, 21*(2). doi:10.1029/2006GB002840.

Bond, T. C., Doherty, S. J., Fahey, D., Forster, P., Berntsen, T., DeAngelo, B., et al. (2013). Bounding the role of black carbon in the climate system: A scientific assessment. *Journal of Geophysical Research: Atmospheres, 118*(11), 5380–5552.

Boucher, O., & Reddy, M. (2008). Climate trade-off between black carbon and carbon dioxide emissions. *Energy Policy, 36*(1), 193–200.

Cao, G., Zhang, X., & Zheng, F. (2006). Inventory of black carbon and organic carbon emissions from China. *Atmospheric Environment, 40*(34), 6516–6527.

Cao, G., Zhang, X., Gong, S., & Zheng, F. (2008). Investigation on emission factors of particulate matter and gaseous pollutants from crop residue burning. *Journal of Environmental Sciences, 20*(1), 50–55.

Chen, Y., Sheng, G., Bi, X., Feng, Y., Mai, B., & Fu, J. (2005). Emission factors for carbonaceous particles and polycyclic aromatic hydrocarbons from residential coal combustion in China. *Environmental Science and Technology, 39*(6), 1861–1867.

Chen, Y., Zhi, G., Feng, Y., Fu, J., Feng, J., Sheng, G., et al. (2006). Measurements of emission factors for primary carbonaceous particles from residential raw-coal combustion in China. *Geophysical Research Letters, 33*(20).

Chen, Y., Zhi, G., Feng, Y., Liu, D., Zhang, G., Li, J., et al. (2009). Measurements of black and organic carbon emission factors for household coal combustion in China: Implication for emission reduction. *Environmental Science and Technology, 43*(24), 9495–9500.

Cofala, J., Amann, M., Klimont, Z., Kupiainen, K., & Höglund-Isaksson, L. (2007). Scenarios of global anthropogenic emissions of air pollutants and methane until 2030. *Atmospheric Environment, 41*(38), 8486–8499.

Dentener, F., Kinne, S., Bond, T., Boucher, O., Cofala, J., Generoso, S., et al. (2006). Emissions of primary aerosol and precursor gases in the years 2000 and 1750 prescribed data-sets for AeroCom. *Atmospheric Chemistry and Physics, 6*(12), 4321–4344.

Diehl, T., Heil, A., Chin, M., Pan, X., Streets, D., Schultz, M., & Kinne, S. (2012). Anthropogenic, biomass burning, and volcanic emissions of black carbon, organic carbon, and SO2 from 1980 to 2010 for hindcast model experiments. *Atmospheric Chemistry and Physics Discussions, 12*(9), 24895–24954.

Granier, C., Bessagnet, B., Bond, T., D'Angiola, A., Van Der Gon, H. D., Frost, G. J., et al. (2011). Evolution of anthropogenic and biomass burning emissions of air pollutants at global and regional scales during the 1980–2010 period. *Climatic Change, 109*(1–2), 163–190.

Junker, C., & Liousse, C. (2008). A global emission inventory of carbonaceous aerosol from historic records of fossil fuel and biofuel consumption for the period 1860–1997. *Atmospheric Chemistry and Physics, 8*(5), 1195–1207.

Kleeman, M. J., Robert, M. A., Riddle, S. G., Fine, P. M., Hays, M. D., Schauer, J. J., & Hannigan, M. P. (2008). Size distribution of trace organic species emitted from biomass combustion and meat charbroiling. *Atmospheric Environment, 42*(13), 3059–3075.

Lamarque, J.-F., Bond, T. C., Eyring, V., Granier, C., Heil, A., Klimont, Z., et al. (2010). Historical (1850–2000) gridded anthropogenic and biomass burning emissions of reactive gases and aerosols: Methodology and application. *Atmospheric Chemistry and Physics, 10*(15), 7017–7039.

Li, X., Wang, S., Duan, L., Hao, J., Li, C., Chen, Y., & Yang, L. (2007). Particulate and trace gas emissions from open burning of wheat straw and corn stover in China. *Environmental Science and Technology, 41*(17), 6052–6058.

Li, X., Wang, S., Duan, L., Hao, J., & Nie, Y. (2009). Carbonaceous aerosol emissions from household biofuel combustion in China. *Environmental Science and Technology, 43*(15), 6076–6081.

Mieville, A., Granier, C., Liousse, C., Guillaume, B., Mouillot, F., Lamarque, J.-F., et al. (2010). Emissions of gases and particles from biomass burning during the 20th century using satellite data and an historical reconstruction. *Atmospheric Environment, 44*(11), 1469–1477.

Novakov, T., Ramanathan, V., Hansen, J., Kirchstetter, T., Sato, M., Sinton, J., et al. (2003). Large historical changes of fossil-fuel black carbon aerosols. *Geophysical Research Letters, 30*(6).

Olivares, G., Ström, J., Johansson, C., & Gidhagen, L. (2008). Estimates of black carbon and size-resolved particle number emission factors from residential wood burning based on ambient monitoring and model simulations. *Journal of the Air and Waste Management Association, 58*(6), 838–848.

Saud, T., Gautam, R., Mandal, T., Gadi, R., Singh, D., Sharma, S., et al. (2012). Emission estimates of organic and elemental carbon from household biomass fuel used over the Indo-Gangetic Plain (IGP), India. *Atmospheric Environment, 61*, 212–220.

Schultz, M. G., Heil, A., Hoelzemann, J. J., Spessa, A., Thonicke, K., Goldammer, J. G., et al. (2008). Global wildland fire emissions from 1960 to 2000. *Global Biogeochemical Cycles, 22*(2).

Shen, G., Yang, Y., Wang, W., Tao, S., Zhu, C., Min, Y., et al. (2010). Emission factors of particulate matter and elemental carbon for crop residues and coals burned in typical household stoves in China. *Environmental Science and Technology, 44*(18), 7157–7162.

Shen, G., Siye, W., Wen, W., Yanyan, Z., Yujia, M., Bin, W., et al. (2012). Emission factors, size distributions, and emission inventories of carbonaceous particulate matter from residential wood combustion in rural China. *Environmental Science and Technology, 46*(7), 4207–4214.

Shen, G., Tao, S., Wei, S., Chen, Y., Zhang, Y., Shen, H., et al. (2013). Field measurement of emission factors of PM, EC, OC, parent, nitro-, and oxy-polycyclic aromatic hydrocarbons for residential Briquette, coal cake, and wood in rural Shanxi, China. *Environmental Science and Technology, 47*(6), 2998–3005.

van der Werf, G. R., Randerson, J. T., Giglio, L., Collatz, G. J., Kasibhatla, P. S., & Arellano, A, Jr. (2006). Interannual variability in global biomass burning emissions from 1997 to 2004. *Atmospheric Chemistry and Physics, 6*(11), 3423–3441.

van der Werf, G. R., Randerson, J. T., Giglio, L., Collatz, G., Mu, M., et al. (2010). Global fire emissions and the contribution of deforestation, savanna, forest, agricultural, and peat fires (1997–2009). *Atmospheric Chemistry and Physics, 10*(23), 11707–11735.

Wang, R., Tao, S., Balkanski, Y., Ciais, P., Boucher, O., Liu, J., et al. (2014a). Exposure to ambient black carbon derived from a unique inventory and high-resolution model. *Proceedings of the National Academy of Sciences, 111*(7), 2459–2463.

Wang, R., Tao, S., Shen, H., Huang, Y., Chen, H., Balkanski, Y., et al. (2014b). Trend in global black carbon emissions from 1960 to 2007. *Environmental Science and Technology.*

Zhang, Y., Schauer, J. J., Zhang, Y., Zeng, L., Wei, Y., Liu, Y., et al. (2008). Characteristics of particulate carbon emissions from real-world Chinese coal combustion. *Environmental Science and Technology, 42*(14), 5068–5073.

Chapter 8
Concentration, Ambient Exposure, and Inhalation Intake of Black Carbon

8.1 Modelled Surface Concentrations of BC

Based on the developed PKU-BC inventory (E_{PKU}) and two versions of the LMDZ-OR-INCA model (M_{INz} and M_{IN}), the simulated surface concentrations of BC are derived and mapped in Fig. 8.1. The spatial patterns simulated by the two versions of the LMDZ-OR-INCA model are similar to each other, which is dependent on the spatial distribution of BC emissions. There are three hot-spot regions, including the North China Plain in the north of China, the Sichuan Basin in the southwest of China, and the Indo-Gangetic Plain in Indian Peninsula. Meanwhile, there are some differences in the regional distribution of BC surface concentrations, with a more detailed distribution of BC captured by the model of M_{INz} at a high resolution over Asia and M_{IN} at a high resolution in the remaining regions of the world.

In comparison, surface concentrations of BC were also simulated by two versions of the LMDZ-OR-INCA model using a reference MACCity inventory (E_{MAC}). The results are shown in Fig. 8.2. The major hot-spot regions of BC emissions are also the hot-spot regions of BC surface concentrations. There are significant differences in the spatial patterns of BC surface concentrations simulated by using the E_{PKU} and E_{MAC} inventories. First, the highest concentration simulated by E_{PKU} (>5 $\mu g\ m^{-3}$) is higher than that by E_{MAC} (4.1 $\mu g\ m^{-3}$). Second, the BC concentrations over the Sichuan Basin simulated by using E_{MAC} are lower by a factor of two to four than that simulated by using E_{PKU}. These differences reflect the difference in the emissions estimated by the two inventories.

R. Wang, *Global Emission Inventory and Atmospheric Transport of Black Carbon*,
Springer Theses, DOI 10.1007/978-3-662-46479-3_8

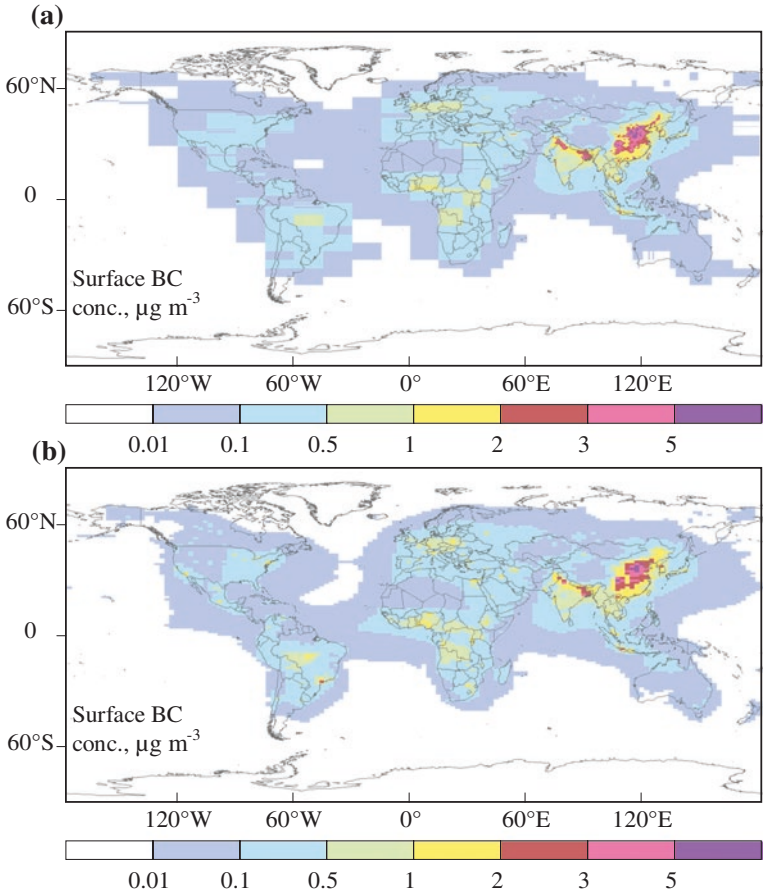

Fig. 8.1 Spatial distributions of surface BC concentrations simulated by using the model M_{INz} zoomed over Asia (**a**) and the regular-grid model M_{IN} (**b**) based on the PKU-BC inventory

8.2 Evaluation of the Modelled Surface BC Concentrations

To evaluate the simulated spatial distributions of surface BC concentrations by the four different combinations of models and emission inventories, namely, E_{PKU}/M_{INz}, E_{MAC}/M_{INz}, E_{PKU}/M_{IN}, and E_{MAC}/M_{IN}, 229 measured surface BC concentration worldwide were collected and used. Table 8.1 lists the information for the 229 measured surface BC observations. All of them were measured during 2003–2010 with five exceptions measured during 1999–2002 in Asia. Observed surface BC concentrations from different years are all used to ensure enough data for model validation. The geographic distribution of 229 observation sites is shown in Fig. 8.3. The measurement sites cover the major regions of East Asia, South Asia, Europe and North America.

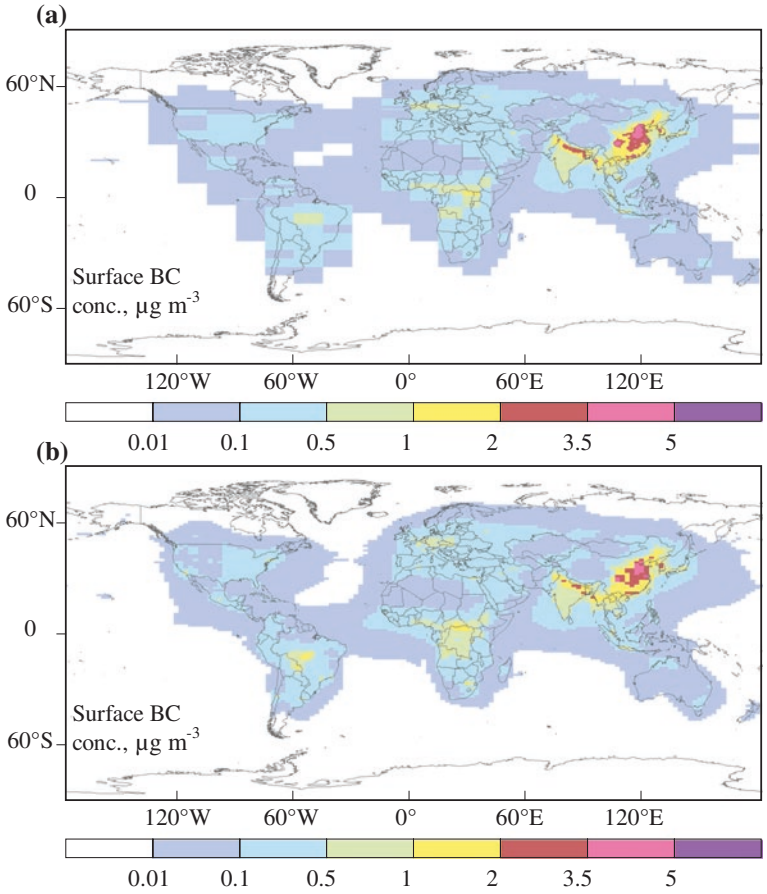

Fig. 8.2 Spatial distributions of surface BC concentrations simulated by using the model M_{INz} zoomed over Asia (**a**) and the regular-grid model M_{IN} (**b**) based on the MACCity inventory

Based on the four simulations, the simulated surface BC concentrations are evaluated by comparing against those measurements in Fig. 8.3, which are plotted in Fig. 8.4. To quantify the influence of uncertainties in PKU-BC-2007, the simulated surface BC concentrations by using the first and third quartiles of PKU-BC-2007 as inputs are shown as error bars. In addition, to quantify the deviation between the modelled and observed BC concentrations, two indexes were calculated, including normalized mean bias (NMB), defined as the difference between arithmetic means of the model minus the observation relative to the observation, and the percentages of sites with the deviation less than a factor of two (F_2). As an improvement by using the high-resolution model and highly disaggregated emission inventory, the NMB is reduced from −88 % in E_{MAC}/M_{IN} to −35 % in E_{PKU}/M_{INz}, with the F_2 increased from 24 to 73 % over all Asian sites. The NMB over all Asian sites is reduced to −73 % if only the updated inventory was used (E_{PKU}/M_{IN}), or −58 %

Table 8.1 Information for observations of surface BC concentrations

Region	Period	Height (m)	Method
Africa	2006 (Jun, Jul)	10	Thermal/optical carbon analysis (NIOSH)
Africa	2005 (Aug, Sep) 2006 (Apr, May)	6	Thermal/optical carbon analysis (Ghent protocol)
Asia	2003 (Jan, Jun, Jul)	6–20	Thermal/optical carbon analysis(IMPROVE-TOR)
Asia	1999 (Apr, Aug, Dec) 2000 (Apr, Aug, Dec)	3	Thermal/optical technique
Asia	2001–2002, annual	2–5	Thermal/optical carbon analysis (XRF)
Asia	2001–2002, annual	4.5	Thermal/optical carbon analysis (CHN method)
Asia	2005 (Jul–Oct)	10	Thermal/optical carbon analysis (IMPROVE-TOR)
Asia	2003–2004, annual	n.a.	Thermal/optical carbon analysis (NIOSH)
Asia	2006, March	10	Thermal/optical carbon analysis (IMPROVE-TOR)
Asia	2008, annual	10	Thermal/optical carbon analysis (IMPROVE-TOR)
Asia	2005–2007, annual	1.5	Thermal/optical carbon analysis (IMPROVE-TOR)
Asia	2003 (Jan, Jun, Jul)	6–20	Thermal/optical carbon analysis (IMPROVE-TOR)
Asia	2008 (Mar, Jun)	n.a.	Radiocarbon analysis
Asia	2003–2006, annual	17	Thermal/optical carbon analysis (NIOSH)
Asia	2000–2001 (Nov–Feb, Jun–Aug)	8	Thermal/optical carbon analysis (modified Dohrmann DC-52 carbon analyzer)
Asia	2006–2007, annual	8	Thermal/optical carbon analysis (IMPROVE-TOR)
Asia	Sep 2006–Feb 2007	n.a.	Thermal/optical carbon analysis (NIOSH)
Asia	1999–2005, annual	n.a.	CHN CORDER MT-3 analyzer
Asia	1998–1999, annual	20	Thermal manganese dioxide oxidation method
Asia	Aug 2004–Feb 2005	2–5	Thermal/optical carbon analysis (IMPROVE-TOR)
Asia	2007–2010, annual	n.a.	Thermal/optical carbon analysis (IMPROVE-TOR)
Asia	2002–2003, annual	4–40	C/H/N elemental analyzer
Asia	Nov 2007–Jun 2009	~10	Thermal/optical carbon analysis (NIOSH protocol)
Asia	2004, Dec	~10	Optical method (Aethalometer)
Asia	2006–2007, annual	~20	Thermal/optical carbon analysis (IMPROVE-TOT)
Asia	2006, annual	4–140	Thermal/optical carbon analysis (IMPROVE-TOR)
Asia	Apr 2009–Jan 2010	30	Thermal/optical carbon analysis (NIOSH)

(continued)

Table 8.1 (continued)

Region	Period	Height (m)	Method
Asia	2009–2010, annual	~10	Thermal/optical carbon analysis (IMPROVE-A)
Asia	2000–2005, annual	~5	Thermal/optical carbon analysis (IMPROVE-A)
Europe	2002–2007, annual	n.a.	Thermal/optical carbon analysis (TOT)
Europe	2003	1–85	Thermal/optical carbon analysis (Sunset TOT, VDI 2465 part 1, VDI 2465 part 2)
Europe	2005	1.8–10	Thermal/optical carbon analysis (NIOSH)
North America	2005	1–85	Thermal/optical carbon analysis (IMPROVE-TOR)

The data are compiled from the literature, as listed in Wang et al. (2014)

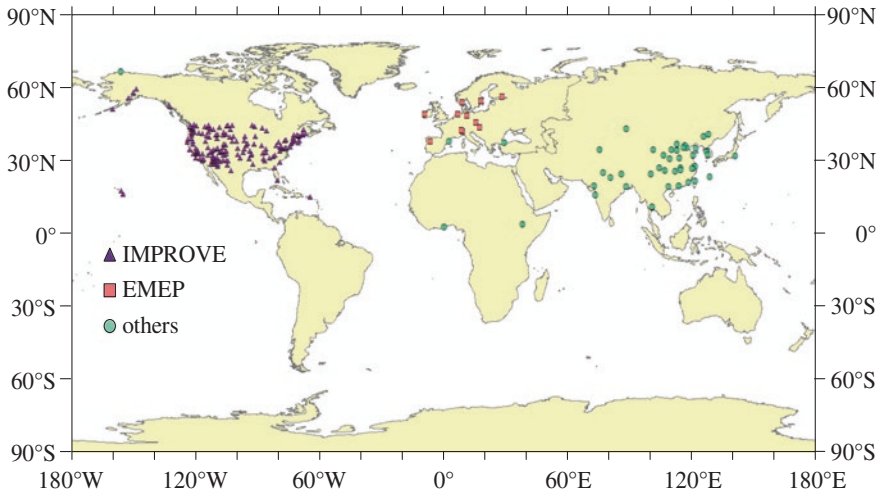

Fig. 8.3 Spatial distribution of the measurement sites. Measured surface BC concentrations are collected from the literature, covering the major regions of East Asia, South Asia, Europe and North America. Reproduced with permission (Wang et al. 2014)

if only the high-resolution model was used (E_{MAC}/M_{INz}), indicating that the final improvement is achieved as a combined effect by using the high-resolution model and highly disaggregated inventory. In addition, regarding the uncertainties in the emission inventory, when the first and third quartiles of PKU-BC-2007 were prescribed, the NMB at all Asian sites was −59 and −7 %, respectively. For the regions other than Asia, the model resolution is coarser in M_{INz}. However, an improvement was achieved by using the updated emission inventory E_{PKU}. When the inventory E_{MAC} was replaced with E_{PKU} in M_{IN}, the NMB was reduced from −32 to −5 % over sites in Africa, from −61 to −49 % over sites in Europe, and remained as

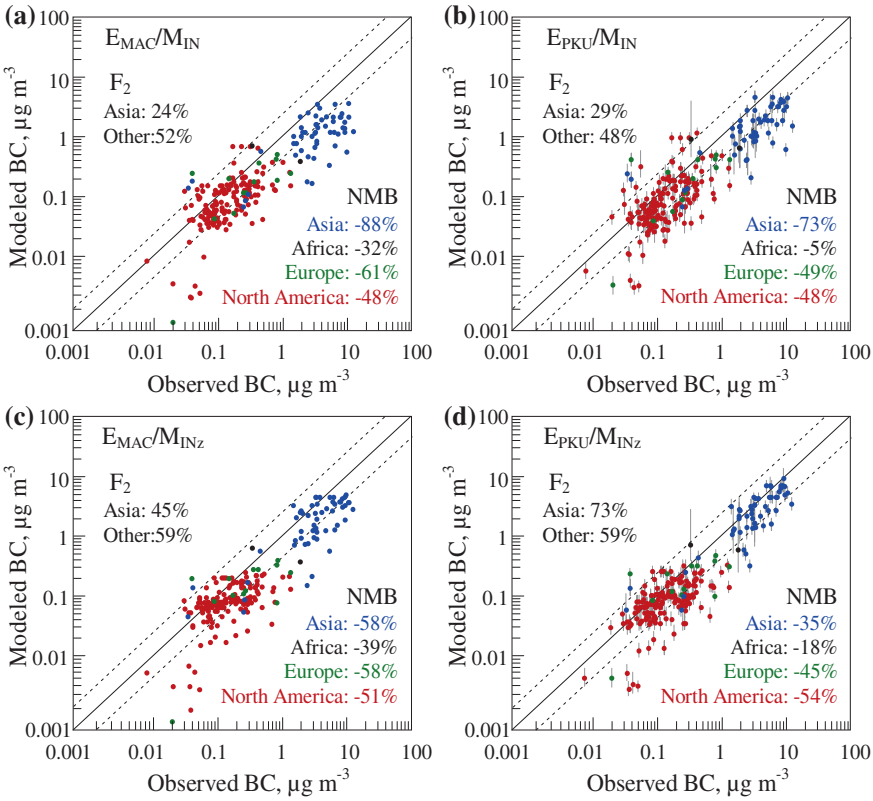

Fig. 8.4 Comparison between the modelled and observed surface BC concentrations in the four inventory/model combinations. **a** E_{MAC}/M_{IN}; **b** E_{PKU}/M_{IN}; **c** E_{MAC}/M_{INz}; **d** E_{PKU}/M_{INz}. Error bars (*vertical lines*) are derived by using the first and third quartiles of PKU-BC-2007. The *dashed lines* show the range of a factor of two deviations of the modeled surface BC concentration from the observations. Reproduced with permission (Wang et al. 2014)

−48 % at all sites in North America. As a combined effect, the NMB at all sites was reduced from −58 % in E_{MAC}/M_{IN} to −45 % if E_{PKU}/M_{INz} was applied in Asia and E_{PKU}/M_{IN} was applied in the regions out of Asia.

Figure 8.5 compares the simulated spatial distribution of surface BC concentrations over South Asia and East Asia to measurements. There was a significant reduction in the bias between the modeled and measured BC concentrations at severely polluted sites, such as the major cities in the North China Plain, the Sichuan Basin, and the Indo-Gangetic Plain. For example, the average surface concentration of BC measured over the North China plain (NCP) (13 sites) was 7.33 g m^{-3}. In comparison, it was simulated to be 2.14 g m^{-3} by E_{MAC}/M_{IN} and 5.31 g m^{-3} by E_{PKU}/M_{INz}. There are two major reasons for the underestimation by E_{MAC}/M_{IN}. First, the BC emission densities were underestimated over the highly populated regions in the traditional inventory E_{MAC}, mainly due to the underestimation of per-capital BC emissions E_{MAC} which assumed a homogeneous

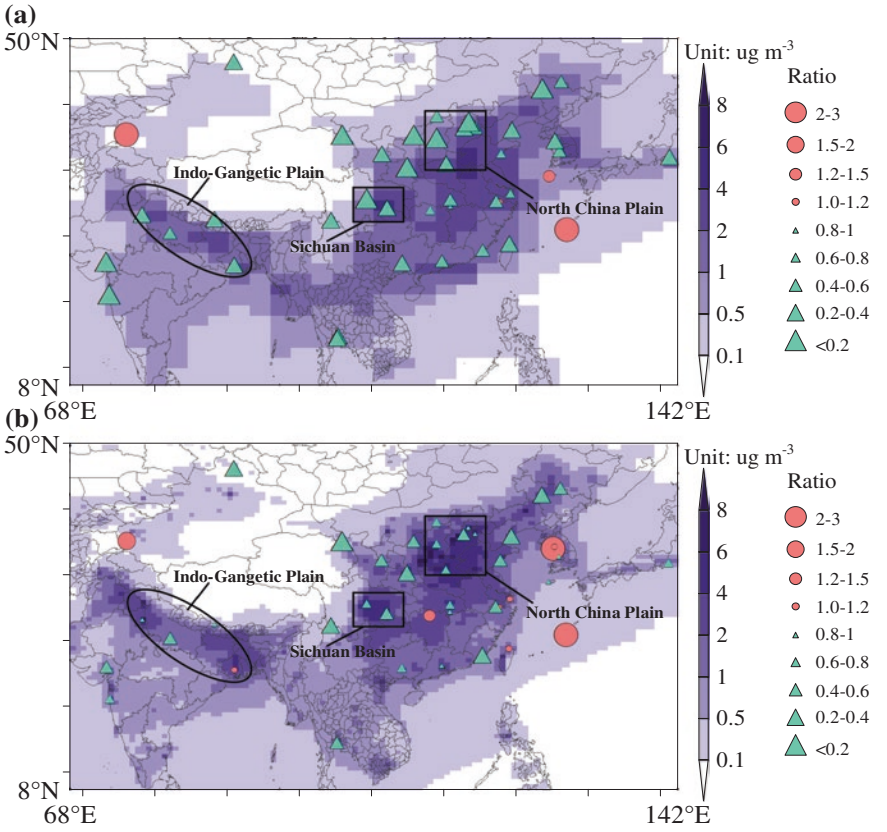

Fig. 8.5 Spatial distribution of the simulated surface BC concentrations in South Asia and East Asia. **a** E_{MAC}/M_{IN}; **b** E_{PKU}/M_{INz}. The site is shown as a *triangle* when the surface BC concentration is underestimated and a *circle* when the surface BC concentration is overestimated. Reproduced with permission (Wang et al. 2014)

distribution of fuel consumptions. Second, the high surface BC concentrations were averaged over a large model grid in a coarse-resolution model, as a spatial smoothing effect (Bond et al. 2013). A better capture of the high BC concentrations over the populated regions has important implications when estimating the exposure risk of BC, which will be discussed below.

8.3 Seasonal Variations of Surface BC Concentrations

There is a seasonal variation of the simulated surface BC concentration, mainly due to the seasonal variation of the emissions and removing rates of BC. The seasonality of the simulated surface BC concentration was also compared to measurements

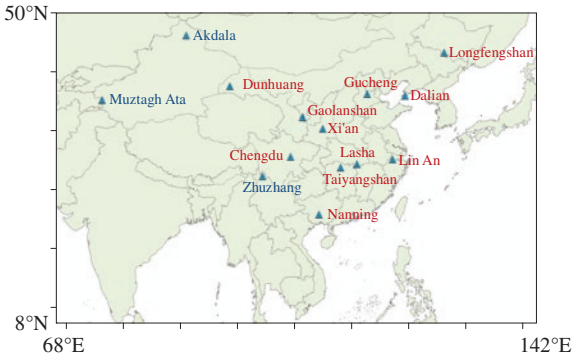

Fig. 8.6 Spatial distribution of BC sites measuring the seasonality of BC concentrations. The three background sites (Akdala, Muztagh Ata, Zhuzhang) are shown as *blue* font. The measured BC concentrations are collected from the literature (Qu et al. 2008; Zhang et al. 2008). Reproduced with permission (Wang et al. 2014)

at fourteen long-term monitoring sites in China, including three background sites. The observed surface BC concentrations are collected from the literature (Qu et al. 2008; Zhang et al. 2008). The spatial locations of the fourteen sites are shown in Fig. 8.6. Since the magnitude of the modeled surface BC concentrations have been evaluated above, the concentrations at these 14 sites are normalized to their annual means, and only the seasonality of BC was evaluated.

Figure 8.7 shows the seasonal variations of surface BC concentrations at the fourteen sites from the three simulations (E_{MAC}/M_{INz}, E_{PKU}/M_{IN}, E_{PKU}/M_{INz}) and observations. As explained above, all concentrations at these sites were normalized to their annual means.

The seasonality of surface BC concentrations at the sites of Xi'an, Chengdu, Nanning, Jinsha, Taiyangshan, Gaolanshan and Longfengshan in the model agrees with the observations very well, with high concentrations in the winter well captured by the model. There are mainly two reasons for the higher concentrations in the winter than that in the summer. First, the BC emissions are generally higher in the winter than that in the summer due to more fuel consumed for heating. Second, the precipitation is mainly concentrated in the summer over the regions influenced by the East Asia monsoon. The modeled seasonal variations of surface BC concentrations at the remaining sites also match the observations, except for that at LinAn and Dunhuang with a notable disagreement in several months. In addition, using the updated inventory and the high-resolution model also influenced the seasonality of modeled surface BC concentrations at several sites. For example, the seasonal trends of the surface BC concentrations modeled by the Asia-zoomed and regular models were significantly different at Muztagh Ata as a background site, due to a different outflow rate of BC from the source region modelled by M_{IN} and M_{INz}. Meantime, there is a higher winter-to-summer ratio of BC concentrations in the north of China such as Dalian, Gucheng, and

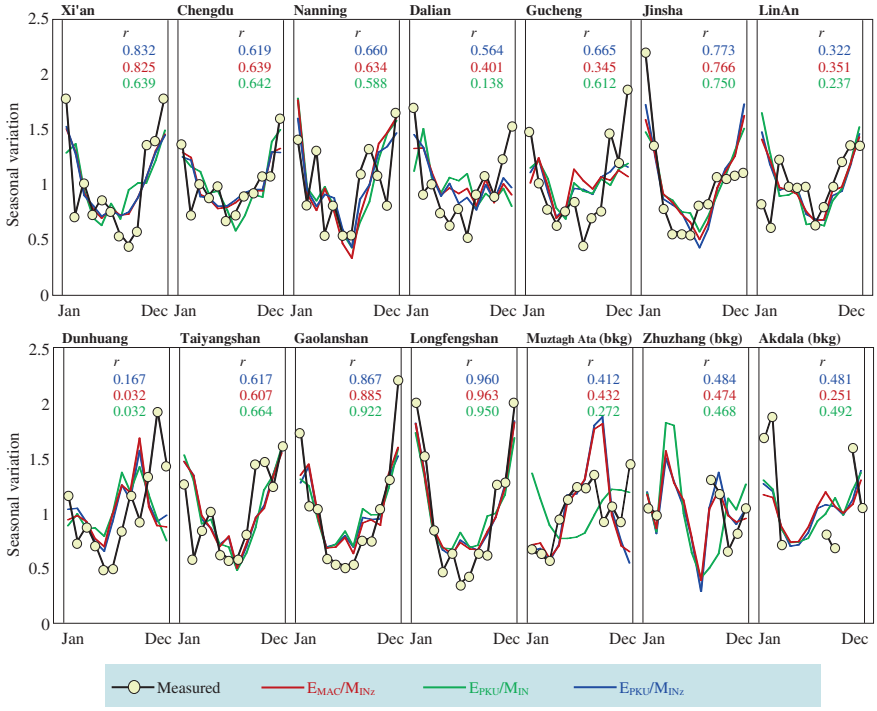

Fig. 8.7 Comparison between the model calculated and field observed monthly mean surface BC concentrations. All concentrations were normalized to their annual means. The correlation coefficients (r) between the modelled and observed concentrations are given in each plot. Reproduced with permission (Wang et al. 2014)

Dunhuang by using E_{PKU}. This can be explained by a higher contribution of residential heating in total BC emissions in E_{PKU} than that in E_{MAC}, in which the emission peaks in the winter.

8.4 Downscaling of BC Concentrations to 0.1° × 0.1°

Although the simulation by E_{PKU}/M_{INz} reaches a high resolution of ~50 km, it is likely that there is still unresolved distribution of BC within the model grid at this resolution. As shown above, the surface BC concentrations are underestimated by ~30 % in Asia. To investigate the influence of insufficient model resolution, a regional chemistry transport model CHIMERE was run off-line at a resolution of 0.1° × 0.1°, which is the original resolution of the emission inventory of E_{PKU}, over the North China Plain, as a typical region with high BC pollution. The simulated BC concentrations over the region were evaluated by observations in Fig. 8.8.

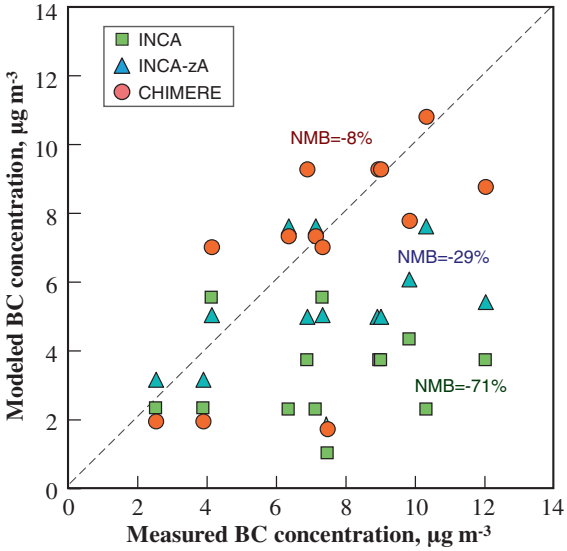

Fig. 8.8 Comparison of the modeled and observed BC concentrations by E_{PKU}/M_{IN}, E_{PKU}/M_{INz}, and E_{PKU}/CHIMERE. All simulations are run with the inventory of E_{PKU}. The normalized mean bias (NMB), defined as the difference of the arithmetic mean of the model minus the observations relative to the observations are marked for each combination. Reproduced with permission (Wang et al. 2014)

The comparison of modeled and observed BC concentrations illustrates that BC concentrations were underestimated by 71 % in the coarse-resolution model (M_{IN}) and by 29 % in the model zoomed over Asia (M_{INz}). In comparison, when the sub-grid distribution of surface BC concentrations were explicitly modeled by the CHIMERE model, the observed and modeled BC concentrations match with a NMB of −8 %. The reduction in the model bias confirms that the emission and concentration of BC are still heterogeneous distributed within the model grid at a resolution of 50 km, as the best resolution of E_{PKU}/M_{INz}, which is densely populated. The spatial distributions of surface BC concentrations modeled by models at the three model resolutions are shown in Fig. 8.9. It shows that the extremely high concentrations can be captured by the regional fine-resolution model CHIMERE, and smoothed in space if the coarse-resolution global model, either M_{IN} or M_{INz}, was used.

However, the 0.1° × 0.1° resolution modeling of atmospheric BC concentration, as had been done using CHIMERE over the North China Plain, cannot be applied globally at present stage due to unaffordable computational load and lack of meteorological data at the same resolution. Therefore, a simplified method to downscale the global surface BC concentrations simulated by M_{INz} in Asia and M_{INz} in the rest region of the world to 0.1° × 0.1° could be an alternative strategy. Assuming that the heterogeneous spatial distribution of BC concentrations is dependent on the distribution of BC emissions, we tried to develop a method to reach a high

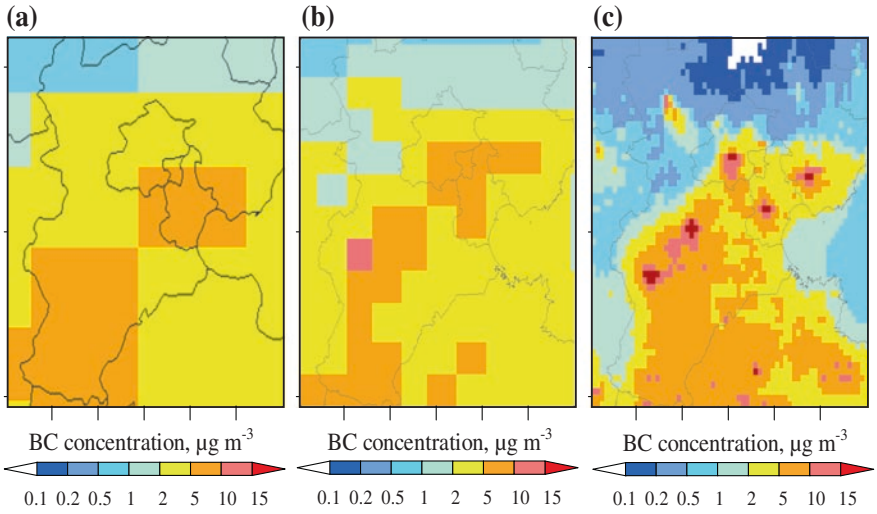

Fig. 8.9 Spatial distribution of the surface BC concentrations modeled by the E_{PKU}/M_{IN} at a resolution of 1.25°× 2.50° (**a**), E_{PKU}/M_{INz} at a resolution of 0.51°× 0.66° (**b**), and E_{PKU}/CHIMERE at a resolution of 0.1°× 0.1° (**c**). Reproduced with permission (Wang et al. 2014)

resolution of BC field using the emission inventory. This is expectable, since the BC concentration is generally higher at the emission centers (Fig. 8.9). However, considering that the dispersion of sub-grid scale emissions might weaken the relationship between the emissions and concentrations, a non-linear downscaling method is applied. The surface BC concentrations calculated by M_{INz} in Asia and by M_{IN} for the remaining regions of the world were downscaled from that modelled over a large model grid (*x, y*) (0.51° × 0.66° grid in M_{INz} or 1.27° × 2.5° grid in M_{IN}) to a 0.1° × 0.1° sub-grid (*i, j*) as:

$$C_{i,j}^{*} = C_{x,y} \frac{E_{i,j}^{\alpha}}{\sum_{i,j} \left(F_{i,j} E_{i,j}^{\alpha} \right)} \tag{8.1}$$

where $C_{i,j}^{*}$ is the downscaled BC concentrations in the 0.1° × 0.1° sub-grid (*i, j*); $C_{x,y}$ is the model-calculated concentration of grid cell (*x, y*) by M_{INz} or M_{IN}; $E_{i,j}$ is the emission density in the sub-grid (*i, j*) derived from the E_{PKU} inventory; $F_{i,j}$ is the area fraction of each sub-grid (*i, j*). The exponent α in Eq. 8.1 is a coefficient describing the dependence of surface BC concentrations on the emissions, which is less than 1.

Subsequently, the optimal exponent α was derived using a trial-and-error method. In detail, different values of α from 0 to 1 were tested at an interval of 0.01 from 0.2 to 0.6, and the deviation as a mean at all sites in Asia and the regions out of Asia was calculated corresponding to each value of α. The variance of the mean misfit as a deviation in the model-observation comparison when

different values of the exponent α were applied is shown in Fig. 8.10. As a result, the lowest model-data misfit can be derived when α equals to 0.3 for either Asia or the regions out of Asia. It should be noted that this optimized exponent α was obtained only for the surface concentrations. The optimal exponent α will change if the method was used to downscale the column load of BC concentrations, which is less dependent on the local emissions and more influenced by transport from

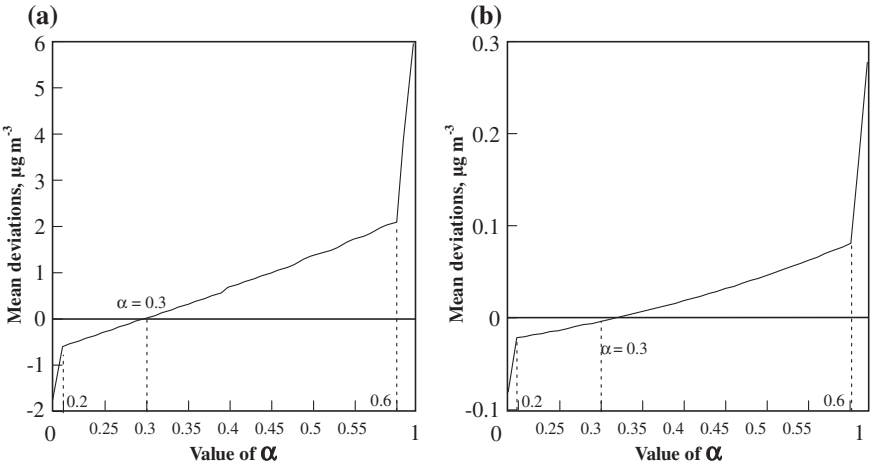

Fig. 8.10 Variance of the mean deviations in the model-observation comparison when different values of the exponent α were applied in Asia (**a**) and the regions out of Asia (**b**). Reproduced with permission (Wang et al. 2014)

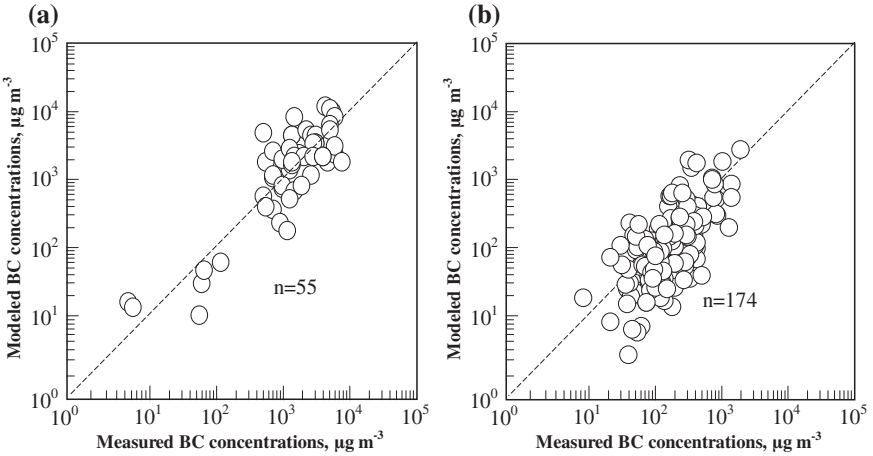

Fig. 8.11 Comparison of the measured and downscaled surface BC concentrations when a exponent α of 0.3 was used in the non-linear downscaling method at sites in Asia (**a**) and the regions out of Asia (**b**). Reproduced with permission (Wang et al. 2014)

surrounding grids. In addition, the method was used to downscale the surface BC concentrations from M_{IN} or M_{INz}, and the optimized exponent α would be different if the concentrations was originally simulated by a model at a spatial resolution different from that in M_{IN} or M_{INz}.

Thus, this optimized value of α (0.3) was used to downscale the modelled BC concentrations by M_{INz} in Asia and M_{IN} for the rest region to 0.1° × 0.1° grids globally. Figure 8.11 shows the comparison of the measured surface BC concentrations and that downscaled to 0.1° × 0.1° from M_{INz} in Asia and M_{IN} in the regions out of Asia. As a result, there was no systematic bias when the modelled concentrations were downscaled to 0.1° × 0.1°.

8.5 Global Ambient Exposure to Black Carbon

Based on the modelled surface BC concentrations at a resolution of 0.1° × 0.1°, we tried to estimate the exposure concentrations of BC globally. Figure 8.12 shows the global distribution of annual mean ambient exposure to BC concentrations in 2007. In general, the spatial pattern is similar to that of the emissions and modelled BC concentrations. Extremely high BC exposure concentrations (>4 μg m^{-3}) were mainly distributed over the developing countries in East Asia and South Asia, while high BC exposure concentrations (>1 μg m^{-3}) were found over the developed countries in Western Europe and North America.

The co-variance of the concentrations and population density was noticed when we estimated the BC exposure. Figure 8.13 shows the geographic distribution of the ambient exposure concentrations of BC over the most polluted regions of East Asia and South Asia, and also the geographic distribution of population. It is noticed that the highest BC concentrations were always corresponding to densely

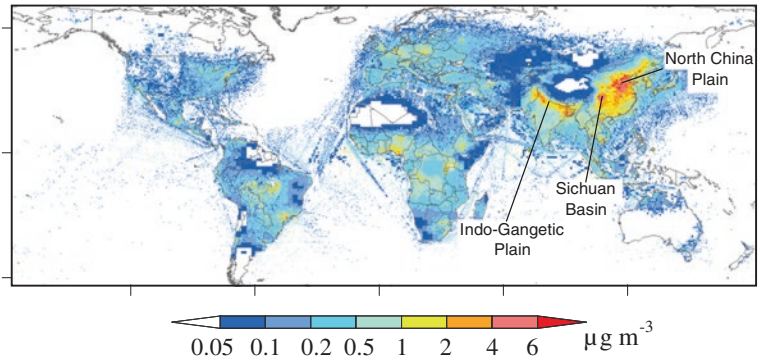

Fig. 8.12 Spatial distribution of the estimated ambient BC exposure concentrations in 2007. The concentrations are derived by downscaling the results from E_{PKU}/M_{INz} in Asia and from E_{PKU}/M_{IN} in the regions out of Asia to 0.1° × 0.1°. Reproduced with permission (Wang et al. 2014)

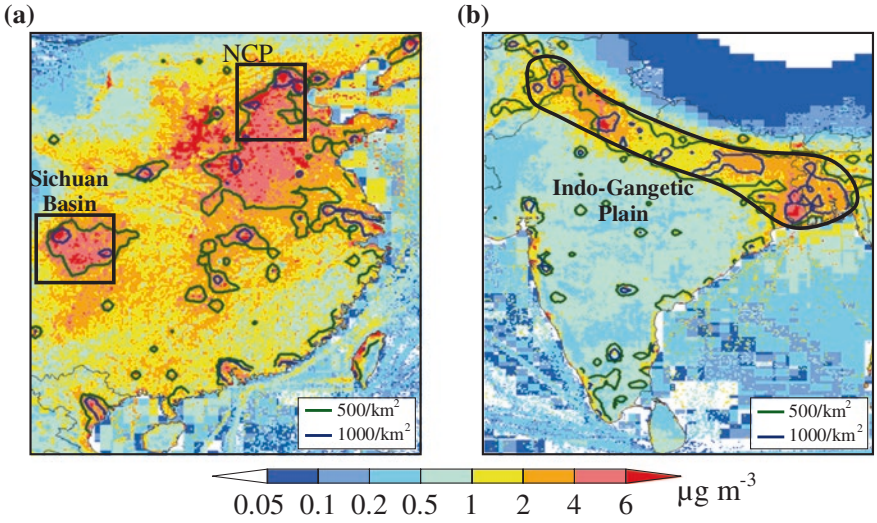

Fig. 8.13 Geographic distribution of population exposure concentrations of BC in East Asia (**a**) and South Asia (**b**) at a resolution of 0.1° × 0.1° in 2007. Population density as contours are shown as the *green* (>500 cap km^{-2}) and *blue* (>1,000 cap km^{-2}) lines. Reproduced with permission (Wang et al. 2014)

distributed population, as a result of the spatial correlation between the emission of BC and the population density. As a result, the global average population-weighted BC concentration (2.14 μg m^{-3}) is significantly higher than the global average area-weighted BC concentration (0.28 μg m^{-3}). As the most seriously polluted regions, the annual mean BC exposure concentrations are as high as 6.68, 5.49 and 4.31 μg m^{-3} averaged over the North China Plain (China), the Sichuan Basin (China), and the Indo-Gangetic Plain (India), respectively. Extremely high BC exposure concentrations (>6 μg m^{-3}) was found in metropolitan areas with a population density over 1000 people per km^2, resulting in a severe health damage.

To study the effect of co-variance of exposure and population, we calculated the cumulative frequency distribution of BC exposure concentrations. As illustrated in Fig. 8.14, the cumulative frequency of BC exposure at the concentrations of 1–10 μg m^{-3} was the lowest in East Asia, indicating the highest percentage of population exposed over this level of BC concentrations. Due to lack of sufficient epidemiological data, there is not a standard criteria of BC exposure concentration that can be used to evaluate the health risk of BC exposure to date (Janssen et al. 2011). In a recent study, Geng et al. (2013) found that, when the ambient BC exposure concentration increases from 2.2 to 4.9 μg m^{-3}, the cardiovascular, respiratory, and total mortality of the population would increase by a percentage of 3.2, 0.6, and 2.3 % in a Chinese city (Shanghai). Meanwhile, the emergency-room and outpatient visits increases by a percentage of 1.33 and 3.35 %, respectively. Thus, we tried to evaluate the health risk of BC exposure concentrations using the two BC exposure criteria reported by Geng et al. (2013), as an initial estimate.

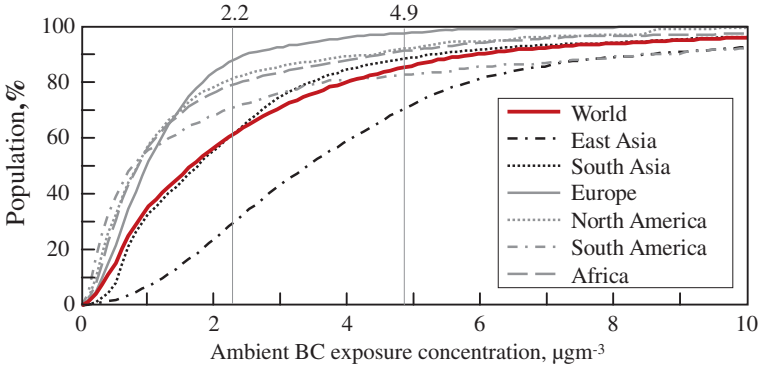

Fig. 8.14 Cumulative frequency distributions of the BC exposure concentration on basis of population. The exposure concentrations are derived by downscaling the results from E_{PKU}/M_{INz} in Asia and from E_{PKU}/M_{IN} in the other regions. Reproduced with permission (Wang et al. 2014)

As a result, the percentage of population exposed to an annual mean BC concentration over 4.9 μg m^{-3} in East Asia and South Asia was as high as 18 and 11 %, respectively. These high-risk populations were mainly distributed in large cities (Fig. 8.13). We expect that the BC exposure risk should be re-evaluated when a comprehensive standard of BC is established.

As a major finding of our work, the modelled BC concentration is sensitive to both the emission and the spatial resolution of transport model. Figure 8.15 compares the BC exposure concentrations averaged over East Asia and South Asia derived from the four inventory/model combinations without downscaling and the combination with downscaling, namely $(E_{PKU}/M_{INz})_d$ (the subscript "d" indicates the downscaling method). The modelled and measured surface-air concentration as an average over all observation sites was used as an evaluator of the model results and also shown in the figure. When the model resolution was enhanced from ~200 to ~50 km, and reached ~10 km, the BC exposure concentration averaged over East Asia was increased from 2.33 μg m^{-3} in E_{PKU}/M_{IN} to 2.80 μg m^{-3} in E_{PKU}/M_{INz}, and 3.91 μg m^{-3} in $(E_{PKU}/M_{INz})_d$. Meantime, this conclusion was partly confirmed by the fact that the modelled BC concentrations at the monitoring sites approach the observations with the model-data misfit reduced from −59 to +1 %. In addition, when the emission inventory was updated, the BC exposure concentration averaged over East Asia was increased from 2.44 μg m^{-3} in E_{PKU}/M_{IN} to 2.80 μg m^{-3} in E_{PKU}/M_{INz}, which was supported by a better agreement of modelled concentration at the observation site (a bias reduced from −47 to −32 %). Similar results are derived in South Asia, where the BC exposure concentration had increased by 55 % from 1.06 μg m^{-3} in E_{MAC}/M_{IN} to 2.36 μg m^{-3} in $(E_{PKU}/M_{INz})_d$.

Similarly, the average BC exposure concentrations in Europe and North America derived from the four inventory/model combinations without downscaling and one combination with downscaling, namely $(E_{PKU}/M_{IN})_d$, are shown in Fig. 8.16. There is a remained model bias of −39 % in Europe, likely due to the relatively low

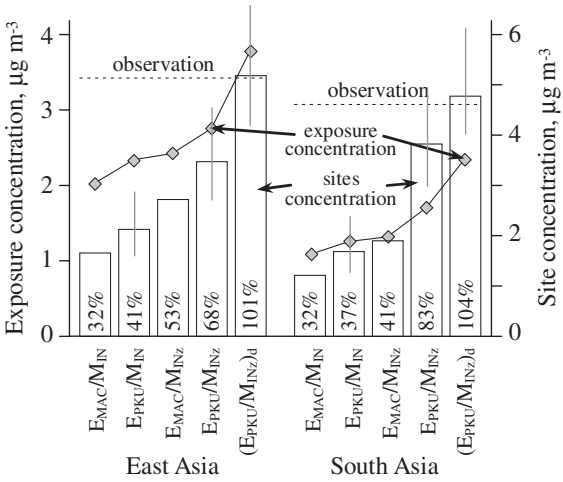

Fig. 8.15 Population exposure concentrations in East Asia and South Asia from the four combinations of emission inventory (E_{PKU} or E_{MAC}) and model (M_{IN} or M_{INz}) and that downscaled from E_{PKU}/M_{INz} ($(E_{PKU}/M_{INz})_d$). The modelled and measured surface-air concentrations averaged over all sites are shown. Error lines for individual *bars* are derived by using the first and third quartiles of PKU-BC-2007. The percentages of modeled concentrations relative to observed ones are listed. Reproduced with permission (Wang et al. 2014)

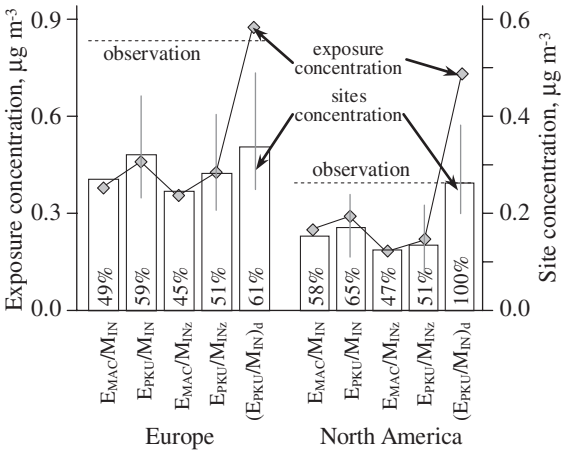

Fig. 8.16 Comparison of the population exposure concentrations in Europe and North America from the four combinations of emission inventory (E_{PKU} or E_{MAC}) and model (M_{IN} or M_{INz}) and that downscaled from E_{PKU}/M_{IN}. The modelled and measured surface-air concentrations averaged over all sites are shown. Error lines for individual *bars* are derived by using the first and third quartiles of PKU-BC-2007. The percentages of modeled concentrations relative to observed ones are listed. Reproduced with permission (Wang et al. 2014)

resolution in M_{IN}. In Europe and North America, the average BC exposure concentrations increased by 100 and 150 % from E_{PKU}/M_{IN} to $(E_{PKU}/M_{IN})_d$, confirming the dependence of BC exposure on model resolution.

8.6 Intake of Black Carbon by Inhalation

According to the simulated BC concentrations by four inventory/model combinations, the intake of BC by inhalation was estimated following a standard exposure estimation method (U.S. Environmental Protection Agency 2011). The lifetime average daily intake (LADI) of BC by a given population via inhalation (ng/kg/day) is calculated by classifying the population into eight age groups (0–2, 2–3, 3–5, 5–10, 10–18, 18–30, 30–60, and >60) and two genders (the superscripts *m* and *f* stand for male and female, respectively):

$$LADI = \sum_{i=1}^{8} \left(\frac{F_i^m \cdot c \cdot R_i^m \cdot T_i^m}{W_i^m} + \frac{F_i^f \cdot c \cdot R_i^f \cdot T_i^f}{W_i^f} \right) \tag{8.2}$$

where F_i^m and F_i^f are fractions of male and female in the ith age group (United States Census Bureau 2012). c is the exposure concentration (ng/m^3). R_i^m and R_i^f are inhalation rate (m^3/day) of male and female in the ith age group (U.S. Environmental Protection Agency 2011). T_i^m and T_i^f are fraction of time expend outdoor of male and female in the ith age group (U.S. Environmental Protection Agency 2011). W_i^m and W_i^f are average body weight (kg) of male and female in the ith age group (U.S. Environmental Protection Agency 2011; Walpole et al. 2012). The uncertainty of the estimated BC intake was derived from a Monte Carlo simulation (10,000 runs) based on the uncertainty distributions of inhalation rate (log-normal), body weight (log-normal), and the fraction of time spend outdoor (normal) from the literature (U.S. Environmental Protection Agency 2011; United States Census Bureau 2012; Walpole et al. 2012).

Based on the simulated 0.1° × 0.1° gridded BC exposure concentrations downscaled from our best inventory/model combination, the LADI were calculated for 222 countries in 2007 individually. The derived national BC LADI is mapped by country in Fig. 8.17. In addition, the LADI for the top 10 countries with the highest BC LADI are listed in Table 8.2. With the largest emission of BC, the LADI is the highest for the Chinese population, reaching 132 ng/kg/day. Although the exposure-response relationship has not been established for BC to date, a large adverse health impact due to BC intake by inhalation can be expected.

Figure 8.18 shows the cumulative distribution of LADI of BC in Chinese, Asian, and non-Asian population according to the different inventory/model combinations. The average LADI is the highest among Chinese population, followed by among Indian and non-Asian population. The percentage of population associated with a

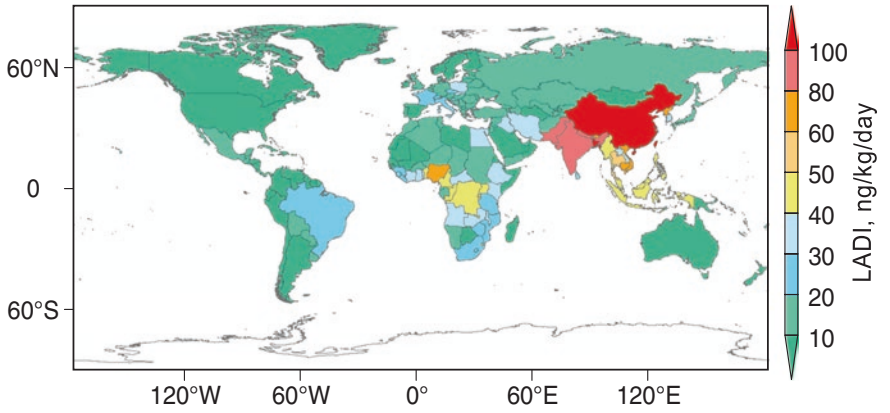

Fig. 8.17 Spatial distribution of the model calculated lifetime average daily intake (LADI) of BC by country in 2007

Table 8.2 The lifetime average daily intake of BC in 2007 calculated for the top 10 countries with the highest lifetime average daily intake

Country	LADI (ng/kg/day)	BC emissions (Gg/year)
China	132	1992
Bangladesh	123	59
Pakistan	86.7	104
India	80.6	629
Nepal	80.2	26
Vietnam	79.4	109
Bhutan	74.7	3.7
North Korea	70.0	29
Cambodian	66.0	53
Nigeria	51.1	228

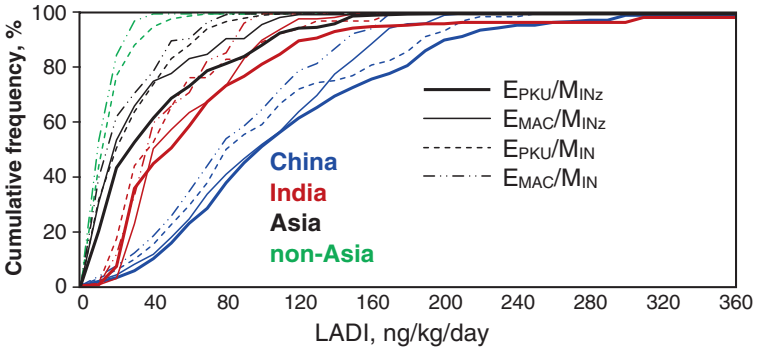

Fig. 8.18 Cumulative frequency distributions of the model calculated lifetime average daily intake (LADI) in Chinese, Asian, and non-Asian populations. The BC exposure concentrations are derived from the four combinations of emission inventory (E_{PKU} or E_{MAC}) and model (M_{IN} or M_{INz})

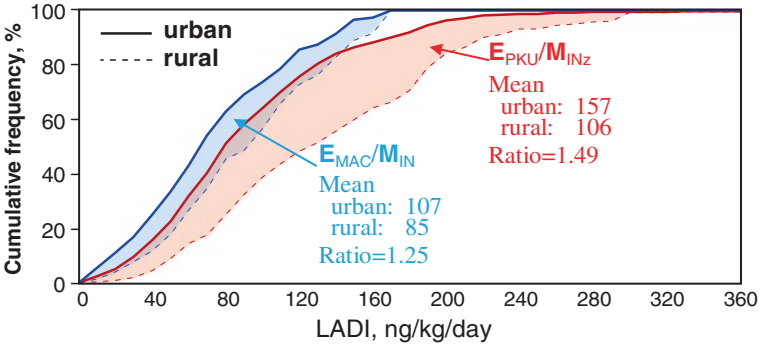

Fig. 8.19 Cumulative frequency distributions of the model calculated the model calculated lifetime average daily intake (LADI) among the population over the urban and rural areas. The BC exposure concentrations are derived from the two inventory/model combinations, namely E_{MAC}/M_{IN} or E_{PKU}/M_{INz}

daily BC intake over a criterion between 0 and 200 ng/kg/day was much higher in E_{PKU}/M_{INz} than that in E_{MAC}/M_{IN}. For example, when the modelling resolution was enhanced from 2.50° × 1.27° in M_{INz} to 0.51° × 0.66° in M_{IN}, the calculated daily BC intake will increase from 97 to 114 ng/kg/day among Chinese population and increase from 31 to 49 ng/kg/day among Indian population. This influence can be enlarged at the high-risk end. According to E_{PKU}/M_{INz}, 10 % of the most vulnerable population exceed an annual mean BC exposure concentration of 200 and 120 ng/m^3 in China and India, respectively, and this concentration reduced to 182 and 101 ng/m^3 when modelled at a resolution of 2.50° × 1.27°. It might be hypothesized that the estimated exposure could be higher if a finer model resolution was used. Both BC concentrations and population distributions are known to peak on very fine scales of a few kilometers. The dependency of exposure, as well as the estimated health impact on model resolution should be further investigated so as to bridge the gap with the data derived from the epidemiological studies.

In addition, based on the high-resolution BC exposure map and an urban-area mask, it is possible to estimate the BC exposure levels over rural and urban areas separately. Figure 8.19 shows the cumulative frequency distributions of the calculated daily BC intakes estimated over the urban and rural areas. As a result, there is a higher urban-rural contrast of BC intakes revealed by using the high-resolution model and inventory. According to E_{PKU}/M_{INz}, there is a difference by a factor of 1.5 in BC intakes by urban and rural populations. According to the population prediction by U.N. Department of Economic and Social Affairs (2011), the population of China and India in cities will increase from 42 and 29 % of the population in 2007, up to 62 and 40 % in 2030, respectively. Thus, even if the surface-air BC concentration remains at the level of 2007 in these two countries, the populated-averaged BC exposure concentration will increase by 15 and 14 % in China and India, respectively, only due to a factor of 2.1 and 3.0 differences in the exposure concentrations between urban and rural populations. It is more and more important

to use high resolution emission inventory and model to estimate the health impact, since the accelerated urbanization in developing countries would cause population to become more unevenly distributed in the future.

References

Bond, T. C., Doherty, S. J., Fahey, D., Forster, P., Berntsen, T., DeAngelo, B., et al. (2013). Bounding the role of black carbon in the climate system: A scientific assessment. *Journal of Geophysical Research: Atmospheres, 118*(11), 5380–5552.

Geng, F., Hua, J., Mu, Z., Peng, L., Xu, X., Chen, R., & Kan, H. (2013). Differentiating the associations of black carbon and fine particle with daily mortality in a Chinese city. *Environmental Research, 120*, 27–32.

Janssen, N., Hoek, G., Simic-Lawson, M., Fischer, P., van Bree, L., ten Brink, H., et al. (2011). Black carbon as an additional indicator of the adverse health effects of airborne particles compared with PM10 and PM2. 5. *Environ Health Perspect, 119*(12), 1691-1699.

Qu, W. J., Zhang, X. Y., Arimoto, R., Wang, D., & Wang, Y. Q. (2008). Chemical composition of the background aerosol at two sites in southwestern and northwestern China: Potential influences of regional transport. *Tellus B, 60B*, 657–673. doi:10.1111/j.1600-0889.2008.00342.x.

U.N. Department of Economic and Social Affairs. (2011). *World population prospects: The 2010 revision*. New York: Department of Economic and Social Affairs of the United Nations.

U.S. Environmental Protection Agency. (2011). *Exposure factors handbook: Chapter 6-inhalation rates*. Retrieved from http://www.epa.gov/ncea/efh/report.html.

United States Census Bureau. (2012). *International data base*. Retrieved from http://www.census.gov/population/international/data/idb.

Walpole, S. C., Prieto-Merino, D., Edwards, P., Cleland, J., Stevens, G., & Roberts, I. (2012). The weight of nations: An estimation of adult human biomass. *BMC Public Health, 12*(1), 439.

Wang, R., Tao, S., Balkanski, Y., Ciais, P., Boucher, O., Liu, J., et al. (2014). Exposure to ambient black carbon derived from a unique inventory and high-resolution model. *Proceedings of the National Academy of Sciences, 111*(7), 2459–2463.

Zhang, X. Y., Wang, Y. Q., Zhang, X. C., Guo, W., & Gong, S. L. (2008). Carbonaceous aerosol composition over various regions of China during 2006. *Journal of Geophysical Research: Atmospheres, 113*(D14111). doi:10.1029/2007JD009525.

Chapter 9
Conclusions

Modelling of the emission, transport and distribution of black carbon (BC) in the atmosphere are associated with large uncertainties. These uncertainties have been well recognized in previous studies, which are reflected by a significant underestimation of the modelled surface BC concentrations. It hampers the quantification of the role of BC in air pollution and climate change. The goal of this thesis is to re-visit the emission inventory of BC and investigate the impact of model resolution on the modelled concentrations of BC in the atmosphere, and applied the new emission inventory and a high-resolution modelling method to assess the exposure concentrations and inhalation intake of BC in the population. These results can be used to evaluate the health risk of BC exposure in air pollution.

A global fuel inventory (PKU-FUEL-2007) and a global carbon inventory (PKU-CO_2-2007) was constructed using a new method, in which uncertainty in fuel data is reduced significantly. Different from traditional fuel inventories, sub-national fuel data were compiled for major countries of fuel consumption and then disaggregated to $0.1° \times 0.1°$ grids. As a result, the bias in the fuel data due to the disaggregation of national fuel data to $0.1° \times 0.1°$ grids was substantially reduced within these countries. Comparing with a reference global carbon inventory ODIAC, the PKU-CO_2-2007 inventory could better characterize the distribution of fuel consumption over rural areas. In the U.S.A., the PKU-CO_2-2007 inventory is in good agreement with a state-of-the-art inventory VULCAN. The fuel inventory can be used to develop the emission inventories of other species which are generated in the combustion.

Based on the constructed fuel inventory, a global high-resolution emission inventory of BC (PKU-BC-2007) was developed with an updated database of BC emission factors. According to the PKU-BC-2007 inventory, global total BC emissions in 2007 from 223 countries/territories were 8895 Gg/year, among which 3700 Gg/year was contributed by Asia. For the remaining regions, Africa, South America, Europe, North America and Oceania contributed to 24, 13.2, 8.5, 6.3 and 2.0 % in the

R. Wang, *Global Emission Inventory and Atmospheric Transport of Black Carbon*,
Springer Theses, DOI 10.1007/978-3-662-46479-3_9

total, respectively. By country, China, Brazil and India were the top three emission countries with a total emission of 1992, 805, and 630 Gg/year, respectively, followed by the U.S.A., Nigeria, Indonesia, Congo, Russia and Angola. Globally, residential coal and biofuels were the major fuels emitting BC, contributing 32 % to the total emissions, which were followed by diesel vehicles, savanna fires, brick production, and deforestation fires.

China was the most important country for BC emissions. In China, residential coal and biofuel contributed over 50 % to national BC emissions, followed by industry (33 %) and on-road motor vehicles (10 %). Spatially, the emission density in the east of China is significantly higher than that in the west of the country. Extremely high BC emission densities were found over the North China Plain, the Weihe Plain, the Sichuan Basin, the Guizhou Plateau, and the Northeast Plain. Temporally, the national BC emission had increased rapidly before the middle of 1990s due to a rapid increase of industry and population, and leveled off since then due to efforts to improve the combustion technology made by the country, including the adjustment of fuel composition, the application of dust removing facilities for industrial boilers, and phase-out of beehive coking plants. In the coming decades, a rapid increase of motor vehicles could be a major motivation leading to an increase in the BC emissions. The most effective approaches to mitigate BC in China include the limitation of vehicle numbers, enhancement of stricter vehicle emission standards and replacement of traditional residential fuels by cleaner fuels.

The constructed BC emission inventory was introduced to a global atmospheric general circulation model LMDZ-OR-INCA. Global transport and distribution of BC in the atmosphere were simulated. Using the same model at two different horizontal resolutions, BC surface concentrations were simulated by using the new PKU-BC-2007 inventory developed in our thesis and also another widely used emission inventory of BC (MACCity). The modelled BC concentrations were evaluated by comparing against a compiled global data set of observations. As a result, the new emission inventory, which updates the emission factors and improves the spatial allocation, produced a better agreement with observations in Asia, when combined with a high-resolution transport model. The normalized mean bias when comparing with observations was reduced from -88 to -35 % in Asia where the new inventory and a high-resolution transport model replace a previous inventory combined with a transport model at a traditional resolution. Furthermore, a nonlinear interpolation method was developed to downscale the BC concentrations to 10 km using emissions as a proxy, and the final bias could be reduced to -12 % globally. In addition, the modelled seasonal trend and vertical distribution of BC were also compared against observations and acceptable agreements were obtained.

According to simulated BC concentrations, ambient exposure and lifetime average daily intake of BC were estimated globally. Based on the new emission inventory and high-resolution model, the global average population-weighted BC concentration was 2.14 $\mu g\ m^{-3}$. Over the most polluted regions of the North China Plain (China), the Sichuan Basin (China), and the Indo-Gangetic Plain

(India), the annual mean BC exposure concentrations were as high as 6.68, 5.49 and 4.31 $\mu g\ m^{-3}$, respectively. Furthermore, the lifetime average daily intake of BC was calculated by country. The top ten lifetime-average-daily-intake countries were China (132 ng/kg/day), Bangladesh (123 ng/kg/day), Pakistan (87 ng/kg/day), India (81 ng/kg/day), Nepal (80 ng/kg/day), Vietnam (79 ng/kg/day), Bhutan (75 ng/kg/day), North Korea (70 ng/kg/day), Cambodia (66 ng/kg/day) and Nigeria (51 ng/kg/day). Although the health effect due to BC exposure cannot be assessed due to lack of exposure-response data, a high health risk is expected in these countries. At last, a contrast was found for the BC exposure over urban and rural areas that BC exposure in urban areas was 2–3 factors higher than that in rural areas. Due to a rapid urbanization in developing countries, more people are moving from rural to urban areas and this re-allocation of population in space would lead to an increase in BC exposure by 10–15 % alone.